

B23261

# THE NIMBUS 6 USER'S GUIDE



**GODDARD SPACE FLIGHT CENTER  
GREENBELT, MARYLAND**



## THE NIMBUS 6 USER'S GUIDE

Prepared By

The LANDSAT/Nimbus Project  
Goddard Space Flight Center  
National Aeronautics and Space Administration

Edited By

John E. Sissala  
Management and Technical  
Services Company  
Beltsville, Maryland

February 1975



## THE NIMBUS 6 USER'S GUIDE

### FOREWORD

This document provides potential data users with background information on the Nimbus 6 spacecraft and experiments as a basis for selecting, obtaining, and utilizing Nimbus 6 data in research studies.

The basic spacecraft system operation and the objectives of the Nimbus 6 flight are outlined, followed by a detailed discussion of each of the experiments. The format, archiving, and access to the data are also described. Finally, the contents and format of the Nimbus 6 Data Catalogs are described. These catalogs will be issued periodically after the launch of Nimbus 6. They will contain representative pictorial data and daily THIR montages obtained during each period, as well as information on the collection and availability of all Nimbus 6 data.

The experimenters for each instrument prepared their section. The assembly and editing of this publication was accomplished by the Management and Technical Services Company (MATSCO), under Contract No. NAS 5-20694 with the Goddard Space Flight Center, NASA, Greenbelt, Maryland.

Don V. Fordyce  
LANDSAT/Nimbus Project Manager  
Goddard Space Flight Center

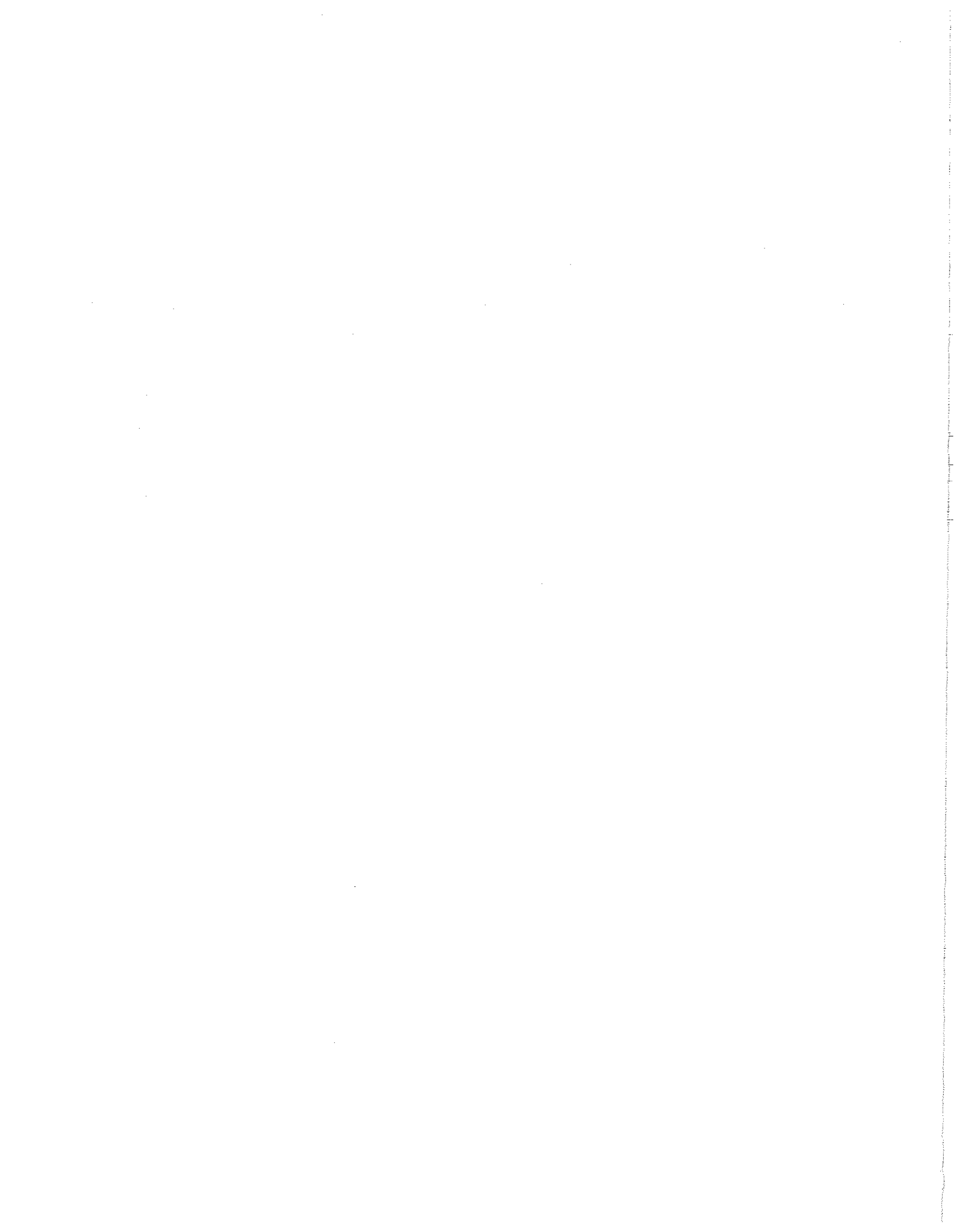


## TABLE OF CONTENTS

	<u>Page</u>
<b>FOREWORD . . . . .</b>	<b>iii</b>
<b>SECTION 1. THE NIMBUS 6 SPACECRAFT SYSTEM . . . . .</b>	<b>1</b>
<b>1.1 Introduction . . . . .</b>	<b>1</b>
<b>1.2 Nimbus 6 Scientific Objectives . . . . .</b>	<b>1</b>
<b>1.3 Spacecraft Attitude . . . . .</b>	<b>3</b>
<b>1.4 Spacecraft Data Systems . . . . .</b>	<b>3</b>
<b>1.4.1 High Data Rate Storage System (HDRSS) . . . . .</b>	<b>5</b>
<b>1.4.2 Versatile Information Processor (VIP) . . . . .</b>	<b>6</b>
<b>1.4.3 Real Time Data Transmission . . . . .</b>	<b>6</b>
<b>1.5 Ground Station Complex . . . . .</b>	<b>6</b>
<b>1.6 Nimbus/ATS Data Utilization Center (NADUC) . . . . .</b>	<b>7</b>
<b>1.7 Archival and Dissemination of Nimbus 6 Data . . . . .</b>	<b>7</b>
<b>1.8 On-Off Operating Mode for each Experiment . . . . .</b>	<b>9</b>
<b>* SECTION 2. THE TEMPERATURE HUMIDITY INFRARED RADIOMETER (THIR) SUBSYSTEM . . . . .</b>	<b>11</b>
<b>2.1 Introduction . . . . .</b>	<b>11</b>
<b>2.2 THIR Operation . . . . .</b>	<b>11</b>
<b>2.2.1 Radiometer . . . . .</b>	<b>11</b>
<b>2.2.2 Scan Sequence . . . . .</b>	<b>14</b>
<b>2.2.3 Scan Geometry . . . . .</b>	<b>18</b>
<b>2.2.4 THIR Transmissions . . . . .</b>	<b>20</b>
<b>2.3 Calibration . . . . .</b>	<b>20</b>
<b>2.3.1 Laboratory Calibration . . . . .</b>	<b>20</b>
<b>2.3.2 Equivalent Blackbody Temperature . . . . .</b>	<b>22</b>
<b>2.4 Data Processing, Archiving, and Availability . . . . .</b>	<b>24</b>
<b>2.4.1 Photofacsimile Film Strips . . . . .</b>	<b>24</b>
<b>2.4.2 Digital Data . . . . .</b>	<b>28</b>

TABLE OF CONTENTS (Continued)

	<u>Page</u>
2.5 Format of the NMRT-THIR . . . . .	30
<b>SECTION 3. THE HIGH RESOLUTION INFRARED RADIATION SOUNDER (HIRS) EXPERIMENT . . . . .</b>	<b>37</b>
3.1 Experiment Description . . . . .	37
3.2 Instrument Description . . . . .	42
3.2.1 Summary . . . . .	42
3.2.2 Optical System . . . . .	43
3.2.3 Signal Electronics . . . . .	47
3.2.4 Interpretation of HIRS Digital Data . . . . .	47
3.3 HIRS Data Processing, Format, and Archiving . . . . .	51
3.3.1 Data Processing . . . . .	51
3.3.2 Image Format . . . . .	51
3.3.3 Tape Format . . . . .	56
3.3.4 Data Archiving . . . . .	56
<b>REFERENCES AND BIBLIOGRAPHY . . . . .</b>	<b>58</b>
<b>SECTION 4. THE SCANNING MICROWAVE SPECTROMETER (SCAMS) EXPERIMENT . . . . .</b>	<b>59</b>
4.1 Introduction . . . . .	59
4.2 Scientific Objectives . . . . .	59
4.3 Experiment Description . . . . .	60
4.4 Description of the Instrument . . . . .	65
4.4.1 Physical Description and Performance Characteristics . .	65
4.4.2 Functional Description . . . . .	67
4.5 Data Processing, Format, and Availability . . . . .	74
4.5.1 Data Processing . . . . .	74
4.5.2 Image Format . . . . .	76
4.5.3 Tape Format . . . . .	83
4.5.4 Data Availability . . . . .	83

TABLE OF CONTENTS (Continued)

	<u>Page</u>
<b>REFERENCES . . . . .</b>	86
<b>*SECTION 5. THE ELECTRICALLY SCANNING MICROWAVE RADIOMETER (ESMR) EXPERIMENT . . . . .</b>	87
<b>5.1 Introduction . . . . .</b>	87
<b>5.2 Instrument Description . . . . .</b>	88
<b>5.2.1 Viewing Geometry . . . . .</b>	88
<b>5.2.2 Operation . . . . .</b>	90
<b>5.2.3 Calibration . . . . .</b>	96
<b>5.3 Data Processing, Format, and Availability . . . . .</b>	102
<b>5.3.1 Data Processing . . . . .</b>	102
<b>5.3.2 Image Format . . . . .</b>	102
<b>5.3.3 Tape Format . . . . .</b>	106
<b>5.3.4 Data Availability . . . . .</b>	108
<b>SECTION 6. THE EARTH RADIATION BUDGET (ERB) EXPERIMENT . . . . .</b>	109
<b>6.1 Scientific Objective . . . . .</b>	109
<b>6.2 Description of the Experiment . . . . .</b>	109
<b>6.2.1 Solar Channels . . . . .</b>	109
<b>6.2.2 Fixed Wide-Angle FOV Channels . . . . .</b>	112
<b>6.2.3 Narrow-Angle FOV Scanning Channels . . . . .</b>	112
<b>6.3 Description of the Instrument . . . . .</b>	123
<b>6.3.1 Physical Layout . . . . .</b>	123
<b>6.3.2 Solar Channels . . . . .</b>	123
<b>6.3.3 Fixed Wide-Angle FOV Channels . . . . .</b>	126
<b>6.3.4 Thermopiles in Channels 1 through 14 . . . . .</b>	127
<b>6.3.5 Interference Filters in Channels 1 through 14 . . . . .</b>	128
<b>6.3.6 Narrow-Angle FOV Scanning Channels . . . . .</b>	128
<b>6.4 Prelaunch Calibration . . . . .</b>	130

## TABLE OF CONTENTS (Continued)

	<u>Page</u>
6.4.1 Solar Channels . . . . .	130
6.4.2 Fixed Wide-Angle Channels . . . . .	132
6.5 In-Flight Calibration . . . . .	133
6.6 Data Processing and Archiving . . . . .	134
<b>REFERENCES . . . . .</b>	<b>139</b>
 <b>SECTION 7. THE LIMB RADIANCE INVERSION RADIOMETER</b>	
<b>(LRIR) EXPERIMENT . . . . .</b>	<b>141</b>
7.1 Introduction . . . . .	141
7.2 Experiment Concept . . . . .	142
7.3 Instrumentation . . . . .	146
7.3.1 LRIR Location and Limb Viewing Geometry . . . . .	146
7.3.2 Instrument Configuration . . . . .	148
7.3.3 Channel Characteristics . . . . .	151
7.4 Calibration . . . . .	154
7.4.1 Preflight Calibration . . . . .	155
7.4.2 Scan Modes and In-Flight Calibration . . . . .	156
7.5 Data Processing, Archiving, and Availability . . . . .	159
<b>REFERENCES . . . . .</b>	<b>161</b>
 <b>SECTION 8. THE PRESSURE MODULATOR RADIOMETER</b>	
<b>(PMR) EXPERIMENT . . . . .</b>	<b>163</b>
8.1 Scientific Objectives . . . . .	163
8.2 Principles of Operation . . . . .	163
8.3 The Instrument . . . . .	166
8.4 Calibration . . . . .	170
8.5 Data Flow and Archiving . . . . .	171
<b>REFERENCES AND BIBLIOGRAPHY . . . . .</b>	<b>171</b>

TABLE OF CONTENTS (Continued)

	<u>Page</u>
<b>SECTION 9. THE TROPICAL WIND ENERGY CONVERSION AND REFERENCE LEVEL EXPERIMENT (TWERLE) . . . . .</b>	<b>173</b>
<b>9.1 Introduction . . . . .</b>	<b>173</b>
<b>9.2 Technical and Scientific Objectives . . . . .</b>	<b>174</b>
<b>9.3 TWERLE Balloon Platform Description . . . . .</b>	<b>174</b>
<b>9.4 Platform Transmissions . . . . .</b>	<b>177</b>
<b>9.5 Random Access Measurement System (RAMS) . . . . .</b>	<b>178</b>
<b>9.5.1 General . . . . .</b>	<b>178</b>
<b>9.5.2 Search and Locate Function . . . . .</b>	<b>179</b>
<b>9.5.3 Search Unit . . . . .</b>	<b>181</b>
<b>9.5.4 Acquisition and Data Recovery . . . . .</b>	<b>181</b>
<b>9.5.5 Formatting and Output Buffering . . . . .</b>	<b>182</b>
<b>9.6 Position and Velocity Determination of Balloon Platforms . . . . .</b>	<b>182</b>
<b>9.7 TWERLE Balloon Platform Data Format and Availability . . . . .</b>	<b>184</b>
<b>9.8 Other Experiments Using RAMS . . . . .</b>	<b>186</b>
<b>9.8.1 Platform Data Sent to Users in Punched Card Format . . . . .</b>	<b>190</b>
<b>9.8.2 Platform Data Sent to Users in Teletype Format . . . . .</b>	<b>191</b>
<b>9.8.3 Platform Data Sent to Users in Line Printer Format . . . . .</b>	<b>201</b>
<b>BIBLIOGRAPHY . . . . .</b>	<b>206</b>
<b>SECTION 10. THE TRACKING AND DATA RELAY EXPERIMENT (T&amp;DRE) . . . . .</b>	<b>207</b>
<b>10.1 Introduction . . . . .</b>	<b>207</b>
<b>10.2 Telemetry Data Relay . . . . .</b>	<b>207</b>
<b>10.3 Tracking and Orbit Determination . . . . .</b>	<b>208</b>
<b>10.3.1 Major System Components . . . . .</b>	<b>208</b>
<b>10.3.2 Overall Electronics . . . . .</b>	<b>210</b>
<b>10.3.3 Tracking Measurement Interpretation . . . . .</b>	<b>214</b>
<b>10.3.4 Orbit Determination . . . . .</b>	<b>216</b>
<b>10.4 Data Processing, Archiving, and Availability . . . . .</b>	<b>216</b>

TABLE OF CONTENTS (Continued)

	<u>Page</u>
BIBLIOGRAPHY . . . . .	218
SECTION 11. THE NIMBUS 6 DATA CATALOG . . . . .	219
APPENDIX A. ABBREVIATIONS AND ACRONYMS . . . . .	221
APPENDIX B. A DIRECT READOUT GROUND STATION FOR NIMBUS 6 ESMR DATA . . . . .	225

## LIST OF FIGURES

<u>Figure</u>		<u>Page</u>
1-1	Nimbus 6 Satellite . . . . .	2
1-2	Nimbus Attitude Axes . . . . .	4
1-3	Nimbus 6 Spacecraft Data Handling System . . . . .	5
2-1	The Temperature Humidity Infrared Radiometer . . . . .	12
2-2	THIR Optical Schematic . . . . .	13
2-3	Relative Spectral Response of the $6.7\mu\text{m}$ and $11.5\mu\text{m}$ Channels . . . . .	16
2-4	THIR Scan Angle Information . . . . .	17
2-5	Relationship between Nadir Angle and Ground Resolution for the THIR $11.5\mu\text{m}$ Channel at 1100 km . . . . .	19
2-6	Simplified Block Diagram of the THIR Subsystem . . . . .	21
2-7	Nimbus 6 THIR Film Labeling . . . . .	26
2-8	Simplified Block Diagram of the THIR A/D Processing System . . . . .	29
3-1	HIRS Filter Responses . . . . .	41
3-2	Weighting Functions for the HIRS Temperature and Water Vapor Channels . . . . .	42
3-3	Scan Grid Patterns for HIRS and SCAMS . . . . .	44
3-4	Schematic of the HIRS Optical System . . . . .	45
3-5	Photograph of the HIRS Instrument . . . . .	46
3-6	HIRS EIS Display Format . . . . .	52
4-1	SCAMS Antenna Reflector Positions . . . . .	62
4-2	SCAMS Weighting Functions . . . . .	64
4-3	SCAMS with Infrared Shield Removed to Show Blackbody Calibration Loads and Antenna Structure . . . . .	66
4-4	SCAMS Functional Block Diagram . . . . .	68
4-5	SCAMS System Block Diagram . . . . .	69
4-6	SCAMS Timing Diagram for a 16-second Cycle . . . . .	75
4-7	Antenna Pattern for Channel 1 at Position 8 . . . . .	76
4-8	Antenna Pattern for Channel 1 at Position 6 . . . . .	77
4-9	SCAMS EIS Display Format . . . . .	78
5-1	ESMR Antenna Scan Geometry . . . . .	89
5-2	Great Circle Distances of ESMR Beam Positions from the Subpoint and the Projection of the Half-power Contours for Four Beam Positions . . . . .	91
5-3	Typical ESMR Coverage of the Earth for a 24 Hour Period . . . . .	92
5-4	Simplified Block Diagram of the ESMR Instrument . . . . .	93
5-5	ESMR EIS Display Format . . . . .	103
6-1	Spectral Intervals Monitored by the ERB Solar Channels . . . . .	113

## LIST OF FIGURES (Continued)

<u>Figure</u>		<u>Page</u>
6-2	ERB Scan Grid Earth Patterns . . . . .	115
6-3	ERB Scan Modes . . . . .	116
6-4	ERB Scanning Channel Views of a Geographical Area Near the Subpoint Track . . . . .	117
6-5	ERB Scanning Channel Views of a Geographical Area Away From the Subpoint Track . . . . .	118
6-6	ERB Radiometer Unit . . . . .	124
6-7	Spectral Response Functions of ERB Optical Channels . . . . .	125
6-8	Transmittance of ERB Suprasil W and Schott Colored Glasses . . . . .	126
6-9	ERB Processing System . . . . .	135
7-1	LRIR Limb Viewing Geometry . . . . .	142
7-2	Computed Limb Radiances as a Function of Tangent Height for Broad ( $585\text{-}705 \text{ cm}^{-1}$ ) and Narrow ( $630\text{-}685 \text{ cm}^{-1}$ ) Channels in the $15 \mu\text{m}$ band of CO . . . . .	145
7-3	Location of the LRIR Instrumentation on the Nimbus 6 Sensory Ring and Associated Limb Viewing Geometry . . . . .	147
7-4	LRIR Scan Track for the Northern Hemisphere . . . . .	149
7-5	LRIR Scan Track for the Southern Hemisphere . . . . .	150
7-6	LRIR Instrument Configuration . . . . .	151
7-7	LRIR Field of View Dimensions . . . . .	152
7-8	LRIR System Block Diagram . . . . .	153
7-9	LRIR Instrumentation During Primary Calibration . . . . .	156
7-10	LRIR Scanning Modes During Limb Acquisition, Limb Scanning, and In-flight Calibration Sequences . . . . .	157
7-11	LRIR Data Reduction Flow . . . . .	160
8-1	Pressure Modulator Cell Showing Method of Modulation . . . . .	164
8-2	Weighting Functions for Different PMR Mean Cell Pressures . . . . .	165
8-3	Weighting Function for the PMR Illustrating the Effect of Doppler Scanning . . . . .	166
8-4	Electronics Block Diagram for One Channel of the PMR . . . . .	167
8-5	Signal versus Radiance for One of the Channels of the Engineering Model PMR . . . . .	170
9-1	Flight Train of TWERLE Balloon System . . . . .	175
9-2	Platform Transmission Format . . . . .	177
9-3	RAMS Block Diagram . . . . .	179
9-4	Conceptual Diagram of the RAMS Time Compressor . . . . .	180
9-5	Line Printer Format of TWERLE Platform Data . . . . .	202

**LIST OF FIGURES (Continued)**

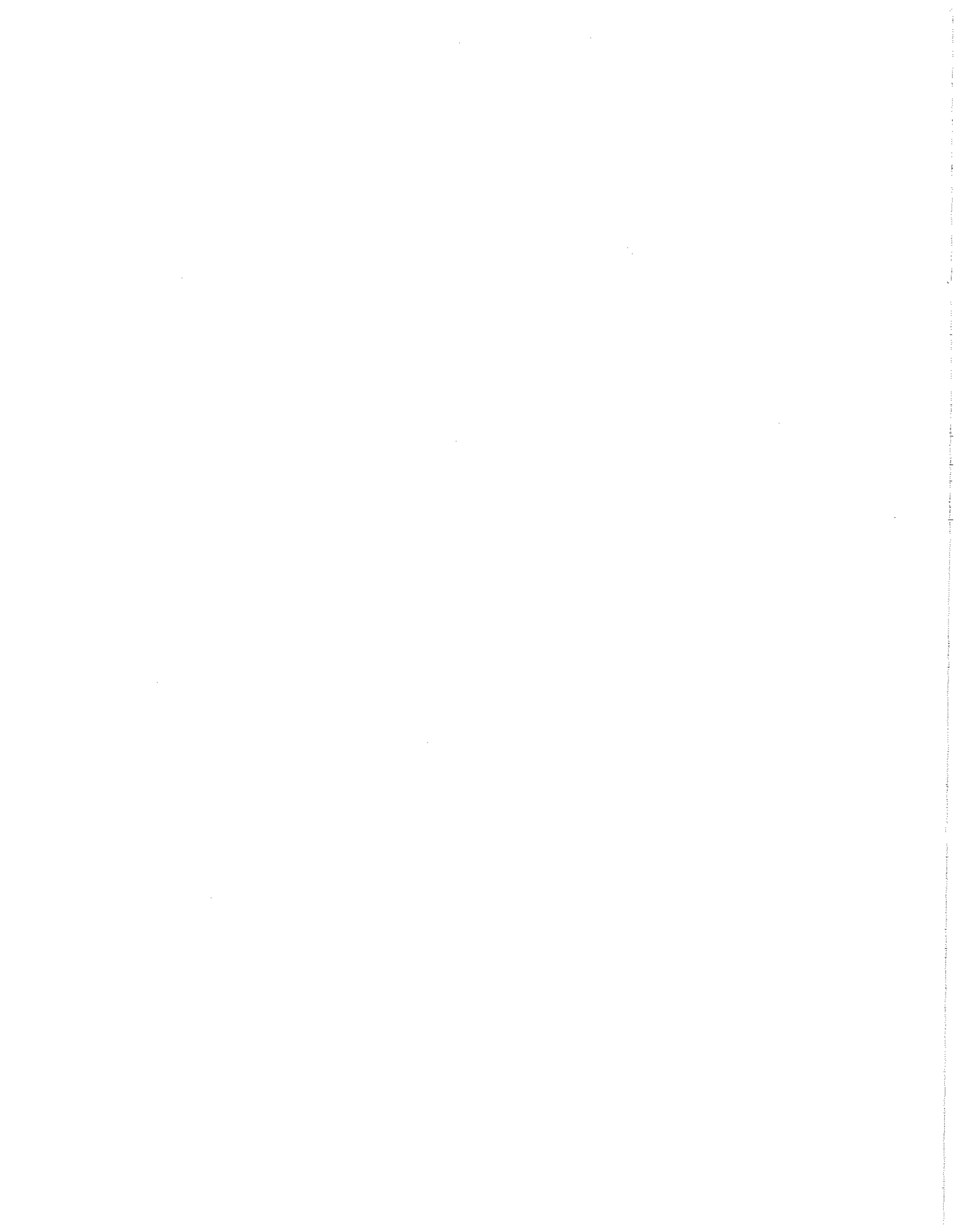
<u>Figure</u>		<u>Page</u>
10-1	T&DRE Geometry . . . . .	209
10-2	Tracking Signal Power Levels and Pointing . . . . .	210
10-3	Orbit Determination Processing System Using T&DRE Data . .	211
10-4	Ground Station Signal Generation to ATS 6 . . . . .	212
10-5	Signal Translations by the ATS 6 Transponder . . . . .	213
10-6	Signal Translations by the Nimbus 6 Transponder . . . . .	214
10-7	Nimbus 6 and ATS 6 Orbit Solution . . . . .	217

## LIST OF TABLES

Table	Page
2-1 Relative Spectral Response of the $6.7\mu\text{m}$ and $11.5\mu\text{m}$ Channels . . . . .	15
2-2 Effective Radiance ( $N$ ) versus Equivalent Blackbody Temperatures ( $T_B$ ) . . . . .	22
2-3 THIR output Voltages versus Equivalent Blackbody Temperatures at Different Bolometer Temperatures for the $11.5\mu\text{m}$ Channel . . . . .	23
2-4 THIR Output Voltages versus Equivalent Blackbody Temperatures at Different Bolometer Temperatures for the $6.7\mu\text{m}$ Channel . . . . .	24
2-5 NMRT-THIR Documentation Record Format . . . . .	32
2-6 NMRT-THIR Data Record Format . . . . .	33
2-7 Definition of Flags Describing Each THIR Swath . . . . .	35
3-1 Functions of the HIRS Channels . . . . .	38
3-2 Summary of HIRS Optical Parameters . . . . .	39
3-3 Coefficients used to Derive Instrument Temperatures and Radiances from Telemetered Count Levels . . . . .	48
3-4 Algorithms for Subsidiary HIRS System Parameter . . . . .	49
3-5 HIRS Gray Scale Number versus Brightness Temperature for each HIRS Channel Displayed on an EIS Image . . . . .	54
3-6 HIRS Calibrated, Located Radiance Tape Format . . . . .	57
4-1 SCAMS Flight Model Performance Characteristics . . . . .	60
4-2 SCAMS Data Format in the VIP Digital A Matrix . . . . .	72
4-3 SCAMS Digital B Status Indicators . . . . .	73
4-4 SCAMS Analog Data Output and Sampling Rates . . . . .	74
4-5 Gray Scale Number versus SCAMS Antenna Temperature for Image Swaths labeled 1, 2, 6, and 7 on the SCAMS EIS Displays . . . . .	79
4-6 Gray Scale Number versus Water Vapor and Liquid Water Values for Image Swaths Labeled 11 and 12 on the SCAMS EIS Displays . . . . .	80
4-7 Temperature Values for the Three SCAMS Oxygen Channels Shown on the SCAMS EIS Displays . . . . .	82
4-8 SCAMS Archival Tape: Tentative Contents for each Major Frame . . . . .	84
5-1 Resolution and Beam Incidence Angles at Various Spacecraft Pitch Angles . . . . .	89
5-2 Digital B Flags Indicating Gain Setting of each Channel and Instrument Status . . . . .	94

## LIST OF TABLES (Continued)

<u>Table</u>		<u>Page</u>
5-3	Sequence of ESMR Information from the Digital A Data . . . . .	95
5-4	Antenna Calibration Parameters . . . . .	98
5-5	Gray Scale Number versus ESMR Brightness Temperature for each Image Swath on the ESMR EIS Displays . . . . .	105
5-6	Format of an ESMR Calibrated Brightness Temperature Tape Logical Record . . . . .	106
6-1	Optical Characteristics of ERB Solar Channels . . . . .	110
6-2	Optical Characteristics of ERB Fixed Wide-Angle FOV Channels . . . . .	111
6-3	Optical Characteristics of ERB Scanning Channels . . . . .	111
6-4	ERB Scanning Channel Target Areas . . . . .	119
6-5	Filter Factors, Sensitivities, Electronic Gains, and Estimated Maximum Irradiances for ERB Channels 1-14 . . . . .	129
6-6	ERB Scan Head Positions During Scan . . . . .	131
6-7	ERB Compacted Archival Tape Format . . . . .	136
7-1	LRIR Science Data Requirements . . . . .	143
7-2	Optical Characteristics of LRIR Channels . . . . .	154
7-3	Volume and Characteristics of LRIR Archival Data . . . . .	161
8-1	Cell CO <sub>2</sub> Pressure Corresponding to Various Temperature Settings on the Sieves . . . . .	168
8-2	Noise Equivalent Temperature for Different Cell Mean Pressures . . . . .	169
9-1	TWERLE-B Format of Balloon Data Processed at NCAR . . . . .	185
9-2	Nimbus RAMS Experiments . . . . .	186
9-3	Format of Card Type 3 for Users Receiving Platform Data in Card Form . . . . .	192
9-4	Format of Card Type 4 for Users Receiving Platform Data in Card Form . . . . .	193
9-5	Format of Card Type 5 for Users Receiving Platform Data in Card Form . . . . .	195
9-6	Teletype Format for Users Receiving Platform Data by Teletype . . . . .	198
10-1	Doppler Cycle Count . . . . .	215



## SECTION 1

### THE NIMBUS 6 SPACECRAFT SYSTEM

by  
Staff Members, LANDSAT/Nimbus Project  
National Aeronautics and Space Administration  
Goddard Space Flight Center

The purpose of this section is to present scientific objectives of the Nimbus 6 experiment, outline the component subsystems of the spacecraft, and present information on data availability.

#### 1. 1 Introduction

The Nimbus 6 spacecraft will be launched from the Western Test Range at Vandenberg Air Force Base, California, aboard a thrust-augmented Delta vehicle. The satellite will be placed in an 1100 kilometer, sun-synchronous polar orbit, having local noon (ascending) and midnight (descending) equator crossings, and an 81 degree retrograde inclination. Successive orbits will cross the equator with 26.8 degrees of longitude separation. The orbital period will be about 107.25 minutes.

In orbit, with its solar panels unfolded, the Nimbus will appear as shown in Figure 1-1. Eight of the nine experiments are mounted on the torus structure at the base of the satellite. The ninth, the antenna and gimbal system of the Tracking and Data Relay Experiment (T&DRE), is mounted on top of the attitude control system.

#### 1. 2 Nimbus 6 Scientific Objectives

The Nimbus 6 mission affords an opportunity to sound the atmosphere with advanced techniques, extending and refining the sounding and atmospheric structure measurement capabilities demonstrated by experiments on Nimbus 3, 4, and 5. The mission will provide an opportunity to assess each instrument's operation in the space environment and to collect a sizable body of data with the global and seasonal coverage needed for support of meteorological experiments. The scientific objectives of the Nimbus 6 are to:

- Achieve a major milestone in the Global Atmospheric Research Program (GARP) to include:

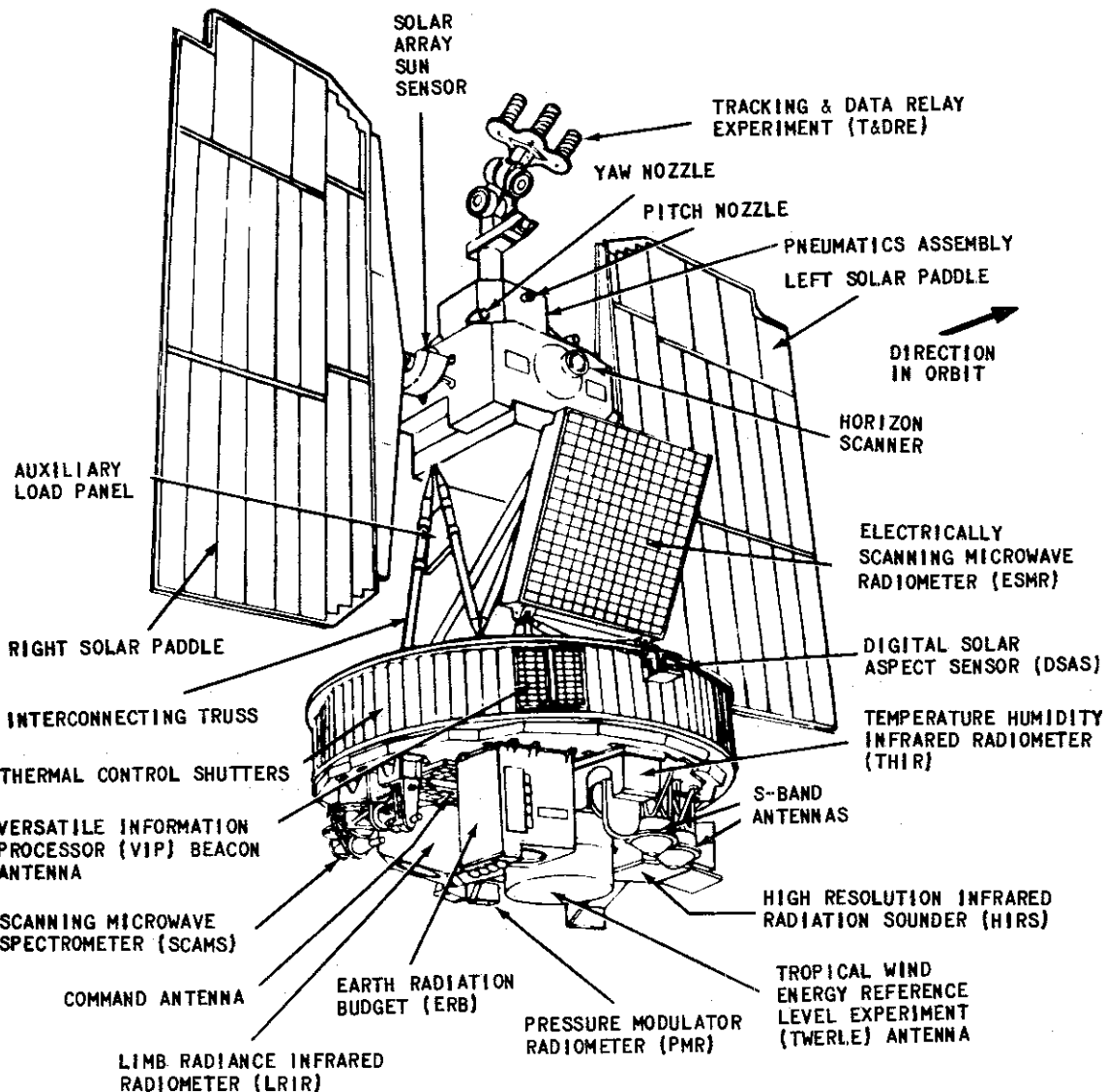


Figure 1-1. Nimbus 6 Satellite

- (a) Refining and further demonstrating techniques to measure global atmospheric mass and wind fields (HIRS, SCAMS, TWERLE)
- (b) Testing the conversion of observations to meteorological analyses for use in numerical models of atmospheric circulation
- Develop and demonstrate techniques for environmental monitoring from space to include:

- (a) Monitoring the temperature and distribution of gasses in the stratosphere (LRIR, PMR)
- (b) Monitoring the planetary radiative energy budget (ERB)
- (c) Monitoring ice cover, sea state, and soil moisture (ESMR)
- Extend vertical sounding capability to the upper stratosphere and develop new sounding techniques (SCAMS, LRIR, PMR, HIRS)
- Measure large-scale atmospheric motions and the conversion of potential energy to kinetic energy, and provide a 150-mb reference level in the Southern Hemisphere (TWERLE)
- Measure sea ice, snow cover ice, surface roughness, moisture, and liquid water content of clouds using microwave imaging (ESMR)
- Develop new technology in the field of low-orbiting satellite communications and tracking utilizing a geostationary satellite (T&DRE)
- Measure the synoptic and planetary earth radiation budget (ERB)

### 1.3 Spacecraft Attitude

The major requirement of the Attitude Control System (ACS) is to stabilize the spacecraft with respect to the earth and orbital plane. The nominal attitude control aligns the yaw axis with the local earth vertical, the roll axis with the spacecraft velocity vector, the pitch axis at right angles to the other two axes, and orients the solar paddles normal to the sun (see Figure 1-2). With Nimbus 6, in order to reduce control system pneumatics consumption, it is planned that the spacecraft will be biased in pitch at +0.6 degrees ('nose up'). The alignment of the pitch and roll axes will be maintained within 0.5 degrees and yaw will be within 1 degree.

### 1.4 Spacecraft Data Systems

Figure 1-3 is a simplified block diagram of the spacecraft data handling system which shows the routing of the sensor data to the Versatile Information Processor (VIP) or to the High Data Rate Storage System (HDRSS). Real-time data links are provided by the beacon and the T&DRE communication channels (via ATS 6), while the HDRSS stored data will be played back to the ground using the S-band channel. TWERLE and T&DRE have their own uplinks from the ground.

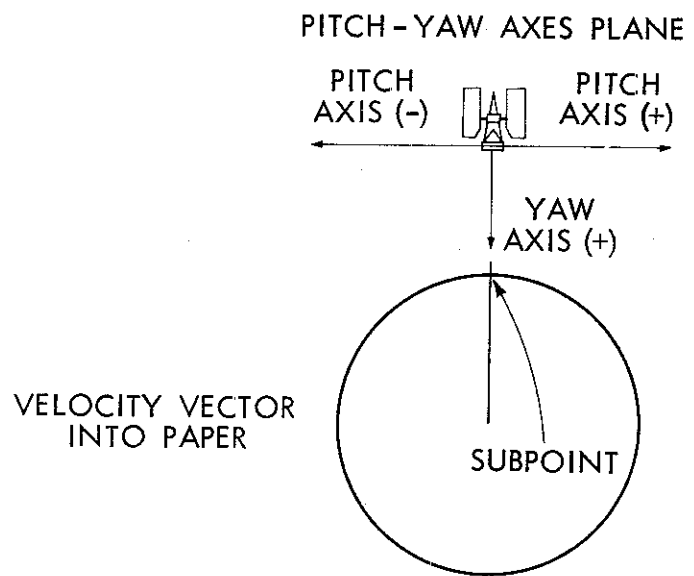
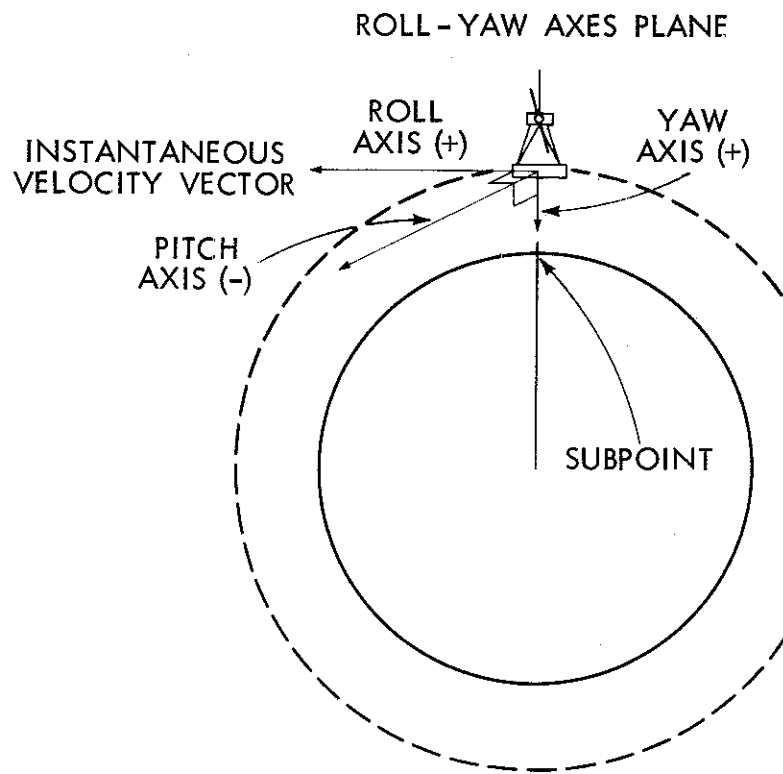


Figure 1-2. Nimbus Attitude Axes

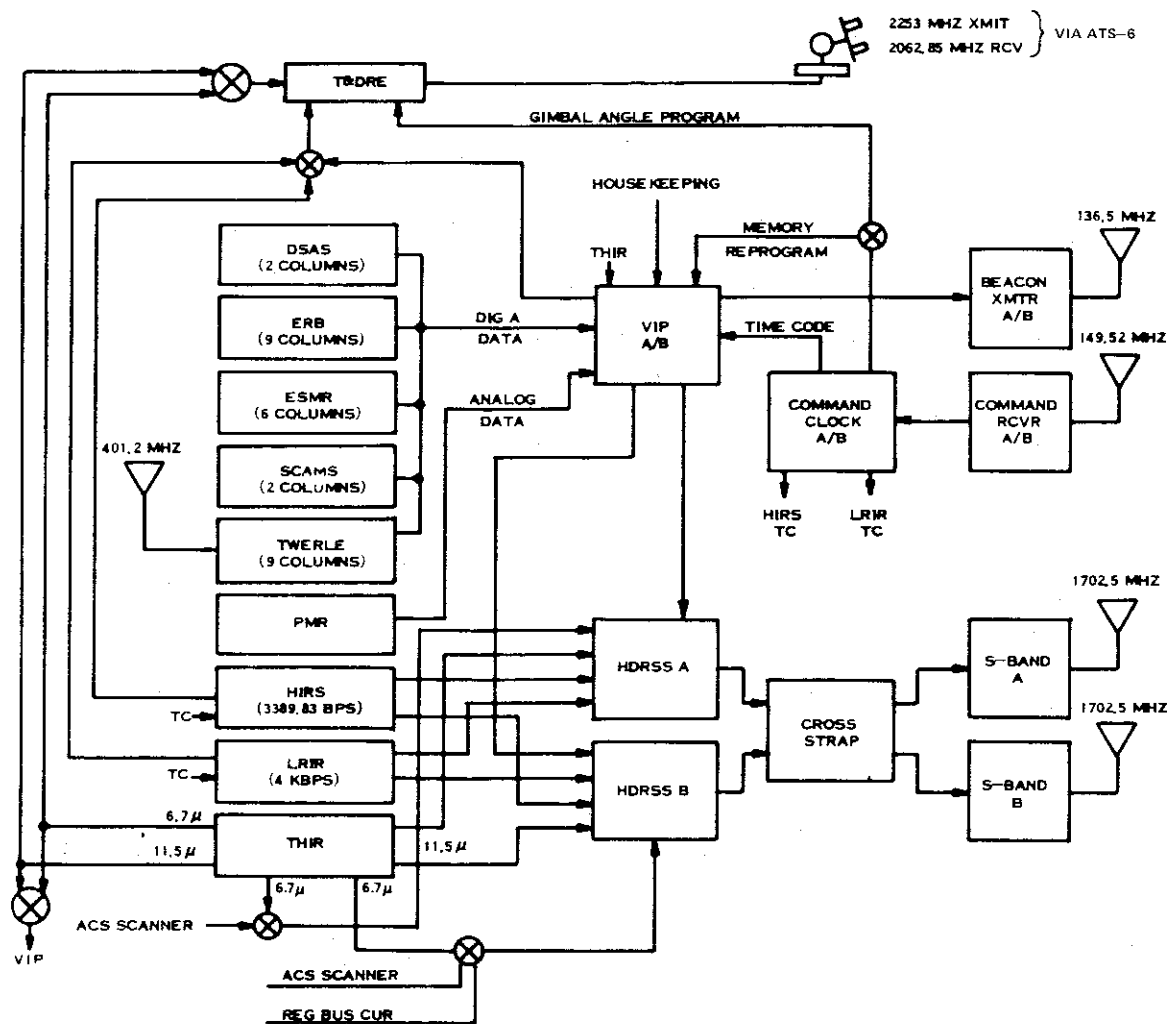


Figure 1-3. Nimbus 6 Spacecraft Data Handling System

#### 1.4.1 High Data Rate Storage System (HDRSS)

The HDRSS consists of a five-channel tape recorder and the associated recording and playback electronics needed for collecting and storing the data from the THIR, HIRS, LRIR, and VIP. Included with this subsystem are the two redundant S-band transmitters and multiplexers used to send the data to the ground. For purposes of redundancy and extending useful data capacity, there are two parallel and independent HDRSS on Nimbus 6. Each HDRSS can record 123 minutes of data. The two HDRSS may be so commanded that one unit is off until the other is filled, allowing 246 minutes of data to be recorded. In addition, while one unit is playing back the other can be recording, thus preventing data loss during playback. Each HDRSS operates into a 5-watt solid-state transmitter.

Data from either HDRSS can be sent to either transmitter for transmission to the ground.

#### 1.4.2 Versatile Information Processor (VIP)

The VIP samples approximately 1,000 outputs from spacecraft systems, processes the data, and inserts it into an output bit stream to be stored on a HDRSS for later transmission to the ground. The sensor data are digitized where necessary, time multiplexed, and formatted into a 4,000 bit per second serial bit stream. The serial bit stream is recorded in biphase on the HDRSS tape recorder and simultaneously may be transmitted over the 136.5 MHz beacon transmission link and the 2253 MHz T&DRE link.

Data processed in the VIP mode include spacecraft subsystem and experiment housekeeping telemetry such as the temperature of components, calibration signals, and voltages, plus the output of five experiments: ERB, ESMR, SCAMS, TWERLE, and PMR.

#### 1.4.3 Real Time Data Transmission

The spacecraft beacon can be used to relay real-time VIP data (ERB, ESMR, SCAMS, TWERLE, and PMR) over areas within range of a Spaceflight Tracking and Data Network (STDN) ground station. The T&DRE system can be used to relay HIRS, LRIR, THIR, or VIP to the ground via ATS 6. Using ATS 6 as a relay station increases the range of coverage of real-time data since the Nimbus views ATS over a greater area of the earth than when Nimbus is within direct range of a ground station.

### 1.5 Ground Station Complex

Real-time data and data from the HDRSS are routinely received at the two STDN stations located near Fairbanks, Alaska, and Rosman, North Carolina. The HDRSS data acquired at Alaska are recorded on pass and then transmitted over a microwave link at reduced rates to the Meteorological Data Handling System (MDHS) at GSFC. HDRSS data acquired at Rosman are relayed directly to GSFC over a wide-band data link.

The Nimbus is within acquisition range of the Alaska STDN during nine or ten orbits each day (of the 13 or 14 orbits per day). The Rosman STDN is within range for the two or three orbits per day missed by Alaska. In addition, the STDN station at Orroral, Australia will have the capability to receive Nimbus 6 S-band data, and will be utilized for processing VIP and HIRS data to eliminate the gap in global coverage that exists with only Rosman and Alaska data collection.

All Nimbus data are initially processed in the MDHS at GSFC. The MDHS generates a photographic image of all ESMR, HIRS, SCAMS, and THIR. Limited quantities of these images are processed and distributed through the Nimbus/ATS Data Utilization Center (NADUC) to NASA-approved users. MDHS-produced digitized magnetic tapes of ERB, ESMR, HIRS, LRIR, SCAMS, and THIR experiment data are distributed by NADUC to the respective experimenters for further data reduction. The MDHS transmits some digital data directly to experimenters. HIRS, PMR, SCAMS, and stripped THIR are transmitted to the Goddard Institute for Space Studies (GISS) in New York City. GISS uses the data for numerical forecast modeling and GARP support. PMR is formatted and transmitted by data link to the PMR experimenter's at Oxford University, Oxford, England. Some TWERLE balloon data are transmitted to the National Center for Atmospheric Research (NCAR). The NADUC mails other TWERLE data, in printout and IBM card form, to various TWERLE experimenters. Some TWERLE data are also transmitted from GSFC via teletype. On request, NADUC delivers T&DRE taped data to the T&DRE experimenter.

#### 1.6 Nimbus/ATS Data Utilization Center (NADUC)

The NADUC performs the following functions for Nimbus 6 data:

- Accounts for and distributes experiment data processed by the MDHS
- Processes all photographic data through to archival products
- Reproduces and distributes photographic data to NASA-approved users
- Generates periodic data catalogs in a format as outlined in Section 11. The Catalogs provide information about all experiment data collected and their availability.
- Provides special technical services to the experimenters and data users
- Maintains a complete photographic data reference file

#### 1.7 Archival and Dissemination of Nimbus 6 Data

Each experimenter is responsible for setting up a procedure to process the data from his experiment and produce archival products. As data are archived they are delivered to the NSSDC where they are used as the source for generating

Nimbus 6 user products. Each Nimbus 6 Data Catalog will announce the quantity of data from each experiment archived and available at the NSSDC. This data availability list will be updated to the time of each catalog's publication date.

The nature and format of the data to be available from each experiment are explained in detail in the respective sections of this guide. The data will be archived and available as described below:

- Photographic data from ESMR, HIRS, SCAMS, and THIR will be archived and available through the National Space Science Data Center (NSSDC), Code 601, Goddard Space Flight Center, Greenbelt, Maryland 20771.
- Digital data tapes from ERB, ESMR, HIRS, LRIR, PMR, SCAMS, and THIR will be archived and available through NSSDC.
- Archival tapes of ERB and HIRS data also will be available through the National Oceanic and Atmospheric Administration (NOAA), National Environmental Satellite Service (NESS), World Weather Building, 5200 Auth Road, Marlow Heights, Maryland 20023, Attention Dr. W. L. Smith.
- Archived LRIR tapes also will be available through the National Center for Atmospheric Research, P. O. Box 3000, Boulder, Colorado 80303, Attention Dr. John C. Gille.
- TWERLE balloon data will be available through the above NCAR address, Attention Dr. Paul R. Julian. Users who desire other TWERLE information or data should write directly to the appropriate experimenter listed in Table 9-2 of this guide.
- Since T&DRE is not a data gathering experiment but an experiment of a new method of relaying data, nothing is archived at the NSSDC. The divisions at GSFC processing and evaluating the data also store these data. Users who desire more information or data from the T&DRE should write to: Mr. Bernard J. Trudell, Tracking and Data Relay Experiment Manager, Code 953, Goddard Space Flight Center, Greenbelt, Maryland 20771.

The NSSDC will furnish limited quantities of data to qualified investigators without charge. The NSSDC may establish a charge for production and dissemination if a large volume of data is requested. Whenever a charge is required, a cost estimate will be provided to the user prior to filling his data request.

All requests from foreign researchers for Nimbus 6 data archived and available through NSSDC must be specifically addressed to:

Director, World Data Center A for Rockets and Satellites  
Code 601, Goddard Space Flight Center  
Greenbelt, Maryland 20771, U. S. A.

When ordering data from either the NSSDC or the World Data Center, a user should specify why the data are needed, the subject of his work, the name of the organization with which he is connected, and any government contracts he may have for performing his study. Of course, each request should specify the experiment data desired, the day and area of interest, plus any other information that would facilitate the handling of the data request.

A user requesting data on magnetic tapes should provide additional information concerning his plans for using the data, e.g., what computers and operating systems will be used. In this context, the NSSDC is compiling a library of routines which can unpack or transform the contents of many of the data sets into formats which are appropriate for the user's computer. NSSDC will provide, upon request, information concerning its services.

When requesting data on magnetic tape, the user must specify whether he will supply new tapes prior to the processing, or return the original NSSDC tapes after the data have been copied.

#### 1.8 On-Off Operating Mode for Each Experiment

If all Nimbus 6 experiments are operating continuously, their combined power requirements are more than is produced by the solar array panels. Thus, on-off operating modes have been established for each experiment to meet the power limitations of the spacecraft. After launch, the following on-off modes may change as data requirements and/or the operational capability of one or more experiments change.

Initially, the T&DRE will be operated to evaluate the experiment. Thereafter, it is planned to operate the experiment only occasionally. The TWERLE will operate about 50 percent of the time, during the earth-daylight portion of each orbit. The ERB and ESMR will alternate in an on-off mode of on for approximately 24 hours and off for 24 hours. HIRS, SCAMS, and LRIR also may have some scheduled off times, but not as frequent as for ERB, ESMR, TWERLE, and T&DRE. Normally, the PMR and THIR will be on continuously.

Each Nimbus 6 Data Catalog will describe the general on-off pattern for each experiment. The Sensors On-Off Table (see Section 11) will give the specific on-off times for each experiment.

## SECTION 2

### THE TEMPERATURE HUMIDITY INFRARED RADIOMETER (THIR) SUBSYSTEM

by

Andrew W. McCulloch

National Aeronautics and Space Administration  
Goddard Space Flight Center

#### 2.1 Introduction

The Nimbus 6 THIR is of the same design and operation as the THIR flown on Nimbus 4 and 5. The two-channel scanning radiometer is designed to measure earth radiation from two spectral bands. A  $10.3 \mu\text{m}$  to  $12.5 \mu\text{m}$  ( $11.5 \mu\text{m}$ ) window channel provides an image of the cloud cover, and temperatures of the cloud tops, land, and ocean surfaces. A  $6.5 \mu\text{m}$  to  $7.1 \mu\text{m}$  ( $6.7 \mu\text{m}$ ) channel provides information on the moisture content of the upper troposphere and stratosphere, and the location of jet streams and frontal systems. The ground resolution at the subpoint is 8.2 km for the  $11.5 \mu\text{m}$  channel and 22.5 km for the  $6.7 \mu\text{m}$  channel. Both will operate continuously to provide day and night global coverage.

#### 2.2 THIR Operation

##### 2.2.1 Radiometer

The THIR consists of an optical scanner (shown in Figure 2-1) and an electronics module (not shown). The optical scanner provides the necessary scan motion to produce cross-course scanning. It contains the radiometer optics, detectors, preamplifiers, detector bias supply, scan drive, and scan synchronization pulse generator (pip) amplifiers. The electronics module provides the necessary amplification and data processing of the detected radiometric signal to achieve the proper levels and formatting compatible with the spacecraft's HDRSS. The electronics module also contains the necessary switching to respond to the spacecraft commands to the THIR, and the appropriate housekeeping telemetry circuits.

The scanner design uses an elliptically shaped plane scan mirror and primary optics, which are common to both channels (Figure 2-2). The scan mirror, set at an angle of 45 degrees to the scan axis, rotates at 48 rpm and scans in a plane perpendicular to the direction of the satellite motion. The scan mirror

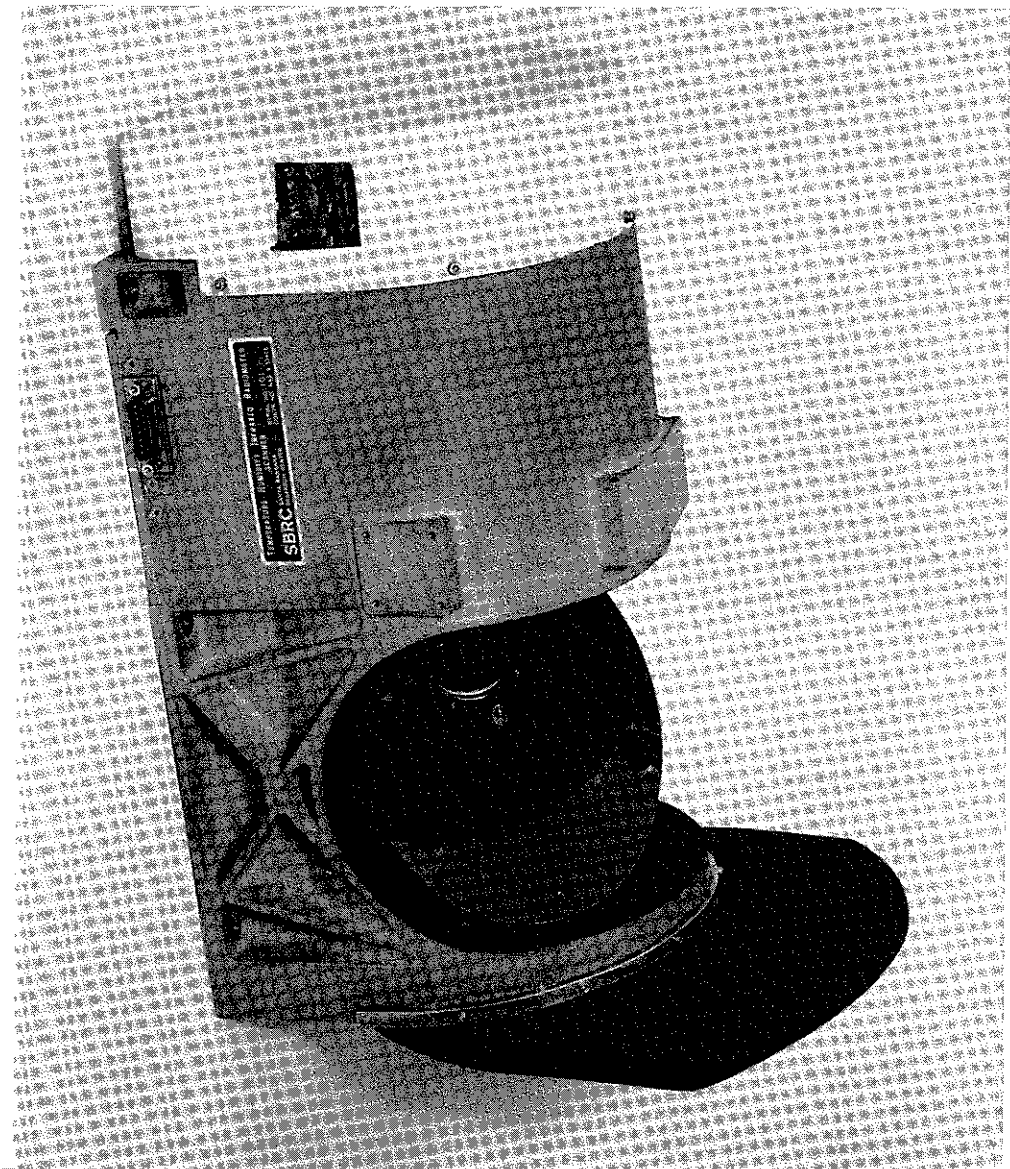


Figure 2-1. The Temperature Humidity Infrared Radiometer

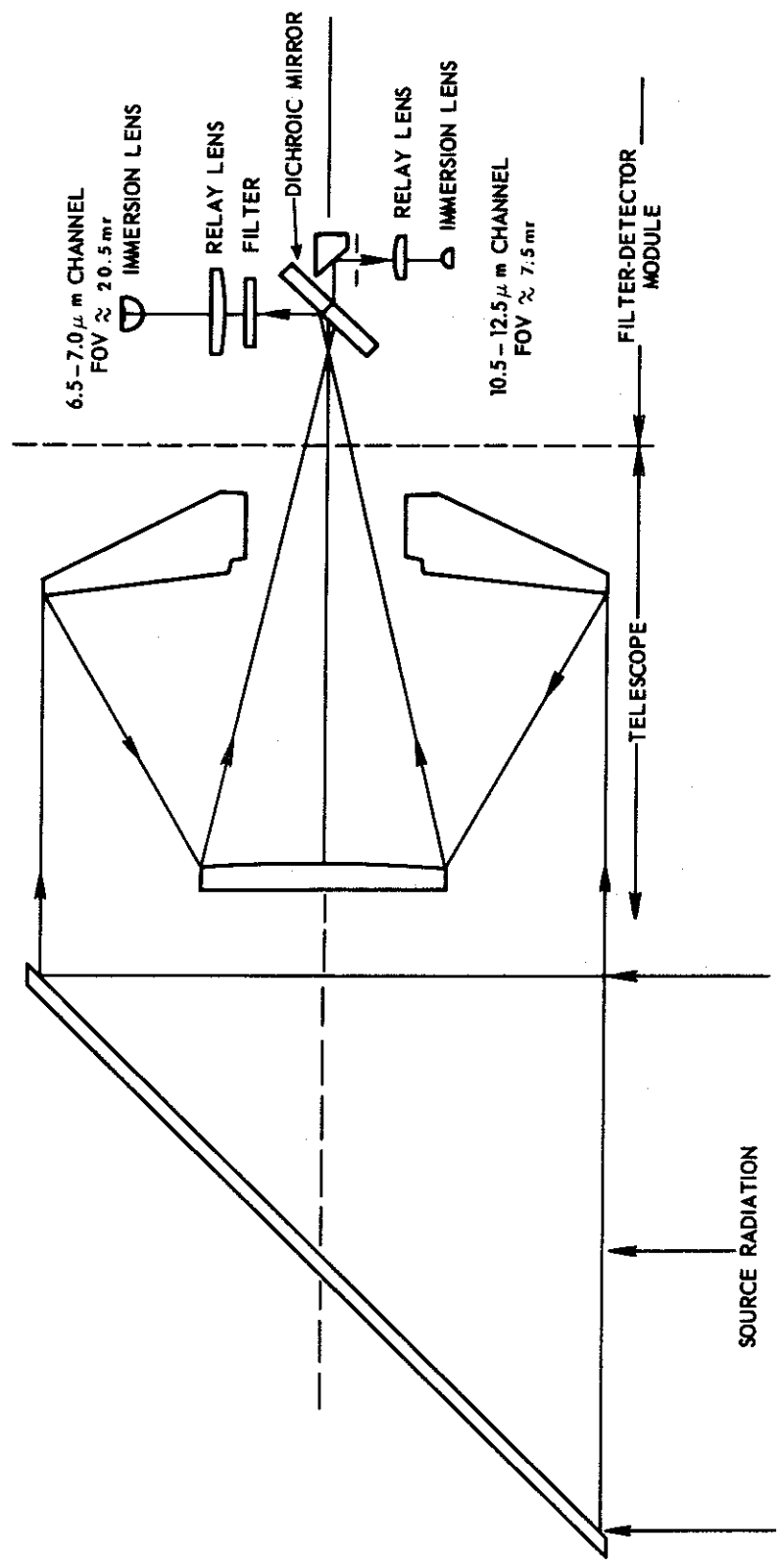


Figure 2-2. THIR Optical Schematic

rotation is such that, when combined with the velocity vector of the satellite, a right-hand spiral results. Therefore, the field of view scans across the earth from east to west in the daytime when traveling northward, and from west to east at night when traveling southward.

The radiation collected by the primary optics is separated into the two infrared bands by a dichroic filter which spectrally divides the energy into two channels. The  $6.7 \mu\text{m}$  data is reflected off the dichroic mirror, through field stops and relay lens, onto the immersed detector-bolometer flake. The  $11.5 \mu\text{m}$  data pass through the dichroic (transmission portion of the dichroic), an Itran-2 relay lens (which also serves as a long-wavelength blocking filter), a folding mirror, and are focused onto a germanium-immersed detector-bolometer flake. The field stops at the image plane of each channel define the field of view;  $20.5 \text{ mr}$  ( $1.17$  degrees) for the  $6.7 \mu\text{m}$  channel and  $7.5 \text{ mr}$  ( $0.43$  degrees) for the  $11.5 \mu\text{m}$  channel. The signals from the detectors are capacitor coupled to the preamplifiers, amplified, and forwarded to the electronics module.

In the electronic module, the signals are further amplified and corrected for detector time constant to provide overall frequency response as required by the subsystem optical resolution. Even though the first stages of amplification are capacitor coupled, the low frequency cutoff ( $0.5 \text{ Hz}$ ) of the data bandwidth is so low that a dc restore circuit is necessary to provide a zero signal reference. This occurs during the portion of the scan when the optics are receiving zero radiation (space). The dc restore circuitry also provides additional gain to raise the signal to the desired output level, and filtering to establish proper frequency characteristics. The signals are processed out of the electronics module through buffer amplifiers.

The tabulated values of the relative spectral response for each channel are shown in Table 2-1, while Figure 2-3 illustrates these data graphically.

### 2.2.2 Scan Sequence

The radiometer scan mirror continuously rotates the field of view of the detector through  $360$  degrees in a plane normal to the spacecraft velocity vector. In sequence, the detector views the in-flight blackbody calibration target (which is part of the radiometer housing), outer space, earth, outer space, and returns again to view the radiometer housing. Figure 2-4 illustrates the radiometer timing sequence relative to the angular position of the scan mirror for each scan cycle. The radiometer Z-axis is oriented  $5$  degrees from the spacecraft zenith. This is done to ensure that the radiometer dc restoration (prior to earth scan) and space check-of-calibration (after earth scan) events will occur when the radiometer is viewing space. This way the correct radiometric data output

Table 2-1  
Relative Spectral Response for the 6.7  $\mu\text{m}$  and 11.5  $\mu\text{m}$  Channels

6.7 $\mu\text{m}$ Channel		11.5 $\mu\text{m}$ Channel			
Wavelength ( $\mu\text{m}$ )	Relative Response	Wavelength ( $\mu\text{m}$ )	Relative Response	Wavelength ( $\mu\text{m}$ )	Relative Response
6.20	0.0000	9.9	0.0000	12.4	0.6863
6.25	0.0018	10.0	0.0237	12.5	0.5658
6.30	0.0036	10.1	0.0825	12.6	0.4474
6.35	0.0245	10.2	0.2215	12.7	0.2754
6.40	0.0455	10.3	0.4486	12.8	0.1111
6.45	0.2245	10.4	0.6062	12.9	0.0413
6.50	0.4036	10.5	0.7242	13.0	0.0097
6.55	0.6713	10.6	0.8540	13.1	0.0000
6.60	0.9390	10.7	0.9236		
6.70	0.9334	10.8	0.9330		
6.75	0.9667	10.9	0.9337		
6.80	1.0000	11.0	0.9402		
6.85	0.9654	11.1	0.9871		
6.90	0.9308	11.2	0.9979		
6.95	0.9541	11.3	1.0000		
7.00	0.9774	11.4	0.9739		
7.05	0.9119	11.5	0.9612		
7.10	0.8463	11.6	0.9451		
7.15	0.5465	11.7	0.9507		
7.20	0.2468	11.8	0.9311		
7.25	0.1347	11.9	0.9309		
7.30	0.0227	12.0	0.8986		
7.35	0.0114	12.1	0.9042		
7.40	0.0000	12.2	0.8437		
		12.3	0.7780		

voltage reference level and the space check-of-calibration of the radiometer will be achieved without ambiguity.

At a scan mirror angle of 5 degrees (referenced to the spacecraft zenith) the radiometer FOV is just starting to leave the scanner housing. At 48 degrees from spacecraft zenith scan mirror position pip No. 1 is generated and the radiometer sync word and calibration sequence is started. At 100 degrees (during the calibration sequence) the radiometer FOV starts to see space fully.

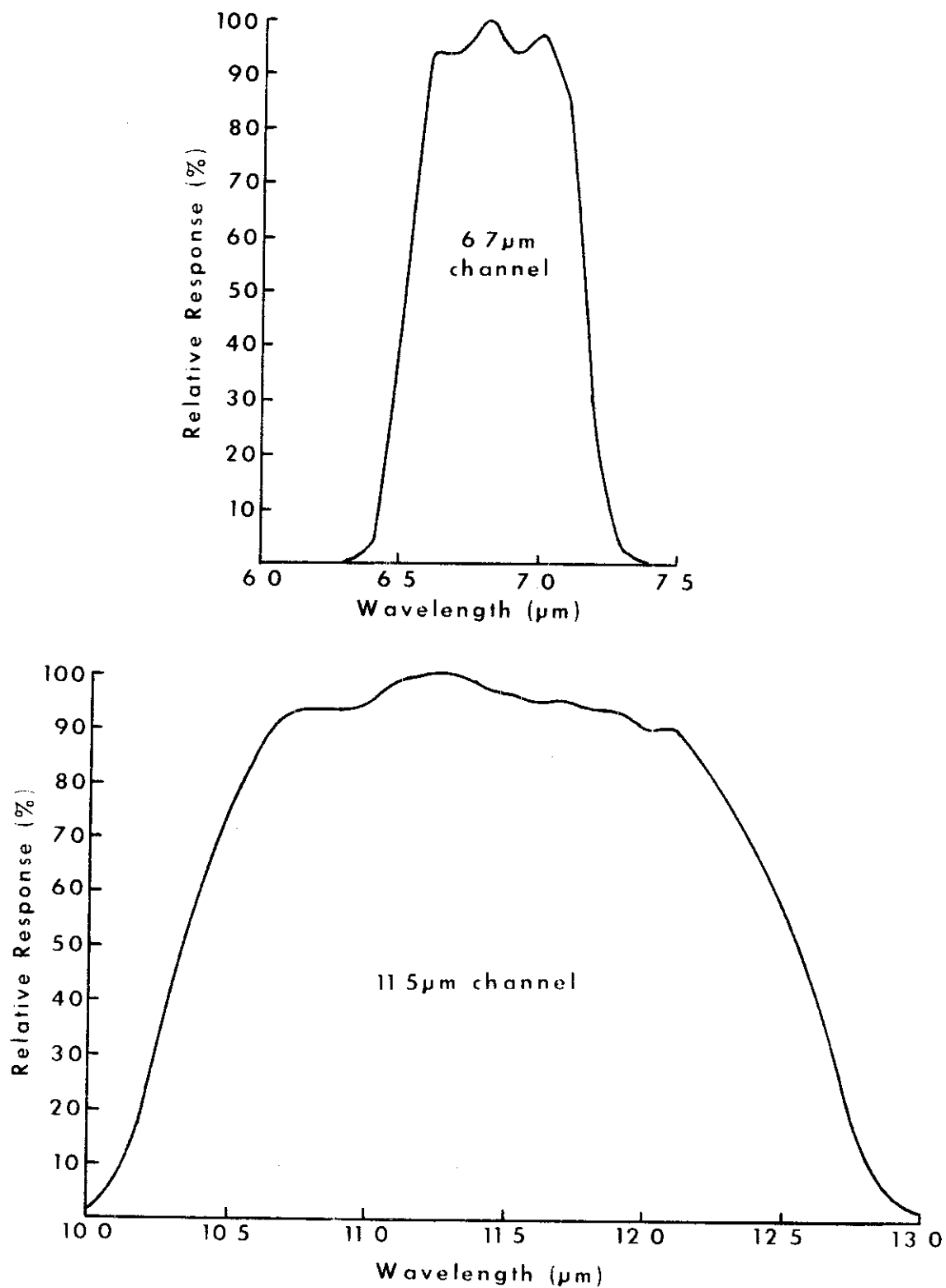
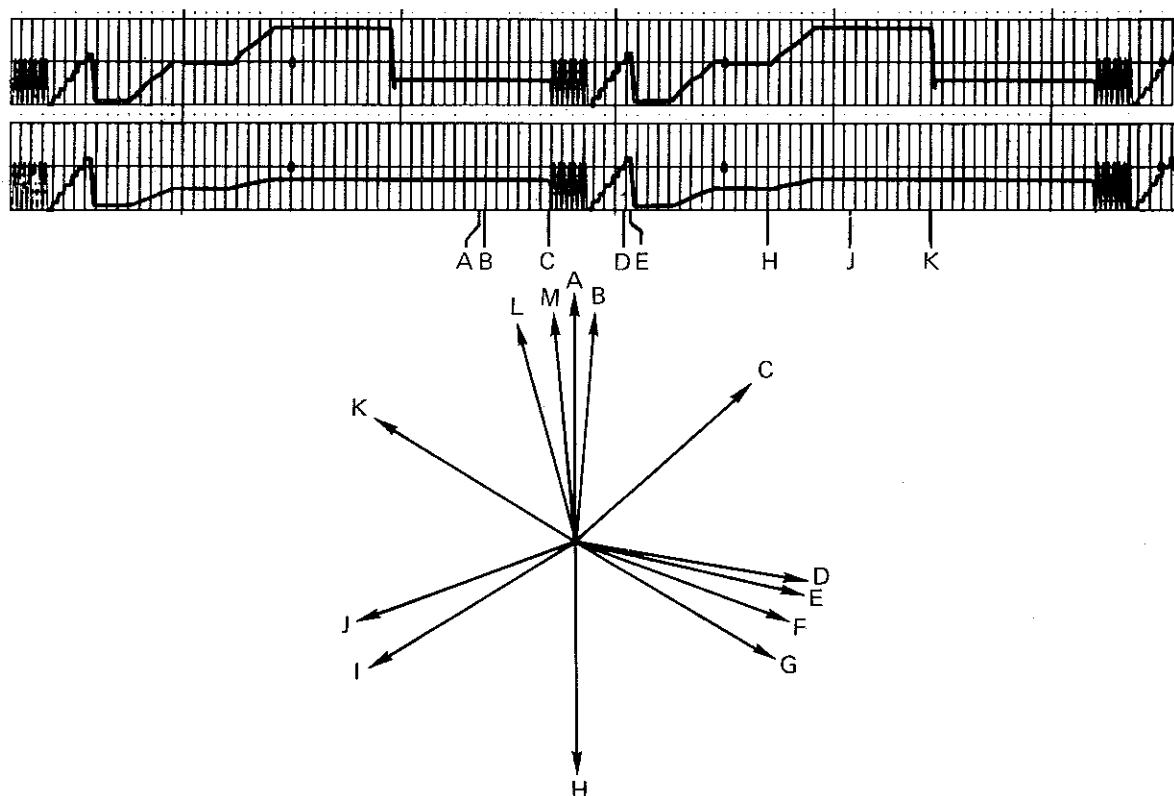


Figure 2-3. Relative Spectral Response of the  $6.7 \mu\text{m}$  and  $11.5 \mu\text{m}$  Channels



LEGEND

Reference Letter	Angle (degrees)	Time (ms)	Event
A :	0	0	Spacecraft zenith
B :	5	17.4	Radiometer IFOV just starting to leave housing
C :	48	166.7	Scan mirror position pip No. 1 occurs and radiometer sync word and calibration signal sequence is started. 6.7 $\mu$ m channel gain returned to normal
D :	100	347.5	Radiometer IFOV just starting to see all of space
E :	103.5	359.4	Calibrate signal sequence ends and restore period starts
F :	110.7	384.4	Restore period ends
G :	121.5	422.2	Earth scan period begins (1100 km orbit)
H :	180	625.0	Spacecraft nadir
I :	238.5	828.8	Earth scan period ends (1100 km orbit)
J :	250	868.9	Radiometer IFOV just starting to see housing
K :	302	1048.5	Scan mirror position pip No. 2 occurs and 6.7 $\mu$ m channel gain is attenuated by a factor of 3
L :	345	1197.9	Radiometer IFOV completely filled by housing
M :	355	1232.6	Radiometer Z-axis

Figure 2-4. THIR Scan Angle Information

At 103.5 degrees the calibration sequence ends and the radiometer dc restore sequence starts. At 110.7 degrees the dc restore sequence ends. The sequence of timing events, starting with the sync word and ending with the radiometer dc restoration, is initiated by scan mirror pip No. 1 and is timed by electronic logic circuits.

At 121.5 degrees (for a nominal 1100 km altitude) the earth scan period begins. At 238.5 degrees the earth-scan period ends; the space check-of-calibration period begins. At 250 degrees the radiometer FOV just starts to see the scanner housing and the space check-of-calibration period ends.

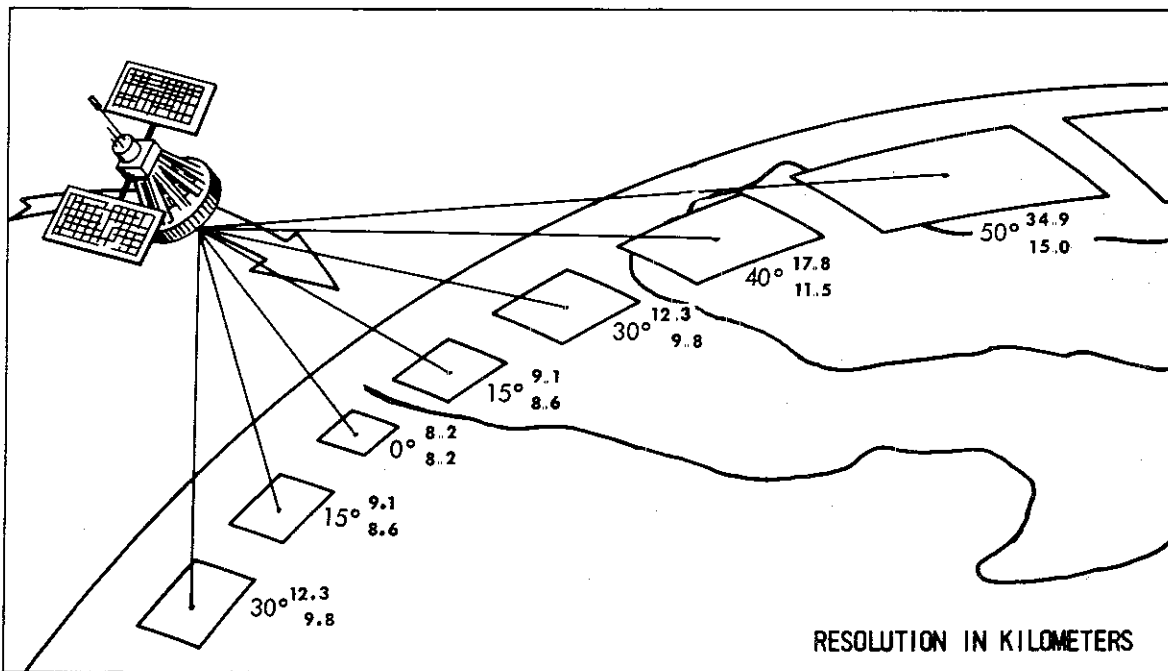
At 302 degrees scan mirror position pip No. 2 is generated and the gain in the  $6.7 \mu\text{m}$  channel is reduced by a factor of 3. (This reduction permits this channel to have a  $0^\circ\text{K}$  to  $270^\circ\text{K}$  dynamic range and still be capable of being calibrated with a scanner housing reference surface temperature as high as  $323^\circ\text{K}$ ). At 345 degrees the radiometer FOV is completely filled by the scanner housing and the second (scanner housing) check-of-calibration period begins. At 355 degrees the scan mirror is parallel with the radiometer Z-axis and the gain of the  $6.7 \mu\text{m}$  channel is returned to normal.

### 2.2.3 Scan Geometry

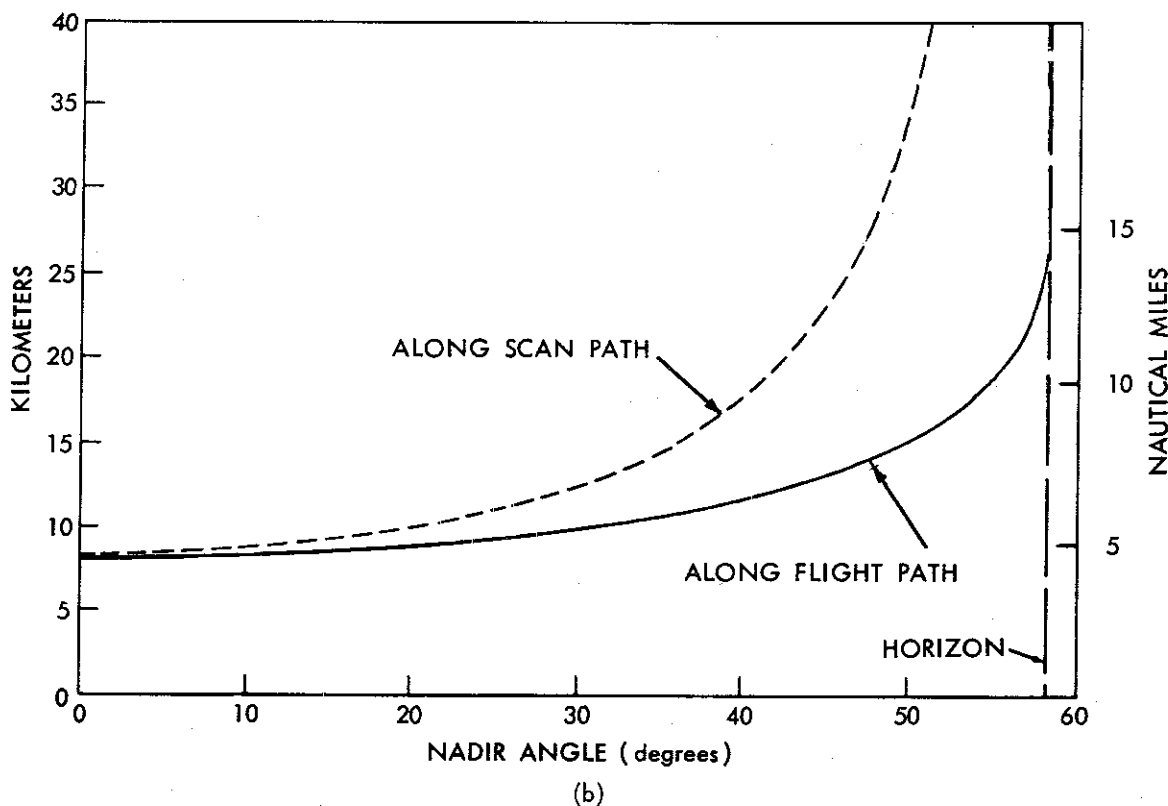
For the  $11.5 \mu\text{m}$  channel the scan rate of 48 rpm, combined with the satellite motion, produces contiguous scan line coverage along the subpoint track. As the scan angle from nadir increases there is increasing overlap between consecutive scan lines, reaching 350 percent overlap at the horizon. There is an even greater increase in ground coverage along the scan line (perpendicular to the line of motion of the satellite) as the angle from nadir increases.

Figure 2-5 shows the relationship between nadir angle and ground resolution for the  $11.5 \mu\text{m}$  channel. Figure 2-5a shows this pictorially while Figure 2-5b is a graph of the relationship. In Figure 2-5a the numbers under each resolution element are nadir angle (in degrees), resolution (in km) along the scan line, and resolution (in km) parallel to the satellite line of motion. At nadir the IFOV of 7.5 mr (0.43 degrees) for the  $11.5 \mu\text{m}$  channel provides a ground resolution of 8.2 km (4.5 nm). At a 50 degree nadir angle the ground resolution element is approximately 35 km long (east to west) by 15 km wide (north to south).

For the  $6.7 \mu\text{m}$  channel the IFOV of 20.5 mr (1.17 degrees) at nadir provides a ground resolution of 22.5 km (12.2 nm). At a 50 degree nadir angle the ground resolution element is approximately 95 km long by 41 km wide.



(a)



(b)

Figure 2-5. Relationship between Nadir Angle and Ground Resolution for the THIR 11.5  $\mu\text{m}$  Channel at 1100 km (a) Pictorial and (b) Graphical

#### 2.2.4 THIR Transmissions

A simplified block diagram of the THIR subsystem is given in Figure 2-6. THIR outputs are normally routed to one of the two HDRSS recorders. Upon command, one of the two THIR channels can be routed to the VIP, or to the T&DRE transponder for relay of data to the ground via ATS 6. Proper coding, timing synchronization, and electrical calibration signals are generated by the THIR electronic logic circuits and applied to the THIR channel outputs.

The varying dc voltage from the THIR modulates a voltage controlled oscillator (VCO), and the voltage variations are recorded on the HDRSS tape recorder. Upon command, the recorder plays back (in reverse) 32 times faster than real time into two channels of the multiplexer (MUX). The signal is doubled and beat against an 805 kHz local oscillator, producing a 657.8 KHz to 602.8 KHz FM signal. This is directed into the S-band transmitter and broadcast to the STDN station along with frequencies of the other experiments.

### 2.3 Calibration

#### 2.3.1 Laboratory Calibration

The main parameters for calibration of all electromagnetic radiation detection devices are essentially the same. Three fundamental quantities must be defined: the effective spectral response,  $\phi_\lambda$ ; the effective radiance,  $\bar{N}$ ; and the equivalent blackbody temperature,  $T_B$ . Here  $\phi_\lambda$  is a composite function involving all of the factors which contribute to the spectral response of the instrument such as filter transmission, mirror reflectances, and the spectral responsivity of the detector.

The effective radiance,  $\bar{N}$ , is defined as

$$\bar{N} = \int_0^{\infty} N_\lambda \phi_\lambda d\lambda \quad (1)$$

where  $N_\lambda$  represents the generally non-Planckian radiation from the earth and its atmosphere.

Because of its narrow field of view, the THIR essentially measures beam radiation or radiance toward the satellite along the optical axis. In the pre-flight laboratory calibration, the FOV of the radiometer was filled by a blackbody target whose temperature could be varied and accurately measured over a range of 190°K to 340°K. From the temperature of the blackbody target,  $T_B$ , the spectral radiance of the target is determined by the Planck function  $B_\lambda$ . The

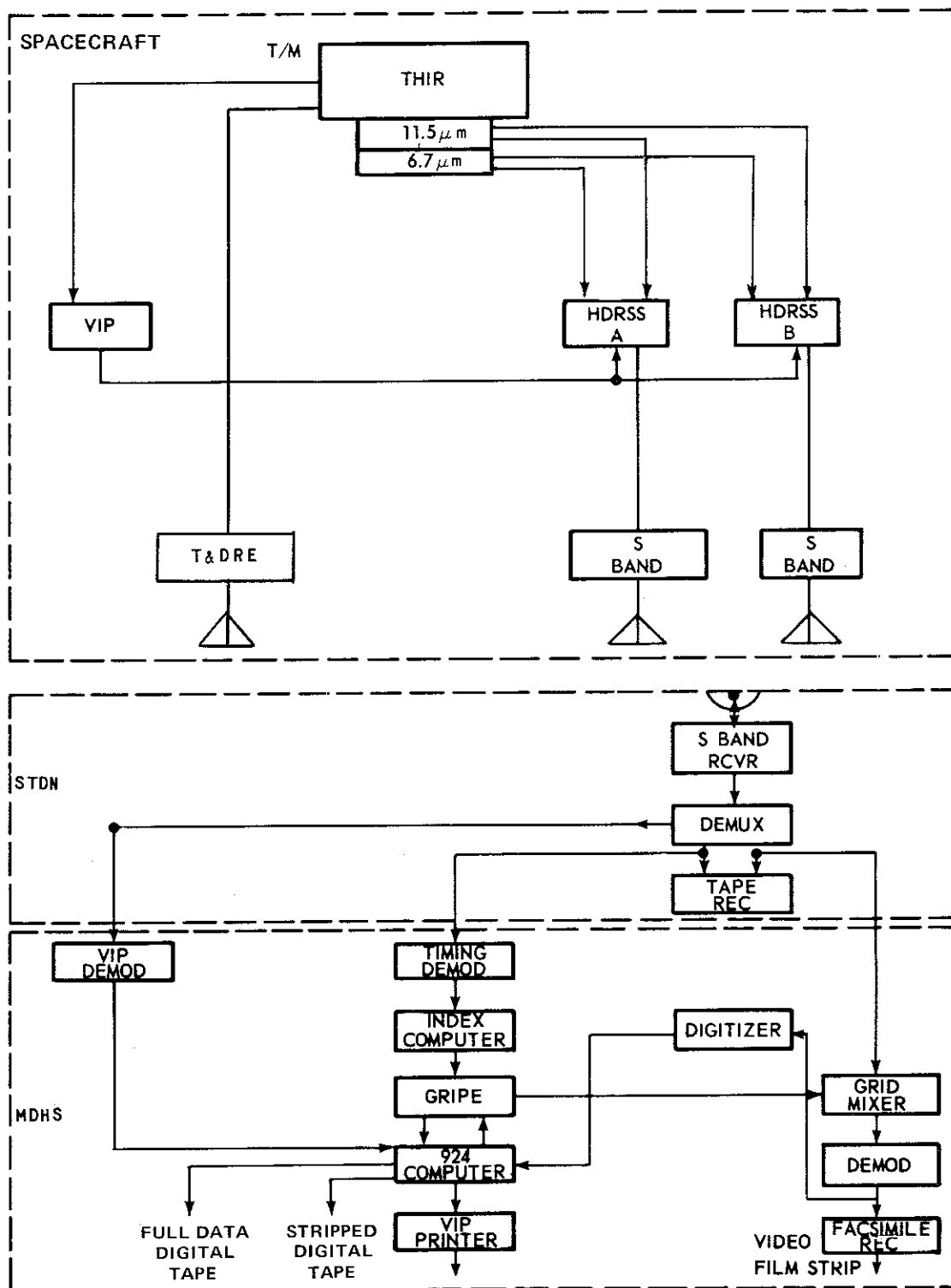


Figure 2-6. Simplified Block Diagram of the THIR Subsystem

integration of this function over the effective spectral response,  $\phi_\lambda$ , yields that portion of the radiance of the target to which the radiometer responds, the "effective radiance,"  $\bar{N}$ , given by

$$\bar{N} = \int_0^\infty B_\lambda(T_B) \phi_\lambda d\lambda \quad (2)$$

### 2.3.2 Equivalent Blackbody Temperature

The effective radiance to which the orbiting radiometer responds may be expressed by

$$\bar{N} = \int_0^\infty N_\lambda \phi_\lambda d\lambda \quad (3)$$

where  $N_\lambda$  is the spectral radiance in the direction of the satellite from the earth and its atmosphere. It is convenient to express the measurement from the orbit in terms of an equivalent temperature of a blackbody filling the field of view which would cause the same response from the radiometer. From Equations 2 and 3 it is seen that this "equivalent blackbody temperature" corresponds to the target temperature,  $T_B$ , of the blackbody used in the laboratory calibration. Therefore, the radiometer measurements can be expressed either as values of effective radiance,  $\bar{N}$ , or as equivalent blackbody temperatures,  $T_B$ . The  $\bar{N}$  versus  $T_B$  function from Equation 2 is given in Table 2-2 for both channels. THIR output voltages versus equivalent blackbody temperatures for both channels are given in Tables 2-3 and 2-4.

Table 2-2  
Effective Radiance ( $\bar{N}$ ) versus Equivalent Blackbody Temperature ( $T_B$ )

Blackbody Temperature (°K)	Effective Radiance (w/m <sup>2</sup> ster)	
	6.7 μm Channel	11.5 μm Channel
150	0.0042	0.2908
160	0.0100	0.4893
170	0.0216	0.7750
180	0.0428	1.167
190	0.0790	1.685
200	0.1372	2.346
210	0.2260	3.166
220	0.3558	4.160
230	0.5387	5.340

Table 2-2 (Continued)

Blackbody Temperature (°K)	Effective Radiance (w/m <sup>2</sup> ster)	
	6.7 μm Channel	11.5 μm Channel
240	0.7880	6.716
250	1.118	8.297
260	1.545	10.08
270	2.084	12.10
280	2.752	14.32
290	3.566	16.76
300	4.542	19.42
310	5.696	22.30
320	7.043	25.40
330	8.598	28.71
340	10.37	32.22
350	12.39	35.94

Table 2-3  
THIR Output Voltages versus Equivalent Blackbody Temperatures at  
Different Bolometer Temperatures for the 11.5 μm Channel

	Bolometer Temperature (°C)				
	0	10	20	30	40
180	-0.583	-0.596	-0.607	-0.605	-0.602
190	-0.664	-0.677	-0.687	-0.683	-0.677
200	-0.768	-0.781	-0.789	-0.784	-0.773
210	-0.898	-0.910	-0.917	-0.909	-0.893
220	-1.057	-1.069	-1.073	-1.062	-1.040
230	-1.246	-1.257	-1.258	-1.244	-1.214
240	-1.467	-1.478	-1.475	-1.458	-1.418
250	-1.722	-1.733	-1.726	-1.704	-1.653
260	-2.012	-2.022	-2.010	-1.984	-1.921
270	-2.338	-2.347	-2.330	-2.298	-2.222
280	-2.700	-2.709	-2.685	-2.647	-2.556
290	-3.099	-3.107	-3.077	-3.032	-2.924
300	-3.535	-3.541	-3.504	-3.452	-3.326

Table 2-3 (Continued)

Blackbody Temperature $T_B$ (°K)		Bolometer Temperature (°C)				
		0	10	20	30	40
310	-4.007	-4.013	-3.968	-3.908	-3.762	
320	-4.516	-4.520	-4.467	-4.398	-4.231	
330	-5.060	-5.063	-5.001	-4.924	-4.734	

Table 2-4  
THIR Output Voltages versus Equivalent Blackbody Temperatures at Different Bolometer Temperatures for the 6.7  $\mu\text{m}$  Channel

		Bolometer Temperature (°C)				
		0	10	20	30	40
180	-0.599	-0.609	-0.613	-0.629	-0.622	
190	-0.681	-0.691	-0.695	-0.710	-0.702	
200	-0.814	-0.824	-0.827	-0.840	-0.831	
210	-1.016	-1.027	-1.029	-1.039	-1.028	
220	-1.313	-1.324	-1.324	-1.330	-1.317	
230	-1.730	-1.741	-1.739	-1.740	-1.723	
240	-2.298	-2.311	-2.305	-2.298	-2.277	
250	-3.051	-3.065	-3.056	-3.038	-3.010	
260	-4.024	-4.040	-4.025	-3.994	-3.958	
270	-5.254	-5.272	-5.250	-5.201	-5.155	

## 2.4 Data Processing, Archiving, and Availability

Nimbus 6 THIR data are available from the NSSDC in photofacsimile film strips or computer-processed digital data. The form of data most readily available to the user is the film strip. Computer processing of the complex and voluminous data will be accomplished whenever requested by a user, as indicated in Section 2.4.2.

### 2.4.1 Photofacsimile Film Strips

At the STDN site the THIR information is demultiplexed and recorded on magnetic tape. It is then transmitted to the Goddard Space Flight Center where

the FM signal is demodulated, synchronized, integrated with geographic grid marks and displayed by a photofacsimile processor. The facsimile processor converts the radiometer output signals and the grid marks into a continuous strip image, line by line, on 70 mm film. Blanking circuits in the recorder reject unwanted sections of each scan line. Only the earth scan and, for calibration purposes, very small portions of the space scan are recorded on the film strip. The  $6.7 \mu\text{m}$  and  $11.5 \mu\text{m}$  data are split and separate tape and film files are compiled for user convenience. All of the THIR data are available on photofacsimile film strips.

The original photofacsimile film strips are processed by the NADUC photographic laboratory and archived at the NSSDC. A copy created from the original film is used as a master for producing all film strips requested by the users.

#### 2.4.1.1 Film Gray Shades

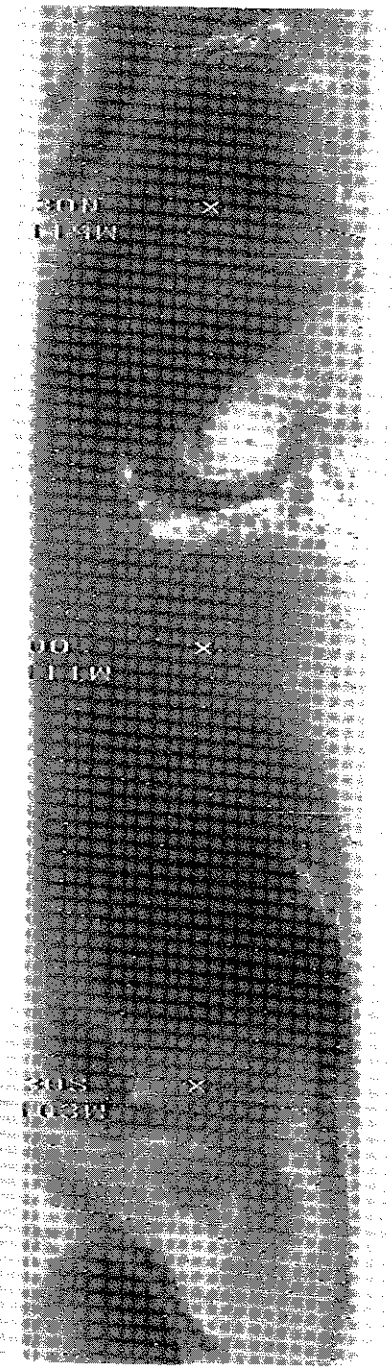
The gray shades in each image correspond to temperature variations of the land, sea, and clouds. On a film positive the lightest tones represent cold temperatures, usually cold clouds, snow, or ice. The darkest tones represent hot temperatures such as those found over the deserts at mid-day.

To maintain uniform film processing, a ten step gray scale wedge is generated just prior to the receipt of THIR data. Since the gray scale is calibrated as a range of temperatures expected in the imagery, the gray scale could be used to estimate image temperatures. But, because film processing is such that variations in density can and do occur, these gray scale values only approximate the image gray shades and accurate quantitative measurements cannot be obtained from the film. Therefore, a gray scale wedge will be furnished to a user only if specifically requested.

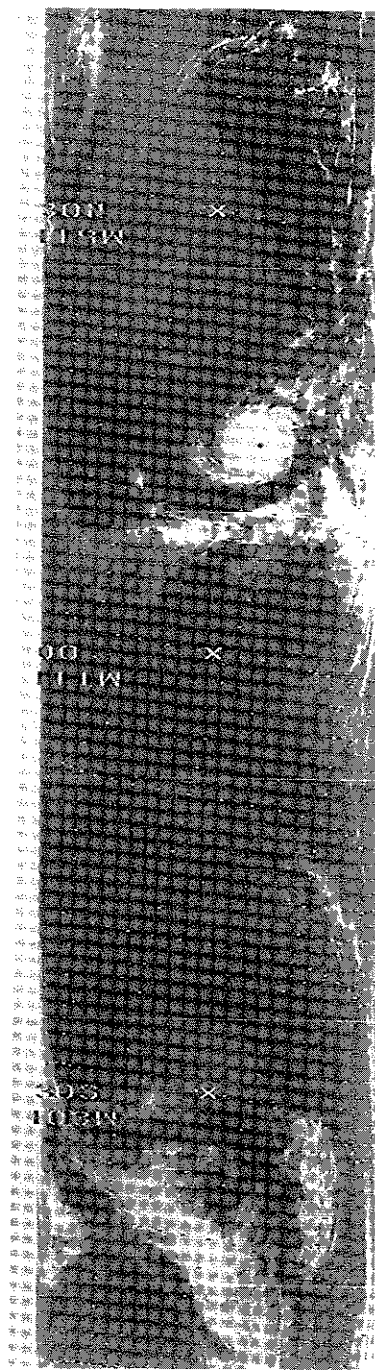
#### 2.4.1.2 Film Strip Labeling

THIR data are archived in separate  $6.7 \mu\text{m}$  and  $11.5 \mu\text{m}$  daytime and nighttime swaths. Thus, the approximate coverage of a full swath is from pole to pole. Each swath is identified by a label with the data orbit number, the channel ( $6.7 \mu\text{m}$  or  $11.5 \mu\text{m}$ ) and whether it is daytime or nighttime. The nighttime swath is labeled with the orbit number followed by N. The daytime swath is identified by the ascending node orbit number (within the swath) followed by a D. Each data block is also provided with a label showing the day of the year and the correct GMT of the data scan nearest the label.

Figure 2-7 shows two THIR film strips with the Nimbus 5 label format. The same will be used on Nimbus 6. The film strip has been gridded for daytime data. The label indicates a day (164), hour (18), minute (35), second (00), data



TIME 164 183500 UT  
DATA ORBIT 7376 D  
6 7 NIMBUS 5



TIME 164 183500 UT  
DATA ORBIT 7376 D  
11 5 NIMBUS 5

Figure 2-7. Nimbus 6 THIR Film Labeling

orbit (7376), daytime data (D), and that the imagery is from the  $11.5 \mu\text{m}$  (right) and  $6.7 \mu\text{m}$  (left) channels of Nimbus 5.

#### 2.4.1.3 Film Strip Gridding

The geographical location of each picture element scanned by the radiometer depends on the stability of the spacecraft. The Nimbus 6 control system has a pointing accuracy of about  $\pm 1$  degree in pitch, roll, and yaw. From an altitude of 1100 km a pointing error of 1 degree corresponds to an error of 20 km (11 nm) in the location of a picture element near the subpoint. On a global basis, this is an acceptable error for most meteorological analyses.

Automatic gridding of the data is accomplished by utilizing a CDC 924 computer to compute geographic coordinates, and a grid mixer which generates the grid points and adds them to the THIR data in analog form. These grid points are electrically superimposed on the film and manually checked to see that they are kept within 60 nm of their correct location at the subpoint. Referring to Figure 2-7, the grid point array makes lines for every 10 degrees of latitude and longitude, with points spaced at 2 degree intervals along each 10 degree line between  $60^\circ\text{N}$  and  $60^\circ\text{S}$  latitude. Outside of  $60^\circ\text{N}$  and  $60^\circ\text{S}$  latitude (not shown) there are latitude lines each 10 degrees, longitude lines each 20 degrees, latitude points each 2 degrees and longitude points each 5 degrees.

A small cross is placed where the subpoint track intersects the  $60^\circ\text{N}$ ,  $30^\circ\text{N}$ ,  $0^\circ$ ,  $30^\circ\text{S}$ , and  $60^\circ\text{S}$  latitude lines. The first cross from the bottom of Figure 2-7 marks the intersection of the subpoint track at  $30^\circ\text{S}$  and  $103^\circ\text{W}$ . The longitude and latitude of each cross (rounded to the nearest degree) is displayed at the extreme right (nighttime) or left (daytime) edge of the picture opposite that cross (latitude above longitude). The latitude format is  $XXY$  where  $00 \leq XX \leq 90$  degrees, and Y is N or S. The longitude format is  $XXX Y$  where  $000 \leq XXX \leq 180$  degrees, and Y is E or W.

#### 2.4.1.4 Ordering THIR Film Strips

When ordering THIR photographic data from NSSDC the following information should be given (in addition to that in Section 1.7):

- Satellite (e.g., Nimbus 6)
- Date of Data
- Data orbit number, channel ( $11.5 \mu\text{m}$  or  $6.7 \mu\text{m}$ ), and whether day or night data

- Data format, i.e., positive or negative transparencies, or prints
- Area of interest defined by latitude and longitude

The THIR imagery in the Nimbus 6 Data Catalogs should be used to obtain the data orbit numbers and to find relevant data.

#### 2.4.2 Digital Data

Quantitative data are obtained when the original analog signals are digitized with full fidelity and the digital data are processed by an IBM 360 computer where calibration and geographic referencing are applied automatically.

A simplified block diagram of the analog-to-digital (A/D) processing system is shown in Figure 2-8. The analog magnetic tape is fed to an A/D converter which utilizes a CDC 924 computer to prepare a digital tape. This tape is then operated upon by the IBM 360 which prepares a reduced radiation data tape called the Nimbus Meteorological Radiation Tape-THIR (NMRT-THIR). The NMRT can be used to generate grid print maps or to accomplish special scientific analyses. The format of this tape, the same as for Nimbus 5 THIR, is given in Section 2.5.

##### 2.4.2.1 Ordering Processed Digital THIR Data

Due to the large volume and the long computer running time required for processing THIR into NMRTs, Nimbus 6 THIR digital data are not routinely reduced to final NMRT format. Only those data which are specifically requested by the user will be processed. Requests should be made through NSSDC. It is anticipated that requested NMRT-THIR will begin to be available through NSSDC six months after launch. The user is urged to make full use of the film strips which are abundantly available in nearly real time from the NSSDC.

A series of programs produce printed and contoured data referenced to a grid on Polar Stereographic or Mercator map bases. These are called grid print maps. The advantages of the grid print map presentation are the display of absolute values of temperatures in their approximate location, geographical rectification of the data, and the possibility of automatically composing measurements from the consecutive orbits into quasi-synoptic maps. Grid print maps may be produced for either a single orbit or a composite of several orbits. The following standard options are available and should be specified when requesting grid print maps from NSSDC.

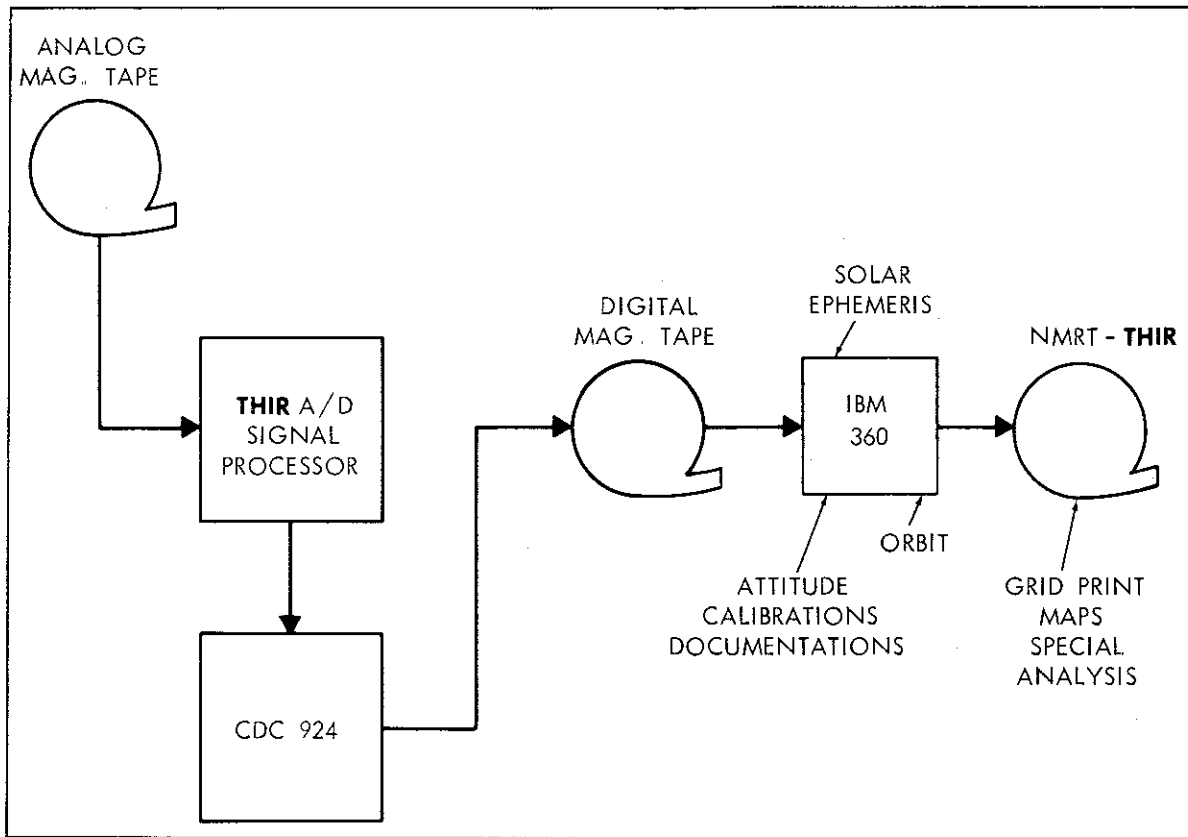


Figure 2-8. Simplified Block Diagram of the THIR A/D Processing System

- Map and Approximate Scale
  - a. Polar Stereographic, 1:30 million
  - b. Polar Stereographic, 1:10 million
  - c. Multi-resolution Mercator maps are available down to 1:1 million scale.
- Maximum Scan Angle (50 degrees is practical limit)
- Field Values and Contouring. Unless otherwise specified, all maps will include field values and contouring except Mercator maps of scales larger than 1:20 million. A data population map, indicating the number of individual measurements contained in each grid point average, as well as a latitude-longitude description for geographically locating the data, will be provided along with each grid print map.

When ordering grid print map data, the following identifying information should be given (in addition to that listed in Section 1.7):

- Satellite (e.g., Nimbus 6)
- Sensor (THIR)
- Channel ( $6.7 \mu\text{m}$  or  $11.7 \mu\text{m}$ )
- Data Orbit Number
- Calendar Date of Equator Crossing
- Beginning and Ending Times of Data in GMT
- Latitude and Longitude Limits of Area of Interest
- Format Desired (either a, b, or c above)

When ordering NMRTs, the "Calendar Date of Equator Crossing" and "Format Desired" can be omitted.

The THIR information in The Nimbus 6 Data Catalog should be used to obtain the data orbit number and the beginning and end times of the data of interest.

## 2.5 Format of the NMRT-THIR

The Nimbus Meteorological Radiation Tape-THIR will be a basic repository for requested radiation data from the Nimbus Temperature-Humidity Infrared Radiometer. This tape will contain data in binary mode at a density of 800 bits per inch.

The first file on this tape contains a BCD label. The label consists of fourteen words of BCD information followed by an end-of-file. The remaining files on this tape contain formatted THIR data in the format described on the following pages. The first record in this data file is a documentation record which describes the data to be found in the succeeding records. This first record contains seventeen words (see Table 2-5). The remaining records in the file will be of variable length, but this length will be consistent within the file (see Table 2-6). The length (L) of the data record can be computed as follows:

$$L = (\text{SWATHS PER RECORD}) \times (\text{WORDS PER SWATH}) \\ + (\text{NUMBER OF NADIR ANGLES}) + 7$$

Ninety degrees are added to all latitudes and attitude data to eliminate negative signs.

Table 2-7 defines the flags which appear in the data records.

Table 2-5  
NMRT-THIR Documentation Record Format

Word No.	Quantity	Units	Scaling	Remarks
1	Channel ID	Integer	B= 35	Equals 115 for 11.5 $\mu\text{m}$ channel and 67 for 6.7 $\mu\text{m}$ channel
2	Date	MMDDYY	B= 35	Date of interrogation for this orbit, i.e., 2/5/64 would be (020504) <sub>8</sub> . Only the last digit of year is used.
3	Nimbus Day	—	B= 35	Start time for this file of data
4	Hour	Z hour	B= 35	
5	Minute	Z minute	B= 35	
6	Seconds	Z seconds	B= 35	
7	Nimbus Day	—	B= 35	End time for this file of data
8	Hour	Z hour	B= 35	
9	Minute	Z minute	B= 35	
10	Seconds	Z seconds	B= 35	
11	Mirror Rotation Rate	Deg/Sec	B= 26	Rotation rate of radiometer mirror
12	Sampling Frequency	Samples/Sec	B= 35	Digital sampling of frequency per second of vehicle time
13	Orbit Number	—	B= 35	Orbit Number
14	Station Code	—	B= 35	Data acquisition site identification code
15	Swath Block Size (325)	—	B= 35	Number of 35-bit words per swath
16	Swaths/Record	—	B= 35	Number of swaths per record
17	Number of Locator Points	—	B= 35	Number of anchor points per swath for which latitudes and longitudes are computed.

Table 2-6  
NMRT-THIR Data Record Format

Word No.	Quantity	Units	Scaling	Remarks
1D	Nimbus Day	-	B= 17	Start time for this record of data
1A	Hour	Z hour	B= 35	
2D	Minutes	Z minute	B= 17	
2A	Seconds	Z seconds	B= 35	
3D	Roll Error	Degrees	B= 14	Roll error at time specified in words one and two.
3A	Pitch Error	Degrees	B= 32	Pitch error at time specified in words one and two.
4D	Yaw Error	Degrees	B= 14	Yaw error at time specified in words one and two.
4A	Height	Kilometers	B= 35	Height of spacecraft at time specified in words one and two.
5D	Detector Temperature	Degrees K	B= 17	Measured temperature of detector cell at time specified in words one and two.
5A	Electronics Temperature	Degrees K	B= 35	Measured temperature of electronics at time specified in words one and two.
6D	Reference Temperature A	Degrees K	B= 17	}
6A	Reference Temperature B	Degrees K	B= 35	
7D	Reference Temperature C	Degrees K	B= 17	
7A	Reference Temperature D	Degrees K	B= 35	

Table 2-6 (Continued)

Word No.	Quantity	Units	Scaling	Remarks
8	Nadir Angle	Degrees	B=29	Nadir angles corresponding to each locator point, and measured in the plane of the radiometer
N	Nadir Angle	Degrees	B=29	
(N+1)D	Seconds	Z Seconds	B=8	Seconds past time in words 1A & 2D for beginning of this swath.
(N+1)A	Data Population	-	B=35	Number of data points in this swath.
(N+2)D	Latitude	Degrees	B=11	Latitudes of subsatellite point for this swath
(N+2)A	Longitude	Degrees	B=29	Longitude of subsatellite point for this swath, positive westward 0 to 360°.
N+3	Flags	-	-	Reserved for flags describing this swath
(N+4)D	Latitude	Degrees	B=11	Latitude of viewed point for the first anchor spot
(N+4)A	Longitude	Degrees	B=29	Longitude of viewed point for first anchor spot, positive westward 0 to 360°.
MD	Latitude	Degrees	B=11	Latitude and longitude for
MA	Longitude	Degrees	B=29	Mth anchor spot
(M+1)D	THIR Data	-	B=14	THIR measurements. Tag
(M+1)A	THIR Data	-	B=32	and prefix reserved for flags.
K(A or D)	THIR Data	-	B=32 B=14	Last THIR data measurement

The above data constitute what is essentially the documentation portion of a data record. These data will be followed by several blocks of data with each block representing a swath. The number of these blocks in a record as well as the size of each block is specified in the documentation record represented on the previous page.

All remaining or unused portions of a swath data block are set to zero, giving a swath block size as specified in the documentation record. The above data on this page are repeated for the number of swaths in each record.

Table 2-7  
Definition of Flags Describing Each THIR Swath

Flag	Bit	Definition	Yes	No
1	35	Summary flag (all checks defined by flags 2 thru 12 are satisfactory, i.e., each flag is zero)	0	1
2	34	Consistency check between sampling rate and vehicle time is satisfactory	0	1
3	33	Vehicle time is satisfactory	0	1
4	32	Vehicle time has been inserted by flywheel	1	0
5	31	Vehicle time carrier is present	0	1
6	30	Vehicle time has skipped	1	0
7	29	Water vapor data	1	0
8	28	Sync pulse recognition was satisfactory	0	1
9	27	Dropout of data signal was detected	1	0
10	26	Window data	1	0
11	25	Unassigned		
12	24	Swath size is satisfactory when compared with the theoretical swath size	0	1
13	23	Unassigned		

Flags For Individual Measurements

Prefix	Tag	Definition	Yes	No
S	18	The particular measurement is below the earth-space threshold	1	0
1	19	Unassigned		
2	20	Unassigned		



### SECTION 3

## THE HIGH RESOLUTION INFRARED RADIATION SOUNDER (HIRS) EXPERIMENT

by

W. L. Smith, P. G. Abel, and H. M. Woolf

National Environmental Satellite Service

National Oceanic and Atmospheric Administration

Washington, D. C.

and

A. W. McCulloch and B. J. Johnson

National Aeronautics and Space Administration

Goddard Space Flight Center

Greenbelt, Maryland

### 3.1 Experiment Description

The Nimbus 6 HIRS is a third generation infrared radiation sounding experiment possessing many new features for greatly improving the capability of sounding the earth's atmosphere from an orbiting spacecraft. HIRS measurements in the  $4.3 \mu\text{m}$  and  $15 \mu\text{m}$   $\text{CO}_2$  band permit better vertical temperature profile resolution to be achieved in the lower troposphere and extend vertical coverage up to the stratopause. It has a channel to measure reflected sunlight to improve the capability of recognizing cloud contamination during the day, especially that caused by low altitude or small element clouds which are difficult to sense with infrared window measurements. Similar to its Nimbus 5 predecessor (ITPR), the HIRS obtains simultaneous measurements in the  $3.7 \mu\text{m}$  and  $11 \mu\text{m}$  window channels to enable the detection of cloudiness, both day and night, and to permit accurate specification of the temperature of the earth's surface, even under partly cloudy sky conditions. Water vapor channels in the weak and strong portions of the  $6.3 \mu\text{m}$   $\text{H}_2\text{O}$  band permit the specification of the abundance of water vapor of the lower and upper troposphere and aid in the detection of thin cirrus cloudiness. Quantitative estimates of the heights and amounts of clouds within the HIRS field of view are obtained from radiance observations in the three most transparent  $15 \mu\text{m}$   $\text{CO}_2$  band channels in a manner previously demonstrated with the Nimbus 5 ITPR radiance observations (Reference 3). High spatial resolution of 25 km (13 nm) and contiguous geographical sampling enable profiles to be obtained down to the earth's surface under all but extensive overcast cloud conditions. In overcast situations the profile derivations are limited to altitudes above the clouds.

With a cross-course scan, described in Section 3.2, the HIRS provides nearly complete sounding coverage of the earth's atmosphere every twelve hours.

A summary of the functions of the seventeen HIRS channels is presented in Table 3-1. A detailed description of these spectral intervals and the spectral response functions for the HIRS are given in Table 3-2, and Figure 3-1, respectively. The weighting functions ( $dB/dT \times d\tau/d \ln(p)$ ) for the temperature and water vapor sounding channels (computed for standard atmospheric conditions) are given in Figure 3-2.

The techniques to be used to process the Nimbus 6 HIRS data are similar to those used for the processing of Nimbus 5 ITPR data as described in Reference 3. As part of the GARP program, the HIRS observations are amalgamated with Nimbus 6 THIR and SCAMS observations to produce optimum global meteorological data sets. These meteorological data sets are used for the development of numerical weather prediction models as well as for research on synoptic scale and mesoscale weather processes. The spatial resolution and geographical spacing of the meteorological parameters derived for these data sets is 200 km. For special small-area research purposes, these same parameters are derived for the full HIRS resolution of 25 km.

The parameters which comprise the Nimbus 6 sounding data sets include:

- Surface temperature
- Vertical temperature profile from the surface to the 40-km level
- Vertical water vapor profile from the surface to the 10-km level
- Vertically integrated liquid water content of clouds
- Pressure altitudes and amounts of clouds
- Total outgoing long wave flux
- Surface albedo and averaged total albedo

**Table 3-1**  
**Functions of the HIRS Channels**

Channel Number	Channel Central Wave-number	Central Wavelength ( $\mu\text{m}$ )	Principal Absorbing Constituents	Level of Peak Energy Contribution	Purpose of the Radiance Observation
1	668	15.0	$\text{CO}_2$	30 mb	
2	679	14.7	$\text{CO}_2$	60 mb	
3	690	14.4	$\text{CO}_2$	100 mb	
4	702	14.2	$\text{CO}_2$	250 mb	
5	716	14.0	$\text{CO}_2$	500 mb	
6	733	13.6	$\text{CO}_2/\text{H}_2\text{O}$	750 mb	
7	749	13.4	$\text{CO}_2/\text{H}_2\text{O}$	900 mb	
8	900	11.0	Window	Surface	Surface Temperature and cloud detection.
9	1224	8.2	$\text{H}_2\text{O}$	900 mb	
10	1496	6.7	$\text{H}_2\text{O}$	400 mb	Water Vapor Sounding. Provide water vapor corrections for $\text{CO}_2$ and window channels. The 6.7 $\mu\text{m}$ channel is also used to detect thin cirrus cloud
11	2190	4.57	$\text{N}_2\text{O}$	950 mb	
12	2212	4.52	$\text{N}_2\text{O}$	850 mb	
13	2242	4.46	$\text{CO}_2/\text{N}_2\text{O}$	700 mb	
14	2275	4.40	$\text{CO}_2/\text{N}_2\text{O}$	600 mb	
15	2357	4.24	$\text{CO}_2$	5 mb	Temperature Sounding. The 4.3 $\mu\text{m}$ band channels provide better sensitivity to the temperature of relatively warm regions of the atmosphere than can be achieved with the 15 $\mu\text{m}$ band channels. Also, the short-wavelength radiances are less sensitive to clouds than those for the 15 $\mu\text{m}$ region.
16	2692	3.71	Window	Surface	Surface Temperature. Much less sensitive to clouds and $\text{H}_2\text{O}$ than 11 $\mu\text{m}$ window. Used with 11 $\mu\text{m}$ channel to detect cloud contamination and derive surface temperature under partly cloudy sky conditions.
17	14,443	0.69	Window	Cloud	Cloud Detection. Used during the day with 3.7 $\mu\text{m}$ and 11 $\mu\text{m}$ window channels to define clear fields of view and to specify any reflected solar contributions to the 3.7 $\mu\text{m}$ channel.

Table 3-2  
Summary of HIRS Optical Parameters

Type of Instrument	Multichannel filter radiometer, Cassegrainian telescope before the filter wheel/chopper assembly. Dichroic and refractive elements between this point and the detectors.
Detector summary	Two cooled detectors at 120°K: LnSe for six short wave IR channels, HgCdTe for ten long wave IR channels. One (300°K) Si detector for the visible channel.
Signal treatment	The signal through each filter is sampled for an integral number of cycles (between 1 and 7 cycles depending on the filter). The rectified signal is integrated over the integral number of cycles, beginning and ending at a positive peak in signal amplitude. The output voltage is digitized to 12 bits, plus a sign bit and a parity bit. Thus the maximum digital range of the output is ±4095 bits in all channels.
Commands	There are 9 bits available for command status.
Field of View	Circular, half amplitude separation 1.24 degrees. Scans to 36.9 degrees from nadir across the point tract, with 21 steps along a scan line on each side of nadir (42 total).
Calibration	Two internal blackbody sources (at 270°K and 300°K), and space. Calibration approximately every 90 seconds (every twenty scan lines).

Channel Number	Central Wave Number ( $\text{cm}^{-1}$ )	Interval Between 50% Response Points ( $\text{cm}^{-1}$ )	Characteristics			
			Noise Equivalent Radiance ( $\text{mw/m}^{-2}\text{ster cm}^{-1}$ )	$T_D = 118^\circ\text{K}$	$T_D = 124^\circ\text{K}$	Noise Equivalent Temperature (NEAT) Source Temp. = 290°K
1	668	2.8	3.0	6.0	1.90	3.80
2	679	13.7	0.66	1.5	0.41	0.94
3	690	12.6	0.45	0.75	0.28	0.47
4	702	15.9	0.27	0.44	0.17	0.27
5	716	17.5	0.52	0.85	0.32	0.52
6	733	17.6	0.23	0.38	0.14	0.23
7	749	18.4	0.27	0.42	0.16	0.26
8	900	34.6	0.19	0.30	0.12	0.19
9	1224	63.4	0.15	0.24	0.14	0.23
10	1496	87.6	0.13	0.19	0.21	0.31
11	2190	20.6	0.012	0.012	0.13	0.13
12	2212	22.5	0.003	0.003	0.04	0.04
13	2242	21.6	0.006	0.006	0.08	0.08
14	2275	35.2	0.002	0.002	0.03	0.03
15	2357	23.0	0.003	0.003	0.06	0.06
16	2692	296.9	0.001	0.001	0.06	0.06
17	14,443	892.2	—	—	—	—

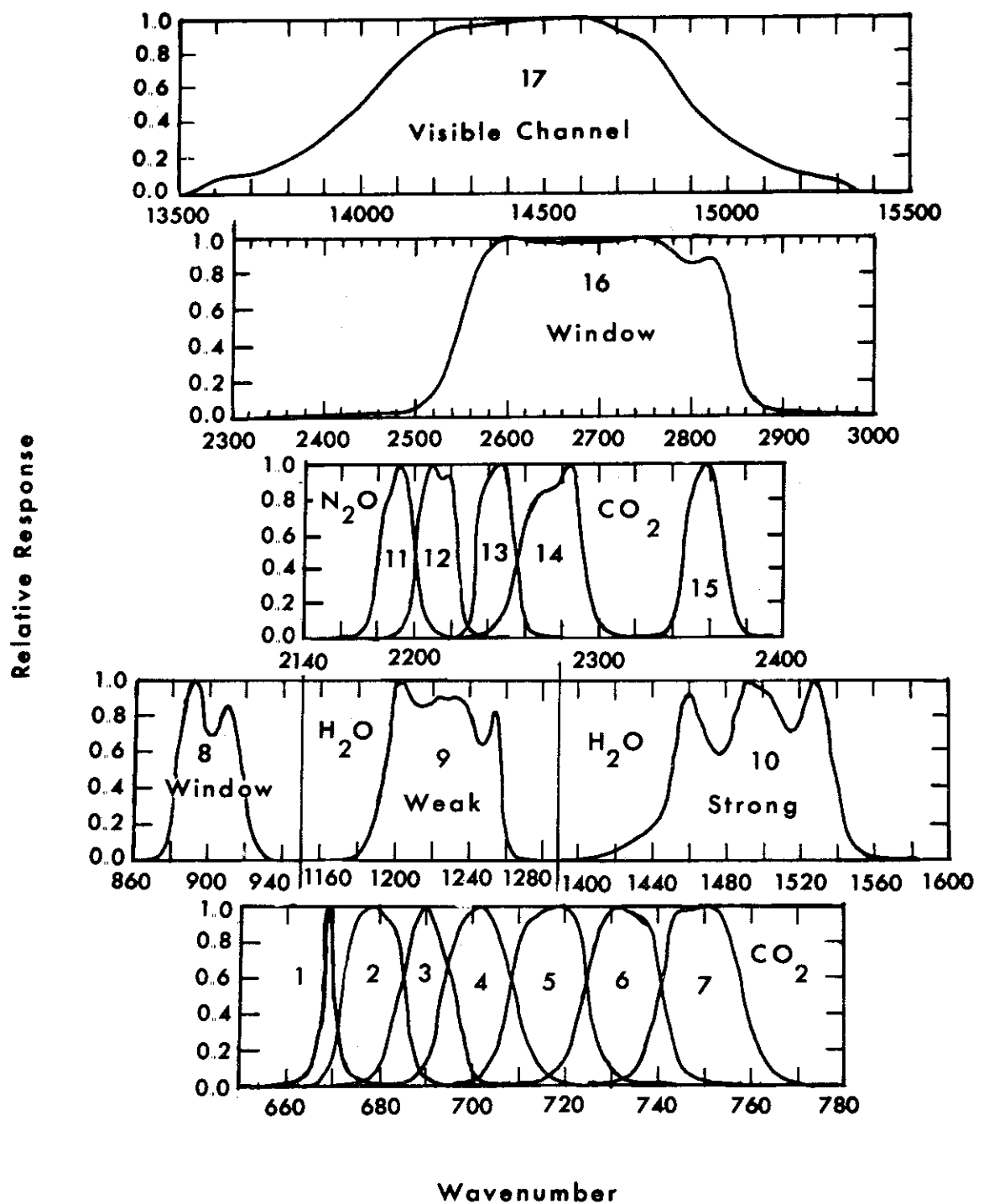


Figure 3-1. HIRS Filter Responses

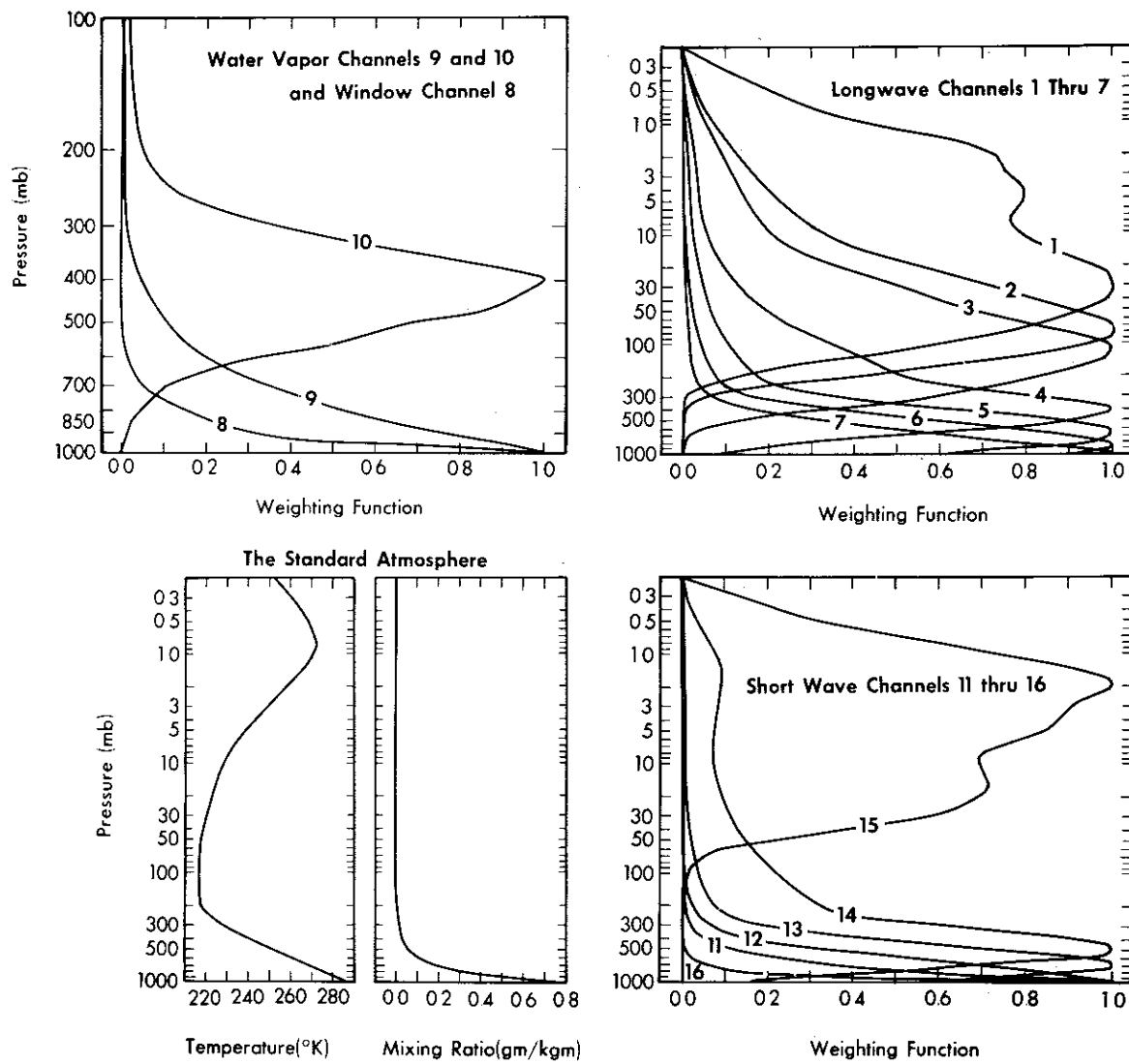


Figure 3-2. Weighting Functions for the HIRS Temperature and Water Vapor Channels

### 3.2 Instrument Description

#### 3.2.1 Summary

The instrument senses radiation in 17 discrete spectral intervals. One is in the visible part of the spectrum, the others being in the  $2 \mu\text{m}$  to  $15 \mu\text{m}$

wavelength range. The ac voltage amplitude from the detectors is proportional to the difference between the radiance of the unknown scene and that of the temperature-controlled filter chopper inside the instrument. Calibration of all the infrared channels in terms of absolute radiance is achieved approximately every 90 seconds, when the system views space and two blackbody targets on board the spacecraft. The space view gives an effectively zero radiance source. The targets are maintained at accurately measured temperatures near 255°K and 300°K.

The field of view of the instrument (between 50 percent amplitude response points) is about 1.24 degrees (equivalent to a circle with an approximate diameter of 25 km at nadir on the ground). The instrument scans along a direction perpendicular to the subpoint track. There are 21 scan elements on each side of the subpoint track, as may be seen in Figure 3-3. Each element is observed for 71 ms, with a step and settle period between observations of 35 ms. Calibration occurs after every 20 completed scan lines.

A summary of the optical parameters appears in Table 3-2.

### 3.2.2 Optical System

Figure 3-4 is a schematic of the HIRS optical system. A photograph of the device appears in Figure 3-5. The first dichroic element transmits the long wave channels (1-10) and reflects the short wave and visible channels. There are, consequently, two field stops for the system, one for each spectral component of the divided beam. Immediately below the field stops, the filters are arranged on a special filter wheel. The short wave and visible filters are arranged along the circumference of an outer radius, while the long wave filters form a concentric inner circle. For the long wave filters a concentric counter-rotating chopper produces a chopping rate of 900 Hz, each filter being viewed for up to seven cycles of the chopper waveform. The short wave chopper is rigidly attached to the filter wheel and each short wave filter extends under several blades of the chopper to produce a chopping rate of 390 Hz. The chopping rates were chosen to produce the maximum detectivity from the system. Since the signal through the visible channel is high, the integration in this case extends over a single cycle of the chopper waveform. The number of cycles in other channels has been chosen to optimize the signal-to-noise ratios.

The two-lens relay system following the field stops in the long and short wave optical trains serves two purposes. It allows the two detectors flexibility in positioning relative to the optics, which is important since they are attached to a radiative cooler and therefore their location is restricted. The relay system also focuses the primary mirror aperture on the detectors, rather than an

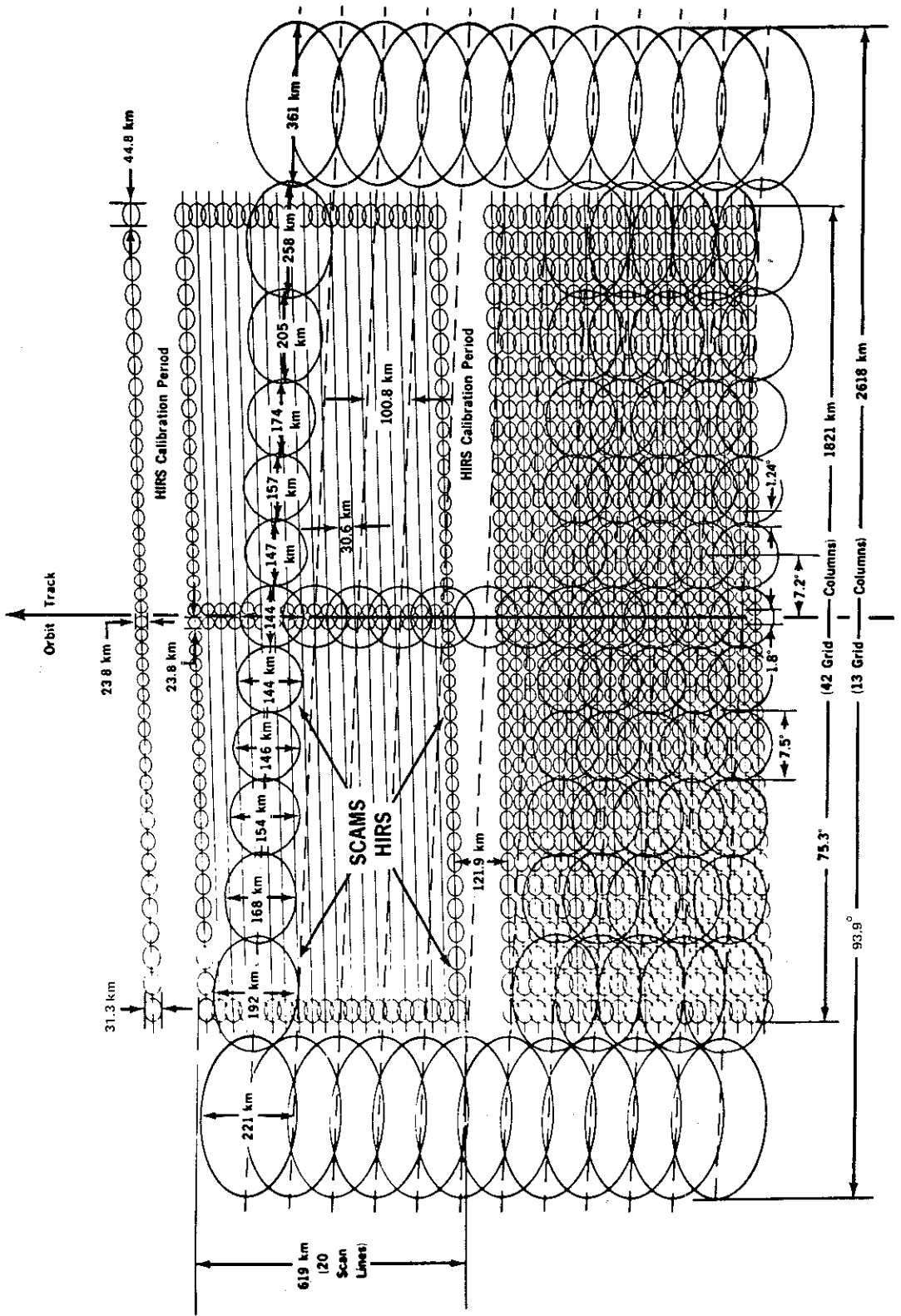


Figure 3-3. Scan Grid Patterns for HIRS and SCAMS

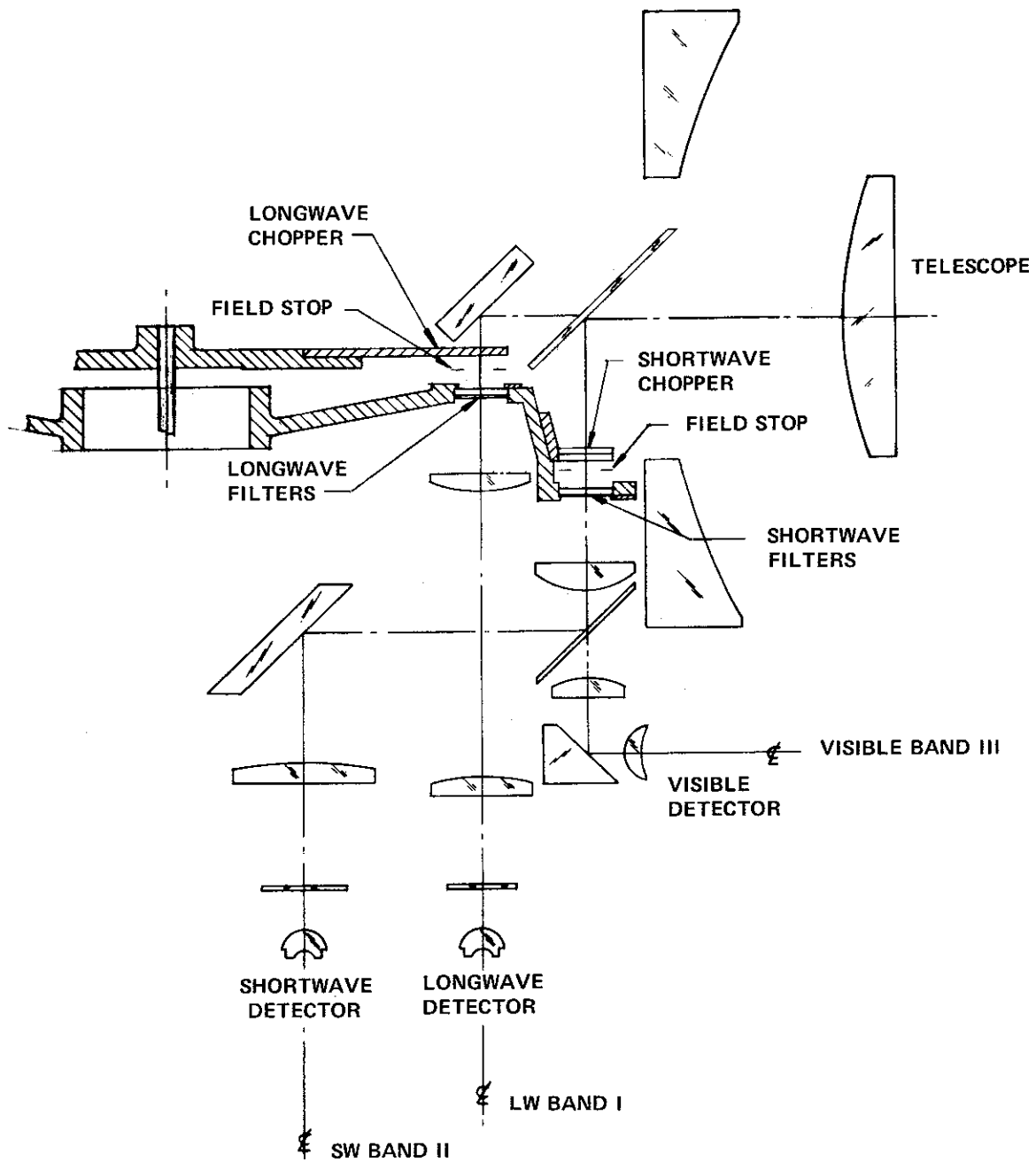


Figure 3-4. Schematic of HIRS Optical System

image of the source. This gives a much more uniform illumination of the detector surface when, for example, the instrument is observing an area of broken cloud cover. The effect of nonuniform detector response across its area, which is pronounced for the long wave detector, is much reduced.

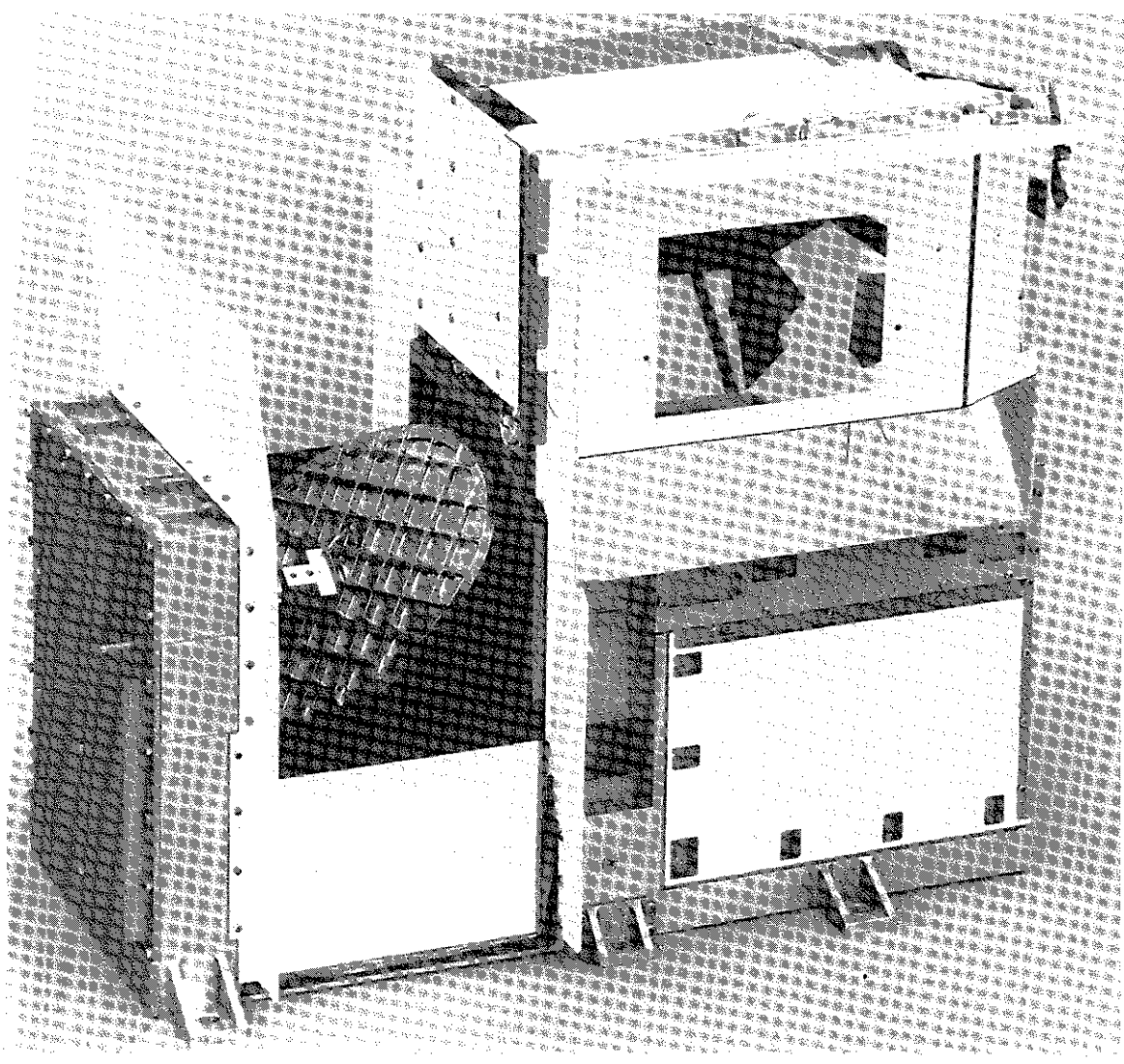


Figure 3-5. Photograph of the HIRS Instrument

Cooled detectors are used for all infrared channels because of their high detectivity and short response time. Since detectivity is higher for smaller detectors, the final element in the optical path is designed to converge the incident rays onto the smallest practicable detector size. The detectors are operated either at a controlled temperature of 124°K, which is just low enough to permit useable performance in the longest wavelength channel (Channel 1), or in an uncontrolled mode. Detection temperatures as low as 118°K are expected in orbit in the uncontrolled mode. The cooler itself is a conventional two-stage device with the detectors mounted on the central black radiating patch.

In front of each cooled detector is a window, held at a temperature of about 180°K, shielding the detectors from most of the contaminant stream which otherwise would reach them. It is also possible to close the door in front of the cooler aperture to space if decontamination becomes necessary. The cooler housing, first stage, and cooled patch, may be heated above 0°C for dispersion of ice crystals or contaminants.

### 3.2.3 Signal Electronics

There are two amplifier chains, one for the long wave channels, and one for the short wave channels and the visible channel. All three detectors have separate low-noise preamplifiers. In the short wave and visible channel preamplifiers, the output is switched at appropriate times (phased with the filter wheel rotation) into the joint main amplifier chain. AC output from the main amplifiers is phase sensitivity rectified using a reference signal derived from sensors monitoring the chopper rotation. This rectified signal is then integrated over an integral number of cycles of the chopper waveform. The output voltage is digitized to 12 bits with two extra bits for sign and parity (i. e., 14 bits total, range  $\pm 4095$  counts).

### 3.2.4 Interpretation of HIRS Digital Data

This section describes the algebra for deriving instrument temperatures and radiances from telemetered count levels.

The calibration blackbody target temperature sensor circuits have built-in voltage stabilizers. From ground calibration, the output count level ( $c_j$ ) and absolute temperature ( $T_j$ ) may be connected by the empirical relation

$$T_j = \sum_{i=1}^4 a_{ij} c_j^{(i-1)} \quad (1)$$

The coefficients  $a_{ij}$  (derived by ITT, the HIRS fabricator) are shown in Table 3-3, for the patch and target temperatures. ITT algorithms for other HIRS temperatures and system parameters are shown in Table 3-4.

Table 3-3  
Coefficients Used to Derive Instrument Temperatures and  
Radiances from Telemetered Count Levels

Coefficients $a_{ij}$ for Various Sensors					
j \ i	1	2	3	4	Location
1	97.393	$-4.04341 \times 10^{-2}$	$2.66559 \times 10^{-6}$	$-2.78578 \times 10^{-10}$	Patch
2	239.204	$-1.43181 \times 10^{-2}$	$4.28189 \times 10^{-7}$	$-1.8147 \times 10^{-11}$	Cool target
3	269.429	$-1.43313 \times 10^{-2}$	$4.266631 \times 10^{-7}$	$-1.78694 \times 10^{-11}$	Warm target
Coefficients $b_{ik}$ for Effective Target Temperatures					
Channel (k)	$\nu_{ok}$	$b_{1k}$	$b_{2k}$		
1	669.19	0.002	1.00001		
2	679.38	-0.029	1.00010		
3	690.45	-0.022	1.00009		
4	701.91	0.008	1.00004		
5	716.83	-0.048	1.00016		
6	732.55	-0.039	1.00014		
7	749.18	-0.005	1.00007		
8	899.99	0.013	1.00019		
9	1223.22	-0.180	1.00056		
10	1508.29	-0.775	0.99939		
11	2191.02	-0.020	1.00003		
12	2211.97	-0.020	1.00005		
13	2244.21	-0.020	1.00002		
14	2274.63	-0.074	0.99993		
15	2357.66	-0.021	1.00004		
16	2691.20	-2.194	1.00316		
17	N/A	N/A	N/A		

The radiance calibration for each channel is derived from the on board target temperatures. For a monochromatic filter at wavenumber  $\nu_o$ , the idealized target radiance is the Planck function  $B(\nu_o, T)$  at the temperature  $T$  of the source. From the true filter profile it is possible to establish an effective target temperature such that the Planck function of the effective temperature gives the true radiance. The effective temperature ( $T_e$ ) may be

**Table 3-4**  
**Algorithms for Subsidiary HIRS System Parameters**

FUNCTION	ALGORITHM									
Patch Power	$P_{\mu W} = 1.16 (VIM)^2 \times 1000$									
Cone Cover Deployed Voltage	$VIM = -1.2 \pm 0.5 \text{ V}$									
Cone Cover Stored Voltage	$VIM = -5.34 \pm 0.5 \text{ V}$									
+15 VDC TM	$V_X = \left\{ K (R_1) \left[ (4.5158) 10^{-4} (VIM) - 1.503 (10^{-4}) V_{15} \right] + VIM \right\}$									
+10 VDC TM										
+5 VDC TM	where      X                  R <sub>1</sub> K <table border="1" style="margin-left: auto; margin-right: auto;"> <tr> <td>+15</td> <td><math>13.3 \times 10^3</math></td> <td>1.0</td> </tr> <tr> <td>+10</td> <td><math>7.87 \times 10^3</math></td> <td>0.99</td> </tr> <tr> <td>+5</td> <td><math>6.65 \times 10^3</math></td> <td>1.0</td> </tr> </table>	+15	$13.3 \times 10^3$	1.0	+10	$7.87 \times 10^3$	0.99	+5	$6.65 \times 10^3$	1.0
+15	$13.3 \times 10^3$	1.0								
+10	$7.87 \times 10^3$	0.99								
+5	$6.65 \times 10^3$	1.0								
-15 VDC TM	$V_{-15} = 2.991 \text{ (VIM)}$									
-24.5 VDC TM	$V_{-24.5} = 4.48 \text{ (VIM)}$									
F/C Motor Current	$I = 0.198 \text{ (VIM) amps}$									
Scan Motor Current	$I = 0.40486 \text{ (VIM) amps}$									
Scan Mirror Temp	(1) $R_I = (3.48 \times 10^4 \times VIM)/(V_{-24.5} - 2.955 \text{ VIM})$									
Pri Telescope Temp	(2) $I_C = \left\{ \left  \frac{1}{(1.02674 \times 10^{-3})} + (2.39508 \times 10^4) \right. \right.$									
Sec Telescope Temp	$\left. \times (\text{LOG}_e R_I) + 1.55404 \times 10^{-7} \right. \right. \\ \left. \left. \times (\text{LOG}_e R_I)^3 \right  - 273.15 \right\}$									
F/C Motor Temp										
Baseplate Temp										
Electronics Temp										
Scan Motor Temp										
Cooler Housing Temp	(1) $R_I = (3.48 \times 10^4 \times VIM)/(V_{-24.5} - 3.540 \text{ VIM})$ (2) $I_C = \left\{ \left  \frac{1}{(1.02674 \times 10^{-3})} + (2.39508 \times 10^4) \right. \right.$ $\left. \times (\text{LOG}_e R_I) + 1.55404 \times 10^{-7} \right. \right. \\ \left. \left. \times (\text{LOG}_e R_I)^3 \right  - 273.15 \right\}$									

Table 3-4 (Continued)

FUNCTION	ALGORITHM																							
F/C Housing Temp	$T^{\circ}K = K_2 V^2 + K_1 V + K_0$ where <table border="1"> <thead> <tr> <th>F/C HSG</th> <th><math>K_2</math></th> <th><math>K_1</math></th> <th><math>K_0</math></th> </tr> </thead> <tbody> <tr> <td>#1</td> <td><math>3.3385 \times 10^{-2}</math></td> <td>-3 3172</td> <td>293.01</td> </tr> <tr> <td>#2</td> <td><math>3.3312 \times 10^{-2}</math></td> <td>-3.3158</td> <td>293.09</td> </tr> <tr> <td>#3</td> <td><math>3.3255 \times 10^{-2}</math></td> <td>-3 3148</td> <td>292.84</td> </tr> <tr> <td>#4</td> <td><math>3.3326 \times 10^{-2}</math></td> <td>-3.3109</td> <td>292.82</td> </tr> </tbody> </table>				F/C HSG	$K_2$	$K_1$	$K_0$	#1	$3.3385 \times 10^{-2}$	-3 3172	293.01	#2	$3.3312 \times 10^{-2}$	-3.3158	293.09	#3	$3.3255 \times 10^{-2}$	-3 3148	292.84	#4	$3.3326 \times 10^{-2}$	-3.3109	292.82
F/C HSG	$K_2$	$K_1$	$K_0$																					
#1	$3.3385 \times 10^{-2}$	-3 3172	293.01																					
#2	$3.3312 \times 10^{-2}$	-3.3158	293.09																					
#3	$3.3255 \times 10^{-2}$	-3 3148	292.84																					
#4	$3.3326 \times 10^{-2}$	-3.3109	292.82																					
Radiant Cone Temp	$T^{\circ}K = K_2 V^2 + K_1 V + K_0$ where <table border="1"> <thead> <tr> <th>Cone Temp</th> <th><math>K_2</math></th> <th><math>K_1</math></th> <th><math>K_0</math></th> </tr> </thead> <tbody> <tr> <td>153°K to 183°K</td> <td>2.2414</td> <td>-17.390</td> <td>131.56</td> </tr> <tr> <td>183°K to 323°K</td> <td>2.4163</td> <td>-16.320</td> <td>133.21</td> </tr> </tbody> </table>				Cone Temp	$K_2$	$K_1$	$K_0$	153°K to 183°K	2.2414	-17.390	131.56	183°K to 323°K	2.4163	-16.320	133.21								
Cone Temp	$K_2$	$K_1$	$K_0$																					
153°K to 183°K	2.2414	-17.390	131.56																					
183°K to 323°K	2.4163	-16.320	133.21																					
Patch Temp	$T^{\circ}K = K_2 V^2 + K_1 V + K_0$ where <table border="1"> <thead> <tr> <th>Patch Temp</th> <th><math>K_2</math></th> <th><math>K_1</math></th> <th><math>K_0</math></th> </tr> </thead> <tbody> <tr> <td>103°K to 143°K</td> <td>1.6727</td> <td>-24.585</td> <td>97.98</td> </tr> <tr> <td>143°K to 323°K</td> <td>1.7787</td> <td>-24.087</td> <td>98.61</td> </tr> </tbody> </table>				Patch Temp	$K_2$	$K_1$	$K_0$	103°K to 143°K	1.6727	-24.585	97.98	143°K to 323°K	1.7787	-24.087	98.61								
Patch Temp	$K_2$	$K_1$	$K_0$																					
103°K to 143°K	1.6727	-24.585	97.98																					
143°K to 323°K	1.7787	-24.087	98.61																					

expressed as a polynomial of the true temperature of the source. A linear fit giving adequate accuracy is:

$$\text{Radiance (Channel } k) = B(\nu_{ok}, T_{ek}), \quad (2)$$

where

$$T_{ek} = \sum_{i=1}^2 b_{ik} T^{(i-1)}$$

The coefficients  $b_{ik}$  for channels  $k = 1-16$  are shown in Table 3-3. The radiance error of this approximation is much less than the noise equivalent radiances specified in Table 3-2.

### **3.3 HIRS Data Processing, Format, and Archiving**

#### **3.3.1 Data Processing**

All HIRS data will be acquired at the Rosman, Orroral, and Alaska STDN stations and relayed to the MDHS at GSFC. The MDHS will produce 4" x 5" negatives and digital data tapes of all HIRS data acquired from each interrogation orbit. The imagery is sent to the NADUC for production of required photographic copies. Images are also reduced to 70 mm roll format and sent to the NSSDC for archiving and filling requests for imagery.

The HIRS digital data will be transmitted via computer-to-computer data link from the MDHS to the Goddard Institute for Space Studies (GISS), New York City, on an orbit-by-orbit basis immediately after decommutation from the spacecraft data stream. Multi-orbit magnetic tapes containing the same data will be courier-delivered to NOAA/NESS, Suitland, Maryland, for developmental, back-up processing, and research purposes.

#### **3.3.2 Image Format**

All HIRS data will be converted to 4" x 5" black and white images at the MDHS at GSFC. The NADUC will reproduce and distribute initial copies of these images. The format and details of the planned HIRS display is described below. Figure 3-6 is a sample of the HIRS display and should be used as reference for the following description.

- **NIMBUS 6 - HIRS**

This identifies the satellite (Nimbus 6) and the experiment (HIRS).

- **DATE**

This identifies the Greenwich month, day, and year the data were recorded on board the satellite.

- **SCALE (F, P1, or P2)**

The data from each orbit will be displayed as an image at full vertical scale (F) or at partial vertical scale (P). In the full scale mode up to 125 minutes of data will be output on a single image (and labeled as SCALE - F). In the partial scale mode the data are displayed at twice the vertical scale used in the full scale mode. Usually, in the partial scale mode, two images are needed to display all the data. The last

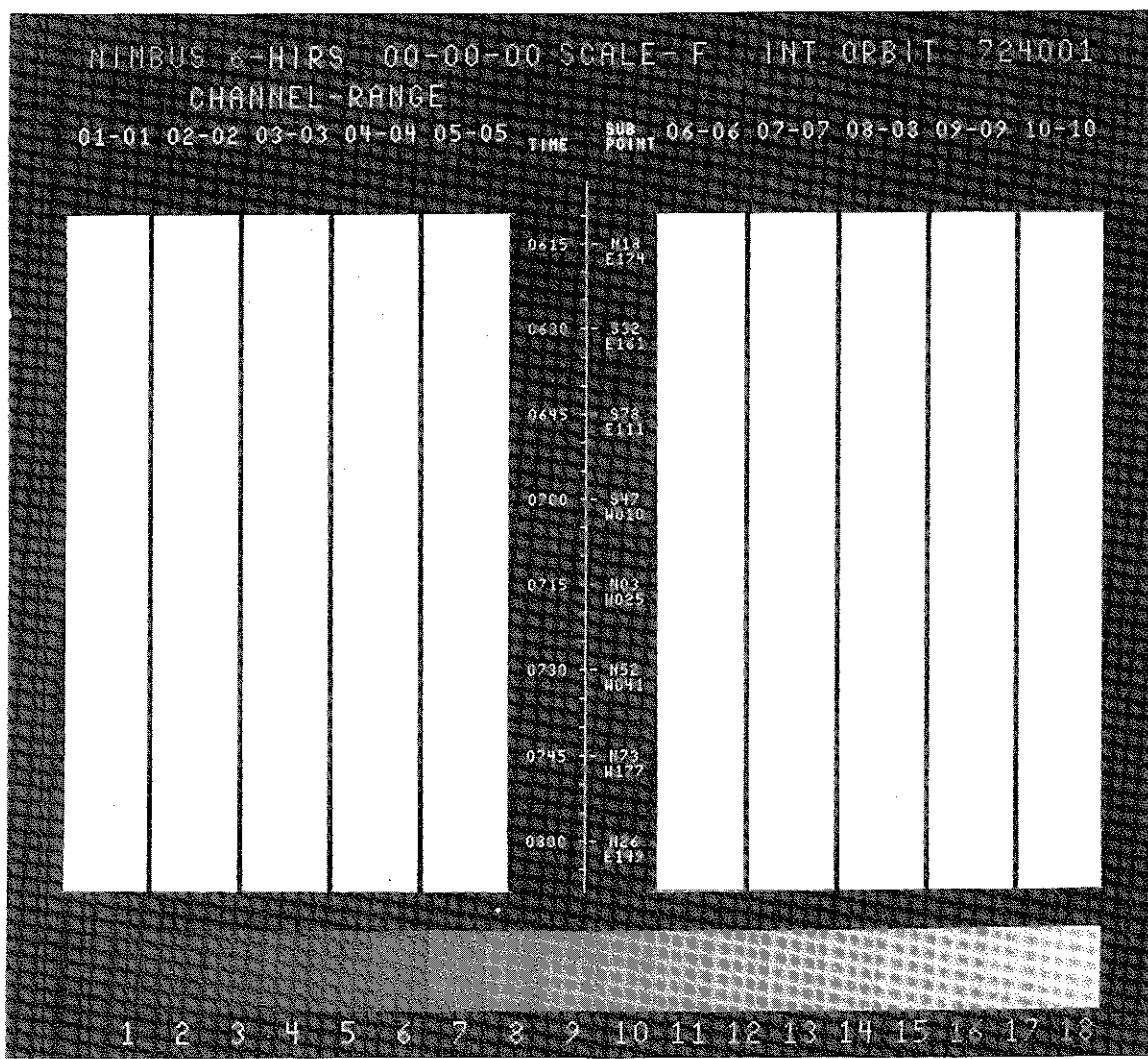


Figure 3-6. HIRS EIS Display

60 minutes of the data are output first (and the image is labeled SCALE-P2). Any remaining data from each interrogation orbit are output on a second image (and labeled SCALE-P1). Note that P1 contains the data acquired earliest. If there is less than 65 minutes of data from an interrogation orbit, only a P2 image is produced. In the full scale (F) mode each scan line of HIRS data are displayed once. In partial scale (P) mode each scan line is displayed twice in succession. In both modes, each of the 42 scan spot elements across a scan is displayed four times for a total of 168 display spots across each line.

- GRAY SCALE

Each image has an 18-step gray scale along the bottom of the display. The gray scale defines the brightness temperature for each of the ten swaths by assigning a different brightness temperature range to the gray scale for each swath. Table 3-5 defines the planned temperature range of gray scale values for each HIRS channel used in the swath displays. If these assigned values should be changed after launch, The Nimbus 6 Data Catalogs will list the new values.

- INT ORBIT

The interrogation orbit identifies the orbit during which the recorded data are transmitted to a STDN station. Usually parts of two data orbits are on the same display. The interrogation orbit number will only identify the last orbit of each display.

- TIME (and) SUBPOINT

Satellite time and latitude-longitude information are presented along the vertical line down the center of each display. The line represents the satellite subpoint track which is located down the center of each of the swaths on each display. TIME is GMT with ticks along the left side of the line at each five minute mark (on the five minutes). TIME is annotated (hour and minute) every 15 minutes (on the quarter hour). SUBPOINT information presents latitude and longitude positions of the satellite subpoint. Each tick mark on the right side of the vertical line is annotated with the subpoint latitude and longitude (to the nearest degree). Latitude is labeled N (north) or S (south). Longitude is labeled E (east) or W (west).

- CHANNEL-RANGE

There are 21 display options of the 17 channels of HIRS data. Only ten, however, can be shown on each image display. All swaths on each display contain the same coverage information, but each contains different temperature and spectral information.

Each swath is identified by a header block label such as 1-1, 6-6, etc. The ten header labels on each display identify the ten HIRS channels displayed. Table 3-5 shows the temperature value versus gray scale number for each channel number. The planned swath display is the following:

**Table 3-5**  
**HIRS Gray Scale Number versus Brightness Temperature**  
**for each HIRS Channel Displayed on an EIS Image**  
**(Brightness Temperature in °K)**

Gray Scale Number	HIRS Channel Number*										
	1-1	2-2	3-3	4-4	5-5	6-6	7-7	8-8	9-9	10-10	11-11
(black) 1	>276	>262	>238	>248	>262	>276	>286	>326	>286	>257	>298
2	276-272	262-258	238-236	248-246	262-259	276-272	286-281	326-322	286-281	257-254	298-295
3	272-268	258-256	236-233	246-243	259-256	272-268	281-277	322-318	281-277	254-252	295-293
4	268-264	256-253	233-231	243-241	256-253	268-264	277-272	318-313	277-272	252-249	293-290
5	264-261	253-250	231-229	241-239	253-250	264-261	272-268	313-309	272-268	249-246	290-288
6	261-257	250-247	229-227	239-237	250-247	261-257	268-263	309-305	268-263	246-243	288-285
7	257-253	247-244	227-224	237-234	247-244	257-253	263-259	305-301	263-259	243-241	285-283
8	253-249	244-241	224-222	234-232	244-241	253-249	259-254	301-297	259-254	241-238	283-280
9	249-245	241-238	222-220	232-230	241-238	249-245	254-250	297-293	254-250	238-235	280-278
10	245-241	238-234	220-218	230-228	238-234	245-241	250-246	293-288	250-246	235-232	278-275
11	241-237	234-231	218-216	228-226	234-231	241-237	246-241	288-284	246-241	232-229	275-273
12	237-233	231-228	216-213	226-223	231-228	237-233	241-237	284-280	241-237	229-227	273-270
13	233-229	228-225	213-211	223-221	228-225	233-229	237-232	280-276	237-232	227-224	270-268
14	229-226	225-222	211-209	221-219	225-222	229-226	232-228	276-272	232-228	224-221	268-265
15	226-222	222-219	209-207	219-217	222-219	226-222	228-223	272-268	228-223	221-218	265-263
16	222-218	219-216	207-204	217-214	219-216	222-218	223-219	268-263	223-219	218-216	263-260
17	218-214	216-213	204-202	214-212	216-213	218-214	219-214	263-259	219-214	216-213	260-258
(white) 18	<214	<213	<202	<202	<213	<214	<214	<259	<214	<213	<258

Table 3-5 (Continued)

Gray Scale Number	12-12	13-13	14-14	15-15	HIRS Channel Number*				
					16-16	17-17	18-18	8-19	11-20
(black)	>286	>276	>257	>276	>336	0-6	0-3	>322	>295
1	286-281	276-272	257-254	276-272	336-333	6-11	3-6	322-313	295-290
2	281-277	272-268	254-252	272-268	333-329	11-17	6-9	313-305	326-318
3	277-272	268-264	252-249	268-264	329-326	17-22	9-12	305-297	285-280
4	272-268	264-261	249-246	264-261	326-322	22-28	12-15	297-288	280-275
5	268-263	261-257	246-243	261-257	322-318	28-33	15-18	288-280	275-270
6	263-259	257-253	243-241	257-253	318-315	33-38	18-21	280-272	270-265
7	259-254	253-249	241-238	253-249	315-311	38-44	21-24	272-263	265-260
8	254-250	249-245	238-235	249-245	311-308	44-50	24-26	263-255	260-255
9	250-246	245-241	235-232	245-241	308-304	50-56	26-29	255-247	255-250
10	246-241	241-237	232-229	241-237	304-300	56-61	29-32	247-238	250-245
11	241-237	237-233	229-227	237-233	300-297	61-67	32-35	238-230	245-240
12	237-232	233-229	227-224	233-229	297-293	67-72	35-38	230-222	240-235
13	232-228	229-226	224-221	229-226	293-289	72-78	38-41	222-213	235-230
14	228-223	226-222	221-218	226-222	289-286	78-83	41-44	213-205	230-225
15	223-219	222-218	218-216	222-218	286-282	83-88	44-47	205-197	225-220
16	219-214	218-214	216-213	218-214	282-279	88-94	47-50	197-188	220-215
17	<214	<214	<213	<214	<279	94-100	>50	<188	<215
(white)	18							<217	

\*The HIRS channel number is the number before the hyphen. The number after the hyphen is the computer program table of temperature versus gray scale as given here. Channel 17-17 is the 0.69  $\mu\text{m}$  visible wavelength channel. The values 17-17 are of albedo, which is dependent on the sun angle and surface characteristics. The “channel” numbered 18-18 (window channel difference) is used to present the difference in temperature between HIRS channel 16 and 8. The “channels” 8-19, 11-20, and 16-21 are used to define a second output range of temperatures versus gray scale for channels 8, 11, and 16. Table 3-1 provides spectral information and the purpose of each of the 17 HIRS channels.

<u>Swath Location</u>	<u>Channel Number</u>
1	8-8
2	9-9
3	10-10
4	16-16
5	17-17
6	18-18 (window channel difference)
7	12-12
8	14-14
9	3-3
10	15-15

This swath display and the temperature versus gray scale table are preliminary. The brightness temperature table values are based on preflight data and, consequently, will change after launch. After launch the table will be updated and other displays, if any, will be presented in The Nimbus 6 Data Catalog.

### 3.3.3 Tape Format

The raw digital data will be routinely processed at GISS using computer software developed by NOAA/NESS. Primary output will be tapes containing calibrated, located radiances. These tapes will be produced on the IBM 360/95 at GISS or the 360/195 at NOAA, and will be nine track, 1600 bpi, and parity. Logical records (one per scan line) of 900 32-bit words will require about 280 feet of tape; therefore one reel will hold six to seven orbits (data files). The orbits will not necessarily be in precise chronological order. A double end-of-file (DEOF) will denote end of information on the tape. Table 3-6 provides a description of the calibrated, located radiance tape format.

### 3.3.4 Data Archiving

The NSSDC will maintain an archival file of all HIRS imagery, and tapes of calibrated, located radiances in the format described in Table 3-6.

Imagery will be archived in 70 mm roll format and will be available to the users as either positive or negative film, or paper products. When requesting imagery, a user should specify the date, orbit, and area of interest (by latitude and longitude), as well as the photographic product desired. All available HIRS photographic data will be listed in The Nimbus 6 Data Catalogs.

Table 3-6  
HIRS Calibrated, Located Radiance Tape Format

Word	Format	Description
1	I	Time (GMT in Seconds)
2	I	Julian Day (1-366)
3	I	Year (74, 75 or 76)
4-45	I	Days (Data Quality)
46-759	SPEC	IR Calibrated Channel Data (17 x 42)
760-801	F2	Latitude (+ is North)
802-843	F2	Longitude (+ is East)
844-885	F2	Zenith Angle (+ is North of Trackline)
886-900	-	Zero Fill
I	Integer quantities right adjusted in 32 bit fields.	
F2	Floating point quantities multiplied by a scaling factor of 100 and rounded (i.e., -145.824 would appear as -14582).	
F4	Floating point quantities multiplied by a scaling factor of 10000 and rounded (i.e., 10.98756 would appear as 109876).	
SPEC	This is a special format and is a combination of the I, F2, and F4 formats. The 17 IR channels will be repeated for each of the 42 earth samples. The long wave channels (1-10) will be in F2 format. The short wave channels (11-16) will be in F4 format. The visible channel (17) will be in the I format.	
Negative qualities are two's complement.		

When requesting HIRS calibrated, located radiance tapes, the user should specify the year, day, and time of data requested, as well as orbits and area of interest. The day and time (GMT) are important since this information is given for each scan of data. The Nimbus 6 Data Catalog HIRS information should be used to extract this data.

The address of the NSSDC and user ordering procedure are described in Section 1.7 of this report.

Tapes containing derived clear-column radiance and atmospheric parameters determined therefrom will be archived at GISS and/or at NOAA/NESS. Formats

of these tapes will be provided at the time of request. Specific requests for such processed data should be directed to:

Dr. W. L. Smith  
NOAA/NESS  
World Weather Building  
5200 Auth Road  
Marlow Heights, Maryland 20023

#### REFERENCES AND BIBLIOGRAPHY

1. Chen, Y. M., Woolf, H. M., Smith, W. L.: Vertical Resolution of Temperature Profiles for HIRS. NOAA Technical Report NESS 67, NESS, January 1974.
2. Davis, Paul A.: Atmospheric Transmittance Models for Infrared Radiometer Measurements. Final Report for NESS Contract 3-35208, March 1974.
3. Smith, W. L., Woolf, H. M., Abel, P. G., Hayden, C. M., Chalfont, M., and Grody, N: Nimbus-5 Sounder Data Processing System Part 1: Measurement Characteristics and Data Reduction Procedures. NOAA Technical Memorandum NESS 57, NESS, June 1974.

## SECTION 4

### THE SCANNING MICROWAVE SPECTROMETER (SCAMS) EXPERIMENT

by

D. H. Staelin, A. H. Barrett, and P. W. Rosenkranz

Massachusetts Institute of Technology

Cambridge, Massachusetts 02139

F. T. Barath, E. J. Johnson, J. W. Waters, and A. Wouters

Jet Propulsion Laboratory

California Institute of Technology

Pasadena, California 91103

and

W. B. Lenoir

Johnson Space Flight Center

Houston, Texas 77058

#### 4.1 Introduction

The Scanning Microwave Spectrometer (SCAMS) is a five-channel radiometer. Observations by the instrument will be used to produce global maps of tropospheric temperature profiles and, over ocean surfaces, the abundances of liquid water and water vapor in the atmosphere. Knowledge of these parameters is important for meteorological purposes, such as providing initial boundary conditions for numerical weather forecasting. Information about snow cover, ice type, soil moisture, and ocean roughness will also be contained in these multifrequency maps of the earth (References 4, 5, and 6).

SCAMS is an advancement of the successful microwave spectrometer experiment (NEMS) on Nimbus 5 (Reference 5). Whereas NEMS observed atmospheric parameters only at nadir along the subpoint track, SCAMS will scan to either side of this track and produce maps of these parameters with nearly full earth coverage every 12 hours, and with spatial resolution of about 145 km (80 nm) near nadir and 330 km (180 nm) at the scan limit.

#### 4.2 Scientific Objectives

The objectives of the SCAMS experiment are to:

- Determine the ability of SCAMS to map atmospheric temperature profiles from 0 km to 20 km, and to determine over oceans the abundance

of liquid water and water vapor in the atmosphere in the presence of clouds.

- Determine the usefulness of global maps of these meteorological variables and of other parameters such as snow and ice properties.
- Demonstrate improvements in the determinations of temperature profiles and other parameters available through combinations of microwave, infrared, and other data.
- Acquire a unique global data set for research and trial operational use. The data may be useful in GARP programs and could be incorporated in the DST program.

#### 4.3 Experiment Description

The SCAMS has five microwave channels, each centered on a different frequency. The frequency of channel 1 lies on a water vapor line near 22 GHz. Channel 2 is an atmospheric window near 32 GHz, and channels 3, 4, and 5 are within the oxygen band near 54 GHz. Table 4-1 gives the exact frequencies and performance characteristics of each channel. Each frequency is affected to a different degree by the terrestrial surface, clouds, precipitation, water vapor, and the atmospheric temperature profile. Therefore, by appropriately interpreting a set of simultaneous equations, most of these meteorological parameters can be estimated separately (References 2 and 7).

Table 4-1  
SCAMS Flight Model Performance Characteristics

Characteristics	Tolerance	Channel				
		1	2	3	4	5
Frequency (MHz)	+5	22.235	31.650	52.850	53.850	55.450
	Measured	22.231	31.650	52.863	53.845	55.445
RF Bandwidth (MHz)	+30, -10	220	220	220	220	220
Integration Time (ms)	±5	950	950	950	950	950
$\Delta I_{rms}$ ( $^{\circ}$ k/sec) (including antenna loss)	Max	1.0	1.0	1.5	1.5	1.5
	Measured	0.2	0.2	0.6	0.5	0.5

Table 4-1 (Continued)

Characteristics	Tolerance	Channel				
		1	2	3	4	5
Dynamic Range ( $^{\circ}$ K)	$\pm 20$	0-350	0-350	0-350	0-350	0-350
Absolute Accuracy ( $^{\circ}$ K rms) (Long Term)	Max	2 0	2 0	2 0	2 0	2 0
IF Frequency Range (MHz)	$\pm 10$	10-110	10-110	10-110	10-110	10-110
	Measured	6-117	7-114	8-118	7-120	7-122
Antenna Beamwidth (deg)	$\pm 0.2$	7.5	7.5	7.5	7.5	7.5
	Measured	7.5	7.5	7.6	7.5	7.4
Antenna Beam Efficiency (%) (within 10 deg. of center)	Measured	97.3	97.3	96.9	97.1	97.4

Scanning is achieved by stepping a reflector in front of each antenna. Each reflector, inclined at 45 degrees to its antenna, scans the antenna beam in a lefthanded sense with respect to the spacecraft velocity vector. A 360 degree scan takes 16 seconds. Figure 4-1 shows a schematic representation of the stepping direction, sequence, and time required to move to the sample position. Thirteen earth data samples, each separated by a 7.2 degree scan step, are recorded between 43.2 degrees to the left of the nadir and 43.2 degrees to the right of the nadir. The step-plus-sample for each earth location takes one second. Three seconds at the end of each earth scan are reserved for calibration and reflector rotation. Calibration includes one-second views of space and of an instrument blackbody source.

The antenna beamwidths of 7.5 degrees give ground resolutions of approximately 145 km (80 nm) at nadir and 330 km (180 nm) at 43 degrees from nadir. The  $\pm 43.2$  degrees of earth scan cover a 2400 km (1300 nm) swath, thus providing overlapping coverage above middle latitudes on successive orbits.

The polarization vector rotates as the beam scans. At nadir, polarization is parallel to the satellite velocity vector for all the channels except the channel 5 oxygen channel. For channel 5, at nadir, the polarization is perpendicular.

The instrument outputs are sampled once per second by VIP, and stored on a HDRSS for transmission to the ground. Normally all channels will operate simultaneously. However, any subset of the channels could operate alone should spacecraft power limitations make it necessary.

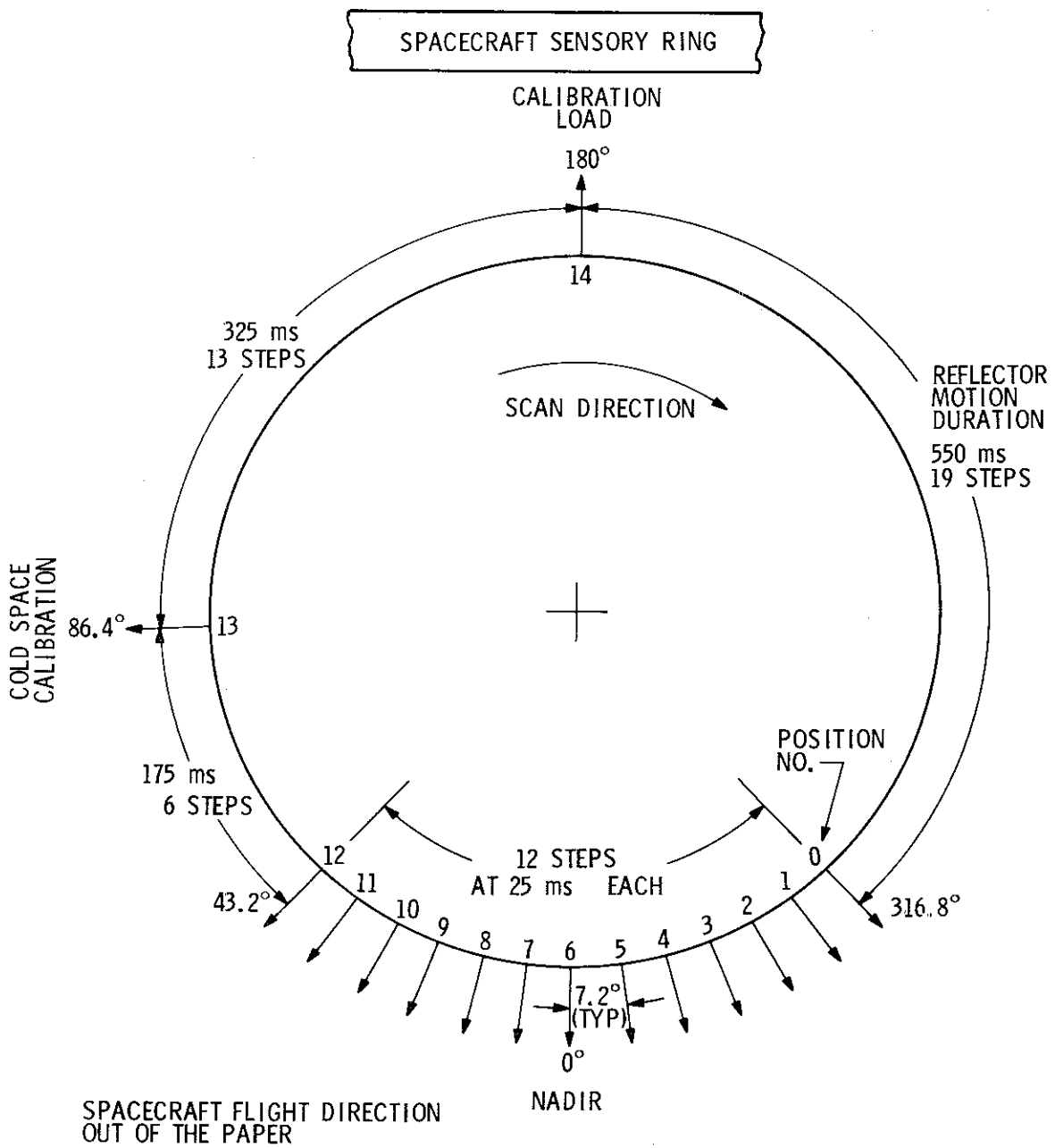


Figure 4-1. SCAMS Antenna Reflector Positions

The experiment can be considered as composed of two parts: 1) The three channels near 5 mm wavelength which are used to obtain atmospheric temperature profiles and, 2) the two channels near 1 cm wavelength which are sensitive

over oceans to atmospheric water vapor and liquid water, and over land to surface emissivity and temperature. Although these two parts could operate separately, the performance is superior when they are interpreted simultaneously; the water vapor and liquid water measurements will improve the temperature profile measurements and vice versa.

The intensity of microwave radiation is customarily expressed in terms of an equivalent brightness temperature  $T_B$  ( $^{\circ}$ K), which is the temperature of a blackbody that would radiate the same power. The brightness temperature perceived by the satellite has a surface and an atmospheric component. These can be expressed as

$$T_B(\nu) = \epsilon T_S e^{-\tau\nu} + \int_0^{\infty} T(h) W(h, \nu) dh. \quad (1)$$

The component contributed by the surface is equal to the average over the antenna beamwidth of the product of the surface emissivity  $\epsilon$ , the surface temperature  $T_B$ , and the atmospheric transmissivity  $e^{-\tau\nu}$ .

The atmospheric component for the oxygen channels, where the atmosphere is nearly opaque, can be expressed as the integral of the atmospheric temperature profile,  $T(h)$ , weighted by the weighting function  $W(h, \nu)$  (Reference 1). The weighting function is weakly dependent upon atmospheric water content, temperature profile, and surface reflectivity, and more strongly dependent on view angle. Each channel corresponds to a different weighting function  $W(h, \nu)$ , similar to those at infrared wavelengths, where  $h$  is altitude and  $\nu$  is frequency. The weighting function of the three oxygen band channels are shown in Figure 4-2 at nadir and at the maximum view angle (43.2 degrees). The temperature profile determinations should be nearly unaffected by cirrus clouds or clouds with less than  $0.01 \text{ gm/cm}^2$  liquid water. For more dense clouds ( $0.1 \text{ gm/cm}^2$ ) the error should normally be less than about  $2^{\circ}\text{K}$  over land and  $1^{\circ}\text{K}$  over ocean. Since such clouds rarely fill the entire viewing zone, the error is usually less. After calibration, the accuracy of the radiometer measurements should be approximately  $1^{\circ}\text{K}$ , and the accuracy of the infrared temperature profile should normally be  $1^{\circ}\text{K}-4^{\circ}\text{K}$  when compared with the National Meteorological Center 0<sup>h</sup> GMT and 12<sup>h</sup> GMT analyses.

The two channels near 1 cm wavelength permit water vapor and cloud water content over the ocean to be estimated separately. This is possible because over the ocean the 9 mm channel is approximately twice as sensitive to clouds as the 13 mm channel, but is only 0.4 times as sensitive to water vapor. Water vapor may be estimated with approximately  $0.2 \text{ gm/cm}^2$  accuracy, and clouds

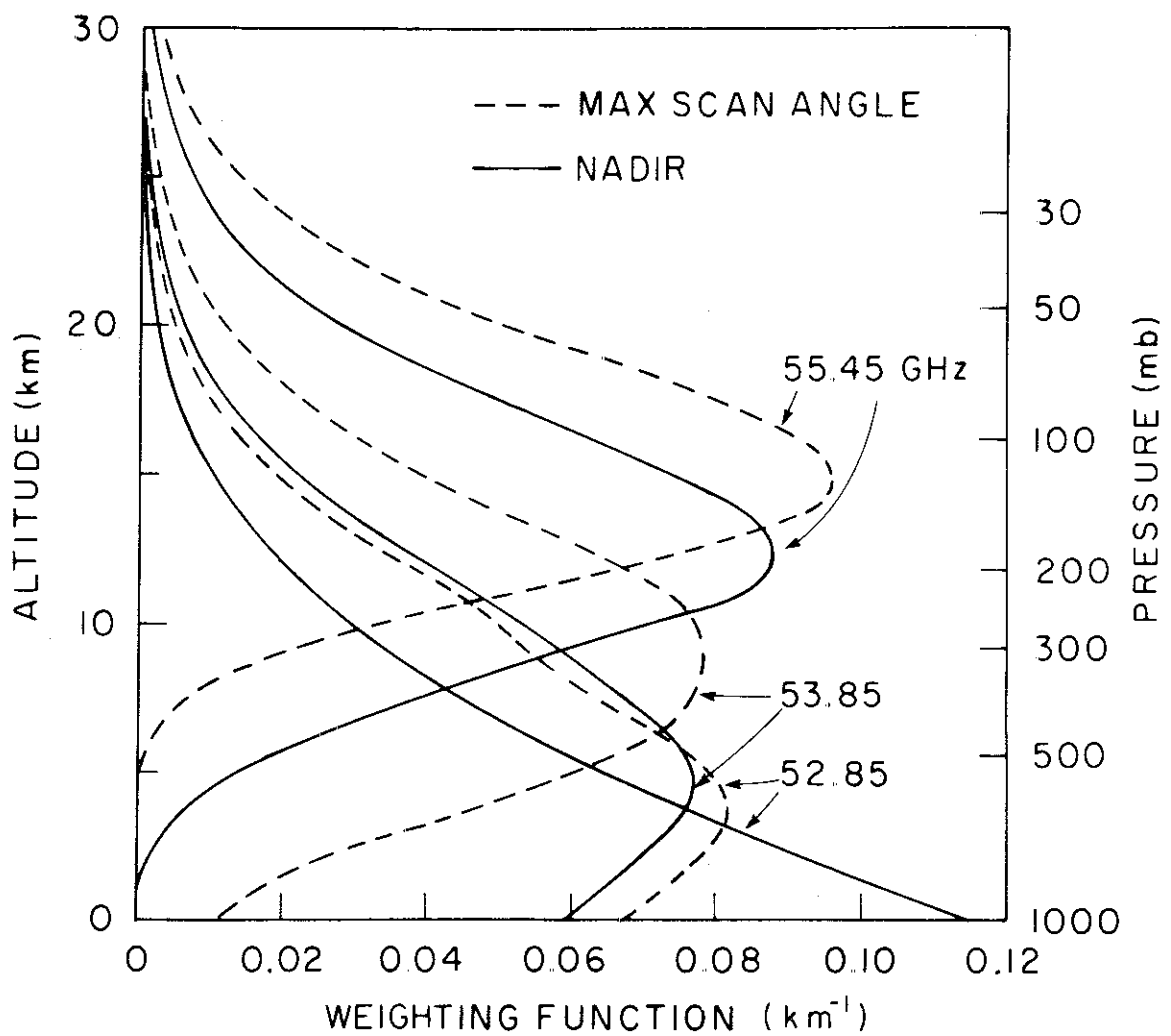


Figure 4-2. SCAMS Weighting Functions. These include a component which is reflected from the surface, assumed to be seawater.

with approximately  $0.02 \text{ gm/cm}^2$  accuracy. Significant sources of error include uncertainties in the altitude distribution of water vapor, heavy seas with much foam, and the reflection of sunlight near the equator at noon (Reference 3).

In addition to the measuring atmospheric parameters, SCAMS measurements can be used to study the properties of ice types, snow cover, and soil moisture. Over land, the two water channels will yield an estimate of surface temperature for regions where the surface emissivity has been calibrated by comparison of microwave and direct temperature measurements, and estimates of surface emissivity in those regions where surface temperature is known.

The SCAMS experimenter computer processes the data to obtain estimates of:

- Antenna temperatures
- Brightness temperatures
- Atmospheric temperature profiles
- Water vapor abundances
- Liquid water abundances

Many of these analyzed products will then be compared with the Nimbus THIR observations, other Nimbus sounding data, radiosondes, ground-based weather reports, etc. These comparisons will determine:

- The accuracy of SCAMS estimates
- The relationship between the estimate accuracy and the nature of the clouds, precipitation, surface effects, water vapor profile, and temperature profile
- The improvements in weather forecasting and modeling available from combinations of sensor types, such as microwaves, infrared, surface measurements, super-pressure balloons, etc.
- The character of any interesting meteorological phenomena observed during SCAMS operations

#### 4.4 Description of the Instrument

##### 4.4.1 Physical Description and Performance Characteristics

A photograph of the SCAMS instrument mounted in its assembly fixture is shown in Figure 4-3. The assembly fixture simulates the Nimbus spacecraft mounting ring and provides support for the instrument during testing and shipping. The O<sub>2</sub> module, containing channels 3, 4, and 5, and antenna/scan support assembly with the single O<sub>2</sub> antenna is mounted to the left. The H<sub>2</sub>O module containing channels 1 and 2, with the antenna/scan support assembly and two antennas, is in the middle and right portions of the photograph. The power supply is in the upper right portion. The O<sub>2</sub> and H<sub>2</sub>O scan mechanisms are

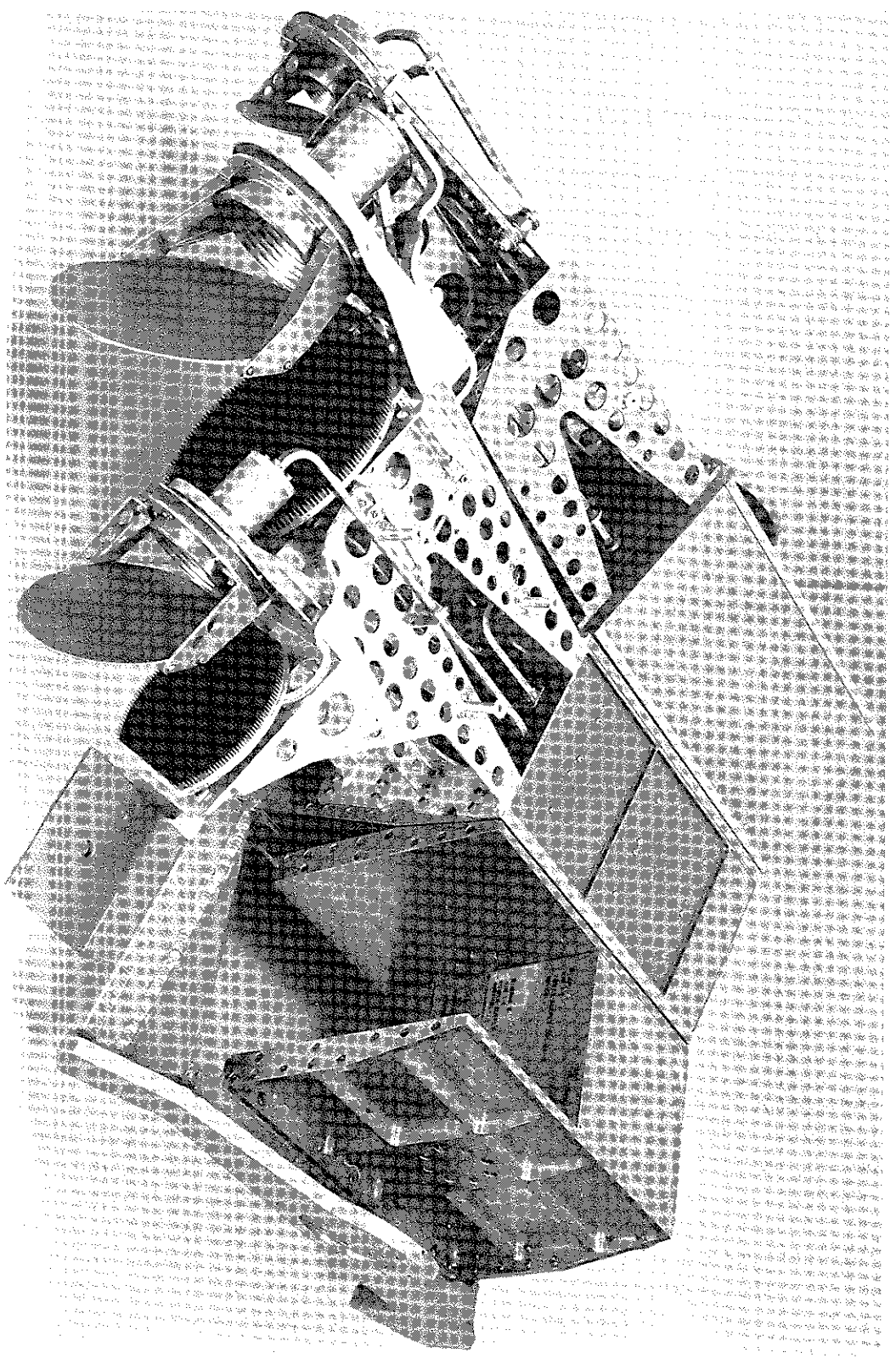


Figure 4-3. SCAMS with Infrared Shield Removed to Show Blackbody Calibration Loads and Antenna Structure

connected by a flexible shaft coupling, which allows separate installation of the O<sub>2</sub> and H<sub>2</sub>O modules into the Nimbus ring. The three blackbody calibration targets may be seen mounted directly below each antenna. Normally the calibration targets are covered with an IR shield, but this has been removed so the ridged type structure may be viewed.

The SCAMS flight model performance characteristics are listed in Table 4-1.

#### 4.4.2 Functional Description

A functional block diagram of the SCAMS system is shown in Figure 4-4. The six functional units are:

- The H<sub>2</sub>O radiometer (Channels 1 and 2)
- The O<sub>2</sub> radiometer (Channels 3, 4, and 5)
- The scan subsystem
- The data unit
- The power supply
- The bench checkout equipment (BCE)

The first five of these are flight equipment, the sixth one is ground support and calibration equipment.

The functional block diagram of the SCAMS instrument proper is shown in Figure 4-5. To a large extent, the blocks in Figure 4-5 represent physical components within the assemblies, e.g., each radiometer has the following separate components:

- Calibration target
- Signal antenna
- Dicke switch
- Isolator
- Reference and base loads

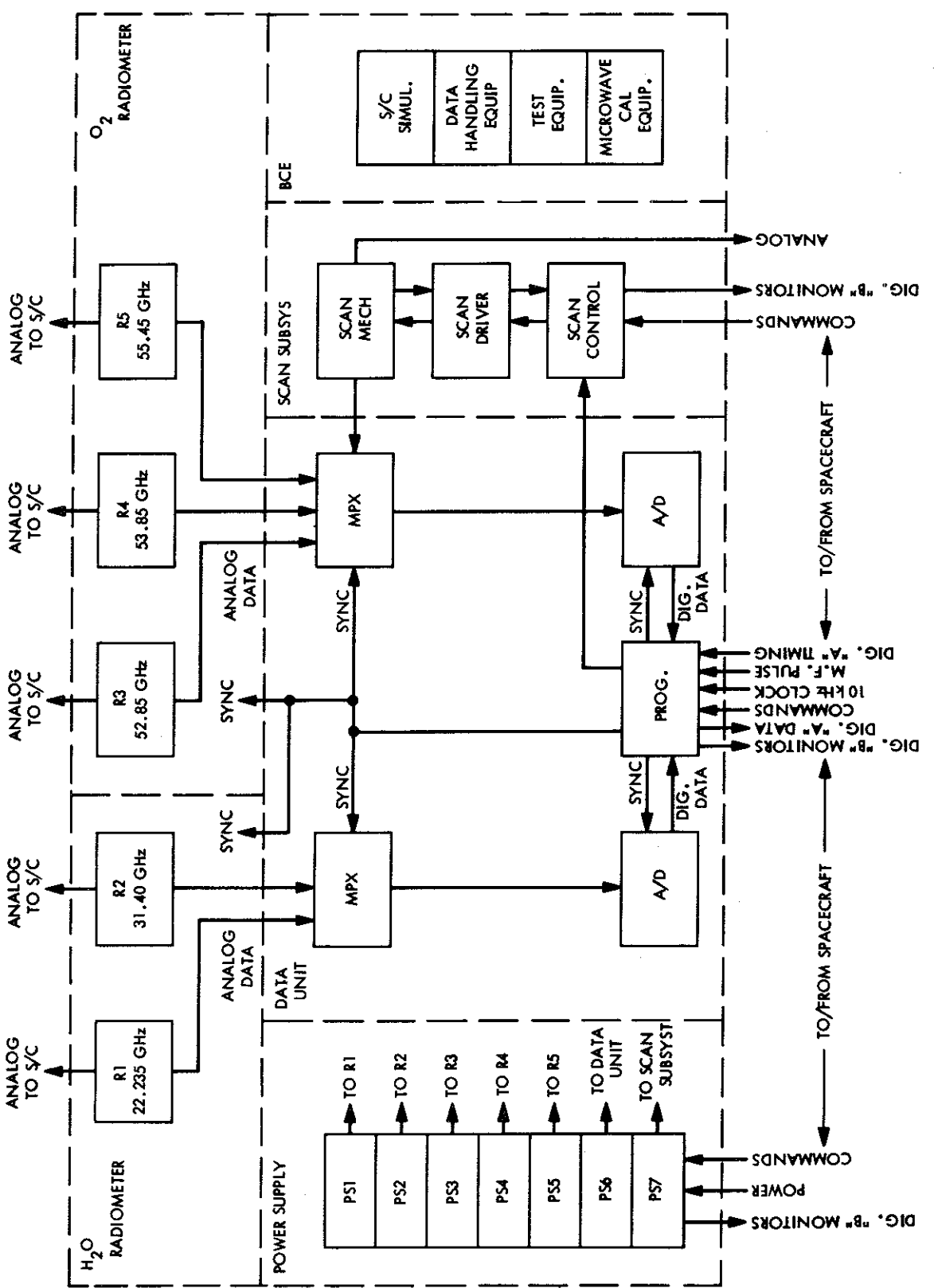


Figure 4-4. SCAMS Functional Block Diagram

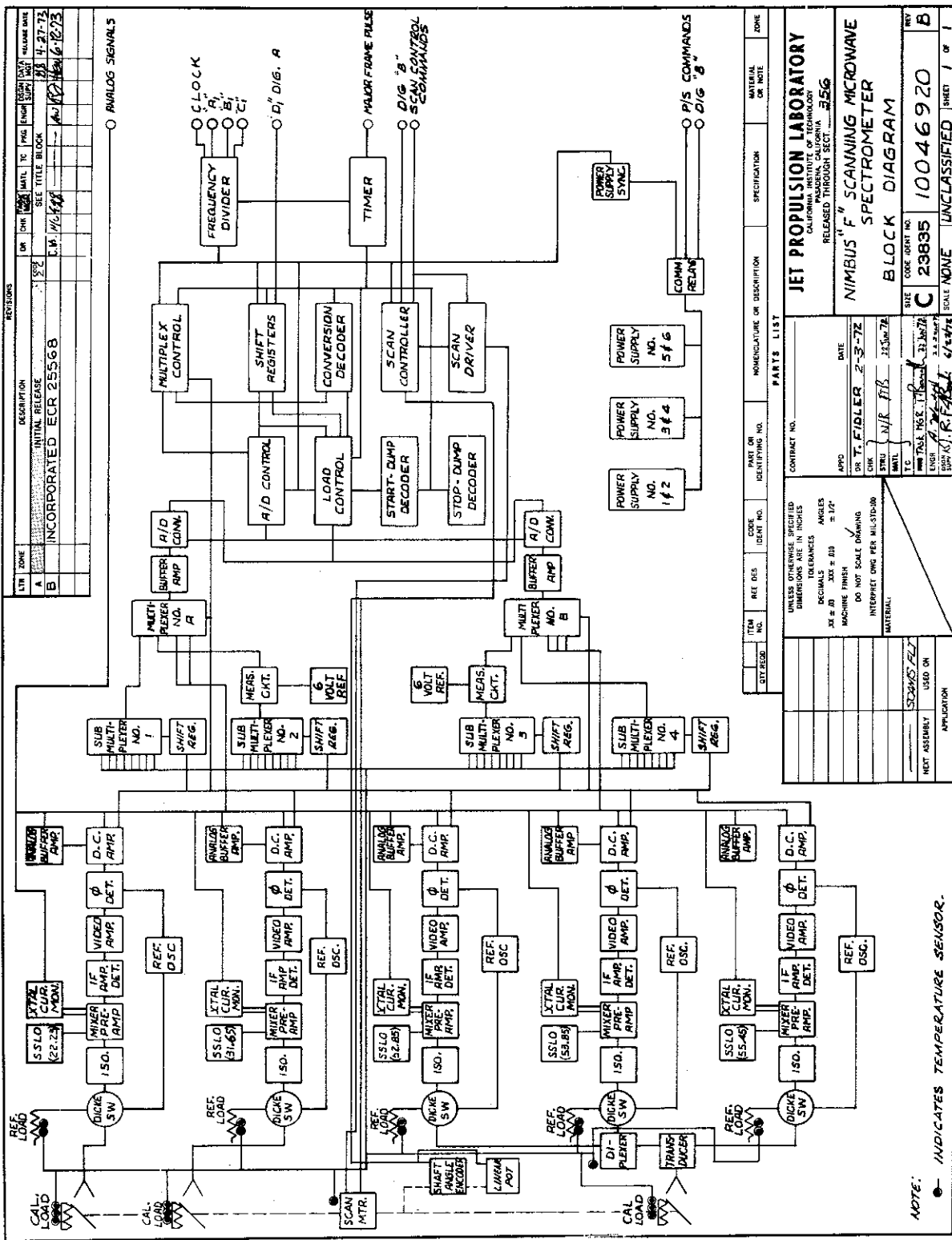


Figure 4-5. SCAMS System Block Diagram

- Mixer, IF preamp
- Solid state local oscillator
- IF amp, detector, video amp
- Video, phase detector, dc amp
- Reference oscillator switch trigger and switch driver
- Temperature and engineering monitor transducers

The 22.2 GHz and 31.65 GHz radiometer channels are completely independent, sharing no components in common. The three O<sub>2</sub> radiometer channels share a common calibration target and antenna. A channelizing filter separates the frequencies of two of the O<sub>2</sub> channels, and starting with the Dicke switches, all three O<sub>2</sub> channels are independent and have a configuration identical to the H<sub>2</sub>O channels.

The scan subsystem consists of the scan controller, the scan drive, and the scan mechanism. The scan controller receives the scan program and controls the scan stepping and timing sequences. The scan driver system includes the scan motor, motor drive electronics, and position readouts. The scan mechanism consists of a shaft, pulleys, belts, and bearings. None of the scan mechanisms are sealed. Due to their physical mounting on the scan mechanism structure, the calibration targets are included in this subsystem.

The scan controller receives inputs from the data programmer, the spacecraft commands, the shaft angle encoder, and the scan motor, and delivers the control signals to the scan driver. The scan driver sends drive pulses to the scan motor coils. The scan mechanism then steps the reflectors. The magnitude, duration, and sequence of pulses are commanded by the scan controller. Power for the drive is derived from the spacecraft regulated voltage and includes appropriate filtering. Redundant digital and analog motor shaft angle readouts are provided.

The system is designed so alignment and synchronization of the three antenna beams is achieved to within  $\pm 0.2$  degrees without major adjustments on the spacecraft and is maintained throughout the spacecraft test, launch, and in-orbit environment.

The primary radiometer data are integrated, then sequentially sampled by two primary multiplexers A and B. The auxiliary radiometer data are sampled

by submultiplexers one through four. By digitizing the analog data in an A/D converter within each of the two radiometer modules, the noise from the spacecraft is minimized. The commutated digitized data are placed in shift registers and read out by the spacecraft into the VIP Digital A spacecraft data system at a rate of one word per tenth of a second. There are two words per minor frame and 160 words per major frame. It takes 16 seconds to accumulate a major frame. Since ten data words at a time are loaded in rapid sequence into the registers, the slower VIP readout introduces a delay in the SCAMS data stream of as much as one second with respect to real time. This, however, does not represent a problem since the data incorporate an index every 16 seconds. Key radiometer analog signals and digital indications of radiometer state are fed into the spacecraft Digital B data system to meet spacecraft requirements and to supply redundant data capability.

The Digital A data constitute the primary output of the instrument. Included are the outputs of five radiometer channels, the scan position encoder, the mixer crystal currents, several temperatures, and other information necessary for complete reduction of the instrument data and for monitoring instrument performance. The five radiometer channel outputs and the scan position encoder are read out once per second; the other data are sampled at longer intervals through submultiplexing. The sub-multiplexers go through two complete cycles during each major frame. All analog to digital conversions in the instrument are performed to an accuracy of 10 bits.

The output format of the digital data is shown in Table 4-2. Word 0, set to 1777, base 8 (1023, base 10) is used to index the data. Word 80 is an instrument serial number indicator. The total of 160 words per major frame is divided in a fixed sequence into any two VIP data matrix columns. The E-CAL and T-CAL samples are known high or low voltages which calibrate the voltage or temperature sensors, respectively.

Digital B indications of radiometer status will be supplied as indicated in Table 4-3.

Buffered analog output of the five radiometer channels, of the scan position indicator, and of other key instrument parameters are provided for quick-look capability and for backup in case of digital data failure. The analog outputs of the instruments and required sampling rates are listed in Table 4-4.

Figure 4-6 is the SCAMS timing diagram.

The antenna patterns are not significantly affected by the view angle and have high beam efficiencies, which simplifies the conversion of the antenna

**Table 4-2**  
**SCAMS Data Format**  
**in the VIP Digital A Matrix**

150 H <sub>2</sub> O E-CAL LO	151 H <sub>2</sub> O T-CAL HI	152 O <sub>2</sub> I-CAL HI	153 O <sub>2</sub> E-CAL LO	154 SCAN POS 14	155 DATA CAL CH 1	156 DATA CAL CH 2	157 DATA CAL CH 3	158 DATA CAL CH 4	159 DAIA CAL CH 5
0 SCAMS INDEX 1777	1 22.2 CAL LOAD	2 O <sub>2</sub> CAL LOAD	3 +XIAL CH 3	4 SCAN POS X	5 ZERO CHECK CH 1	6 ZERO CHECK CH 2	7 ZERO CHECK CH 3	8 ZERO CHECK CH 4	9 ZERO CHECK CH 5
10 +XIAL CH 1	11 31.6 CAL LOAD	12 O <sub>2</sub> CAL LOAD	13 -XTAI CH 3	14 SCAN POS 0	15 DATA CH 1	16 DAIA CH 2	17 DAIA CH 3	18 DAIA CH 4	19 DAIA CH 5
20 -XIAL CH 1	21 22.2 CAL LOAD	22 FILIER TEMP	23 +XIAL CH 4	24 SCAN POS 1	25↑	26↑	27↑	28↑	29↑
30 +XIAL CH 2	31 31.6 CAL LOAD	32 52.8 REF LOAD	33 -XIAL CH 4	34 SCAN POS 2	35	36	37	38	39
40 -XIAL CH 2	41 22.2 REF LOAD	42 53.8 REF LOAD	43 +XIAL CH 5	44 SCAN POS 3	45	46	47	48	49
50 -XIAL CH 5	51 31.6 REF LOAD	52 55.4 REF LOAD	53 5V REF	54 SCAN POS 4	55	56	57	58	59
60 H <sub>2</sub> O E-CAL HI	61 H <sub>2</sub> O T-CAL LO	62 O <sub>2</sub> I-CAL LO	63 O <sub>2</sub> E-CAL HI	64 SCAN POS 5	65↓	66↓	67↓	68↓	69↓
70 H <sub>2</sub> O E-CAL LO	71 H <sub>2</sub> O T-CAL HI	72 O <sub>2</sub> I-CAL HI	73 O <sub>2</sub> E-CAL LO	74 SCAN POS 6	75 DAIA CH 1	76 DATA CH 2	77 DATA CH 3	78 DATA CH 4	79 DATA CH 5

Table 4-2 (Continued)

80 INSIR S/N	81 22.2 CAI LOAD A	82 O2 CAI LOAD A	83 +XIAL CH 3	84 SCAN POS 7	85 DATA CH 1	86 DATA CH 2	87 DATA CH 3	88 DATA CH 4	89 DATA CH 5
90 +XIAL CH 1	91 31.6 CAI LOAD A	92 O2 CAL LOAD B	93 -XIAL CH 3	94 SCAN POS 8	95 ↑	96 ↑	97 ↑	98 ↑	99 ↑
100 -XIAL CH 1	101 22.2 CAI LOAD B	102 FILTER TEMP	103 +XIAL CH 4	104 SCAN POS 9	105	106	107	108	109
110 +XIAL CH 2	111 31.6 CAI LOAD B	112 52.8 REF LOAD	113 -XTAL CH 4	114 SCAN POS 10	115	116	117	118	119
120 -XIAL CH 2	121 22.2 REF LOAD	122 53.8 REF LOAD	123 +XIAL CH 5	124 SCAN POS 11	125 ↓	126 ↓	127 ↓	128 ↓	129 ↓
130 -XIAL CH 5	131 31.6 REF LOAD	132 55.4 REF LOAD	133 5V REF	134 SCAN POS 12	135 DATA CH 1	136 DATA CH 2	137 DATA CH 3	138 DATA CH 4	139 DATA CH 5
140 H <sub>2</sub> O E-CAI HI	141 H <sub>2</sub> O T-CAI LO	142 O <sub>2</sub> I-CAI LO	143 O <sub>2</sub> E-CAI HI	144 SCAN POS 13	145 DATA SKY CH 1	146 DATA SKY CH 2	147 DATA SKY CH 3	148 DATA SKY CH 4	149 DATA SKY CH 5

Table 4-3  
SCAMS Digital B Status Indicators

Level 1	Level 0
Channel 1 on Channel 2 on Channel 3 on Channel 4 on Channel 5 on Data Subsystem on Scan Subsystem on System Reset Zero Position Defeat	Channel 1 off Channel 2 off Channel 3 off Channel 4 off Channel 5 off Data Subsystem off Scan Subsystem off Scan Enable Zero Position Enable

Table 4-4  
SCAMS Analog Data Output and Sampling Rates

Data	Samples/Second
Channel 1 data	1/1
Channel 2 data	1/1
Channel 3 data	1/1
Channel 4 data	1/1
Channel 5 data	1/1
Scan Position	1/1
Ch. 1 Cal target temp.	1/16
Ch. 2 Cal target temp.	1/16
Ch. 1 Ref. load temp.	1/16
Ch. 2 Ref. Load temp.	1/16
O <sub>2</sub> Cal target temp.	1/16
Scan motor temp.	1/16
Ch. 3 Ref. load temp.	1/16
Ch. 4 Ref. load temp.	1/16
Ch. 5 Ref. load temp.	1/16
H <sub>2</sub> O Thermistor bias	1/16
O <sub>2</sub> Thermistor bias	1/16

temperatures to brightness temperatures. The antenna pattern for channel 1 at position 8 (14.4 degrees from nadir) is shown in Figure 4-7, where the plot covers  $\pm 100$  degrees from boresight and the base is at -50 dB. A more quantitative antenna pattern is presented for channel 1 at position 6 (nadir) in Figure 4-8. The plane of this pattern is parallel to the spacecraft velocity vector. The two major sidelobes near 60 degrees and 90 degrees result from the spillover energy toward the rear of the spacecraft passing the lip of the reflector plate.

#### 4.5 Data Processing, Format, and Availability

##### 4.5.1 Data Processing

All SCAMS data will be acquired at the Rosman and Alaska STDN stations and relayed to the MDHS at GSFC. After each interrogation orbit, the MDHS will produce one 4" x 5" negative of the SCAMS data and a SCAMS User Formatted Output tape containing SCAMS, ESMR, and NOAA Forecast Data. These tapes and copies of the SCAMS imagery will be mailed to the SCAMS experimenter at MIT. There, the data will be processed to yield estimates of the antenna and brightness temperatures, atmospheric temperature profiles, water vapor

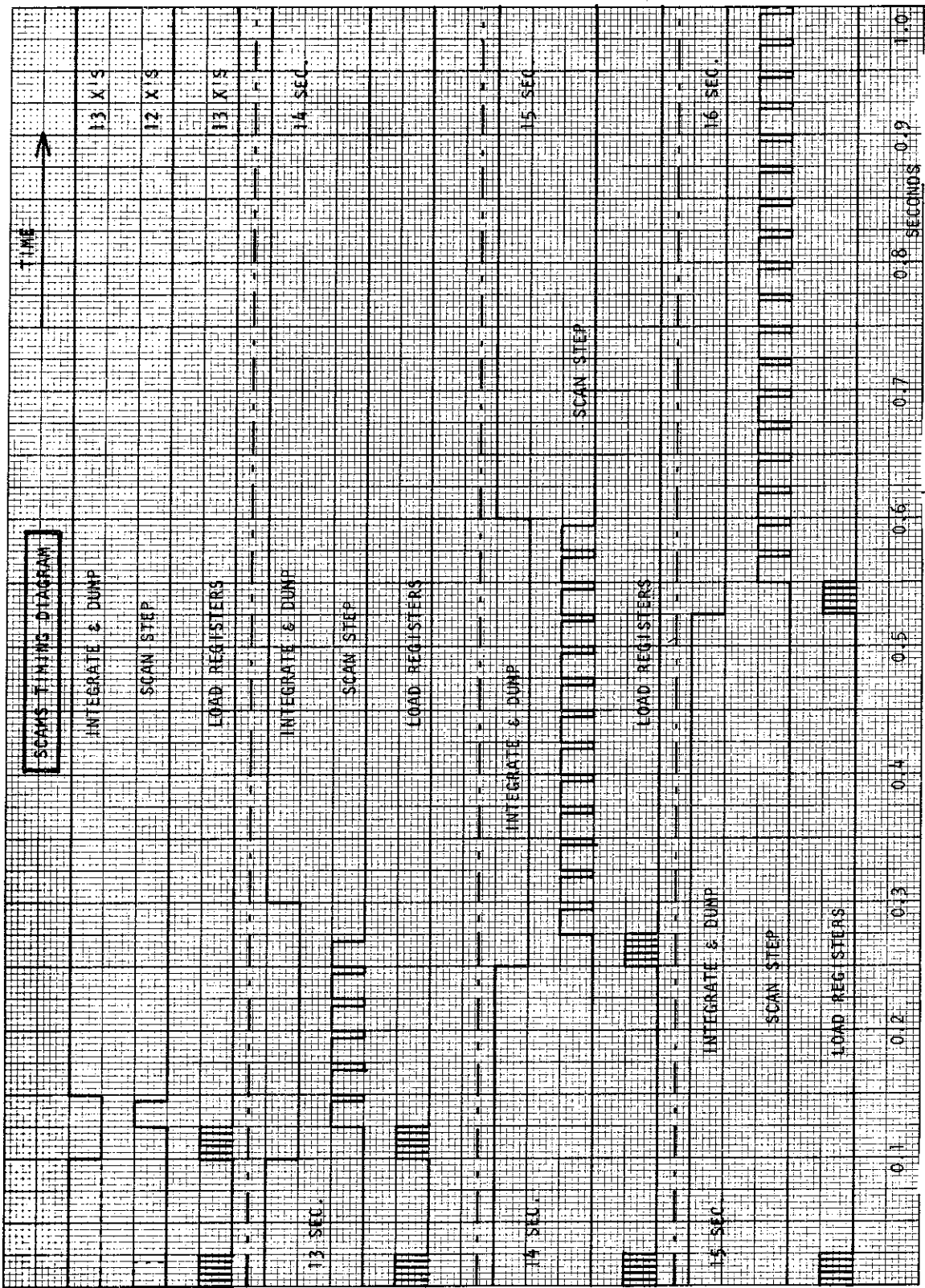


**Figure 4-6.** SCAMS Timing Diagram for a 16-second Cycle. It shows periods when the data is integrated, the antenna is stepped to its next position, and the data registers are loaded for subsequent transmission to VIP.

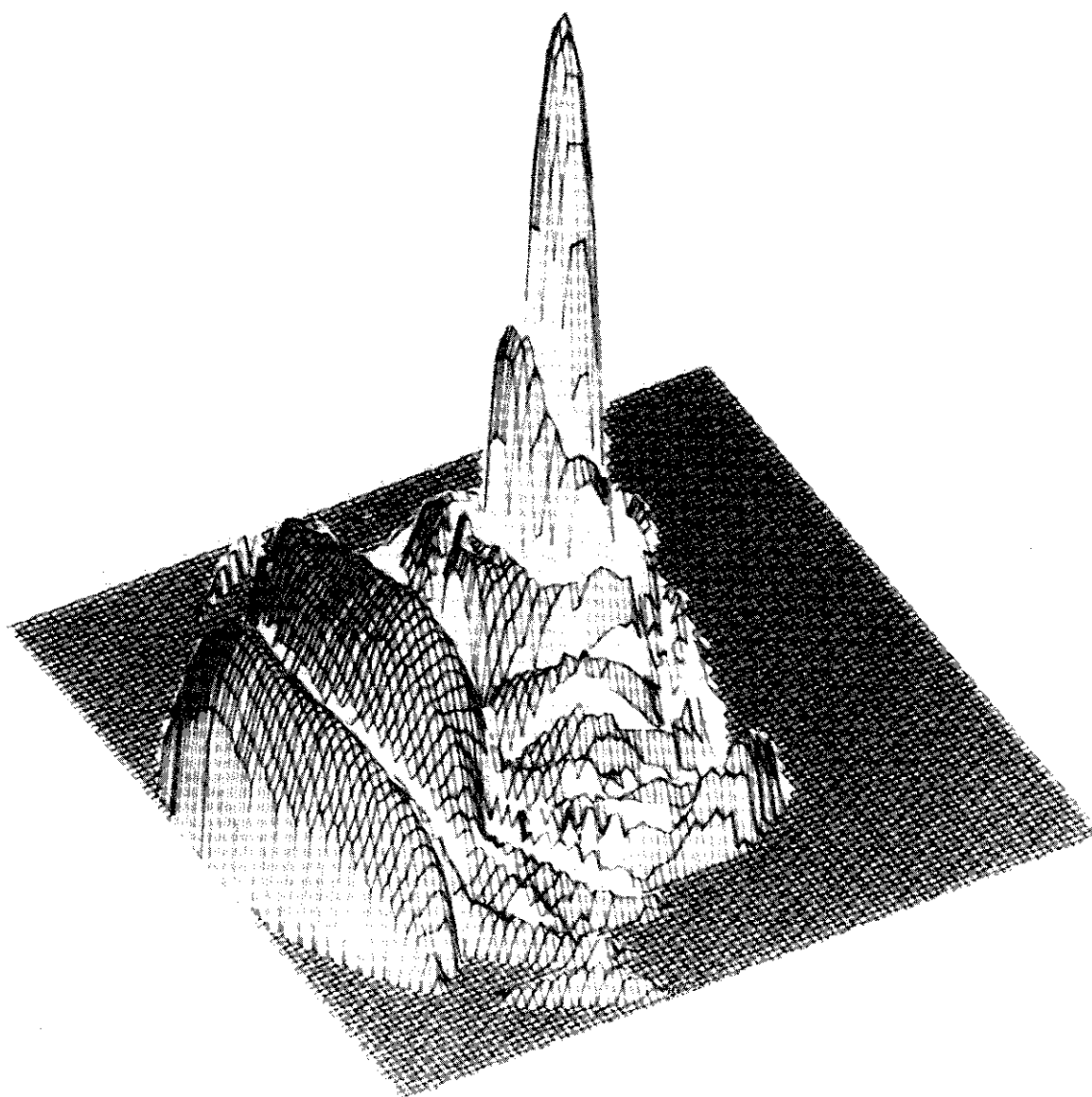


**Figure 4-7.** Antenna Pattern for Channel 1 at Position 8. Plot is  $\pm 100$  degrees from boresight and the base is at -50 dB.

and liquid abundances. These estimates, the original SCAMS data, and other coordinated information will be formatted as archival tapes on nine-track magnetic tapes. These tapes will be sent to the NSSDC at GSFC.

#### 4.5.2 Image Format

All SCAMS data will be converted to 4" x 5" black and white images at the MDHS at GSFC. The NADUC will reproduce and distribute initial copies of

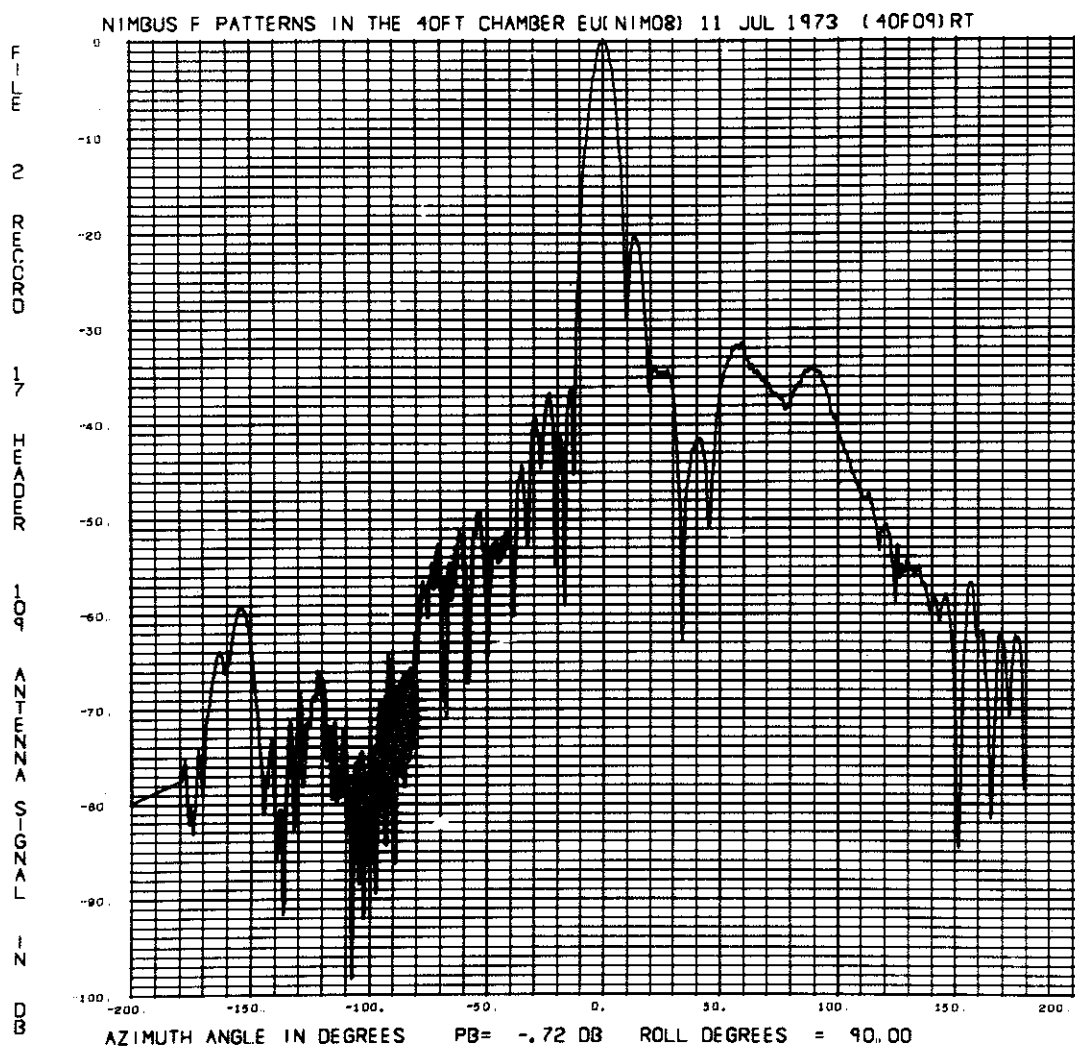


Figure 4-8. Antenna Pattern for Channel 1 at Position 6. Plot is along ground track, with positive angles corresponding to positions behind the spacecraft. Vertical scale is dB.

these images. Normally, the SCAMS data will be displayed by itself. However, there is an MDHS option to display a combination of SCAMS and ESMR data. The combination display will be a composite of standard display options for SCAMS and ESMR and, therefore, is not presented in detail in this report. The format and details of the planned SCAMS display is described below. Figure 4-9 is a sample of the SCAMS display and should be used as a reference for the following description.

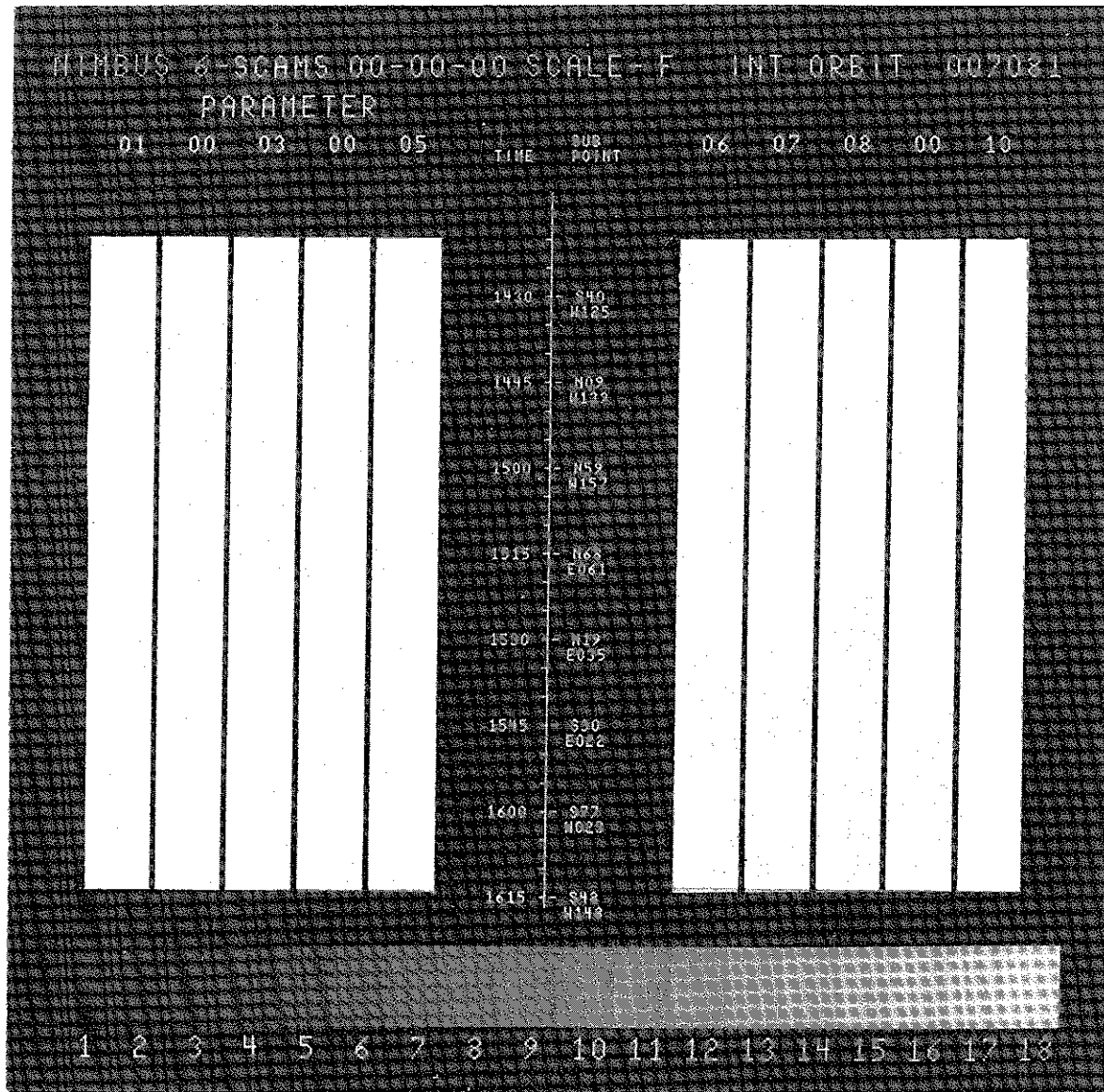


Figure 4-9. SCAMS EIS Display Format

- NIMBUS 6-SCAMS

This identifies the satellite (Nimbus 6) and the experiment (SCAMS).

- DATE

This identifies the Greenwich month, day, and year the data was recorded on board the satellite.

- SCALE (F, P1, or P2)

The data from each orbit will be displayed as an image at full vertical scale (F) or at partial vertical scale (P). In the full scale mode, up to 125 minutes of data will be output on a single image (and labeled as SCALE-F). In the partial scale mode the data is displayed at twice the vertical scale used in the full scale mode. Usually, in the partial scale mode, two images are needed to display all the data. The last 60 minutes of the data is output first (and the image is labeled SCALE-P2). Any remaining data from each interrogation orbit is output on a second image (and labeled SCALE-P1). Note that P1 contains the data acquired earliest. If there is less than 65 minutes of data from an interrogation orbit, only a P2 image is produced. In the full scale (F) mode each scan line of SCAMS data is displayed three times in succession.

In the partial scale (P) mode, each scan line is displayed six times in succession. In both modes, each of the 13 scan spot elements across a scan is displayed ten times for a total of 130 display spots across each line.

- GRAY SCALE

Each image has an 18-step gray scale along the bottom of the display. The gray scale defines the brightness temperature for the swaths labeled 1, 2, 6, 7, 11, and 12 by assigning a different brightness temperature range to the gray scale for each of these swath displays. Tables 4-5 and 4-6 define the planned temperature range of gray scale values for each of these swath displays. If these assigned values should be changed after launch, The Nimbus 6 Data Catalogs will list the new values.

Table 4-5  
Gray Scale Number versus SCAMS Antenna Temperature for Image Swaths Labeled 1, 2, 6, and 7 on the SCAMS EIS Displays

Gray Scale Number	Antenna Temperature (°K)
(black) 1	<100
2	100-114
3	114-128
4	128-141
5	141-155
6	155-169

Table 4-5 (Continued)

Gray Scale Number	Antenna Temperature (°K)
7	169-183
8	183-196
9	196-210
10	210-224
11	224-238
12	238-251
13	251-265
14	265-279
15	279-293
16	293-306
17	306-320
(white) 18	> 320

The image swaths labeled 1 and 6 present data for SCAMS channel 1 (22 GHz water vapor channel)

The image swaths labeled 2 and 7 present data for SCAMS channel 2 (32 GHz window channel)

The displays of antenna temperatures for image swaths labeled 1 and 2 are uncorrected for scan angle from nadir. Swaths labeled 6 and 7 are corrected for scan angle from nadir.

Table 4-6  
Gray Scale Number versus Water Vapor and Liquid Water Values for Image Swaths Labeled 11 and 12 on the SCAMS EIS Displays

Gray Scale Number	Swath #11 Water Vapor (gm/cm <sup>2</sup> )	Swath #12 Liquid Water (gm/cm <sup>2</sup> )
(black) 1	< 0.35	< 0.18
2	0.35-0.71	0.18-0.35
3	0.71-1.06	0.35-0.53
4	1.06-1.41	0.53-0.71
5	1.41-1.76	0.71-0.88
6	1.76-2.11	0.88-1.06
7	2.11-2.47	1.06-1.24
8	2.47-2.82	1.24-1.41

Table 4-6 (Continued)

Gray Scale Number	Swath #11 Water Vapor (gm/cm <sup>2</sup> )	Swath #12 Liquid Water (gm/cm <sup>2</sup> )
9	2.82-3.18	1.41-1.59
10	3.18-3.53	1.59-1.76
11	3.53-3.88	1.76-1.94
12	3.88-4.24	1.94-2.12
13	4.24-4.59	2.12-2.29
14	4.59-4.94	2.29-2.47
15	4.94-5.29	2.47-2.65
16	5.29-5.65	2.65-2.82
17	5.65-6.00	2.82-3.00
(white) 18	> 6.00	> 3.00

The image swath labeled 11 contains data derived from SCAMS channel 1 (22 GHz water vapor channel).

The image swath labeled 12 contains data derived from SCANS channel 2 (32 GHz window channel).

- INT ORBIT

The interrogation orbit identifies the orbit during which the recorded data are transmitted to a STDN station. Usually parts of two data orbits are on the same display. The interrogation orbit number will only identify the last orbit of each display.

- TIME (and) SUBPOINT

Satellite time and latitude-longitude information are presented along the vertical line down the center of each display. The line represents the satellite subpoint track, which is located down the center of each swath on each display. TIME is GMT with time ticks along the left side of the line at each five minute mark (on the five minutes). TIME is annotated (hour and minute) every 15 minutes (on the quarter hour). SUBPOINT information presents latitude and longitude positions of the satellite subpoint. Each tick mark on the right side of the vertical line is annotated with the subpoint latitude and longitude (to the nearest degree). Latitude is labeled N (north) or S (south). Longitude is labeled E (east) or W (west).

- PARAMETER

There are 15 possible swath display options of the five channels of SCAMS data. Only ten, however, can be shown on each image display. All swaths on each display contain the same coverage information, but each contains different temperature or spectral information. Swaths labeled 1 through 5 show the antenna temperatures of channels 1 through 5 uncorrected for scan angle from nadir. Swaths labeled 6 through 10 show the same antenna temperatures corrected for the attenuation of temperature as the scan angle increases from nadir. Swaths 11 and 12 show the water vapor and liquid water content of the atmosphere as derived from the data in SCAMS channels 1 and 2. The swaths labeled 13, 14, and 15 (using SCAMS channels 3, 4, and 5) give the average temperature between the 1000 mb-500 mb, 500 mb-250 mb, and the 250 mb-100 mb levels.

Each swath is identified by a header block label (number 1 through 15). These headers identify the class of SCAMS data for each swath. Tables 4-5 and 4-6 define the SCAMS channel 1 and 2 data displayed in swaths labeled 1, 2, 6, 7, 11, and 12 and the temperature range of the shades of gray for each swath. Table 4-7 defines the SCAMS channel 3, 4, and 5 data displayed in swaths labeled 3, 4, 5, 8, 9, 10, 13, 14, and 15. Temperature data in these swaths is contoured with the contour ranges and intervals for each swath shown in Table 4-7.

Table 4-7  
Temperature Values for the Three SCAMS Oxygen Channels  
Shown on the SCAMS EIS Displays

SCAMS Channel Number	Image Swath Number	Contour Range (°K)	Contour Interval (°K)	Item
3	3	210-300	2	Antenna temperature uncorrected for scan angle from nadir
4	4	200-280	2	
5	5	180-240	2	
3	8	210-280	2	Antenna temperature corrected for scan angle from nadir
4	9	210-270	2	
5	10	210-230	2	
3	13	240-290	2	Avg. temp. between 1000-500 mb

Table 4-7 (Continued)

SCAMS Channel Number	Image Swath Number	Contour Range (°K)	Contour Interval (°K)	Item
4	14	210-260	2	Avg. temp. between 500-250 mb
5	15	200-230	2	Avg. temp. between 250-100 mb
SCAMS channel 3 is at 52.85 GHz				
SCAMS channel 4 is at 53.85 GHz				
SCAMS channel 5 is at 55.45 GHz				

These swath displays and temperature ranges of each swath are preliminary. After launch other displays and temperature ranges may be used which will show more information. Any post-launch changes will be presented in The Nimbus 6 Data Catalogs.

#### 4.5.3 Tape Format

The format for the archival tape produced by the experimenter at MIT has not yet been fixed, but it should approximate the following.

The tapes will be standard 9-track 1600 BPI tapes each containing five files, i.e., a short header file which identifies the data contained on the tape, and four data files, one for each of four days. Each day contains an integral number of orbits and begins with the orbit in progress at 0<sup>h</sup> GMT.

The tapes are written in a blocked FORTRAN format with 1400 bytes per major frame, and a block size of 4200. Thus, three 16 second major frames comprise one 4200-byte block. The tape contents for each major frame are listed in Table 4-8.

#### 4.5.4 Data Availability

All 4" x 5" SCAMS negatives will be optically reduced to 70 mm film format by the NADUC and forwarded to the NSSDC. Upon request, the NSSDC will furnish a user with either positive or negative SCAMS photographic products. All SCAMS photographic products will be listed in The Nimbus 6 Data Catalogs.

Table 4-8  
SCAMS Archive Tape: Tentative Contents for Each Major Frame

Parameter	Number of Elements	Variable Type	Dimensional Units	Multiplier Used
Day	1	I*2	-	1
Minutes	1	I*2	-	1
Seconds	1	I*2	-	1
Altitude (of satellite)	1	I*2	km	1
Latitude (of satellite)	1	R*4	°N	1
Longitude (of satellite)	1	R*4	°E	1
Data Missing somewhere flag	1	L*1	-	1
Ascending: yes/no	1	L*1	-	1
Lost frames since last frame	1	I*2	-	1
Pitch error	4	I*2	Deg	32
Roll error	4	I*2	Deg	32
Digital A data	160	I*2	-	1
Playback orbit	1	I*2	-	1
Reference orbit	1	I*2	-	1
Spares	2	I*2	-	-
Housekeeping Temps	12	R*4	°K	1
T <sub>A</sub> channel 1	13	I*2	°K	32
T <sub>A</sub> channel 2	13	I*2	°K	32
T <sub>A</sub> channel 3	13	I*2	°K	32
T <sub>A</sub> channel 4	13	I*2	°K	32
T <sub>A</sub> channel 5	13	I*2	°K	32
Surface elevation (of spot viewed)	13	I*2	km	32
Latitude (of spot viewed)	13	I*2	°N	32
Longitude (of spot viewed)	13	I*2	°E	32
T <sub>B</sub> channel 1	13	I*2	°K	32
T <sub>B</sub> channel 2	13	I*2	°K	32
T <sub>B</sub> channel 3	13	I*2	°K	32
T <sub>B</sub> channel 4	13	I*2	°K	32
T <sub>B</sub> channel 5	13	I*2	°K	32
Surface reflectivity	13	I*2	%	32
H <sub>2</sub> O Vapor, integrated	13	I*2	mm	32
H <sub>2</sub> O Liquid, integrated	13	I*2	mm	32

Table 4-8 (Continued)

Parameter	Number of Elements	Variable Type	Dimensional Units	Multiplier Used
1000-500 mb Geo-potential thickness	13	I*2	Dm	32
500-250 mb Geo-potential thickness	13	I*2	Dm	32
250-100 mb Geo-potential thickness	13	I*2	Dm	32
1000 mb Temperature	13	I*2	°K	32
850 mb Temperature	13	I*2	°K	32
700 mb Temperature	13	I*2	°K	32
500 mb Temperature	13	I*2	°K	32
400 mb Temperature	13	I*2	°K	32
300 mb Temperature	13	I*2	°K	32
250 mb Temperature	13	I*2	°K	32
200 mb Temperature	13	I*2	°K	32
150 mb Temperature	13	I*2	°K	32
100 mb Temperature	13	I*2	°K	32
70 mb Temperature	13	I*2	°K	32
50 mb Temperature	13	I*2	°K	32
30 mb Temperature	13	I*2	°K	32
10 mb Temperature	13	I*2	°K	32
Spares	52	I*2	°K	32
Flags	13	I*2	°K	32
Total = 1400 bytes/frame				
BLKSIZE = 4200				
RECFM = FB				

The SCAMS archival tapes (described in Section 4.5.3) will be available from NSSDC. The address of the NSSDC and user ordering procedure are described in Section 1.7 of this report.

## REFERENCES

1. Meeks, M. L., and Lilley, A. E.: The Microwave Spectrum of Oxygen in the Earth's Atmosphere. *J. Geophys. Res.*, vol. 68, no. 6, 1963, pp. 1683-1703.
2. Rosenkranz, P. W., Barath, F. T., Blinn III, J. C., Johnston, E. J., Lenoir, W. B., Staelin, D. H., and Waters, J. W.: Microwave Radiometric Measurements of Atmospheric Temperature and Water from an Aircraft. *J. Geophys. Res.*, vol. 77, no. 30, 1972, pp. 5833-5844.
3. Rosenkranz, P. W. and Staelin, D. H.: Microwave Emissivity of Ocean Foam and its Effect on Nadiral Radiometric Measurements. *J. Geophys. Res.*, vol. 77, no. 33, 1972, pp. 6528-6538.
4. Staelin, D. H.: Passive Remote Sensing at Microwave Wavelengths. *Proc. IEEE*, vol. 57, no. 4, 1969, pp. 427-439.
5. Staelin, D. H., Barrett, A. H., Waters, J. W., Barath, F. T., Johnston, E. J., Rosenkranz, P. W., Gaut, N. E., and Lenoir, W. B.: Microwave Spectrometer on the Nimbus 5 Satellite: Meteorological and Geophysical Data. *Science*, vol. 182, no. 4119, 1973, pp. 1339-1341.
6. Tomiyasu, K.: Remote Sensing of the Earth by Microwaves. *Proc. IEEE*, vol. 62, no. 1, 1974, pp. 86-92.
7. Westwater, E. H., and Strand, O.: Statistical Information Content of Radiation Measurements used in Indirect Sensing. *J. Atmos. Sci.*, vol. 25, no. 5, 1968, pp. 750-758.

## SECTION 5

### THE ELECTRICALLY SCANNING MICROWAVE RADIOMETER (ESMR) EXPERIMENT

by

T. Wilheit

National Aeronautics and Space Administration  
Goddard Space Flight Center

#### 5.1 Introduction

The Nimbus 6 ESMR receives the thermal microwave radiation upwelling from the earth's surface and atmosphere in a 250 MHz band centered at 37 GHz (0.81 cm). The antenna beam is scanned electrically through 71 discrete positions on each sweep. Each sweep takes 5 1/3 seconds. Brightness temperatures are measured at each scan position. At GSFC these temperatures are used to produce images and digital tapes of microwave brightness temperatures. The data will be used to map the liquid water content of the clouds, the distribution and variation of sea ice cover and snow cover on the ice, and characteristics of land surfaces.

The Nimbus 6 ESMR instrument operating principles and physics of the microwave measurements are similar to the ESMR on Nimbus 5. The user is referred to The Nimbus 5 User's Guide (Section 4) for a more extensive discussion of microwave radiometry as it relates to ESMR. The significant differences between the two are in wavelength, polarization, and scanning geometry.

The operating wavelength is 0.81 cm (37.0 GHz) for the Nimbus 6 ESMR and 1.55 cm (19.35 GHz) for the Nimbus 5 ESMR. The most significant effect of this wavelength difference is roughly to triple the instrument's sensitivity to water droplets while keeping its sensitivity to water vapor essentially the same. This change will make it easier to distinguish light rain areas from areas of high water vapor. A secondary effect will be roughly to double the contrast between first year ice and multi-year ice. However, there will be a slight increase in ambiguity in the determination of the percent of open water in the ice within the IFOV, but this problem is not expected to be significant. The decrease in operating wavelength will also decrease the brightness temperature over snow, making it possible to identify and map snowfields.

The Nimbus 5 ESMR measured only the horizontally polarized component of the microwave radiation. The Nimbus 6 ESMR will measure both horizontal and

vertical components by using two separate radiometer channels. The polarization information will facilitate the quantitative interpretation of radiometric measurements. In particular, the surface reflectivity of sea ice is substantially unpolarized while the reflectivity of a water surface is highly polarized. These factors will be used to reduce the ambiguity in determining ice type. Similarly, ocean roughness, caused by winds, appears significantly different in the two polarizations. This information will be used to estimate wind speeds over oceans and to refine the estimates of water vapor and liquid water content of the atmosphere over oceans.

The Nimbus 5 ESMR scan caused a peak-to-peak variation of incidence angle of approximately 60 degrees at the earth's surface. The Nimbus 6 ESMR scan is along a cone such that the angle of incidence at the earth's surface varies by less than 1 degree. Keeping the incidence angle constant facilitates both qualitative and quantitative data interpretation.

## 5.2 Instrument Description

### 5.2.1 Viewing Geometry

The antenna beam of the ESMR scans ahead of the spacecraft along a conical surface with a constant angle of 45 degrees with respect to the antenna axis (see Figure 5-1). The beam scans in azimuth  $\pm 35$  degrees about the forward direction in 71 steps such that beam position 1 is 35 degrees azimuth angle to the right of the spacecraft, beam position 36 views straight ahead, and beam position 71 views 35 degrees to the left. In azimuth, the angular resolution varies from 0.95 degrees at beam position 36 to 1.17 degrees at the 35 degree scan extremes, and in elevation it varies from 1.00 degrees at position 36 to 0.84 degrees at the extremes of the scan.

The antenna axis is tipped 5 degrees forward of the vertical axis of the spacecraft. This orientation permits the antenna beam to intersect the earth at a nearly constant incidence angle throughout the scan. The beam incidence angle (in degrees) at the earth ( $\theta_z$ ) can be expressed as

$$\theta_z = 48.8 + 1.37P + 0.01P^2 + (1.4 - 0.38P + 0.02P^2) R_j^2, \quad (1)$$

where  $P$  is the spacecraft pitch angle in degrees (+ pitch is "nose up"),  $j$  is the beam position number, and  $R_j$  is equal to  $(36 - j)/35$ .

For the expected spacecraft pitch bias of  $+0.6$  degrees the incidence angle varies between an angle of 50.8 degrees for scan positions 1 and 71 and 49.6

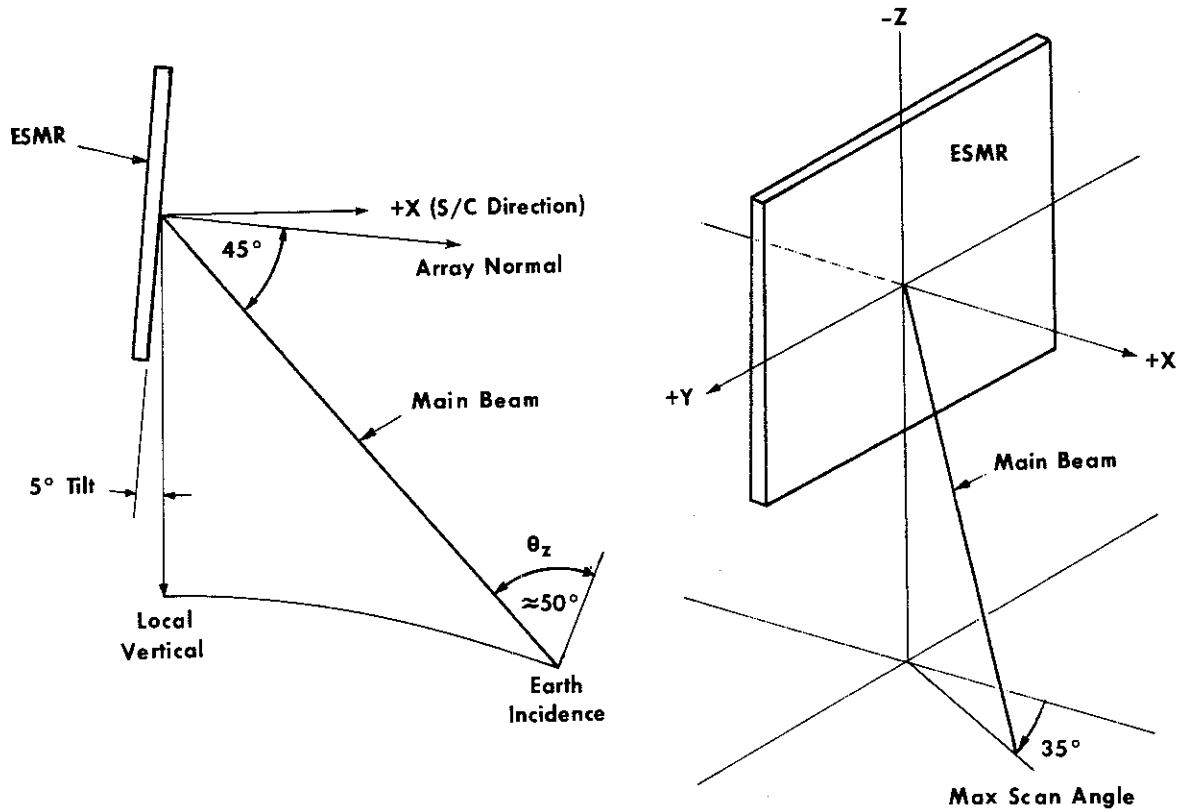


Figure 5-1. ESMR Antenna Scan Geometry

degrees for position 36, or  $\pm 0.6$  degrees across the scan. This should be easy to correct for in the data analysis. Table 5-1 presents incidence angles at various spacecraft pitch angles.

Table 5-1  
Resolution and Beam Incidence Angles at Various  
Spacecraft Pitch Angles

Spacecraft Pitch Angle (degrees)	Beam Incidence Angle (degrees)		Cross-track Resolution (km)	Down-track Resolution (km)
	Position 1 & 71	Position 36		
5.0	55.9	55.9	22	54
0.6	50.8	49.6	20	43.5
0.0	50.2	48.8	20	42
-5.0	46.0	42.2	18	35

The antenna beam is designed to step in the increments of constant  $\sin \phi$ , where  $\phi$  is the azimuthal angle. Beam pointing angles are accurate to within  $\pm 0.2$  degrees of their indicated positions. Each beam position can be converted to earth location distance from the subpoint by the equations

$$Y (\text{km}) = 991 + 41.6P + P^2 - (177 + 6.4P + 0.28P^2) R_j^2 \quad (2)$$

and

$$X (\text{km}) = (639 + 10.8P + 0.32P^2) R_j$$

where Y is the great circle distance along the satellite motion direction from the subpoint to the viewed point, and X is the great circle distance perpendicular to the satellite motion direction from the subpoint to the viewed point. Figure 5-2 shows the location of beam positions on the surface of the earth, as well as the projections of the half-power (3 dB) contours for four of the beam positions. Note that these instantaneous fields of view are oval, each is oriented approximately parallel to the satellite track, and the 3 dB contours of the adjacent beam positions are very close (within 1 km) to tangent. The arrow drawn from beam position 1 toward the subpoint is intended to show that the elongated dimension of the oval IFOV is more nearly aligned with the subpoint track than with the cross-track scan motion. As Table 5-1 shows, a variation in pitch does not significantly change the 3 dB resolution in the cross-scan direction but does significantly vary the down-track resolution.

The expected typical ESMR coverage of the earth for a 24-hour period is shown in Figure 5-3. Since the width of the image area is only 1272 km (for 0 degrees pitch), there are substantial coverage gaps in the equatorial region. These gaps decrease away from the equator and disappear at 60 degrees latitude. Areas polewards of 85.7 degrees will not be viewed since the satellite subpoint track only reaches to 80 degrees of latitude. Areas shaded dark and all areas between 60 degrees and 85 degrees are covered at least twice during each 24-hour period. Coverage in Figure 5-3 was generated from actual Nimbus 5 data and thus reflects the blind orbit and interrogation problems that limit the total amount of data actually received.

### 5.2.2 Operation

A simplified block diagram of the instrument is shown in Figure 5-4. The independent portions of the horizontal and vertical polarization channels are in separate dashed boxes, while those elements common to both channels are shown in the center. The radiation in both polarizations is received and separated in the phased array antenna. The polarization signal and various calibration data for each channel are fed to a ferrite switch which sequentially selects the

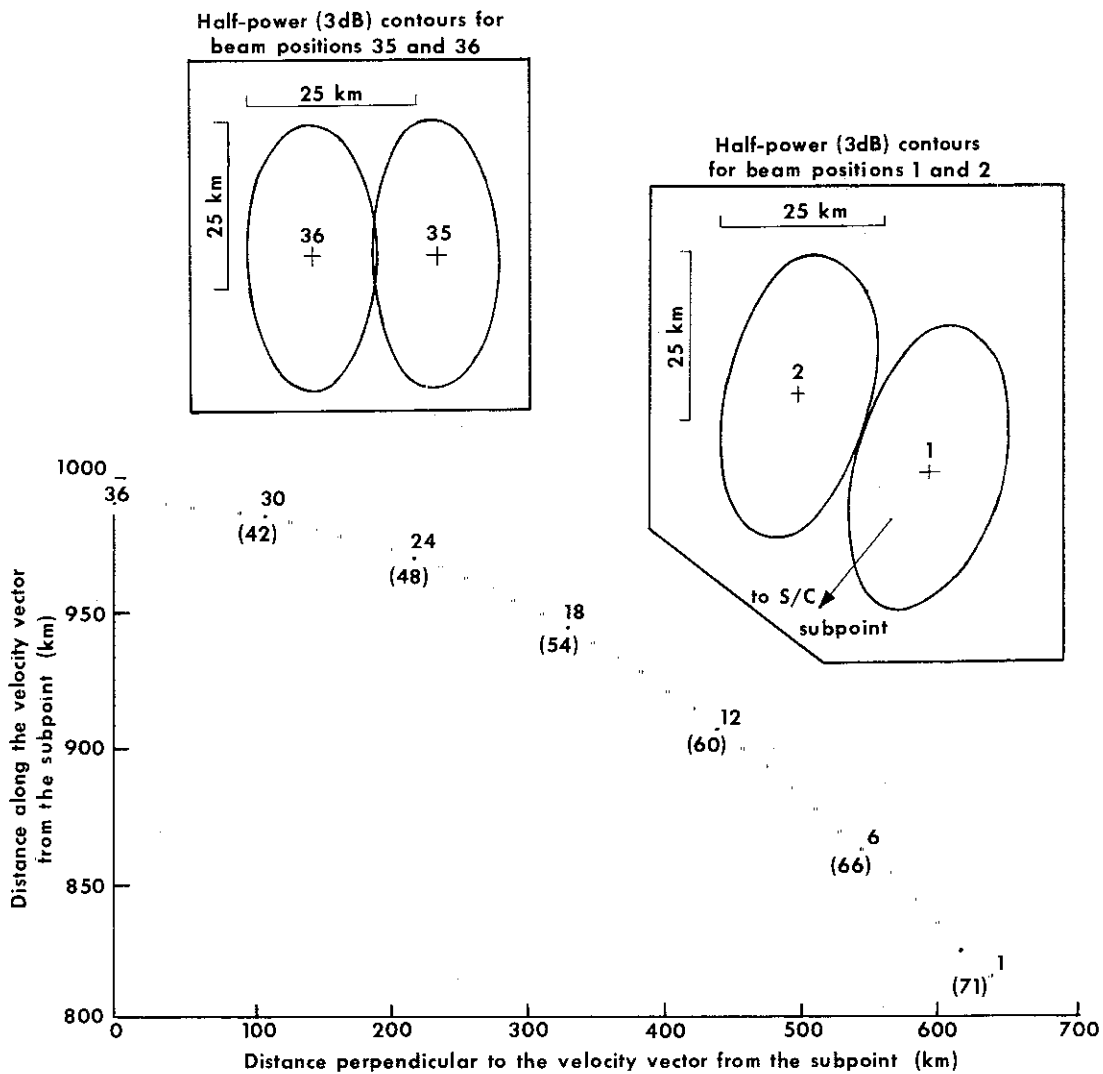


Figure 5-2. Great Circle Distances of ESMR Beam Positions from the Subpoint and the Projection of the Half-power Contours for Four Beam Positions. Beam positions 37 through 71 are located at mirror image positions of 35 through 71, respectively.

information to be sent to the receiver. The selected signal is then beat in the mixer portion of the receiver with the 37 GHz signal from the Gunn diode local oscillator. That portion of the resulting signal that is within the 10 to 125 MHz intermediate frequency bandpass is then amplified. Each receiver, centered at a frequency of 37 GHz, is thus sensitive to a 250 MHz wide frequency band with a 20 MHz gap in the middle. The signal is then detected, further amplified, and synchronously demodulated to detect the amplitude modulation coming from the ferrite switch. The multiplex switch in the vertical channel selects between the

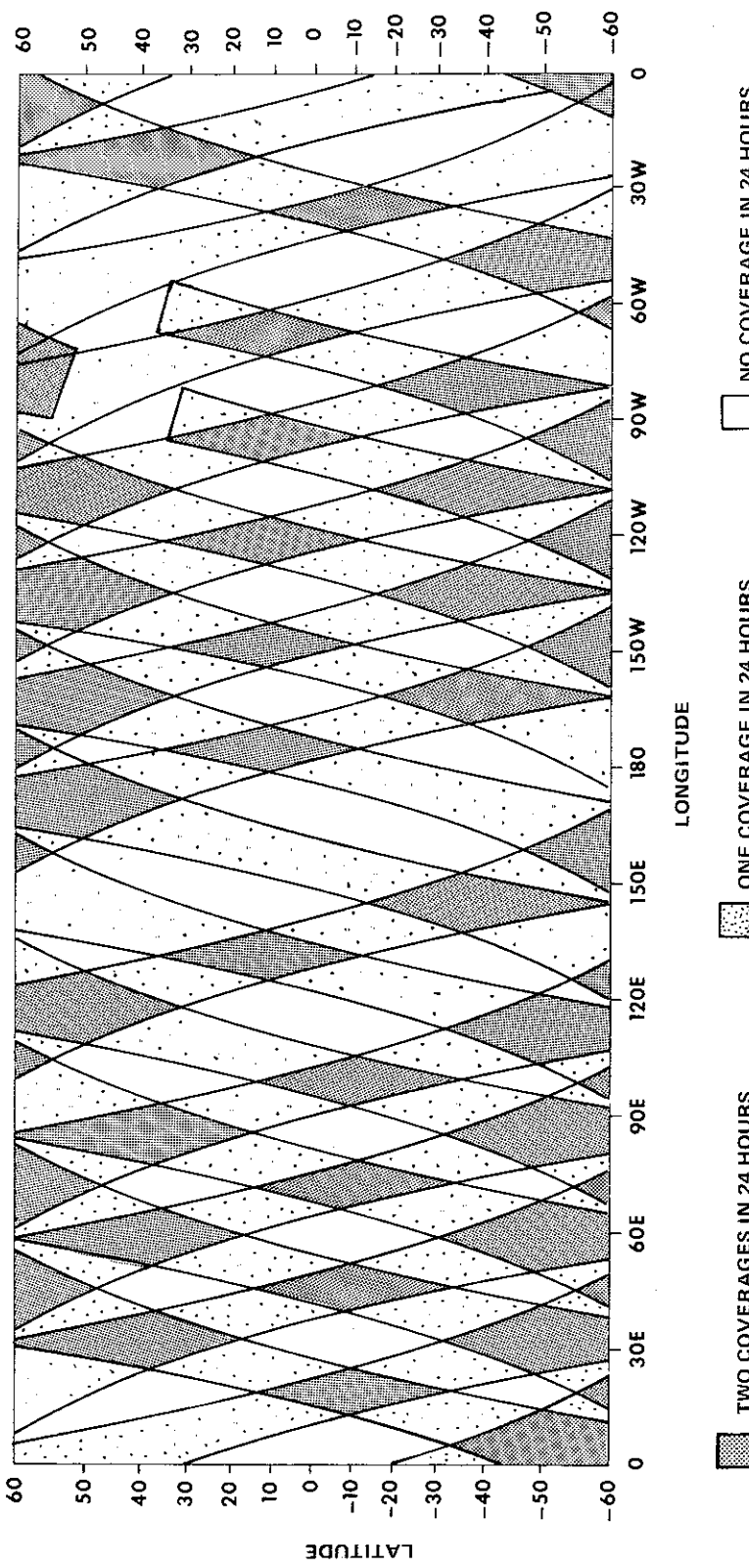


Figure 5-3. Typical ESMR Coverage of the Earth for a 24-hour Period.  
This coverage was derived from Nimbus 5 data.

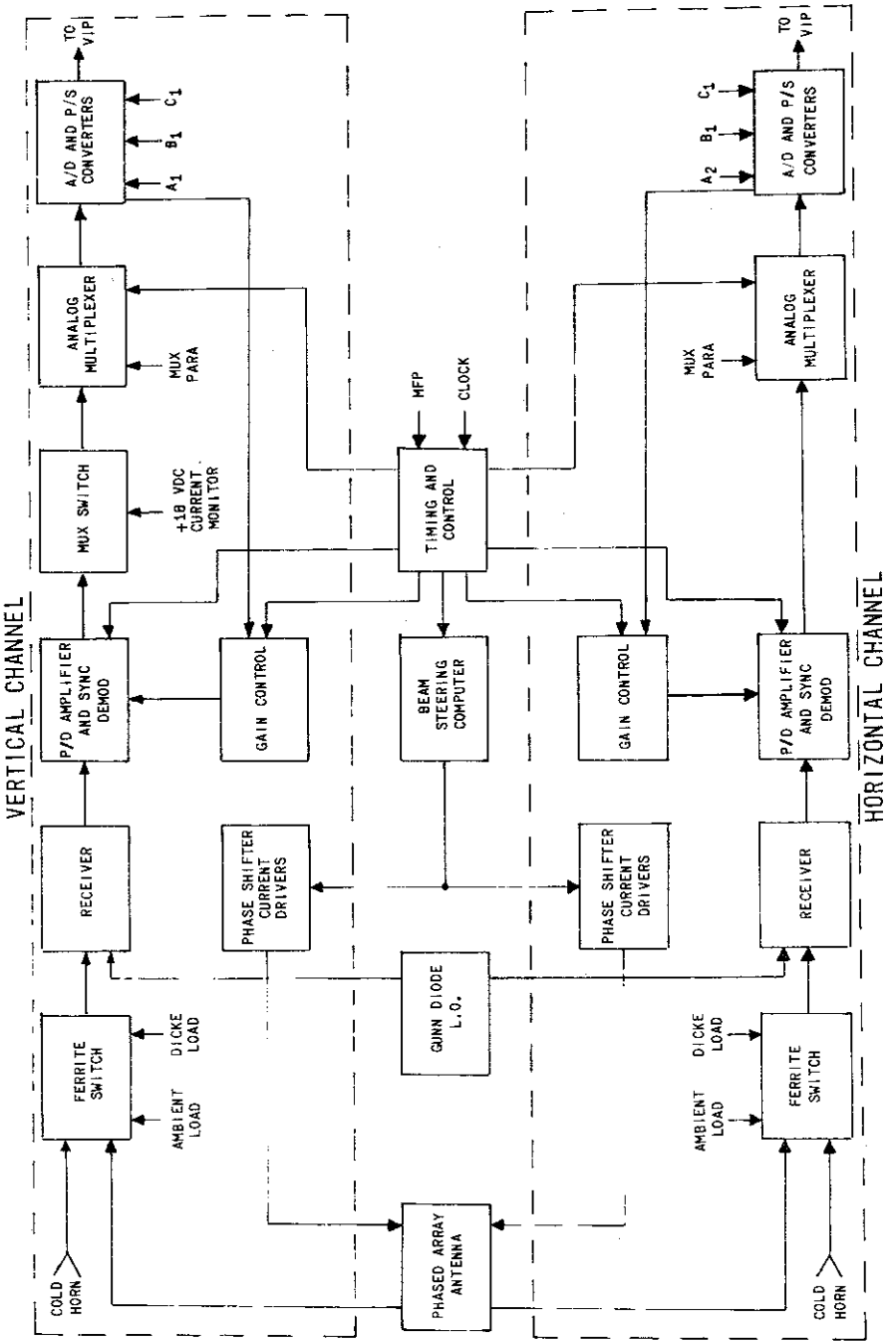


Figure 5-4. Simplified Block Diagram of the ESMR Instrument

signal from the synchronous demodulator and a signal proportional to the total phase shifter current. The phase shifter current value is used for diagnostic purposes only. Normally the switch will be left in the radiometer mode. The analog multiplexer selects among the various thermisters within the instrument and the radiometer signal. The chosen signal is digitized to 10 bits and fed serially to the spacecraft VIP data system.

When the instrument is in the cold calibration mode (measuring the space-view signal from the cold horn), the digitized signal is automatically examined. If it is not within the range 769 to 991, the gain is adjusted by about 10 percent to bring it toward or into this range. There are 32 such steps available and the instrument can step through them at a rate of one step each 5 1/3 seconds. This feature may be overridden by commanding both channels to manual gain control and stepping the gain one step at a time by command.

ESMR data is recorded in the VIP and transmitted to the ground in three forms: analog, digital A, and digital B. The analog data are of engineering significance only and will not be discussed here. The digital B data are a set of single bit digital flags indicating the instrument status and gain setting of each channel. The 15 digital B flags and their normal operating values are given in Table 5-2. If the flags depart from these values the data may be subject to analysis limitations. These would be discussed in The Nimbus 6 Data Catalog.

Table 5-2  
Digital B Flags Indicating Gain Setting of Each  
Channel and Instrument Status

Flag Number	Description	I/O	Normal Value	Bit Value On CBTT
1	Radiometer Power	ON/OFF	ON	1
2	Load Power	ON/OFF	ON	2
3	Phase Shifter Monitor	ON/OFF	OFF	4
4	Horizontal Gain	AUTO/MANUAL	AUTO	8
5	Horizontal Gain	$2^0/0$	$17 \pm 3$	16
6	Horizontal Gain	$2^1/0$		
7	Horizontal Gain	$2^2/0$		
8	Horizontal Gain	$2^3/0$		
9	Horizontal Gain	$2^4/0$		
10	Vertical Gain	AUTO/MANUAL	AUTO	
11	Vertical Gain	$2^0/0$	$12 \pm 3$	
12	Vertical Gain	$2^1/0$		
13	Vertical Gain	$2^2/0$		
14	Vertical Gain	$2^3/0$		
15	Vertical Gain	$2^4/0$		

The primary data are the two digital A streams, one for each polarization. These data consist of two columns of 240 ten-bit positive integers recorded during each 16 second VIP major frame. Each data frame stands as a logical record, interpretable as a unit. However, some averaging and smoothing of the calibration data over a longer time period will be performed by the Atmospheric and Hydrospheric Applications Division (AHAD) at GSFC.

The format of the ESMR digital A data is given in Table 5-3. The data words labeled MUX 1 through 30 are temperature measurements used in the calibration process. Beam positions 1 through 71 (words 3-73, 83-153, and 163-237) are proportional to the radiometric output when the radiometer is switched (through the ferrite switch network) to the antenna as it scans. Word 239 (MUX cal) should have the value  $670 \pm 1$ . A value greater than  $670 \pm 1$  for either channel represents a drift in a voltage standard and all the MUX data for that channel would be scaled to bring the value back to 670. Words 238 and 240 are included for testing convenience and need not be considered for data interpretation.

Table 5-3  
Sequence of ESMR Information from the Digital A Data

Frame Time Increment	Horizontal Channel	Vertical Channel
1	Ant. Temp. AA (MUX 1)	Ant. Temp. BB (MUX 2)
2	Ant. Temp. CC (MUX 3)	Ant. Temp. DD (MUX 4)
3	Beam Pos. 1H	Beam Pos. 1V
.	.	.
73	Beam Pos. 71H	Beam Pos. 71V
74	Amb. Ref. H	Amb. Ref. V
75	Cold Ref. H	Cold Ref. V
76	Cold Ref. H	Cold Ref. V
77	P.S. Temp. HA (MUX 5)	P.S. Temp. VA (MUX 6)
78	P.S. Temp. HB (MUX 7)	P.S. Temp. VB (MUX 8)
79	P.S. Temp. HC (MUX 9)	P.S. Temp. VC (MUX 10)
80	P.S. Temp. HD (MUX 11)	P.S. Temp. VD (MUX 12)
81	Feed Array Temp. HA (MUX 13)	Feed Array Temp. VA (MUX 14)
82	Feed Array Temp. HB (MUX 15)	Feed Array Temp. VB (MUX 16)
83	Beam Pos. 1H	Beam Pos. 1V
.	.	.
153	Beam Pos. 71H	Beam Pos. 71V
154	Amb. Ref. H	Amb. Ref. V
155	Cold Ref. H	Cold Ref. V

Table 5-3 (Continued)

Frame Time Increment	Horizontal Channel	Vertical Channel
156	Cold Ref. H	Cold Ref. V
157	Waveguide Temp. H (MUX 17)	Waveguide Temp. V (MUX 18)
158	Fer. Sw. Temp. HA (MUX 19)	Fer. Sw. Temp. VA (MUX 20)
159	Ant Load Temp. AA (MUX 21)	Ant Load Temp. BB (MUX 22)
160	Hot Ref. Temp. H (MUX 23)	Hot Ref. Temp. V (MUX 24)
161	Amb. Load Temp. H (MUX 25)	Amb. Load Temp. V (MUX 26)
162	Cold Horn Temp. H (MUX 27)	Cold Horn Temp. V (MUX 28)
163	Beam Pos. 1H	Beam Pos. 1V
233	Beam Pos. 71H	Beam Pos. 71V
234	Amb. Ref. H	Amb. Ref. V
235	Cold Ref. H	Cold Ref. V
236	Cold Ref. H	Cold Ref. V
237	Cold Horn W/G Temp. H (MUX 29)	Cold Horn W/G Temp. V (MUX 30)
238	+18 VDC Monitor H (MUX 31)	+18 VDC Monitor V (MUX 32)
239	MUX Cal. Voltage H (MUX 33)	MUX Cal. Voltage V (MUX 34)
240	System Mode	Frame Sync.

### 5.2.3 Calibration

The calibration of the radiometer depends on a linear response of the system between the input brightness temperature at, or ahead of, the Dicke switch and the digital output to the VIP. The equation used to obtain the antenna/radiometer interface brightness temperature ( $T_B$ ) is

$$T_B = \frac{I_A - (I_C - I_A)(C - C_A)}{(C_C - C_A)}, \quad (3)$$

where  $T_A$  is the effective temperature of the ambient calibration load,  $T_C$  is the effective brightness temperature of the cold calibration horn,  $C$  is the digital output from the radiometer to be converted into brightness temperature, and  $C_A$  and  $C_C$  are the corresponding digital outputs of the ambient calibration load and the cold horn calibration, respectively (when the radiometer is measuring the radiation from the calibration loads). The values of the effective calibration temperatures ( $T_A$  and  $T_C$ ) have been calculated as function of the temperatures of the ferrite switch and waveguides (referred to the antenna/radiometer interface). The equation used to determine  $T_A$  and  $T_C$  are

$$\begin{pmatrix} I_C \\ T_A \end{pmatrix}_{\text{vertical}} = \begin{pmatrix} -0.09 & 0.11 & 0.00 & 0.07 & 0.06 \\ -0.09 & 0.10 & 1.03 & 0.00 & 0.00 \end{pmatrix} \cdot \begin{pmatrix} t_{18} \\ t_{20} \\ t_{26} \\ t_{28} \\ t_{30} \end{pmatrix} - \begin{pmatrix} 24.5^\circ K \\ 12.3^\circ K \end{pmatrix},$$

(4)

and

$$\begin{pmatrix} I_C \\ T_A \end{pmatrix}_{\text{horizontal}} = \begin{pmatrix} -0.12 & 0.02 & 0.00 & 0.06 & 0.04 \\ -0.12 & 0.04 & 1.08 & 0.00 & 0.00 \end{pmatrix} \cdot \begin{pmatrix} t_{17} \\ t_{19} \\ t_{25} \\ t_{27} \\ t_{29} \end{pmatrix} + \begin{pmatrix} 8.1^\circ K \\ -0.3^\circ K \end{pmatrix},$$

where  $t$  is the temperature of the ferrite switch and waveguides and the subscripts give the multiplex positions. Each equation is derived from measured losses (as a function of temperature) of the ferrite switch and the various waveguides. Since these values are used to calibrate the antenna loss, accumulated errors are largely absorbed in the antenna loss corrections.

Antenna loss is measured by allowing the instrument to scan the sky at a 45 degree zenith angle cone while the sky horns also view the sky at a 45 degree zenith angle through a reflector. The approximate brightness of the sky under clear conditions is typically  $20^\circ K$  to  $40^\circ K$  at 37 GHz, depending on altitude and water vapor content. Knowing the exact temperature is not necessary for the calibration as long as the sky horns and antenna beams observe the same temperature. The equation used to determine the loss ratio ( $L$ ) at each beam position is of the form

$$L = \frac{t_0 - 2.7^\circ K}{t_0 - T_B},$$

(5)

where  $2.7^\circ K$  is the cosmic background for the sky brightness (the same expected in space, and used in above calibration expression),  $T_B$  is the brightness temperature measured for each polarization at each beam position,  $t_0$  is the antenna thermodynamic temperature, which was varied from  $265^\circ K$  to  $320^\circ K$ . The antenna temperature is the average of 12 thermister readings from the horizontal channel (MUX numbers 1, 2, 3, 4, 5, 7, 9, 11, 13, 15, 21, and 22) and 12 from the vertical channel (MUX numbers 1, 2, 3, 4, 6, 8, 10, 12, 14, 16, 21 and 22).

These losses are also a function of the phase shifter temperature as well, but are well approximated by a linear function of the phase shifter temperatures

$$L(I_{ps}) = L_0 + (t_{ps} - 300^\circ K) L_1 , \quad (6)$$

where  $L_0$  is the measured loss ratio at  $300^\circ K$ ,  $t_{ps}$  is the average of the six thermistors on or near the phase shifters for each polarization (MUX numbers 5, 7, 9, 11, 13 and 15 for the horizontal channel and MUX numbers 6, 8, 10, 12, 14 and 16 for the vertical channel), and  $L_1$  is the temperature coefficient of each loss ratio. Table 5-4 lists the loss ratios ( $L_0$ ) at  $300^\circ K$  and their temperature coefficients ( $L_1$ ) for all 71 beam positions for both polarizations.

Table 5-4  
Antenna Calibration Parameters

Beam Position	Horizontal Channel				Vertical Channel			
	$L_0$	$L_1(x10^{-3})$	X	a	$L_0$	$L_1(x10^{-3})$	X	b
1	1.937	1.14	0.632	0.022	1.976	2.27	0.794	0.037
2	1.988	0.74	0.628	0.021	2.028	2.53	0.871	0.035
3	2.154	0.94	0.636	0.020	2.128	2.20	0.833	0.033
4	2.075	1.63	0.875	0.018	2.256	2.66	0.836	0.031
5	2.084	1.16	0.912	0.017	2.246	2.74	0.898	0.029
6	1.950	1.70	0.928	0.016	2.255	3.10	0.904	0.027
7	1.909	1.40	0.928	0.015	2.234	3.31	0.906	0.025
8	1.949	1.64	0.928	0.014	2.249	3.69	0.907	0.024
9	2.006	2.17	0.924	0.013	2.271	3.79	0.911	0.022
10	2.083	2.57	0.923	0.012	2.306	3.79	0.912	0.020
11	2.152	2.79	0.923	0.011	2.315	3.94	0.905	0.019
12	2.232	3.26	0.917	0.010	2.317	3.61	0.915	0.017
13	2.307	3.43	0.923	0.010	2.331	3.79	0.926	0.016
14	2.392	3.36	0.925	0.009	2.349	3.63	0.908	0.015
15	2.463	3.73	0.911	0.008	2.345	4.04	0.924	0.013
16	2.538	4.40	0.911	0.007	2.331	3.51	0.912	0.012
17	2.613	4.57	0.918	0.006	2.326	3.46	0.917	0.011
18	2.667	4.19	0.910	0.006	2.318	3.40	0.910	0.010
19	2.749	5.71	0.910	0.005	2.309	3.43	0.922	0.009
20	2.777	4.69	0.920	0.005	2.300	3.50	0.919	0.008
21	2.821	5.79	0.914	0.004	2.280	3.34	0.926	0.007
22	2.866	6.14	0.916	0.004	2.267	3.19	0.913	0.006
23	2.878	5.07	0.926	0.003	2.252	3.17	0.922	0.005
24	2.904	4.86	0.916	0.003	2.239	3.21	0.920	0.004
25	2.917	5.43	0.919	0.002	2.226	3.14	0.923	0.004
26	2.943	4.57	0.918	0.002	2.213	2.89	0.928	0.003

Table 5--4 (Continued)

Beam Position	Horizontal Channel				Vertical Channel			
	L <sub>0</sub>	L <sub>1</sub> (x10 <sup>-3</sup> )	X	a	L <sub>0</sub>	L <sub>1</sub> (x10 <sup>-3</sup> )	X	b
27	2.933	3.87	0.924	—	2.195	2.67	0.934	—
28	2.966	4.40	0.917	—	2.185	2.83	0.928	—
29	2.948	3.94	0.926	—	2.171	2.79	0.929	—
30	2.977	4.43	0.926	—	2.171	2.51	0.922	—
31	2.977	4.43	0.919	—	2.163	2.57	0.930	—
32	2.967	3.67	0.920	—	2.155	2.76	0.934	—
33	2.993	4.57	0.930	—	2.152	2.66	0.929	—
34	2.969	3.71	0.934	—	2.149	2.54	0.929	—
35	2.980	3.86	0.927	—	2.146	2.66	0.935	—
36	3.007	3.43	0.927	—	2.149	2.79	0.928	—
37	3.006	3.79	0.933	—	2.151	2.64	0.932	—
38	2.986	3.14	0.926	—	2.149	2.47	0.937	—
39	2.979	3.36	0.935	—	2.150	2.70	0.932	—
40	2.977	3.43	0.936	—	2.154	2.53	0.930	—
41	3.007	3.43	0.940	—	2.158	2.61	0.938	—
42	2.963	4.57	0.925	—	2.167	2.53	0.942	—
43	3.917	4.53	0.936	—	2.173	2.57	0.932	—
44	2.974	5.36	0.941	—	2.184	2.80	0.934	—
45	2.967	5.43	0.942	—	2.200	2.93	0.936	—
46	2.953	5.57	0.933	0.002	2.213	3.09	0.936	0.003
47	2.939	5.21	0.943	0.002	2.223	2.91	0.939	0.004
48	2.916	4.79	0.937	0.003	2.235	2.87	0.935	0.004
49	2.859	4.71	0.929	0.003	2.293	3.09	0.938	0.005
50	2.874	5.36	0.940	0.004	2.258	3.01	0.930	0.006
51	2.821	4.64	0.934	0.004	2.277	3.04	0.941	0.007
52	2.801	5.29	0.941	0.005	2.292	3.41	0.929	0.008
53	2.737	5.43	0.936	0.005	2.308	3.44	0.933	0.009
54	2.693	3.81	0.942	0.006	2.315	3.36	0.942	0.010
55	2.216	4.96	0.934	0.006	2.321	3.29	0.926	0.011
56	2.559	5.21	0.939	0.007	2.332	3.54	0.936	0.012
57	2.470	4.29	0.941	0.008	2.330	3.37	0.929	0.013
58	2.384	3.47	0.934	0.009	2.340	3.61	0.933	0.015
59	2.293	3.57	0.942	0.010	2.315	3.61	0.931	0.016
60	2.197	3.43	0.950	0.010	2.293	3.44	0.944	0.017
61	2.162	2.97	0.944	0.011	2.317	3.84	0.937	0.019
62	2.075	2.59	0.943	0.012	2.306	4.14	0.934	0.020
63	2.004	2.07	0.941	0.013	2.261	3.31	0.931	0.022

Table 5-4 (Continued)

Beam Position	Horizontal Channel				Vertical Channel			
	L <sub>0</sub>	L <sub>1</sub> (x10 <sup>-3</sup> )	X	a	L <sub>0</sub>	L <sub>1</sub> (x10 <sup>-3</sup> )	X	b
64	1.904	1.59	0.949	0.014	2.250	3.56	0.931	0.024
65	1.902	1.20	0.938	0.015	2.220	3.14	0.923	0.025
66	1.947	0.93	0.940	0.016	2.254	3.29	0.922	0.027
67	2.070	1.00	0.933	0.017	2.253	2.81	0.902	0.029
68	2.059	1.06	0.808	0.018	2.205	2.39	0.821	0.031
69	2.096	1.33	0.662	0.020	2.083	2.39	0.863	0.033
70	1.970	1.00	0.658	0.021	2.021	2.03	0.818	0.035
71	1.942	0.86	0.633	0.022	1.983	2.33	0.683	0.037

The antenna loss correction ( $T_A$ ) equation is of the form

$$T_A = L T_B - (L - 1)t_0 , \quad (7)$$

where  $L$  is the previously defined loss ratio for each polarization,  $T_B$  is the radiometric temperature measured at the antenna output, and  $t_0$  is as previously defined.

The measured antenna temperature is an integral over a complete solid angle

$$T_A = \frac{\int I_B(\theta, \phi) G(\theta, \phi) \cos \theta d\theta d\phi}{\int G(\theta, \phi) \cos \theta d\theta d\phi} , \quad (8)$$

where  $T_B$  is the brightness temperature in a direction specified by the conventional polar angles  $\theta$  and  $\phi$ .  $G$  is the antenna gain as a function of these same angles. Since the gain function in the  $\theta$  direction is quite well behaved, having sidelobes about 30 dB below the main axis gain, the equation is reduced to a one dimensional problem

$$T_A = \frac{\int I_B(\phi) g(\phi) d\phi}{\int g(\phi) d\phi} , \quad (9)$$

where  $g(\phi)$  is the antenna gain function along the  $\theta = 45$  degree surface.

A matrix method for correcting for the antenna sidelobe on the Nimbus 5 ESMR was described in The Nimbus 5 User's Guide. It proved to be wasteful of

computer time. A simple, but quite adequate, approximation will be used for the ESMR on Nimbus 6. The brightness temperature for the  $i$ -th beam position may be approximated by

$$(\bar{T}_A)_i \cong (A_i, j-1 + A_i, j + A_i, i+1) \bar{T}_B + (1 - A_i, i+1 + A_i, i+A_i, i+1) \bar{T}_B, \quad (10)$$

where the  $A$ 's are the same as discussed on page 86 of The Nimbus 5 User's Guide, and  $\bar{T}_B$  is the brightness temperature averaged across the scan. Further,  $\bar{T}_A$  is approximately equal to  $\bar{T}_B$ , where  $\bar{T}_A$  is the average antenna temperature across the swath, which is readily calculated. Thus the brightness temperature for each beam position ( $T_{Bi}$ ) is

$$T_{Bi} = \frac{I_{Ai} + (X_i - 1)\bar{T}_A}{X_i}, \quad (11)$$

where each  $X_i$  is given in Table 5-4. Note that, as with the Nimbus 5 algorithm, no attempt is made to correct for the contributions from adjacent beam positions as they must be considered part of the main beam contribution. Correcting for adjacent beams would cause unacceptable noise amplification.

The two polarizations received by the antenna are not quite the horizontal and vertical polarizations but rather a mix of the two because of geometric problems inherent to the antenna, the antenna tilt angle, and mechanical tolerances in building the antenna. The equations used to obtain the true temperature ( $T_{true}$ ) for each polarization are of the form

$$T_{\substack{\text{Horizontal} \\ \text{True}}} = (1 - a) T_{\substack{\text{Horizontal} \\ \text{Nominal}}} + a T_{\substack{\text{Vertical} \\ \text{Nominal}}}, \quad (12)$$

and

$$T_{\substack{\text{Vertical} \\ \text{True}}} = (1 - b) T_{\substack{\text{Vertical} \\ \text{Nominal}}} + b T_{\substack{\text{Horizontal} \\ \text{Nominal}}}$$

The values of  $a$  and  $b$  as a function of beam position are given in Table 5-4. This correction is applied to each pair of measured brightness temperatures for each beam position.

In summary the steps applied in calibrating the radiometric signal are to:

- Compute the brightness temperature at the antenna/radiometer interface
- Correct for the loss in the antenna, which depends on the beam position, polarization, and phase shifter temperature

- Correct for the antenna gain function (sidelobes)
- Correct for the polarization mixing

### 5.3 Data Processing, Format, and Availability

#### 5.3.1 Data Processing

All ESMR data will be acquired at the Rosman and Alaska STDN stations and relayed to the MDHS at GSFC. MDHS will produce 4" x 5" negatives and digital tapes of all ESMR data acquired from each interrogation orbit. The imagery is sent to the NADUC for production of required photographic copies. Images are also reduced to 70 mm roll format and sent to the NSSDC for archiving and filling of users' requests for imagery. The ESMR digital data tapes are sent to the IED at GSFC for processing into Calibrated Brightness Temperature Tapes (CBTT). All CBTT are sent to the NSSDC for archiving and to fill user requests for ESMR digital data.

#### 5.3.2 Image Format

All ESMR data will be converted to 4" x 5" black and white images at the MDHS at GSFC. The NADUC will reproduce and distribute initial copies of these images. Normally, the ESMR data will be displayed by itself. However, there is an MDHS option to display a combination of ESMR and SCAMS data. The combination display will be a composite of standard display options for ESMR and SCAMS and, therefore, is not presented in detail in this report. The format and details of the planned ESMR display are described below. Figure 5-5 is a sample of the ESMR display and should be used as a reference for the following description.

- NIMBUS 6-ESMR

This identifies the satellite (Nimbus 6) and the experiment (ESMR).

- DATE

This identifies the Greenwich month, day, and year the data was recorded on board the satellite.

- SCALE (F, P1, or P2)

The data from each orbit will be displayed as an image at full vertical scale (F) or at partial vertical scale (P). In the full scale mode up to

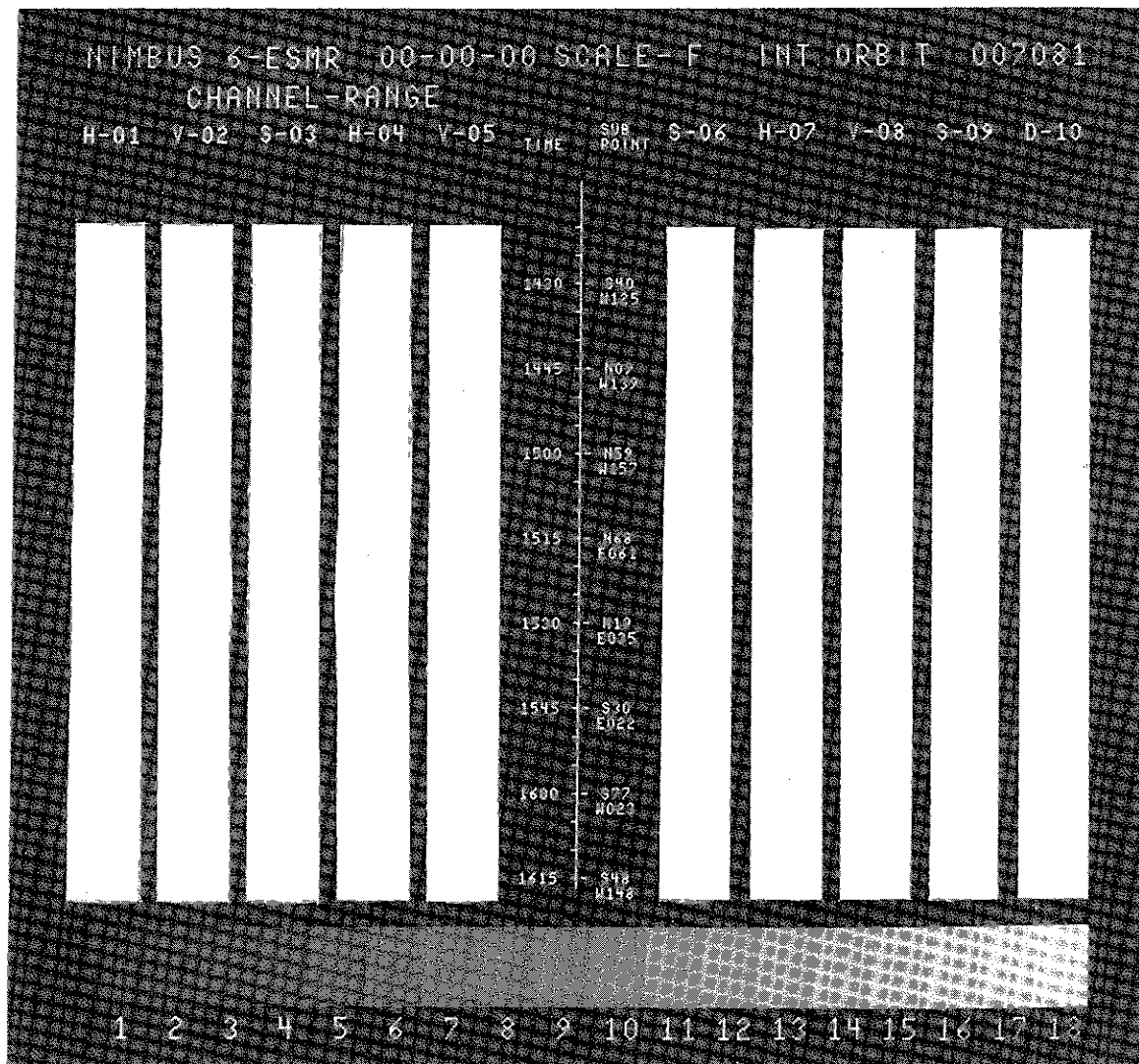


Figure 5-5. ESMR EIS Display Format

125 minutes of data will be output on a single image (and labeled as SCALE-F). In the partial scale mode the data is displayed at twice the vertical scale used in the full scale mode. Usually, in the partial scale mode, two images are needed to display all the data. The last 60 minutes of data is output first (and the image is labeled SCALE-P2). Any remaining data from each interrogation orbit is output on a second image (and labeled SCALE-P1). Note that P1 contains the data acquired earliest. If there is less than 65 minutes of data from an interrogation orbit, only a P2 image is produced. In the full scale (F) mode each scan line of ESMR data is displayed once. In the partial

scale (P) mode each scan line is displayed twice in succession. In both modes, each of the 71 scan spot elements across a scan is displayed twice for a total of 142 display spots across each line.

- GRAY SCALE

Each image has an 18-step gray scale along the bottom of the display. The gray scale defines the brightness temperature for each of the ten swaths by assigning a different brightness temperature range to the gray scale for each swath. Table 5-5 defines the planned temperature range of gray scale values for each swath. If these assigned values should be changed after launch, The Nimbus 6 Data Catalogs will list the new values.

- INT ORBIT

The interrogation orbit identifies the orbit during which the recorded data is transmitted to a STDN station. Usually parts of two data orbits are on the same display. The interrogation orbit number will only identify the last orbit of each display.

- TIME (and) SUBPOINT

Satellite time and latitude-longitude information are presented along the vertical line down the center of each display. The line represents the satellite subpoint track which is located down the center of each of the swaths on each display. TIME is GMT with time ticks along the left side of the line at each five minute mark (on the five minutes). TIME is annotated (hour and minute) every 15 minutes (on the quarter hour). SUBPOINT information presents latitude and longitude positions of the satellite subpoint. Each tick mark on the right side of the vertical line is annotated with the subpoint latitude and longitude (to the nearest degree). Latitude is labeled N (north) or S (south). Longitude is labeled E (east) or W (west).

- CHANNEL-RANGE

Each display contains ten swaths of ESMR data. All swaths on each display contain the same coverage information, but each contains different polarization or temperature information. Each swath is identified by a header block labeled H-01, V-02, etc. These headers identify the class of ESMR data for each swath. Table 5-5 defines each swath and the temperature range of the shades of gray. These swath displays and the temperature ranges of each swath are preliminary. After

Table 5-5  
 Gray Scale Number versus ESMR Brightness Temperature for  
 Each Image Swath on the ESMR EIS Displays  
 (Brightness Temperature in °K)

Gray Scale Number	ESMR Swath Displays									
	H-01	V-02	S-03	H-04	V-05	S-06	H-07	V-08	S-09	D-10
(black) 1	<140	<194	<154	<190	<226	<202	<240	<258	<250	0-3
2	140-143	194-196	154-157	190-193	226-228	202-205	240-243	258-260	250-253	3-6
3	143-146	196-198	157-160	193-196	228-230	205-208	243-246	260-262	253-256	6-9
4	146-149	198-200	160-163	196-199	230-232	208-211	246-249	262-264	256-259	9-12
5	149-152	200-202	163-166	199-202	232-234	211-214	249-252	264-266	259-262	12-15
6	152-155	202-204	166-169	202-205	234-236	214-217	252-255	266-268	262-265	15-18
7	155-158	204-206	169-172	205-208	236-238	217-220	255-258	268-270	265-268	18-21
8	158-161	206-208	172-175	208-211	238-240	220-223	258-261	270-272	268-271	21-24
9	161-165	208-210	175-178	211-215	240-242	223-226	261-265	272-274	271-274	24-26
10	165-168	210-212	178-181	215-218	242-244	226-229	265-268	274-276	274-277	26-29
11	168-171	212-214	181-184	218-221	244-246	229-232	268-271	276-278	277-280	29-32
12	171-174	214-216	184-187	221-224	246-248	232-235	271-274	278-280	280-283	32-35
13	174-177	216-218	187-190	224-227	248-250	235-238	274-277	280-282	283-286	35-38
14	177-180	218-220	190-193	227-230	250-252	238-241	277-280	282-284	286-289	38-41
15	180-183	220-222	193-196	230-233	252-254	241-244	280-283	284-286	289-292	41-44
16	183-186	222-224	196-199	233-236	254-256	244-247	283-286	286-288	292-295	44-47
17	186-190	224-226	199-202	236-240	256-258	247-250	286-290	288-290	295-298	47-50
(white) 18	>190	>226	>202	>240	>258	>250	>290	>290>	>298	>50

The swaths labeled H-01, H-04, and H-07 present successive temperature ranges of data from the horizontal polarization channel.

The swaths labeled V-02, V-05, and V-08 present successive temperature ranges of data from the vertical polarization channel.

The swaths labeled S-03, S-06, and S-09 present the average of the horizontal and vertical polarization temperature for each data point.

The swath labeled D-10 presents the difference between the horizontal and vertical polarization channel temperature for each data point.

These swath displays and the temperature ranges are preliminary. Any post-launch changes will be presented in The Nimbus 6 Data Catalogs.

launch other displays and temperature ranges may be used which will show more information. Any post-launch changes will be presented in The Nimbus 6 Data Catalogs.

### 5.3.3 Tape Format

The format of one logical record of the CBT is given in Table 5-6. These tapes are Fortran readable; all numbers are I\*2. The table shows the format of one logical record (16 seconds of ESMR data). The physical record is ten logical records. Each logical record will have 375 numbers (750 bytes). The radiometric data for the 71 beam positions (positions 5-75 in the format) will be packed to conserve tape space, but the packing format will be easy to decode. The number recorded on the tape for the brightness temperature at the i-th beam position ( $N_i$ ) is determined by using the equation

$$N_i = 256(T_{Hi} - 50) + T_{Vi} - 50 \quad (13)$$

where  $T_{Hi}$  and  $T_{Vi}$  are the brightness temperatures for the horizontal and vertical polarizations, respectively. This form is unambiguous for brightness temperature between 50°K and 306°K. Latitude and longitude locations (format positions 76-85) are given for beam positions 6, 21, 36, 51, and 66. The locations of other beam positions can be determined by interpolation and extrapolation. Digital B flags 1 through 4, and 10 are bits 1 through 5, respectively, for position 86 of the first scan, while the horizontal and vertical AGC numbers are in this position on the next two scans. In a logical record where the values for position 86 change from the preceding record, the radiometric values in the "changed" record should be ignored. The position numbers after 86 are primarily of engineering significance and will not be discussed here.

Table 5-6  
Format of an ESMR Calibrated Brightness Temperature Tape Logical Record

Position	Scan 1	Scan 2	Scan 3
1	Year	Day	Program Version
2	Hour	Hour	Hour
3	Minute	Minute	Minute
4	Second	Second	Second
5	Temp. Beam Pos. 1	Temp. Beam Pos. 1	Temp. Beam Pos. 1
6	Temp. Beam Pos. 2	Temp. Beam Pos. 2	Temp. Beam Pos. 2
•	• • •	• • •	• • •
•	• • •	• • •	• • •
75	Temp. Beam Pos. 71	Temp. Beam Pos. 71	Temp. Beam Pos. 71

Table 5-6 (Continued)

Position	Scan 1	Scan 2	Scan 3
76	Lat. BP 6(x10)	Lat. BP 6(x10)	Lat. BP 6(x10)
77	Lat. BP 21(x10)	Lat. BP 21(x10)	Lat. BP 21(x10)
78	Lat. BP 36(x10)	Lat. BP 36(x10)	Lat. BP 36(x10)
79	Lat. BP 51(x10)	Lat. BP 51(x10)	Lat. BP 51(x10)
80	Lat. BP 66(x10)	Lat. BP 66(x10)	Lat. BP 66(x10)
81	Long. BP 6(x10)	Long. BP 6(x10)	Long. BP 6(x10)
82	Long. BP 21(x10)	Long. BP 21(x10)	Long. BP 21(x10)
83	Long. BP 36(x10)	Long. BP 36(x10)	Long. BP 36(x10)
84	Long. BP 51(x10)	Long. BP 51(x10)	Long. BP 51(x10)
85	Long. BP 66(x10)	Long. BP 66(x10)	Long. BP 66(x10)
86	Digital B Flags	Horizontal AGC	Vertical AGC
87	Avg. Hor. Cold Cal.	Avg. Vert. Cold Cal.	$\sigma_{CC}$ Hor. (x10)
88	$\sigma_{CC}$ Vert. (x10)	Avg. Hor. Warm Cal.	Avg. Vert. Warm Cal.
89	$\sigma_{WC}$ Hor. (x10)	$\sigma_{WC}$ Vert. (x10)	S/C Altitude (km)
90	Pitch (x10)	Roll (x10)	Yaw (x10)
91	MPX Temp. 1(x10)	MPX Temp. 2(x10)	MPX Temp. 3(x10)
92	MPX Temp. 4(x10)	MPX Temp. 5(x10)	MPX Temp. 6(x10)
.	.	.	.
.	.	.	.
100	MPX Temp. 28 (x10)	MPX Temp. 29 (x10)	MPX Temp. 30 (x10)
101	MPX Counts 1	MPX Counts 2	MPX Counts 3
.	.	.	.
.	.	.	.
112	MPX Counts 31	MPX Counts 32	SPARE
113	Analog #1	Analog #2	Analog #3
.	.	.	.
.	.	.	.
119	Analog #16	Analog #17	Analog #18
120	Analog #20	SPARE	SPARE
121	SPARE	SPARE	SPARE
.	.	.	.
.	.	.	.
125	SPARE	SPARE	SPARE

### 5.3.4 Data Availability

The NSSDC will maintain an archival file of all ESMR imagery and CBTTs. Upon request the NSSDC will furnish a user with either, or both, products.

Imagery will be archived in 70 mm roll format and will be available to users as either positive or negative film or paper products. When requesting imagery a user should specify the date, orbits, and area of interest (by latitude and longitude), as well as the photographic product desired. All ESMR photographic data available will be listed in The Nimbus 6 Data Catalogs.

Seven track CBTTs will be available from NSSDC. The user should specify the date, orbits, and area of interest. The most important information is the day and the time (GMT) of data coverage since this is given for each scan of data. The Nimbus 6 Data Catalog ESMR information should be used to extract this data. The address of the NSSDC and user ordering procedure are described in Section 1.7 of this report.

## SECTION 6

### THE EARTH RADIATION BUDGET (ERB) EXPERIMENT

by

W. L. Smith, D. T. Hilleary, H. Jacobowitz, and H. B. Howell  
National Environmental Satellite Service  
National Oceanic and Atmospheric Administration

Washington, D. C.

and

J. R. Hickey and A. J. Drummond\*  
The Eppley Laboratory  
Newport, Rhode Island

#### 6.1 Scientific Objective

The ERB experiment is designed to provide highly accurate (1 percent or better) radiation measurements of the sun and earth from which the terrestrial radiation budget can be determined on both the synoptic and planetary scales. The measurements obtained will serve as an initial bench mark data set for the long-term monitoring of the radiational aspects of the global environment.

Measurements of radiation will be obtained in 22 different optical channels. Ten solar channels (labeled 1 through 10) will measure incoming solar radiation. Four earth-looking channels (11 through 14) with fixed wide-angle FOV's will measure radiation from the entire earth disc. Eight earth-looking scanning channels with narrow-angle FOV's will measure the angular dependence of earth radiation. Four of these channels (15 through 18) will measure short wavelength radiation, while the other four (19 through 22) will measure the long wavelength radiation. Tables 6-1, 6-2 and 6-3 present the spectral characteristics of solar, wide-angle, and narrow-angle channels respectively.

#### 6.2 Description of the Experiment

##### 6.2.1 Solar Channels

The ERB experiment measures the incoming solar radiation in 10 spectral channels as the satellite orbits over the Antarctic, just before it starts its northward trip on the daylight side of the earth. The spectral intervals monitored

---

\*Deceased

Table 6-1  
Optical Characteristics of ERB Solar Channels

Channel	Wavelength Limits ( $\mu\text{m}$ )	Filter	Solar Irradiance Air Mass Zero ( $\text{W m}^{-2}$ )	Approximate Non-amplified Signal Output (mV)	Amplified** Operational Responsivity (Bits/ $\text{W m}^{-2}$ )	Noise Equivalent Irradiance ( $\mu\text{W cm}^{-2}$ )
1	0.2-5.0	Suprasil W	1346.4	15.3	1.338	1.77
2*	0.2-5.0	Suprasil W	1346.4	15.3	1.338	1.77
3	<0.2->5.0	None	1353.0	19.0	1.331	1.43
4	0.530-3.0	OG530	961.8	10.1	1.872	1.94
5	0.695-3.0	RG695	696.2	7.6	2.586	1.91
6	0.394-0.505	Interference Filter	205.4	0.76	8.398	3.58
7	0.345-0.460	Interference Filter	169.6	0.51	10.155	5.73
8	0.300-0.408	Interference Filter	114.4	0.32	13.851	7.55
9	0.264-0.340	Interference Filter	46.1	0.85	34.384	.94
10	0.243-0.312	Interference Filter	21.7	0.17	73.110	1.32

NOTES:

\*Channels 1 and 2 are redundant. Channel 2 is used for in-flight calibration of channel 1.

\*\*Values of channel operational sensitivities include safety factors for temperature effects and irradiance uncertainties.  
10 Volts = 2047 Bits

- Channels 1 through 8 are fitted with N3 type thermopile detectors; channels 9 and 10 have type K2 thermopiles
- The unencumbered FOV for all channels is 10 degrees; the maximum field is 26 degrees for channels 1 through 8 and 28 degrees for channels 9 and 10.

Table 6-2  
Optical Characteristic of ERB Fixed Wide-Angle FOV Channels

Channel	Wavelength Limits ( $\mu\text{m}$ )	Filter	Irradiance Range Anticipated ( $\text{W m}^{-2}$ )	Approximate Non-Amplified Signal Output (mV)	Amplified Operational Sensitivity (Bits/ $\text{W m}^{-2}$ )	Noise Equivalent Irradiance ( $\mu\text{W cm}^{-2}$ )
11	<0.2 to >50	None	-200 to +600	-2.1 to 7.6	1.707	0.655
12*	<0.2 to >50	None	-200 to +600	-2.1 to 7.6	1.707	0.655
13	0.2 to 5.0	2 Suprasil W Hemispheres	0 to 450	0 to 5.7	2.276	0.655
14	0.695 to 3.0	RG695 Hemispheres	0 to 250	0 to 3.2	4.096	0.665
		Between 2 Suprasil W Hemispheres				

NOTES:

- \* Channels 11 and 12 are redundant channels. Channel 11 is used for in-flight calibration of channel 12.
- All channels have type N3 thermopile sensors.
- All channels have an unencumbered FOV of 121 degrees and a maximum FOV of 133.3 degrees.
- Channel 12 has an additional FOV selection of 89.4 degrees unencumbered, 112.4 degrees maximum.

Table 6-3  
Optical Characteristics of ERB Scanning Channels

Channel	Wavelength Limits ( $\mu\text{m}$ )	Filter	FOV (Degrees)	Responsivity (V/W RMS/RMS)	Noise Equivalent Radiance ( $\text{W cm}^{-2} \text{ sr}^{-1}$ )	NEP ( $\text{W Hz}^{-1/2}$ )
15-18	0.2 to 5.0	Suprasil W Deposited Layers On	0.25 X 5.12	50	3.7 X 10 <sup>-5</sup>	6.65 X 10 <sup>-9</sup>
19-22	4.5 to 50	Diamond Substrate	0.25 X 5.12	50	1.8 X 10 <sup>-5</sup>	1.73 X 10 <sup>-9</sup>

by the solar channels are illustrated in Figure 6-1, superimposed on the 1971 standard extraterrestrial NASA curve. These bands were selected to provide measurements of the solar "constant," necessary for earth heat budget computations, and of solar energy in spectral subdivisions in the ultraviolet and visible regions where solar emission variability may occur and where uncertainties exist in present values of the solar emission spectrum.

### 6.2.2 Fixed Wide-Angle FOV Channels

Earth-emitted infrared radiation and reflected solar radiation are measured with fixed, wide-angle FOV (approximately 130 degrees) sensors. The four wide-angle channels (11 through 14) instantaneously view the entire earth disc (of 3330 km in radius when viewed from 1112 km) and provide a direct measure of the total terrestrial flux passing through a unit area at the satellite altitude. An integration of these measurements over the entire globe, together with the solar constant observations, provide a measure of the net radiation balance for the earth-atmosphere system. In principle, the accuracy of this measurement should be compromised only by the diurnal sampling restrictions of the Nimbus sun-synchronous orbit. Measurements of the radiation flux reflected in the short wave region ( $0.2 \mu\text{m}$  to  $5 \mu\text{m}$ ), in addition to those of the total earth radiation flux ( $0.2 \mu\text{m}$  to  $> 50 \mu\text{m}$ ), permit separation of the planetary albedo and long wave flux components of the observed net radiation flux.

An earth flux channel (ch. 14) and a solar flux channel (ch. 5) measure radiation in the  $0.7 \mu\text{m}$  to  $3 \mu\text{m}$  interval enabling the planetary albedo to be defined for the spectral subregions  $\lambda < 0.7 \mu\text{m}$  and  $\lambda > 0.7 \mu\text{m}$ . These two spectral regions separate the molecular-plus-aerosol contribution from the aerosol-dominant spectral contribution to the total backscattered radiation. This separation is important for assessing the contribution of aerosols to any detectable variations of the earth's planetary albedo.

### 6.2.3 Narrow-Angle FOV Scanning Channels

The ERB also obtains measurements of the earth-reflected solar radiation ( $0.2 \mu\text{m}$  to  $4 \mu\text{m}$ ) with channels 15 through 18 and earth-emitted long wave radiation ( $4 \mu\text{m}$  to  $> 50 \mu\text{m}$ ) with channels 19 through 22. These scanning channels, which have a rectangular FOV of 0.25 degrees x 5.12 degrees, are needed to observe the worldwide radiation budget in sufficient detail for use in synoptic scale numerical weather prediction models. Since conversion of directional radiance observations to hemispheric flux requires the use of angular distribution models, the scanning portion of the ERB experiment is designed to obtain a large number of angularly independent views of the same geographical area as the Nimbus spacecraft orbits overhead. Characteristic angular distribution models are derived for a variety of reflecting surface conditions from a

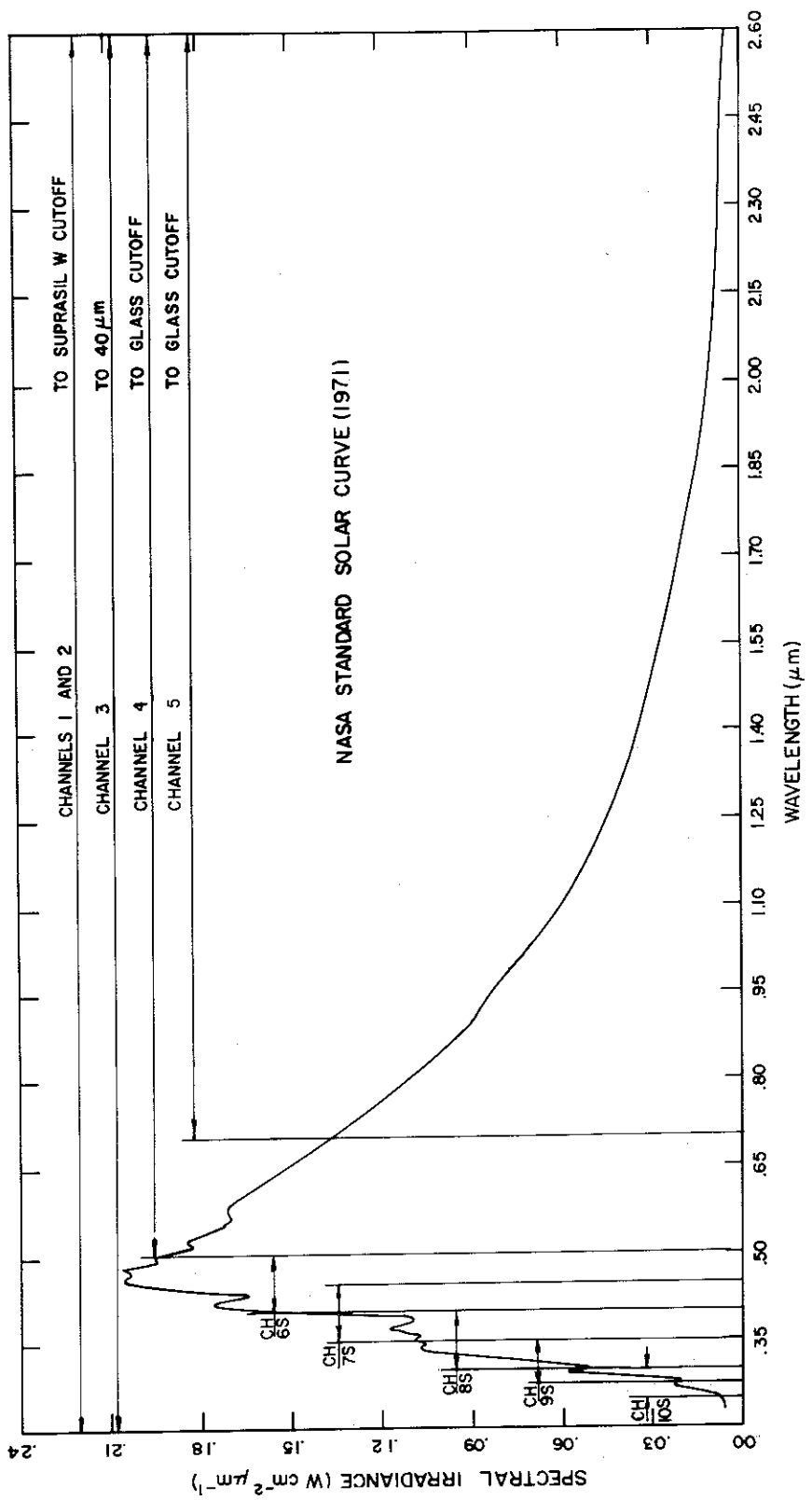


Figure 6-1. Spectral Intervals Monitored by the ERB Solar Channels  
(With 1971 NASA Standard Extraterrestrial Solar Curve)

composite of the scanning channel observations of each area. These models are used to specify the radiation budgets of synoptic scale regions.

#### 6.2.3.1 Scan Geometry and Scan Modes

The basic scan geometry of the ERB is shown in Figure 6-2. The ERB scan is designed to integrate over smaller angular intervals during the horizon portion of the scan to partially maintain the same ground resolution from nadir to horizon. Additional averaging of the radiance data in the ground data processing is performed to eliminate remaining differences in ground resolution as a function of viewing angle.

To observe the radiance from various scenes over a wide variety of incident and emerging angles, there are five different scan modes of operation. These routines are schematically illustrated in Figure 6-3. Four scan patterns are a composite of long and short grids shown in Figure 6-2 (a long grid in the forward direction is followed by a short grid in the cross-track direction and then concluded with a long grid in the aft direction). The fifth scan pattern is a composite of scan pattern 3 followed immediately by scan pattern 4. Scan modes 1, 2, 3, and 4 obtain a maximum number of angular independent views of a given geographical area. When the instrument is in one of these four modes of operation, that scan pattern is repeated every 112 seconds or every 700 km along the subpoint track. These four scan modes ensure the ability to obtain numerous observations in the principal plane of the sun, the plane in which the greatest angular variations in reflected sunlight occur. Scan mode 5, which is the normal mode of operation to obtain maximum earth coverage, is repeated every 224 seconds or every 1400 km along the subpoint track.

Figures 6-4 and 6-5 show a complete scan pattern projected on an imaginary sphere coincident with the earth's surface and fixed with respect to the satellite. The solid line with the arrowheads indicates the motion of a point on the earth's surface relative to the imaginary sphere and scan pattern. The small target areas considered for illustration are located at 40°N latitude in Figure 6-4 and 0° latitude in Figure 6-5. The shaded portions of the scan pattern indicate which FOV's contain the target area. The area is first observed on the forward horizon (in the direction of satellite motion) at a view angle of 58.5 degrees. During succeeding scan patterns, as the satellite approaches the area, the area is viewed at angles of approximately 56, 51, 49, 15, and 0 degrees. As the satellite moves away from the area, radiance observations are made over the other half of the scanning plane at view angles of 15, 40, 51, 57, and 58.5 degrees. Consequently, a fairly complete picture of the angular distribution of radiation emerging from this geographical area in the scanning plane is obtained. Figure 6-5 is presented to illustrate how the side grid scan helps to sense the angular distribution of radiation from geographical areas which are not near the subpoint track.

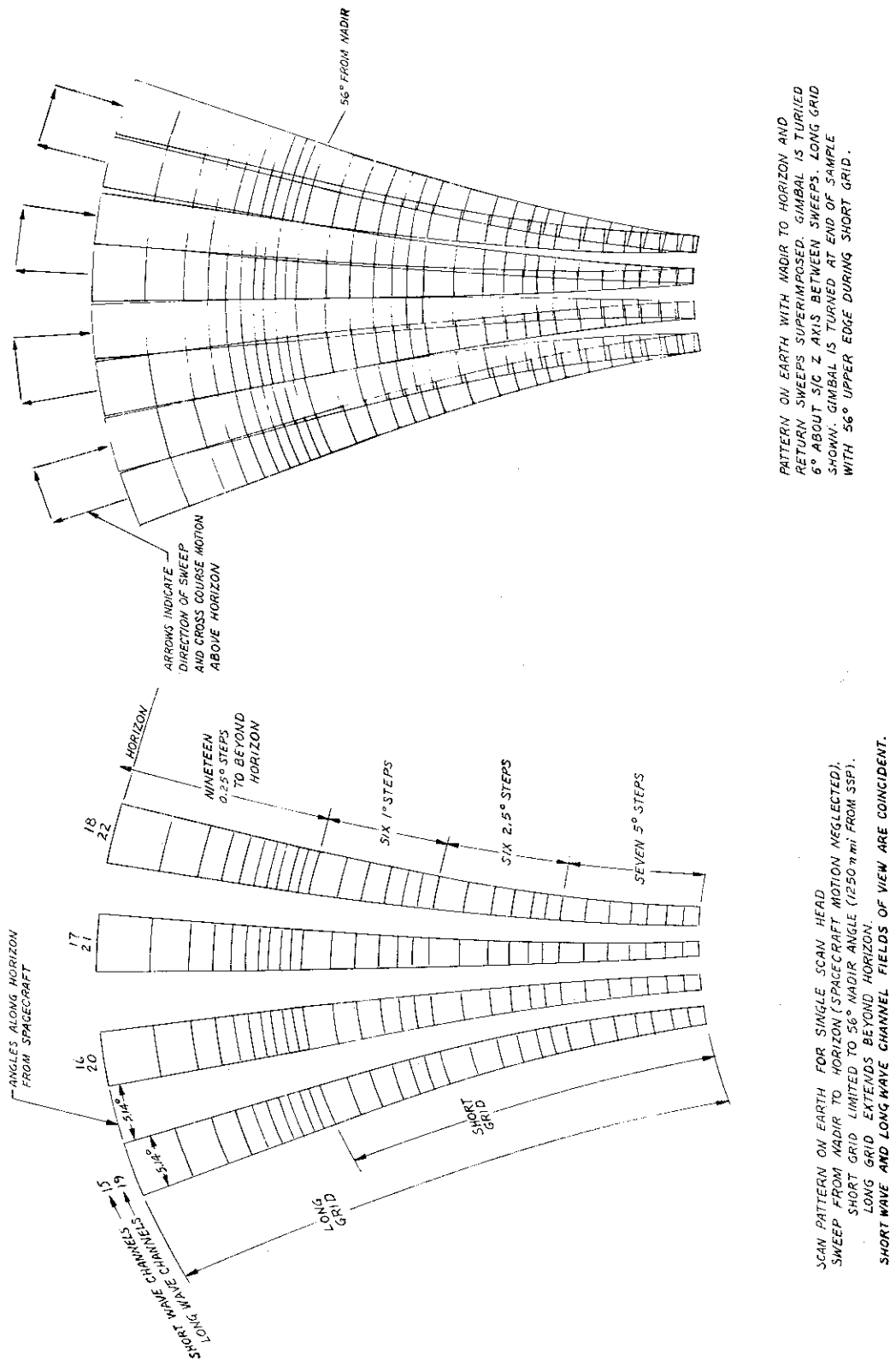


Figure 6-2. ERB Scan Grid Earth Patterns

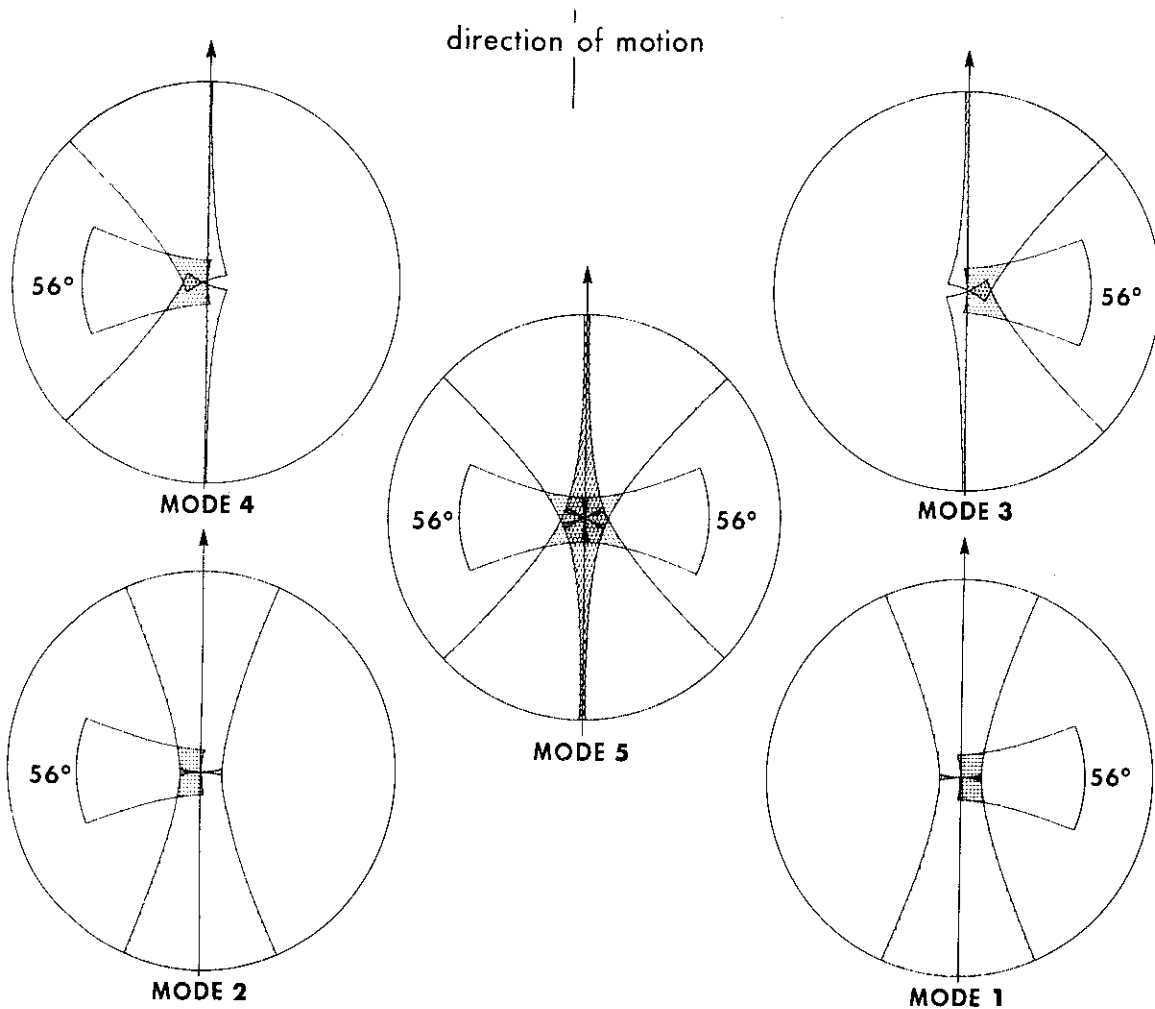
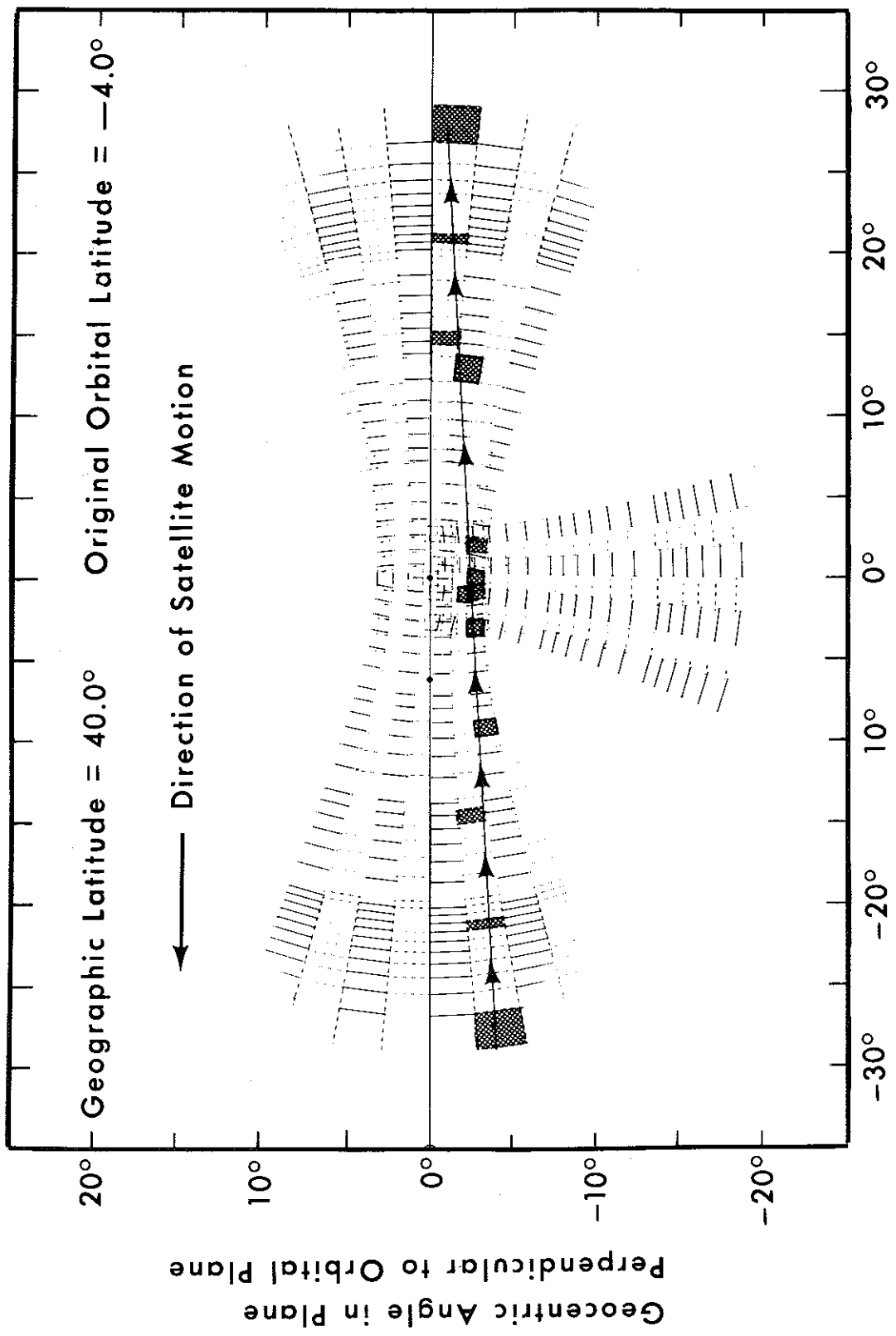


Figure 6-3. ERB Scan Modes

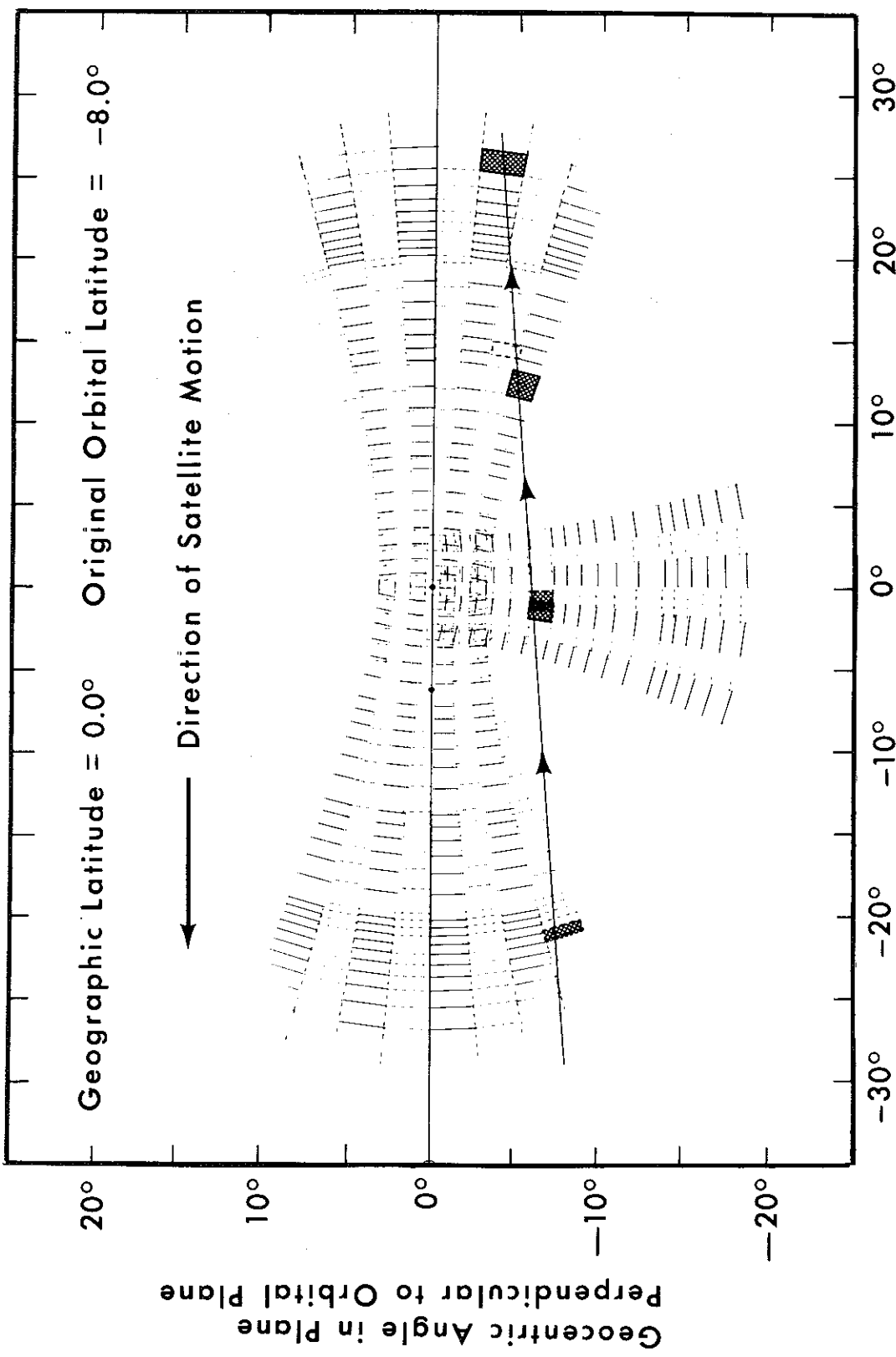
#### 6.2.3.2 Modeling the Angular Distribution of Radiance

The ERB scanning channel observations are used to model the angular distribution of the radiance reflected and emitted by the earth and atmosphere. The surface of the earth is first divided into "target areas" of approximately 500 km x 500 km. As a matter of convenience in the data handling, the boundaries of the target areas are chosen to coincide with the latitudes and meridians specified in Table 6-4. The radiances observed from a particular target area will be weighted according to the geometrical proportion of the FOV which lies within the target area. A weighted average radiance for the target area can then be obtained with observations having approximately the same angles of observation and solar incidence. Since a single target area is seen from as



**Geocentric Angle in Orbital Plane**

**Figure 6-4. ERB Scanning Channel Views of a Geographical Area  
Near the Subpoint Track**



### Geocentric Angle in Orbital Plane

Figure 6-5. ERB Scanning Channel Views of a Geographical Area Away from the Subpoint Track

Table 6-4  
ERB Scanning Channel Target Areas

Latitude Limits		Longitude Interval*
Lower Limit	Upper Limit	
0.0	4.5	4.5
4.5	9.0	4.5
9.0	13.5	4.5
13.5	18.0	4.5
18.0	22.5	5.0
22.5	27.0	5.0
27.0	31.5	5.0
31.5	36.0	5.0
36.0	40.5	6.0
40.5	45.0	6.0
45.0	49.5	6.0
49.5	54.0	7.5
54.0	58.5	8.0
58.5	63.0	9.0
63.0	67.5	10.0
67.5	72.0	12.0
72.0	76.5	18.0
76.5	81.0	22.5
81.0	85.5	40.0
85.5	90.0	120.0

\*For each latitude band the longitude intervals start at the 0 degree meridian and progress east by the increments listed.

many as nine very different directions on a single orbital pass, up to eighteen values of radiance (nine reflected and nine emitted), as well as nine sets of accompanying solar incident and radiant emerging angles are determined for each target area. (The earth location of the FOV corresponding to each position of the scanning channel telescopes are not explicitly computed. However, if the user desires such information it may be readily obtained using the formulas given in Reference 3.)

For each target area, the angular models of observed radiances are based on a statistical composite of its surface and cloud conditions. Each target area has been categorized by its surface characteristics (i. e., land, water, mountains,

snow, ice, and forests) as a function of season. Each target area is further subdivided by the type of cloudiness present at the time of observation. The cloud types are based on the cloud distributions (heights and amounts) provided by the Nimbus 6 HIRS experiment.

From time composites of the radiance data collected for each specific surface and cloud category, the relative angular reflection and emission patterns are obtained. The relative radiant intensity is defined by

$$R_s(\phi_o, \phi, \theta) = \frac{I_s(\phi_o, \phi, \theta)}{I_s(\phi_o, 0, 0)}, \quad (1)$$

and

$$R_L(\phi) = \frac{I_L(\phi)}{I_L(0)}, \quad (2)$$

where  $\phi_o$  and  $\phi$  are the solar and satellite zenith angles, respectively, and  $\theta$  is the azimuth angle of the emerging radiance. The subscripts S and L refer to the short wavelength and long wavelength regions, respectively. Since the intensity of radiation is not measured at all possible combinations of azimuth and zenith angles, supplementary data obtained from aircraft observations and theoretical computations are used to extrapolate the ERB reflected radiation data over the entire upward hemisphere of directions.

From the average angular patterns of relative radiance,  $R_s^c(\phi_o, \phi, \theta)$  and  $R_L^c(\phi)$ , for each surface and cloud category, a general model of the angular distribution of radiance is formulated in terms of empirical orthogonal functions (Reference 2). Specifically the models are:

$$R_s'(\phi_o, \phi_i, \theta_j) = R_s^c(\phi_o, \phi_i, \theta_j) - \bar{R}_s(\phi_o, \phi_i, \theta_j) = \sum_{k=1}^K a_k \xi_{ijk}, \quad (3)$$

and

$$R_L'(\phi_i) = R_L^c(\phi_i) - \bar{R}_L(\phi_i) = \sum_{k=1}^K b_k \psi_{ik}, \quad (4)$$

where the overbar signifies a mean over all surface and cloud categories, and  $\xi_{i,j,k}$  and  $\psi_{ik}$  are statistically derived empirical orthogonal functions. (A survey of methods for computing empirical orthogonal functions is given in Reference 1.) The use of empirical orthogonal functions enables optimum specifications of the radiant fluxes for any specific number of radiance measurements. The first function ( $k = 1$ ) explains the maximum amount of the variance of the observed radiance patterns which can possibly be explained by a single function. The second function ( $k = 2$ ) explains the maximum amount of residual variance (i.e., total variance minus that explained by the first function) which can be explained by a single function. In the same manner, subsequent functions explain successively smaller amounts of the total variance.

Having determined the empirical orthogonal functions, the radiant fluxes are specified routinely from the one or more directional radiance measurements for a given area. It follows from (3) and (4) that the true relative radiance distribution for a specific situation can be expressed as a perturbation of the angular distribution obtained from a composite of observations for similar surface and cloud situations. Specifically, the equations (3) and (4) can be re-written in terms of a departure from the composited radiance distribution obtained for the categorical condition,  $R^c$ . The relations are

$$R_s(\phi_o, \phi_i, \theta_j) - R_s^c(\phi_o, \phi_i, \theta_j) = \sum_k a'_k \xi_{i,j,k}, \quad (5)$$

and

$$R_L(\phi_i) - R_L^c(\phi_i) = \sum_k b'_k \psi_{ik}, \quad (6)$$

where  $a'_k$  and  $b'_k$  are new coefficients.

The next step is to transform (5) and (6) to a system of N equations from which coefficients similar to  $a'_k$  and  $b'_k$  can be determined from the N radiance observations. Multiply (5) and (6) by  $I_s(\phi_o, 0, 0)$  and  $I_L(0)$ , respectively to obtain the system of equations

$$I_s(\phi_o, \phi_i, \theta_j) = a^*_o R_s^c(\phi_o, \phi_i, \theta_j) + \sum_{k=1}^{N-1} a^*_k \xi_{i,j,k}, \quad (7)$$

and

$$I_L(\phi_i) = b^*_o R_L^c(\phi_i) + \sum_{k=1}^{N-1} b^*_k \psi_{ik} \quad i = 1, 2, \dots, N, \quad (8)$$

where  $a^*_o = I_s(\phi_o, 0, 0)$ ,  $b^*_o = I_L(0)$ ,  $a^*_k = I_s(\phi_o, 0, 0)$ ,  $a'_k$  and  $b'_k = b^*_k - I_L(0)$ . After solving for the  $a^*$ 's and  $b^*$ 's, the total short wave and long wave fluxes can be obtained from integrals of (7) and (8) over the upward hemisphere of directions. The resultant integrated flux relations are

$$F_s(\phi_o) = a^*_o F_s^c(\phi_o) + \sum_{k=1}^{N-1} a^*_k \xi_k^*, \quad (9)$$

and

$$F_L = b^*_o F_L^c + \sum_{k=1}^{N-1} b^*_k \psi_k^*, \quad (10)$$

where

$$\xi_k^* = \sum_i \sum_j \xi_{i,j,k} \cos \phi_i \sin \phi_i \Delta \phi_i \Delta \theta_j, \text{ and}$$

$$\psi_k^* = 2\pi \sum_i \psi_{ik} \cos \phi_i \sin \phi_i \Delta \phi_i.$$

From the long wave and short wave fluxes the net radiation,  $F_N$ , is computed as the difference between the incoming solar radiation (obtained from the solar constant measurements and solar zenith) and the sum of estimated outgoing short wave and long wave fluxes.

## 6.3 Description of the Instrument

### 6.3.1 Physical Layout

The ERB instrument consists of one radiometer unit, as shown in Figure 6-6, with the approximate dimensions of 33 cm x 36 cm x 48 cm and weight of 32.7 kg. All ERB electronics and optics are located within the radiometer unit. The rotatable solar channel assembly is located on the +X surface, facing forward in the direction of spacecraft motion. This assembly can be rotated 20 degrees to either side of the spacecraft x-axis in order to acquire an on-axis view of the sun under the expected variation of the satellite orbit plane with respect to the sun. The scanning channel assembly with the gimbal-mounted cylindrical scan head, and the fixed wide-angle earth-flux channels are located on the +Z (nadir) face of the instrument. Adjacent to the solar channel assembly on the +X surface is the diffuser-plate target for in-flight checks on the calibration of the short wave narrow-angle scanning channels.

### 6.3.2 Solar Channels

Each of the 10 solar channels is an independent, individually replaceable modular element with a mated amplifier as part of the unit. The sensors are advanced versions of wirewound-type thermopiles. There are no imaging optics in the solar channels; only filters, windows, and apertures. No optical amplification is required to maintain high signal-to-noise ratios because the thermopile sensitivities are high and state-of-the-art electronics are used. The spectral intervals of the solar channels have been illustrated in Figure 6-1. Channels 1 and 2 are duplicated, channel 1 being the reference for channel 2 for the in-flight calibration program. Channels 4 and 5 contain broad bandpass filters with transmittance spectra (Figure 6-7) matching those of the standard Schott glasses, OG530 and RG695, of the World Meteorological Organization. (The RG695 glass is also used in channel 14, one of the short wave fixed earth-flux channels.) The filters are protected against particle radiation by 4-mm thick windows or hemispheres of fused silica. The interference filters are deposited on Suprasil W (grade III) fused silica substrates to minimize degradation. The transmittance of Suprasil W from  $0.2 \mu\text{m}$  to  $5 \mu\text{m}$  is shown in Figure 6-8. Blocking, outside the primary transmission bands, is achieved by interference layers only. No absorbing glasses are used. The radiation in the  $0.2 \mu\text{m} - 0.53 \mu\text{m}$ ,  $0.53 \mu\text{m} - 0.70 \mu\text{m}$ , and  $0.20 \mu\text{m} - 0.7 \mu\text{m}$  bands is obtained by differential treatment of the channel 4 and 5 data, together with readings obtained from channel 2. Table 6-1 lists the solar irradiances at the receiver, the FOV, and the measurement type for each channel. Channels 1 through 8 have type N3 thermopiles; channels 9 and 10 have type K2. (Section 6.3.4 discusses the thermopiles in detail.) Note that the maximum FOV of channels 9 and 10 are different from the other solar channels.

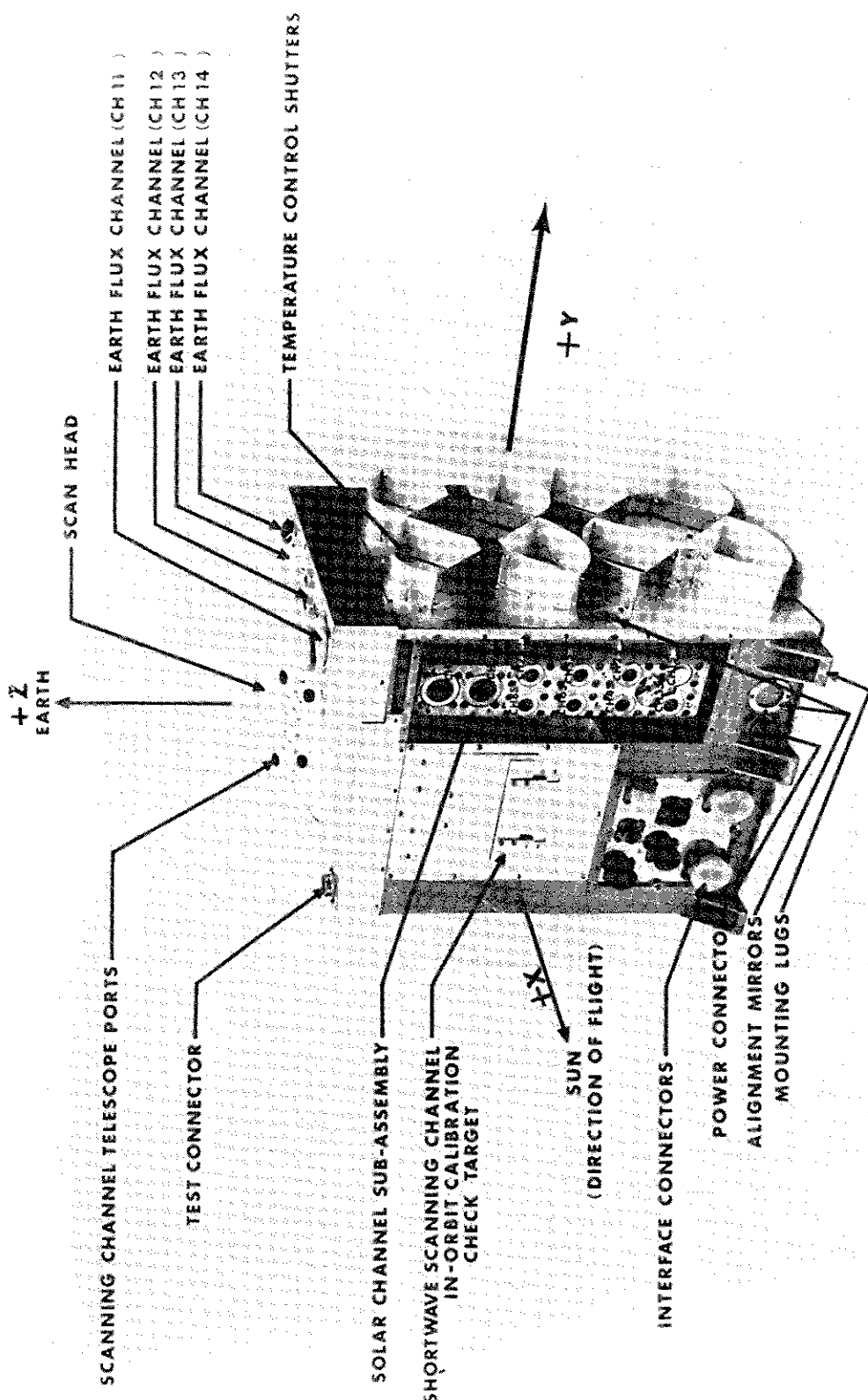


Figure 6-6. ERB Radiometer Unit

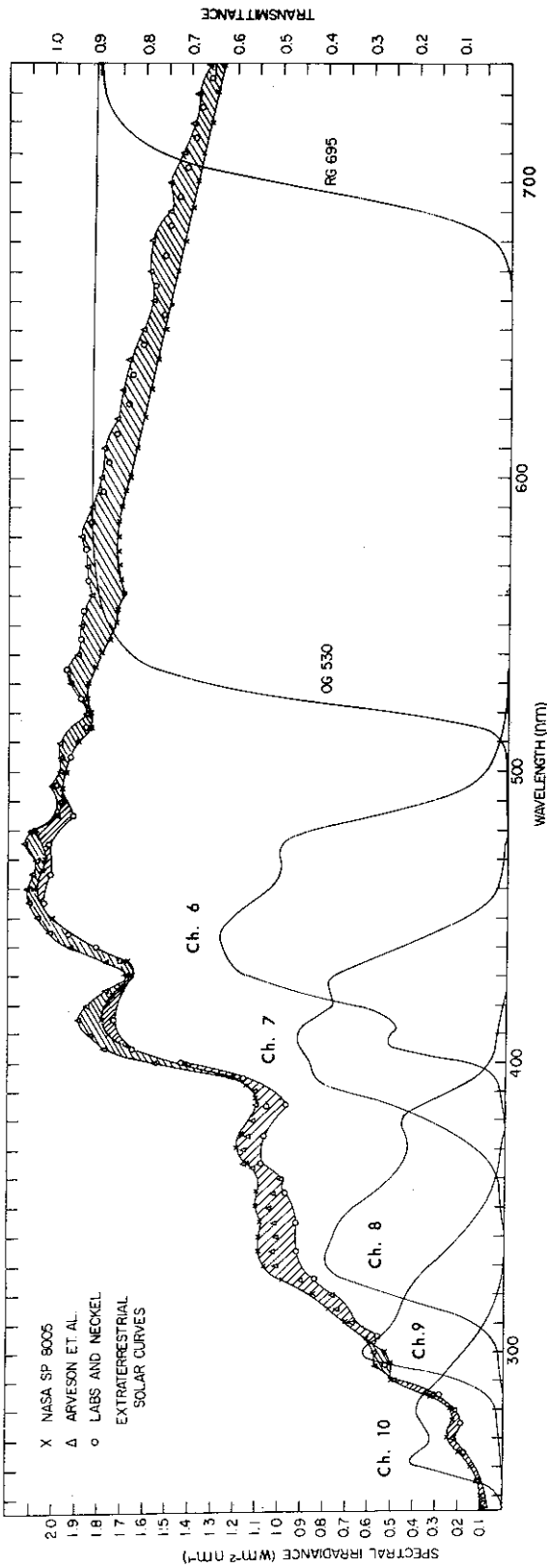


Figure 6-7. Spectral Response Functions of ERB Optical Channels

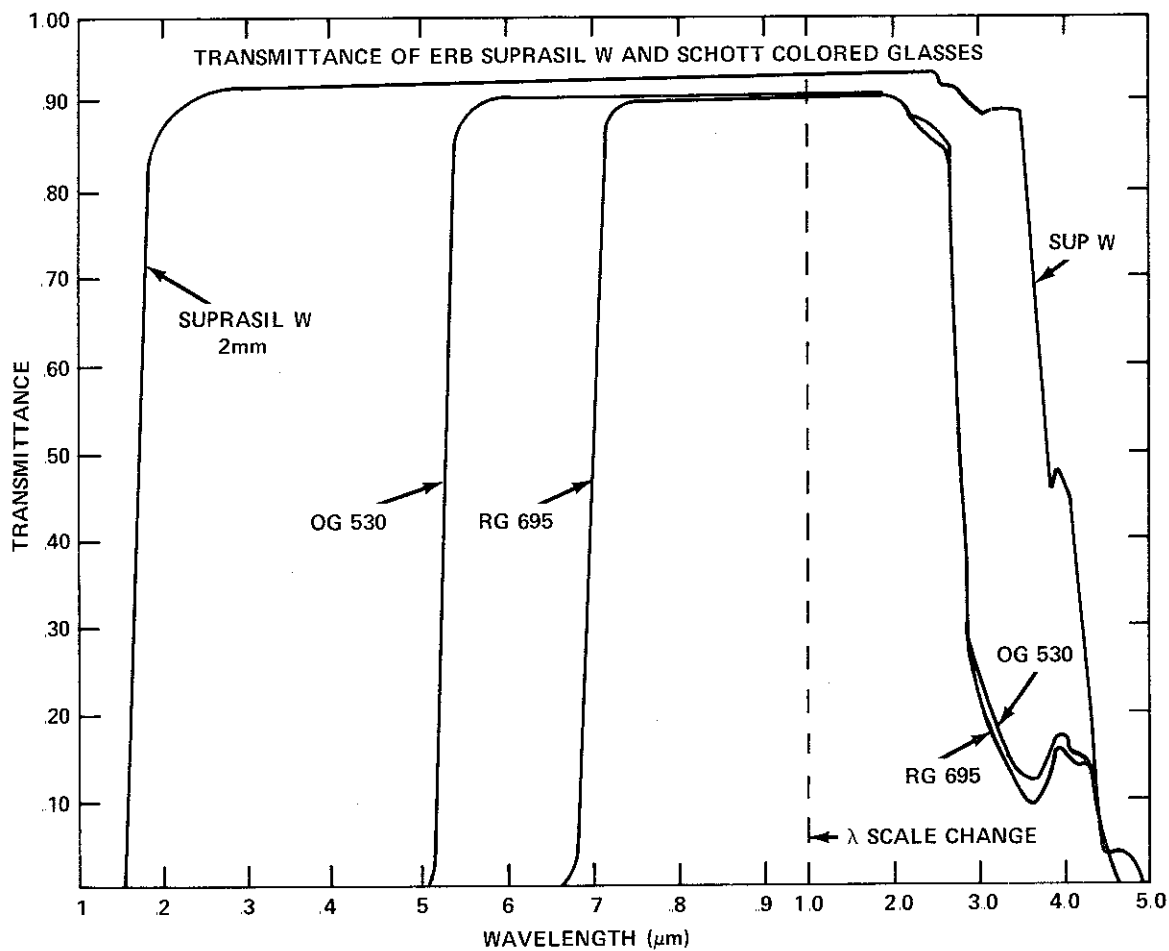


Figure 6-8. Transmittance of ERB Suprasil W and Schott Colored Glasses

As the satellite comes over the Antarctic region each orbit, the sun is viewed within the unencumbered field for about three minutes. The unencumbered field is that for which the entire sun is contained in the receiver FOV. The solar channels are monitored before and after solar acquisition in order to obtain the space radiation reference (or "zero-level" response). The outputs of the solar channels are sampled once per second.

### 6.3.3 Fixed Wide-Angle FOV Channels

The fixed wide-angle FOV channels are numbered 11 through 14. The FOV of each channel encompasses the entire earth surface visible each moment from the Nimbus orbit. To allow for the possibility of a small angular misalignment of these channels with respect to nadir, the FOV acceptance angle is slightly larger than that required to view the earth disc. In addition, channel 12 has an insertable stop so, upon command, it can view slightly less than the entire earth surface.

Channel 11 is a duplicate of 12 and is used only occasionally as a calibration check of channel 12. These two channels, with no filters or windows, measure the absolute irradiance over the band from  $<0.2 \mu\text{m}$  to  $>50 \mu\text{m}$ . The earthward-facing surfaces of these channels are highly polished. Each employs a type N3 thermopile with a circular receiver. These are fabricated from aluminized kapton on which a circle of cured Chemglaze Z-306 paint has been applied and then overcoated with 3M-type 401-C10 black velvet optical paint.

Channel 13, the short wave ( $0.2 \mu\text{m}$  to  $5.0 \mu\text{m}$ ) fixed earth-flux channel, is equipped with two hemispheres of Suprasil W (grade III) fused silica. The spectral band matches that of solar channels 1 and 2. The difference in measured radiation between channel 11 (or 12 with full field) and channel 13 is the long wave terrestrial component. Channel 13 is similar to a precision pyranometer.

Channel 14 has a broadband (RG695 glass) filter hemisphere, to match the band of channel 5. The RG695 hemisphere (partial) of channel 14 is between two Suprasil W, fused silica hemispheres. The outer one is thick to attenuate particle radiation which might damage the glass. The inner hemisphere is the characteristic IR blocker included in all precision pyranometers. The use of RG695 as a separator of the short wave irradiance about its cutoff wavelength of approximately  $0.7 \mu\text{m}$  is a common practice in albedo measurements. After proper correction of the measured irradiance values of channels 13 and 14, the irradiance in the band between  $0.20 \mu\text{m}$  and  $0.7 \mu\text{m}$  is determined. Thus, the primarily scattering and primarily absorbing regions of the short wave reflected radiation are independently assessed.

Table 6-2 lists the magnitudes anticipated for the terrestrial radiances at the receiver as well as the FOV and the type of measurement of each wide-angle FOV channel.

#### 6.3.4 Thermopiles in Channels 1 through 14

The detectors for all the solar and fixed wide-angle FOV channels are improved versions of the wirewound-type thermopiles employed in the Eppley-JPL radiometers. Type N3 is used for channels 1 through 8, and 11 through 14. Those in the earth channels (11 through 14) have a circular blackened area on the receiver, while those in the solar channels 1 through 8 are blackened over the entire square. Channels 9 and 10 have type K2 thermopiles. These are larger than the N3 type, but of similar construction.

The thermopiles are constructed to react to a conductive thermal transient in such a way that both active and reference receivers will respond simultaneously and equally to the temperature offset, thus cancelling any offset in the output signal. Also, the time constants of the actual active and reference couples are

matched by position control during the plating operation. The receivers are matched, coated, and mounted in a manner which assures time constants near balance. This requirement is extremely important because the solar measurements are made during the thermal transition period when the satellite crosses the terminator from darkness to full sunlight. This balance is an especially critical parameter for channels 9 and 10, having type K2 thermopiles, because of the low radiation input signal levels and the high sensitivity of the thermopiles. For this reason, the active and reference junction time constants of the K2 thermopiles must be balanced to within  $\pm 5$  percent to meet the accuracy objectives for the other channels.

#### 6.3.5 Interference Filters in Channels 1 through 14

Since the ideal square wave response cannot be realized, filter factors are used to specify the transmittance characteristics of each filter. These filter factors (the reciprocal of effective transmittance) should differ by less than 1 percent for all possible extraterrestrial solar spectral distributions over the pertinent filter bands. Table 6-5 gives the approximate wavelength limits and the filter factors for the interference filters used in channels 1 through 14 of the ERB radiometer, assuming the NASA solar curve as the source. Figure 6-8 illustrates the spectral transmittance functions for the interference filters.

#### 6.3.6 Narrow-Angle FOV Scanning Channels

The cylindrical scan head contains four telescopes aligned such that the telescope center lines are 12 degrees apart when projected onto the horizontal plane. The telescopes contain off-axis mirror objectives which are deployed to accept a common chopper interrupting the beams immediately ahead of the field stops. In addition to its time-sharing beam splitter function, the chopper also separates the beam energy into the long wavelength ( $4 \mu\text{m}$  to  $50 + \mu\text{m}$ ) and the short wavelength ( $0.2 \mu\text{m}$  to  $4 \mu\text{m}$ ) relays. Each relay consists of a field stop, spectral filter, cross-axis tilted relay mirror, referred aperture stop, and detector. With the off-axis mirror objective and cross-axis tilted relay mirror tilted equally with respect to the optical axis, the effects of polarization induced by reflection are minimized. The detector is a pyroelectric element immune to solar exposure and intentionally defocussed to provide uniformity in field response.

The scan head is on a gimbal mounted on the main frame of the radiometer unit. The gimbal arrangement allows the pointing direction of the scan head to be varied within a vertical plane by rotation of the scan head, and within a horizontal plane by rotation of the gimbal. The pointing direction of the scan head is specified by two angles,  $\alpha$  and  $\beta$ . The angle  $\alpha$ , in the scan plane, is

Table 6-5  
Filter Factors, Sensitivities, Electronic Gains, and Estimated  
Maximum Irradiances for ERB Channels 1-14

Channel No.	$\lambda_1$ ( $\mu\text{m}$ )	$\lambda_2$ ( $\mu\text{m}$ )	FF	S (in air) (mv/mw-cm <sup>2</sup> )	VA Ratio	G (bits/volt)	$W_e$ (w/m <sup>2</sup> )
1	0.200	4.00	1.156	0.0991	1.261	604	1531.2
2	0.200	4.00	1.156	0.0931	1.239	654	1531.2
3	0.200	50.0+	1.000	0.0860	1.249	605	1538.9
4	0.530	3.00	1.255	0.0963	1.297	919	1093.9
5	0.695	3.00	1.256	0.1020	1.277	1,218	791.9
6	0.396	0.5075	2.46687	0.1011	1.301	7,978	242.9
7	0.346	0.460	4.22722	0.1032	1.217	17,227	217.8
8	0.300	0.408	4.78830	0.1140	1.366	21,110	155.1
9	0.277	0.355	7.55508	0.761	*1.83	9,077	58.96
10	0.246	0.312	11.3185	0.787	*1.83	32,052	28.27
11	0.200	50.0+	1.000	0.0936	1.261	706	1200
12	0.200	50.0+	1.000	0.0965	1.249	691	1200
13	0.200	4.00	1.156	0.1090	1.298	817	1000
14	0.695	3.00	1.256	0.1170	1.368	1,569	500

\* Estimated

$\lambda_1, \lambda_2$  — Wavelength Limits

FF — Filter Factor (assuming NASA Solar Curve)

S — Channel Sensitivity

VA — Vacuum-to-air (Sensitivity) ratio

G — Electronic gain

$W_e$  — Estimated Maximum Irradiance (Produces 2047 bits output)

measured between the nadir ( $\alpha = 0^\circ$ ) direction and the curve connecting the upper edges of the FOVs. The angle  $\beta$ , in the plane perpendicular to the scan plane, is measured between the orbital plane and the scan plane. Thus, the scan plane is the XZ plane when  $\beta = 0^\circ$ . The vertical motion is accomplished with a stepper drive which rotates the scan head in steps of 0.25 degrees. The gimbal rotation is driven by a stepper motor which rotates the gimbal in steps of 0.5 degrees.

The FOV's of the four telescopes are rectangular, 0.25 degrees x 5.12 degrees, and are arranged so that with  $\alpha = 58.6$  degrees the upper corners of the FOV's lie along the earth's horizon as shown in Figure 6-2. The narrow-angle (0.25 degrees) side of the FOV is in the direction of vertical ( $\alpha$ ) motion. The FOV's of the short wavelength channels (15 through 18) are coincident, respectively, with those of the long wavelength channels (19 through 22).

The five scan modes described in Figure 6-3 are based on four gimbal position sequences and one scan head rotation sequence. These sequences are defined in Table 6-6 in terms of VIP major frame count from the start of the basic scan routine, the encoder position, and the angle of rotation. Note that many of the channel output samples result from integration over several (4, 10, or 20) fields of view. The scan head rotation speed is varied to accomplish this so that the sampling frequency of two samples per second is constant.

## 6.4 Prelaunch Calibration

### 6.4.1 Solar Channels

The prelaunch calibration plan for the solar channels consists of a number of absolute intercomparisons and transfer operations. The reference for the absolute calibrations is the new cavity radiometer scale which is referenced to other viable radiometric standards, such as the International Pyrheliometric Scale (IPS) 1956 and radiometric references at the U.S. National Bureau of Standards.

The solar modules are calibrated in both natural and simulated solar beams to establish operating levels and reference points for later calibrations. The primary calibration is accomplished by simultaneous viewing of the sun by the channel modules and a self-calibrating cavity radiometer of the PACRAD type. This calibration is primarily for the total short wave and broad bandpass channels (1 through 5). For indoor calibrations using simulated solar radiation the transfer instrument is a Normal Incidence Pyrheliometer (NIP). This instrument has been calibrated against the same reference standards (new cavity radiometer

Table 6-6  
ERB Scan Head Positions During Scan

A. Alpha Encoder Positions\*

Major Frame	Encoder Position
1	0(20)140, 150(10)200, 204(4)224, 225(1)236
2	237(1)243, 3*263, 2*243, 242(-1)224, 220
3	216(-4)200, 190(-10)140, 120(-20)20, 8*0, 20(20)140
4	150(10)200, 204(4)224, 224, 224(-4)200, 190(-10)140, 120(-20)20
5	7*0, 20(20)140, 150(10)200, 204(4)224, 225(1)230
6	231(1)243, 3*263, 2*243, 242(-1)229
7	228(-1)224, 220(-4)200, 190(-10)140, 120(-20)20, 9*0

\*Alpha encoder positions (m) represent the number of steps (1 step = 0.25° of rotation) from the reference position (0°) so that the angle  $\alpha$  is given (in degrees) by  $\alpha = 0.25 \cdot m$  (degrees).

- This sequence of  $\alpha$  angles (encoder positions) is the same for all scan routines.
- The notation  $n_1 \ n_2 \ n_3$  is used for an arithmetic progression  $n_1, n_1 + n_2, n_1 + 2 \cdot n_2, \dots, n_3$ . For example 0(20)140 can be written 0, 20, 40, 60, ..., 140, and 220(-4)200 is the same as 220, 216, 212, ..., 200.
- The notation  $n_1 * n_2$  means  $n_1$  occurrences of the value  $n_2$ .

B. Beta Encoder Positions<sup>+</sup>

Major Frame	Scan Mode	Encoder Positions	Major Frame	Scan Mode	Encoder Positions
1	1	16*512	1	3	16*557
2	1	4*512, M, 11*524	2	3	4*557, M, 11*569
3	1	9*524, 3*M, 4*692	3	3	9*569, 3*M, 4*692
4	1	6*692, M, 9*704	4	3	6*692, M, 9*704
5	1	3*M, 13*872	5	3	3*M, 13*827
6	1	7*872, M, 8*884	6	3	7*827, M, 8*839
7	1	12*884, 4*M	7	3	12*839, 4*M

Table 6-6 (Continued)

Major Frame	Scan Mode	Encoder Positions	Major Frame	Scan Mode	Encoder Positions
1	2	16*524	1	4	16*479
2	2	4*524, M, 11*512	2	4	4*479, M, 11*467
3	2	9*512, 3*M, 4*344	3	4	9*467, 3*M, 4*344
4	2	6*344, M, 9*332	4	4	6*344, M, 9*332
5	2	3*M, 13*164	5	4	3*M, 13*209
6	2	7*164, M, 8*152	6	4	7*209, M, 8*197
7	2	12*152, 4*M	7	4	12*197, 4*M

- + Beta encoder positions ( $n$ ) represent the number of steps (1 step =  $0.5^\circ$  of rotation) from the reference position ( $n_0 = 518$ ) so that the angle  $\beta$  is given (in degrees) by  $\beta = 0.5 \cdot (n - n_0)$
- The letter M in the table means that the scan head is in motion so that the encoder readout may not be repeated exactly at those times.

scale) and also by direct intercomparison with an Angstrom electrical compensation pyrheliometer which is traceable to IPS 1956.

The primary ERB reference instrument is a NIP with serial number 12018E6 having a Suprasil W window matching the ERB channels. It has been directly calibrated against Eppley Laboratory and Canadian standard pyrheliometers, all with extensive intercomparison histories with IPS standards. Two other NIP instruments have been calibrated by similar intercomparisons for use as ERB standards. These bear serial numbers 12016E6 and 10902E4. The last of these is a high sensitivity unit employed principally for calibration of the short wave scanning channels.

The primary calibration is transferred to the ERB Reference Sensor Model (RSM) by sequentially viewing the direct solar beam (outdoors) and the solar simulator beam (indoors) of the reference NIP. The reference NIP is fitted with a filter wheel having matching filters of channels 4 through 10. The RSM instrument is similar in construction to the actual ERB flight units. All further inter-comparisons of flight units during thermal vacuum and ambient testing are performed by direct intercomparison with the RSM in simulated solar radiation.

#### 6.4.2 Fixed Wide-Angle FOV Channels

There are long wave and short wave calibrations of channels 11 and 12. The long wave calibrations are performed during thermal vacuum testing with a

special blackbody source. The source is a double cavity blackbody unit designed for calibrating channels 11 and 12 after they are mounted on the ERB radiometer unit. It operates over a temperature range of 180°K to 390°K with an apparent emissivity under test conditions in vacuum of 0.995 or greater. Temperatures are measured and controlled to an accuracy of 0.1°C during these calibrations.

The short wave calibrations of the RSM channels 11 and 12 are performed by intercomparison with standard pyranometers that have been calibrated against the pyrheliometric standards mentioned above. These intercomparisons are performed by measuring diffuse radiation in an integrating hemisphere and also outdoors by the well-known solar shading technique. Special Suprasil W partial hemispheres are employed on channels 11 and 12 during these short wave intercomparisons. The reference pyranometers are fitted with FOV reduction collars to match the ERB channels.

Channels 13 and 14 are calibrated in the manner described for the short wave calibration of channels 11 and 12. For calibration of channel 14, the standard pyranometer is fitted with an RG695 hemisphere matching that of the channel. The NIP also has a matching RG695 disc for this purpose.

Channels 13 and 14 of the RSM are intercompared with the matching channels of the flight unit during thermal vacuum testing. This is accomplished by sequentially irradiating these channels (on the RSM and flight unit) by the controlled light beam of the Shortwave Earth-Flux Channel Comparator.

## 6.5 In-Flight Calibration

In-flight checks of the degradation of the solar and earth-flux channels will be accomplished by occasionally unshuttering the reference channels 1 and 11 which are duplicates of channels 2 and 12, respectively. Occasionally channel 12 will be shuttered for comparison with the normally-shuttered channel 11.

In addition to these optical calibration checks, the electronic linearity and gain will be checked, on command, by replacing the normal scene signals with fixed staircase input signals. Any changes in electronic calibration will be noted and corrections will be applied to the outputs of channels 1 through 14.

Channel 13 data will be checked by comparison with channel 12 over the illuminated pole, since at this time the channel 12 output is dominated by the short wave ( $0.2 \mu m$  to  $4.0 \mu m$ ) contribution. An additional daily check of channel 13 can be accomplished by integrating the short wave scanning channel data obtained in the normal scan mode (routine 5). Zero-level signals for both

13 and 14 will be obtained as the satellite passes over the dark pole. The calibration of channel 13, with corrections for the energy contributions from the  $3.0 \mu m - 4.0 \mu m$  spectral region, as determined from the long wave scanning channels, will be used to check the prelaunch calibration of channel 14.

In-flight checks of calibration for the short wavelength scanning channels (15-18) are accomplished, upon command, when these channels view a solar-illuminated diffusely-reflecting scatter plate whose apparent reflectance is known.

The long wavelength scanning channels (19-22) are calibrated in flight, upon command, by viewing internal reference blackbodies for a high radiance target, and by numerous views of space during the scan sequence for a cold target. In addition to the space views, which occur during each scan routine, the scan head can be commanded to a constant space look.

## 6.6 Data Processing and Archiving

The User Formatted Output (UFO) Tapes containing the ERB data will be generated at the Nimbus MDHS and carried daily by courier to NOAA/NESS. These tapes will be retained at NOAA/NESS for approximately one month before being returned to the Nimbus MDHS.

The raw data will be routinely processed by NOAA/NESS and the calibrated data, as well as portions of the raw data, will be stored on the ERB Master Archival Tapes (ERBMAT). The ERBMAT will then be input to a number of analysis programs, some of which will produce calibrated maps of the earth's radiative properties for the GARP Data Systems Test. The calibrated data and a minimum of auxilliary information will be stored on the ERB Compacted Archival Tapes (ERBCAT). NOAA/NESS will retain the original ERBCAT set and send a copy to NSSDC. The basic ERB data processing system is illustrated in Figure 6-9.

The ERBCAT is a 9-track, labeled, binary tape written at a density of 1600 bytes per inch. There is one (protected) file on the tape with an end-file mark after the last data record. The first record is a directory record, and contains information about the contents of the tape. Following the directory record are the data records. Each physical record consists of 10 logical records, a logical record containing 340 data words from one VIP major frame (16 seconds). Each physical record consists of 6844 8-bit bytes including the segment descriptor words and block descriptor words. The data from each orbit are separated from the data of the following orbit by an orbital summary

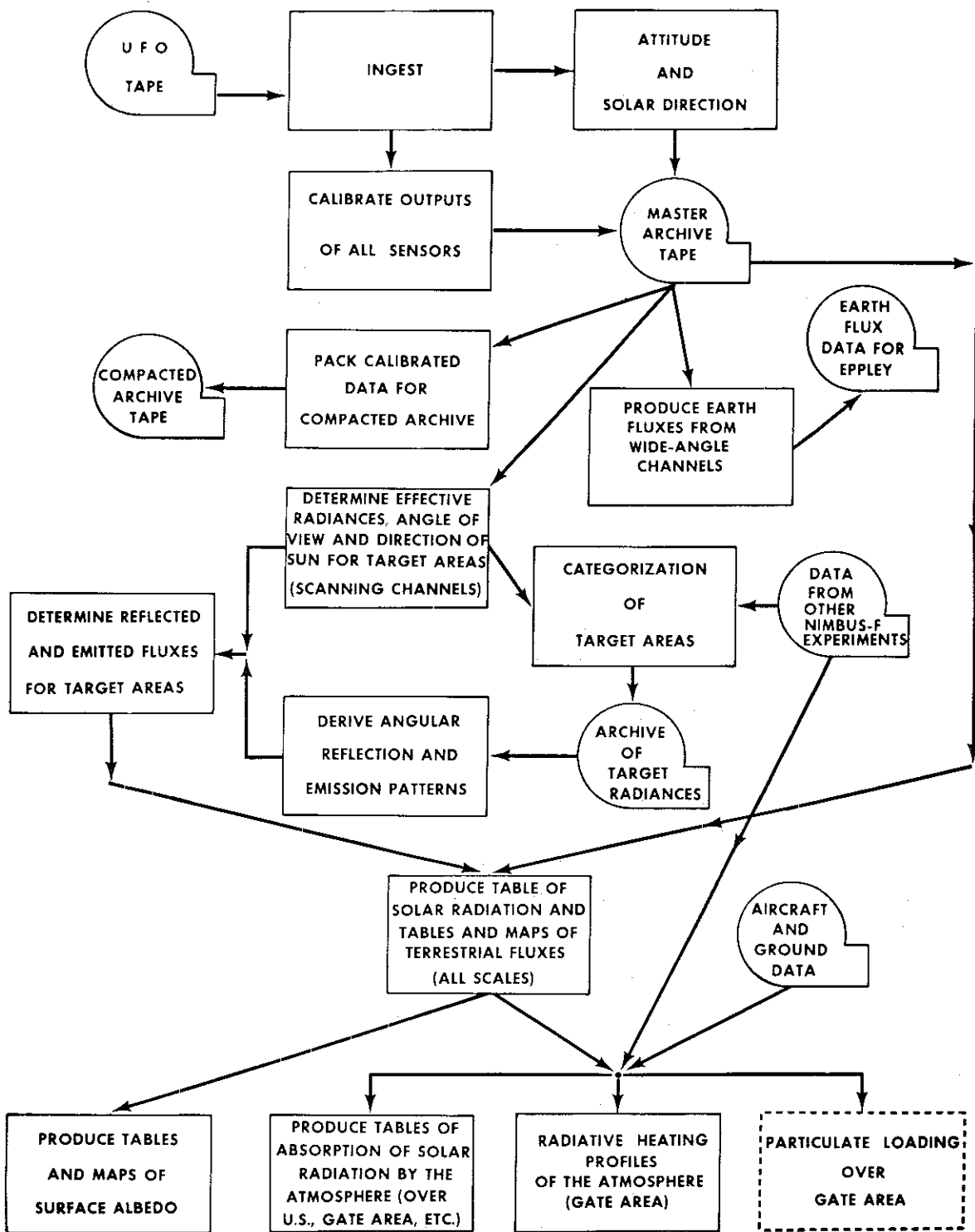


Figure 6-9. ERB Processing System

record of the same length as a logical record and with each of the first four bytes set to FFFF hexadecimal. This record contains some auxilliary data as well as solar irradiances from Channels 1-10. With this format each ERBCAT can contain data from as many as 120 orbits (about 9 days of data) and can be read by standard FORTRAN.

The formats of the directory record, the logical record, and the orbital summary record are described in Table 6-7. Each "word" is an integer of 16 binary bits. The scale factors indicated were used to retain the desired degree of significance. For example the quantity representing subpoint latitude, if floated and divided by its scale factor of 100, will give the subpoint latitude in degrees.

Table 6-7  
ERB Compacted Archival Tape Format

A. Directory Record

Word No.	Description of Quantity
1-4	Tape Identifier (ERBCAT) in EBCDIC
5	Number of orbits on this tape (1-120)
6	Orbit number of first orbit on tape
7	Month at start of first orbit
8	Day at start of first orbit
9	Year at start of first orbit
10	GMT hour and minute (100*Hour+Min) at start of first orbit
11	Month at end of last orbit on tape
12	Day at end of last orbit on tape
13	Year at end of last orbit on tape
14	GMT hour and minute at end of last orbit on tape
15-134	Orbit numbers in order of appearance
135-340	Zero fill

B. Logical Record

Word No.	Description of Quantity	Scale Factor
1	Spacecraft Day number, increasing from zero for day of launch	1
2	Orbit number, increasing from 1	1
3	Year, two least significant digits	1
4	Numeric day of year, 1-365 (or 366), 171 for 20 June 1974	1

Table 6-7 (Continued)

Word No.	Description of Quantity	Scale Factor
5	Hour and Minute (100* Hour + Min) GMT	1
6	Second, 0-59	1
7	Latitude (geodetic), -90°(S) to 90°(N)	100
8	Longitude, -180°(W) to 180°(E)	100
9	Spacecraft Altitude (in km.)	1
10	Spacecraft pitch angle	100
11	Spacecraft roll angle	100
12	Spacecraft yaw angle	100
13-44	32 alpha-encoder positions, 0-511	1
45-60	16 beta-encoder positions, 0-1023	1
61	Gamma-encoder position	1
62-65	4 channel 11 irradiances, 0-12000	10
66-69	4 channel 12 irradiances, 0-12000	10
70-73	4 channel 13 irradiances, 0-9000	10
74-77	4 channel 14 irradiances, 0-5000	10
78-109	32 channel 15 radiances, 0-9000	10
110-141	32 channel 16 radiances, 0-9000	10
142-173	32 channel 17 radiances, 0-9000	10
174-205	32 channel 18 radiances, 0-9000	10
206-237	32 channel 19 radiances, 0-1950	10
238-269	32 channel 20 radiances, 0-1950	10
270-301	32 channel 21 radiances, 0-1950	10
302-333	32 channel 22 radiances, 0-1950	10
334	Instrument status word (normally = 0)	1
	<u>Units decimal digit</u> (indicates position of scan head)	
	0 = Scan mode	
	1 = Nadir position	
	2 = Space position	
	3 = LW check position	
	4 = SW check position	
	9 = Transition mode	
	<u>Tens decimal digit</u> (indicates status of shutters (chs. 1, 11, 12))	
	0 = Reference chs. CLOSED, Ch. 12 OPEN	
	1 = Reference chs. CLOSED, Ch. 12 CLOSED	
	2 = Reference chs. OPEN, Ch. 12 CLOSED	
	3 = Reference chs. OPEN, Ch. 12 OPEN	
	9 = Status unknown	

Table 6-7 (Continued)

Word No.	Description of Quantity	Scale Factor
	<u>Hundreds decimal digit</u> (indicates status of Ch. 12 FOV) 0 = Ch. 12 FOV wide 1 = Ch. 12 FOV narrow 9 = Status unknown	
	<u>Thousands decimal digit</u> (indicates status of El. Cal. and Go/No go heater) 0 = Go/No go heater OFF, El. Cal. OFF 1 = Go/No go heater OFF, El. Cal. ON 2 = Go/No go heater ON, El. Cal. OFF 9 = Status unknown	
335	Scan information word (zero if not in scan mode) Units decimal digit: major framecount (1-7) Tens decimal digit: scan mode (1-5) Hundreds decimal digit: 0 = mode 4 portion of mode 5 1 = mode 3 portion of mode 5 Thousands decimal digit: 0 = no scan errors 1 = $\alpha$ scan errors 2 = $\beta$ scan errors 3 = $\alpha$ and $\beta$ errors	1
336	Solar zenith angle at subsatellite point (0-900)	10
337	Solar azimuth (relative to true north, 0-3599)	10
338	Spacecraft Heading (0-3599)	10
339	Spacecraft illumination indicator (0-4) 0 = none of DSAS sensors are illuminated 1 = sensor 1 illuminated 2 = sensor 2 illuminated 3 = sensor 3 illuminated 4 = sensor 4 illuminated	1
340	Zero fill	

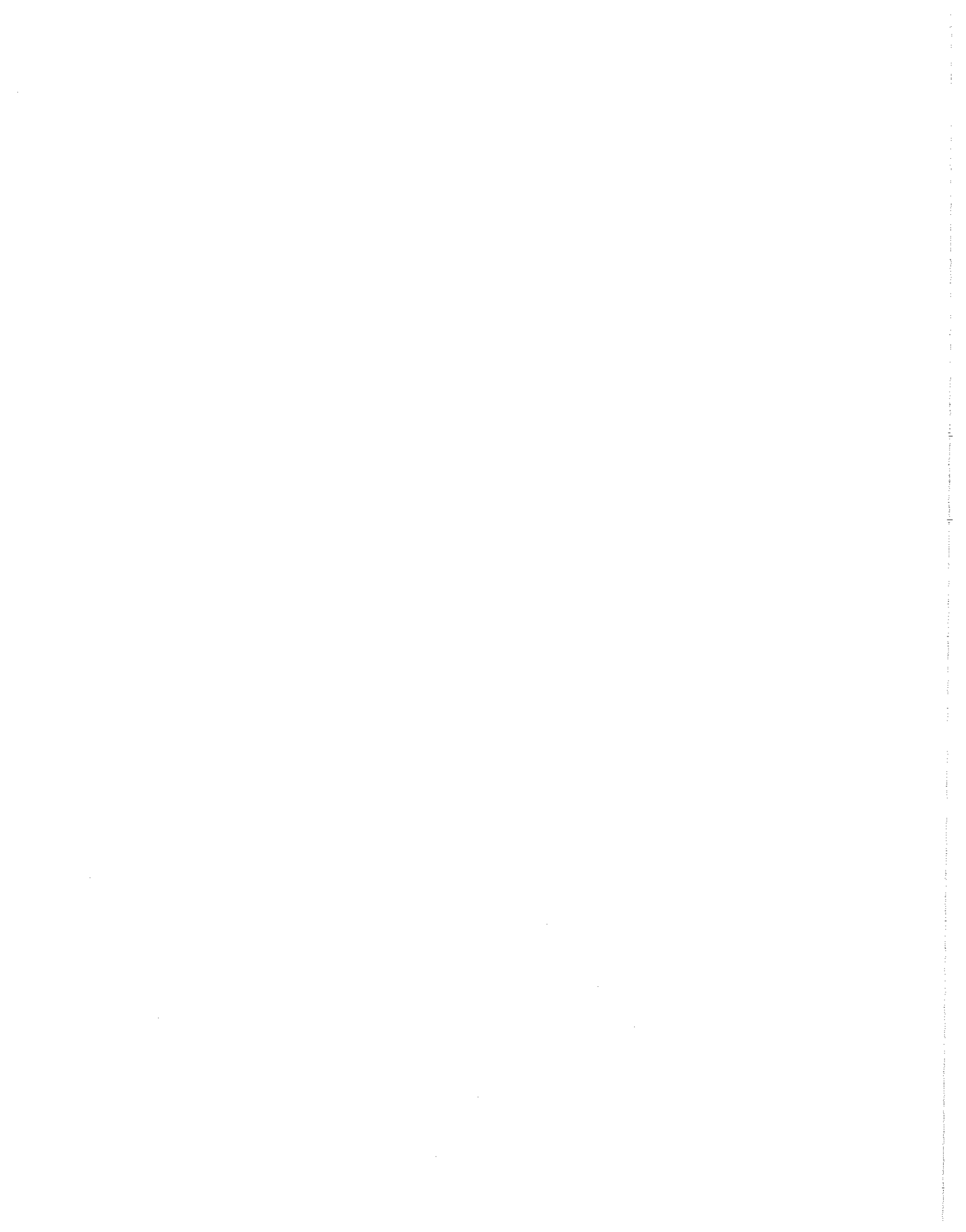
Table 6-7 (Continued)

## C. Orbital Summary Record

Word No.	Description of Quantity	Scale Factor
1	FFFF (Hexidecimal)	1
2	FFFF (Hexidecimal)	1
3	Orbit number	1
4	GMT (100×hours+minutes)	1
5	Numeric day of the year	At the start
6	Year (units and tens digits)	of the orbit
7	Subpoint latitude (-90° to 90°)	100
8	Subpoint longitude (-180° to 180°)	100
9	Number of major frames within the orbit	1
10	GMT	1
11	Numeric day of the year	At the end
12	Year	of the orbit
13	Subpoint latitude	100
14	Subpoint longitude	100
15-16	GMT ( $t_o$ ) of solar chs. peak signal Wd. 15: 100×hours+minutes Wd. 16: seconds	1
17-340	Zero fill	1

## REFERENCES

1. Alishouse, J. C., Crone, L. J., Fleming, H. E., VanCleef, F. L., and Wark, D. Q.: A Discussion of Empirical Orthogonal Functions and Their Application to Vertical Temperature Profiles. Tellus, vol. 19, no. 3, 1967, pp. 477-482.
2. Obukhov, A. M.: The Statistically Orthogonal Expansion of Empirical Functions. Akademiya Nauk, USSR. Izvestiya Seriya Geofizicheskaya 1960, pp. 432-439, (English Translation by the American Geophysical Union, Nov. 1960, pp. 288-291).
3. Ruff, I.: To be published within the National Environmental Satellite Service of the National Oceanic and Atmospheric Administration, 1975.



## SECTION 7

### THE LIMB RADIANCE INVERSION RADIOMETER (LRIR) EXPERIMENT

by

J. C. Gille\* and P. Bailey, NCAR, Boulder, Colorado 80303  
F. B. House, Drexel University, Philadelphia, Pennsylvania 19104  
R. A. Craig, Florida State University, Tallahassee, Florida 32301  
J. R. Thomas, Honeywell Radiation Center, Lexington, Mass. 02173

#### 7.1 Introduction

The Limb Radiance Inversion Radiometer (LRIR) experiment is being conducted to determine the vertical distribution of temperature, ozone, and water vapor from the lower stratosphere (~15 km) through the stratosphere and into the lower mesosphere (~60 km) on a global scale. These vertical distributions will be determined by inverting measured limb radiance profiles obtained by the LRIR, an infrared, multispectral scanning radiometer aboard the Nimbus 6 spacecraft. Measurements are made in each of four spectral regions: two in the  $15 \mu\text{m}$  carbon dioxide band; one in the  $9.6 \mu\text{m}$  ozone band; and one located in the rotational water vapor band ( $23 \mu\text{m}$  to  $27 \mu\text{m}$ ).

A programmed scanning mirror in the radiometer causes the fields-of-view of the four detectors to make coincident, vertical scans across the earth's horizon. (See Figure 7-1 for description of limb-viewing geometry.) The data from these scans are stored on a HDRSS tape recorder for later transmission to the ground. During data reduction the measured limb radiance profiles from the carbon dioxide channels are operated on by inversion algorithms to determine the vertical temperature distribution. This inferred temperature profile, together with the radiance profiles in the ozone and water vapor channels, are then used to infer the vertical distribution of these trace constituents.

Spacecraft hardware consists of a frame housing assembly (FHA) and two electronics units: the frame housing electronics unit (FEU) and the interface electronics unit (IEU). The FHA consists of an optical mechanical package (OMP) and a two-stage solid ammonia-methane cryogen package (SCP) for detector cooling. The FEU conditions radiance signals, controls the scan drive mechanism,

---

\*John C. Gille is principal investigator of the LRIR experiment and coordinates activities of the Science Team, composed of the members above.

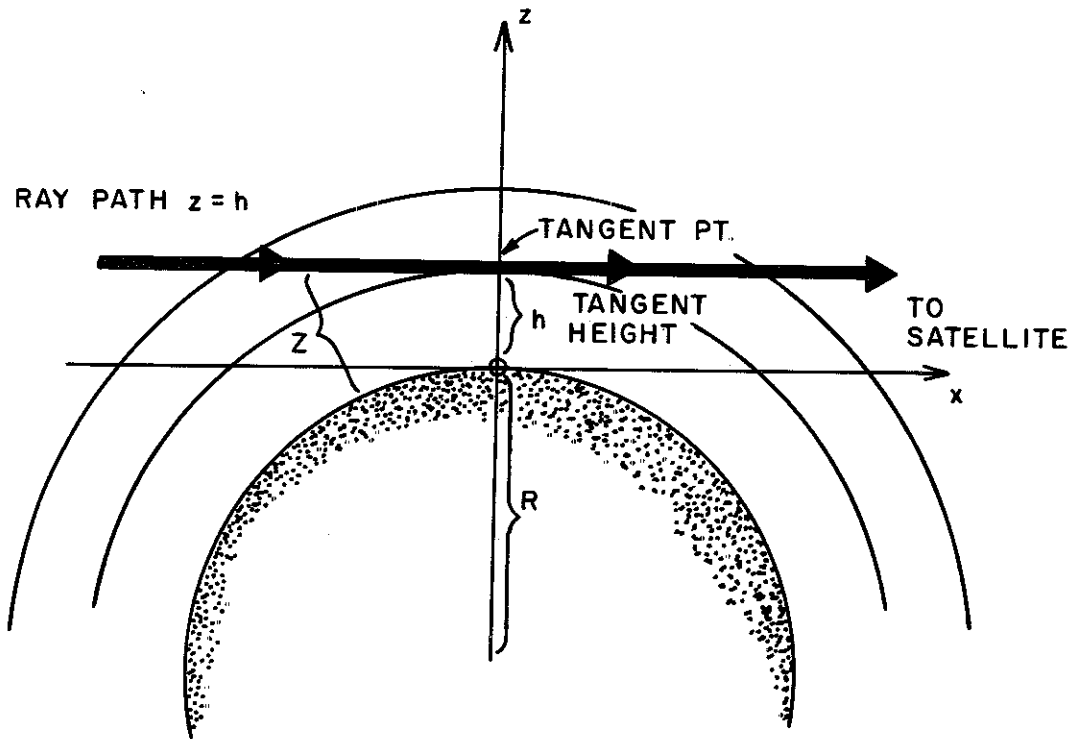


Figure 7-1. LRIR Limb Viewing Geometry

and contains the command relay and command logic assemblies. The IEU interacts with spacecraft systems and performs the functions of signal processing, control, power conversion and digitizing of electronic signals.

## 7.2 Experiment Concept

The scientific objectives of the LRIR experiment are to:

- Acquire and present global measurements of temperature, ozone and water vapor in the stratosphere and lower mesosphere for one year
- Obtain the geostrophic component of the wind up to a level of 1 mb (~48 km) through integration of the temperature profile in the thermal wind equation

In order to meet these scientific objectives, specifications were placed on the instrument design to provide observations of sufficient quality to yield atmospheric parameters to the desired accuracy and precision. In this regard, minimum scientific data requirements were established as indicated in Table 7-1. Instrument specifications were determined relative to these data requirements.

Table 7-1  
LRIR Science Data Requirements

Parameter	Accuracy	Vertical Resolution of Parameters	Altitude Range
Temperature	$\pm 3^{\circ}\text{K}$ RMS	3 km	15-54 km
Ozone	$\pm 20\%$ at 1 mb	3 km	15-48 km (1 mb)
Water Vapor	$\pm 50\%$ at 1 mb	3 km below 30 km 4-5 km above 30 km	15-48 km (1 mb)
Geostrophic winds	$\pm 10$ m/sec (Thickness $\pm 70$ m or $\bar{T}$ to $\pm 1.5^{\circ}\text{K}$ )	Winds at 5, 2 and 1 mb	to 48 km (1 mb)

Referring to Figure 7-1, LRIR receives infrared radiation emitted by the atmosphere along a ray path that may be identified by the height (tangent height) or point (tangent point) closest to the surface. The atmosphere may be scanned by sweeping the view direction from tangent heights  $< 0$  (ray paths intersecting the surface) to large positive values. The following advantageous features of limb scanning are apparent from a consideration of Figure 7-1.

- High inherent vertical resolution

For geometric reasons, a small portion of the signal originates from below the tangent height, and most of the signal originates from a 4 km to 5 km layer above the tangent height.

- Zero background

For  $h > 0$ , all radiation received originates in the atmosphere, and all variations in signal are due to the atmosphere since the radiation is viewed against the cold background of space.

- Large opacity

There is at least 60 times more emitting gas along a horizontal path grazing the surface than there is in a vertical path to the tangent point. Thus, the atmosphere can be sampled to high altitudes.

There are, of course, disadvantages associated with these features. The long paths mean that even for rather transparent spectral regions, it will be difficult to see the solid surface of the planet. A cloud along a path will act as

a body of infinite opacity, and may cause a considerable alteration in the emerging radiation. For the earth's atmosphere, where clouds are present but usually below the tropopause, these facts suggest that reliable operation will be limited to the upper troposphere and above, with even the coverage of the upper troposphere and lower stratosphere being subject to occasional interruption. For these reasons parameters are determined only above a nominal tropopause at 15 km.

The radiative transfer equation for a non-scattering atmosphere in local thermodynamic equilibrium may be written as

$$I_i(h) = \int_{-\infty}^{\infty} B_i[T] \frac{d\tau_i(h; x)}{dx} dx , \quad (1)$$

where  $I$  is the observed radiance at tangent height  $h$  and spectral interval  $i$ ,  $B$  is the Planck blackbody function,  $T$  is temperature,  $x$  the distance coordinate along the ray path, with the origin at the tangent point and positive toward the satellite (located at  $+\infty$ ), and  $\tau(h; z)$  the mean transmission in the spectral interval along the path with tangent height  $h$  from point  $x$  to the satellite.

The temperature inversion problem is to determine  $B$  and therefore  $T$  from measurements of  $I$ , assuming that  $d\tau/dx$  is known. The latter requires that the distribution of the emitting species be known, which in practice means that radiation from  $\text{CO}_2$ , a uniformly mixed gas, is measured. In the limb problem  $d\tau/dx$  is also crucially affected by the atmospheric structure.

In the case of the constituent inversion problem, the solution to the temperature inversion problem is utilized with the constituent limb radiance profile to determine the gas concentration as a function of altitude. In Equation (1),  $B$  is known from the temperature solution. The constituent concentration is determined as an implicit function of transmission  $\tau_i(h; x)$ .

In order to gain a better understanding of the data to be observed by the LRIR, examples of calculated profiles of limb radiance as functions of tangent height are shown from a mid-latitude winter sounding in Figure 7-2.

The broad ( $\text{BCO}_2$ ) channel refers to the  $585-705 \text{ cm}^{-1}$  spectral band, and the narrow ( $\text{NCO}_2$ ) channel covers the band  $630-685 \text{ cm}^{-1}$ . The signals are quite similar at upper levels where only the strong lines near the centers of the bands are contributing. Below about 30 km, the  $\text{BCO}_2$  signal is much larger because the weaker lines in the band wings are contributing energy from the lower atmosphere. The dashed line presents the difference between  $\text{BCO}_2$  and  $\text{NCO}_2$  signals, or the contribution from the  $585-630 \text{ cm}^{-1}$  and  $685-705 \text{ cm}^{-1}$  regions. The

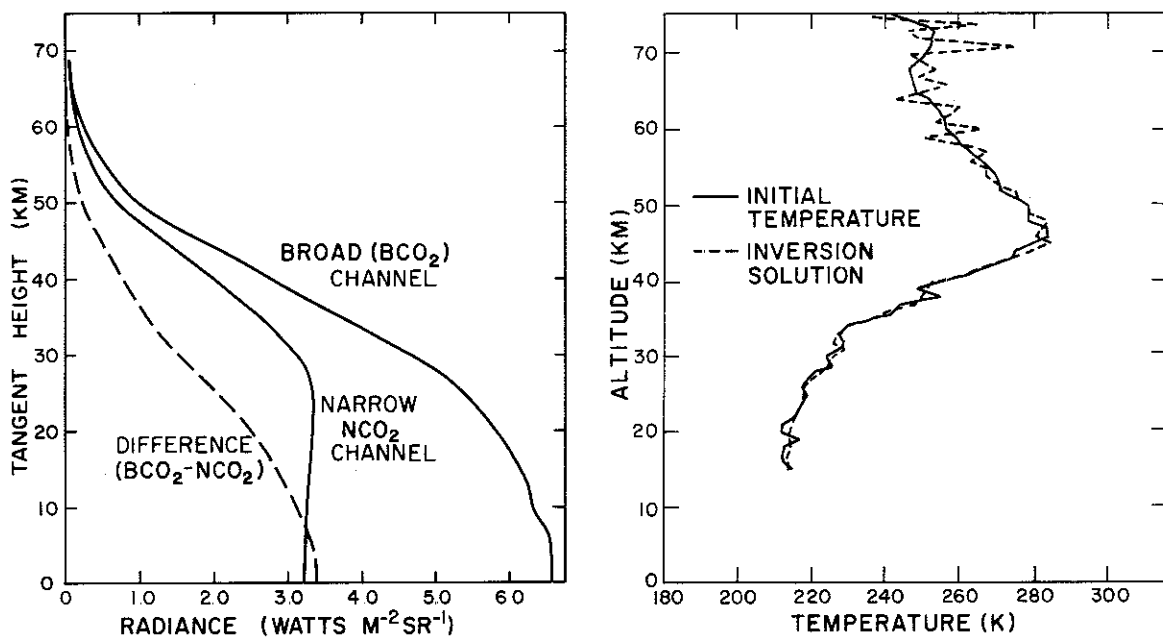


Figure 7-2. Computed Limb Radiances as a Function of Tangent Height for Broad ( $585\text{--}705\text{ cm}^{-1}$ ) and Narrow ( $630\text{--}685\text{ cm}^{-1}$ ) Channels in the  $15\text{ }\mu\text{m}$  Band of  $\text{CO}_2$ .

steeply sloping portions of the curve occur in situations where the whole path through the atmosphere is moderately transparent, and an appreciable portion of the signal is coming from the tangent point. Figure 7-2 demonstrates that the  $\text{BCO}_2$  minus  $\text{NCO}_2$  region provides better information on the lower levels of the stratosphere and upper levels of the troposphere.

The profile depicting inversion results in Figure 7-2 illustrates a realistic solution for typical instrument errors, defined by the science requirements in Table 7-1. These results are based on computed limb radiance profiles in Figure 7-2 which were perturbed for realistic radiometer and pointing errors, and included a 1.5 km instrumental field-of-view. The procedures for inverting  $\text{CO}_2$  radiance profiles to obtain a solution to the temperature distribution are presented in a paper by Gille and House (Reference 1). The inversion results in Figure 7-2 are in good agreement with the initial temperature profile up to about the 55 km level but become more and more "saw-toothed" in nature at higher altitudes. This characteristic is caused by the random error of the instrument which dominates the natural limb signal at high altitudes. In other words, the signal-to-noise ratio of the measurement becomes increasingly smaller as the LRIR scans to higher altitudes. One obvious procedure to employ in the data processing of real observations is to mathematically smooth the solutions

at higher altitudes and/or average adjacent limb profiles before inversion. Mathematical smoothing techniques can also be employed during the inversion procedure.

Solutions to the constituent inversion problem for vertical distributions of ozone and water vapor show characteristics similar to the temperature of inversion results in Figure 7-2. The saw-toothed character of the solution develops in a similar manner and altitude for ozone distributions, but at about a 40 km level for water vapor distributions, since the signal-to-noise ratio degrades at a lower altitude.

### 7.3 Instrumentation

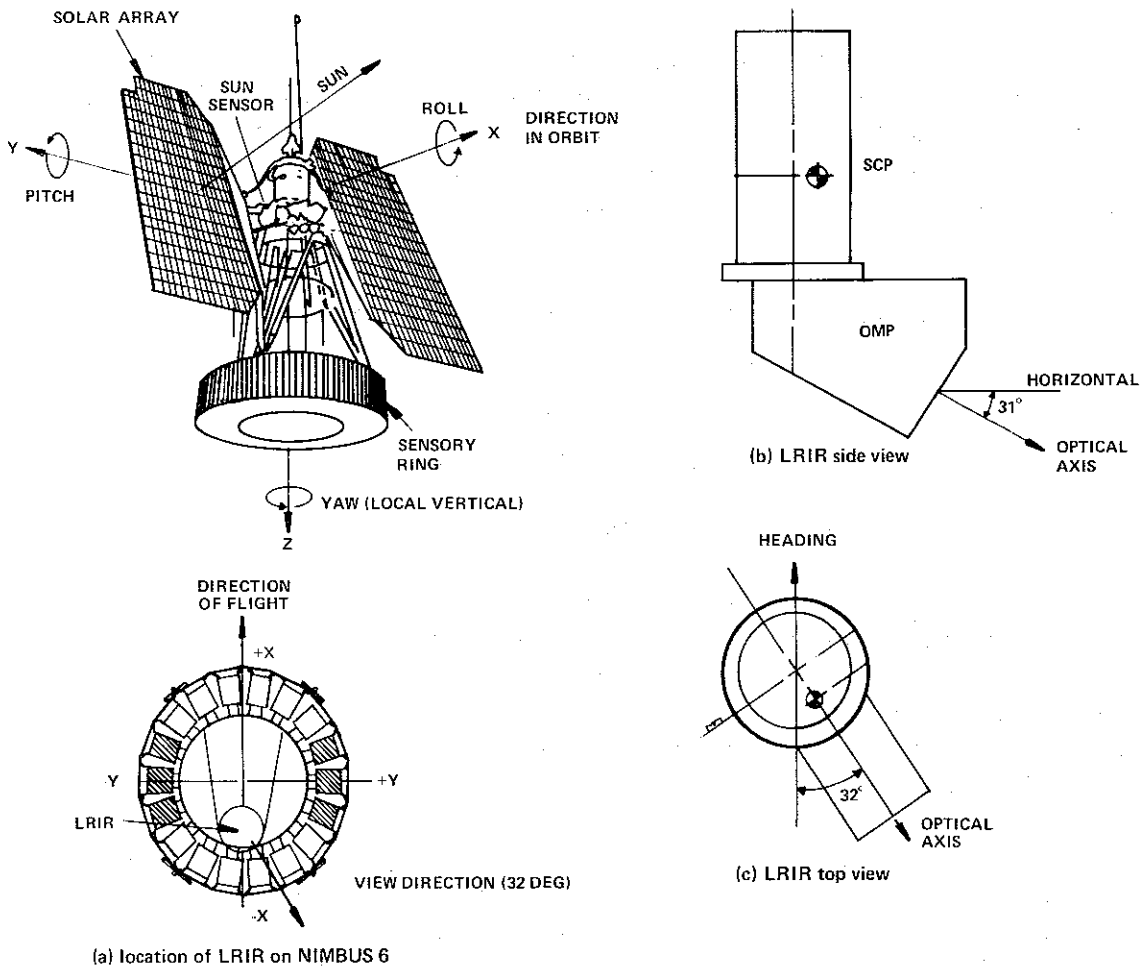
In some respects the LRIR instrumentation is similar to nadir viewing experiments, but in other respects it is considerably different. For example, the radiometer employs a fixed array of cooled detectors whose optical views are directed by a scanning mirror. However, the LRIR scan angle is nominally  $\pm 1$  degree about the earth's horizon, whereas other instruments, like THIR, scan from horizon to horizon across the earth scene. The detectors for LRIR are cooled by a two-stage solid cryogen package incorporating solid ammonia and methane dewars, maintaining the detectors at 65°K. This mechanism of detector cooling is quite different from more widely used radiative coolers.

Since LRIR has a different viewing geometry from nadir viewing experiments, the discussion in this section of the User's Guide first considers the physical location of LRIR on the satellite and the position of view relative to the satellite and relative to the earth's limb. This discussion will help potential users of LRIR data to better understand the relationship between these data and other observations from Nimbus 6. These discussions are followed by details of LRIR instrumentation.

#### 7.3.1 LRIR Location and Limb Viewing Geometry

The information presented in Figure 7-3 illustrates the principal axes of Nimbus 6 and the location of the LRIR relative to these axes and the sensory ring (a). Also shown are associated positions of the optical axis of the radiometer relative to the local horizontal (b) and to the spacecraft heading (c).

As mentioned in Section 7.1, the FHA consists of two components; the cryogen cooler (SCP) and radiometer optics (OMP). The SCP is located to the rear of the sensory ring and directly along the roll axis of the satellite. The OMP is situated beneath the sensory ring with the attached SCP projecting up through



(a) location of LRIR on NIMBUS 6

**Figure 7-3. Location of the LRIR Instrumentation on the Nimbus 6 Sensory Ring and Associated Viewing Geometry**

the ring on the inside. The optical axis of the OMP is positioned 32 degrees to the left of the negative roll axis (-X) in the X-Y plane and 31 degrees below the horizontal of the sensory ring. This positioning is necessary to shield the radiometer from direct solar radiation and to position the mirror scan some 30 to 40 km above the earth's horizon. The mirror in the OMP scans "up and down" through a small angle just above the earth's surface.

It should be emphasized that LRIR views neither the local nadir nor in the orbital plane of the spacecraft. The azimuth of the scan plane is fixed at 32 degrees off the direction of flight. The elevation axis of the scan plane is about 0.6 degrees above the earth's horizon. As a result, the LRIR scan track, when projected to earth, is parallel and to the right of the subpoint track relative to

direction of flight. When the satellite is near the north pole, the LRIR views across the pole. Near the south pole the LRIR views equatorward of the sub-point latitude position. With this geometric configuration, a greater density of observations are provided in the Northern Hemisphere as compared to the Southern Hemisphere. Thus, LRIR data coverage extends from about latitude 83°N to 64°S.

To better understand the LRIR coverage, computer portrayals of successive scan tracks for both hemispheres are presented in Figures 7-4 and 7-5. Note in Figure 7-4 that successive ascending and descending node scans provide equal spacing in mid-latitudes of the Northern Hemisphere in order to provide good spatial coverage in this geographical region of the earth.

### 7.3.2 Instrument Configuration

The LRIR instrument configuration is shown schematically in Figure 7-6. The limb radiance enters the baffled aperture, reflects off the plane scanning mirror, is focused by the primary parabolic mirror through a field stop and collimator via relay optics to the cooled detectors. Details of the SCP and the functional position of the electronics units are also shown in Figure 7-6. (See Figure 7-8 for more details of electronic units.)

The scan mirror can view the earth's horizon by scanning through a  $\pm 5$  degree angle about the optical axis. The mirror can rotate to an angle of 8 degrees above the optical axis in order to view the cold of space for calibration and can rotate further, to an angle of 30 degrees above the optical axis, to view the warm in-flight calibration source. (See Section 7-4 for more details.)

As mentioned previously, the detectors are fixed in position within the detector capsule assembly of the cryogen cooler. Thus, these detectors are fixed relative to each other when the optics are scanning across the limb scene.

It is important when interpreting the data to understand the dimensions and spatial positions of the four channels. The FOV of the LRIR channels and their location relative to the limb scene are presented in Figure 7-7. The angular resolution (in milliradians) of each detector and their angular positions relative to each other are indicated. These angles correspond to the FOV at the radiometer. When this view is projected through the atmosphere at the limb, perpendicular to a vertical plane at the tangent point, the sampled area encompasses a rectangle that is 50 km in the horizontal by 20 km in the vertical. Within this area the O<sub>3</sub> and two CO<sub>2</sub> channels cover areas of 20 km and are positioned in a manner shown in Figure 7-7. The H<sub>2</sub>O channel covers a much larger area, about 50 km by 2.5 km. However, due to excessive noise on the left side of

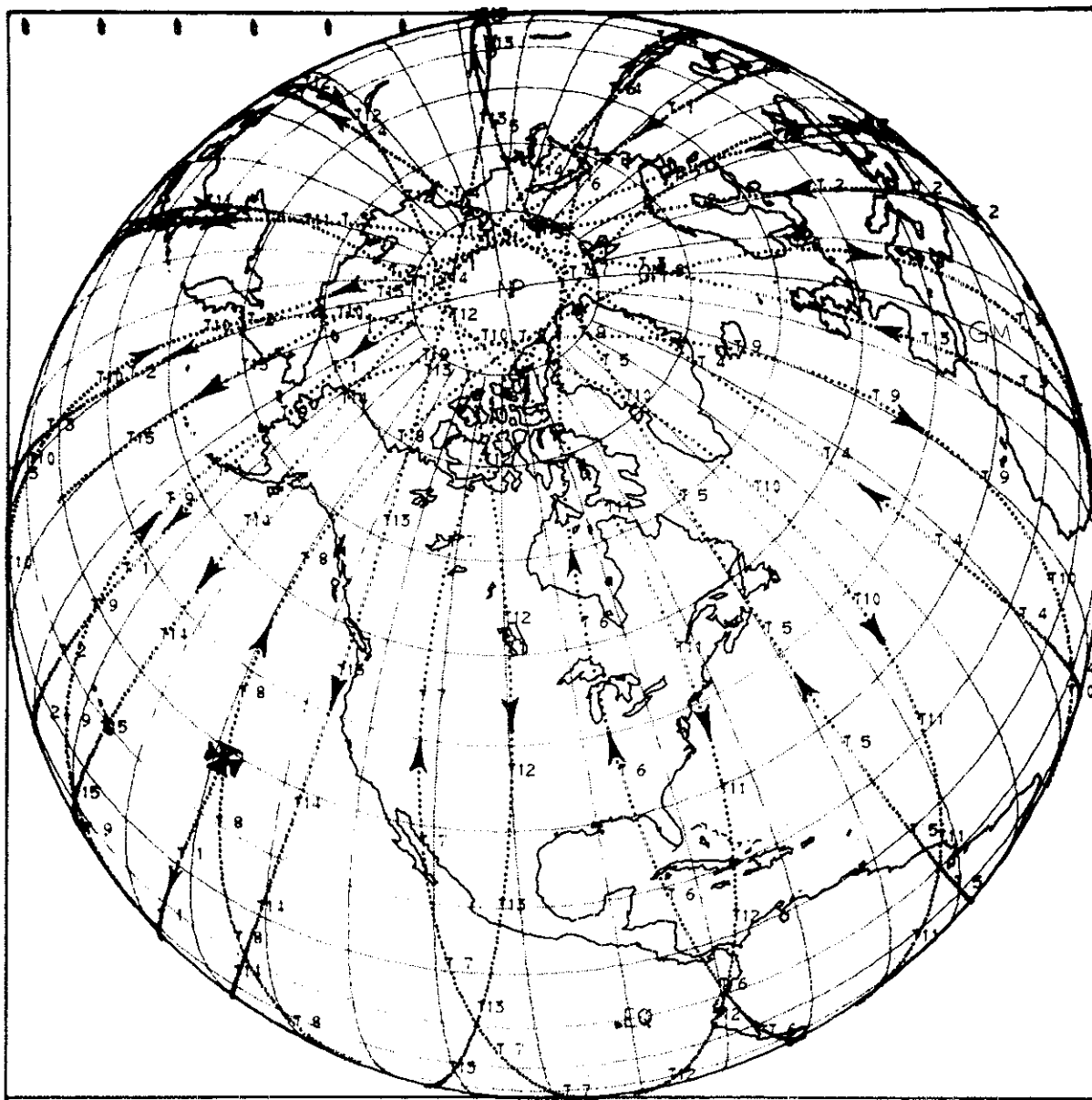


Figure 7-4. LRIR Scan Track for the Northern Hemisphere

channel 4, it was clipped and only the right side of that channel will actively acquire data. One can visualize this configuration as four narrow slits, parallel to the earth's surface and stacked one on the other as shown in Figure 7-7. For all practical purposes, observations by each channel are coincident in time and only slightly displaced from each other in the spatial domain.

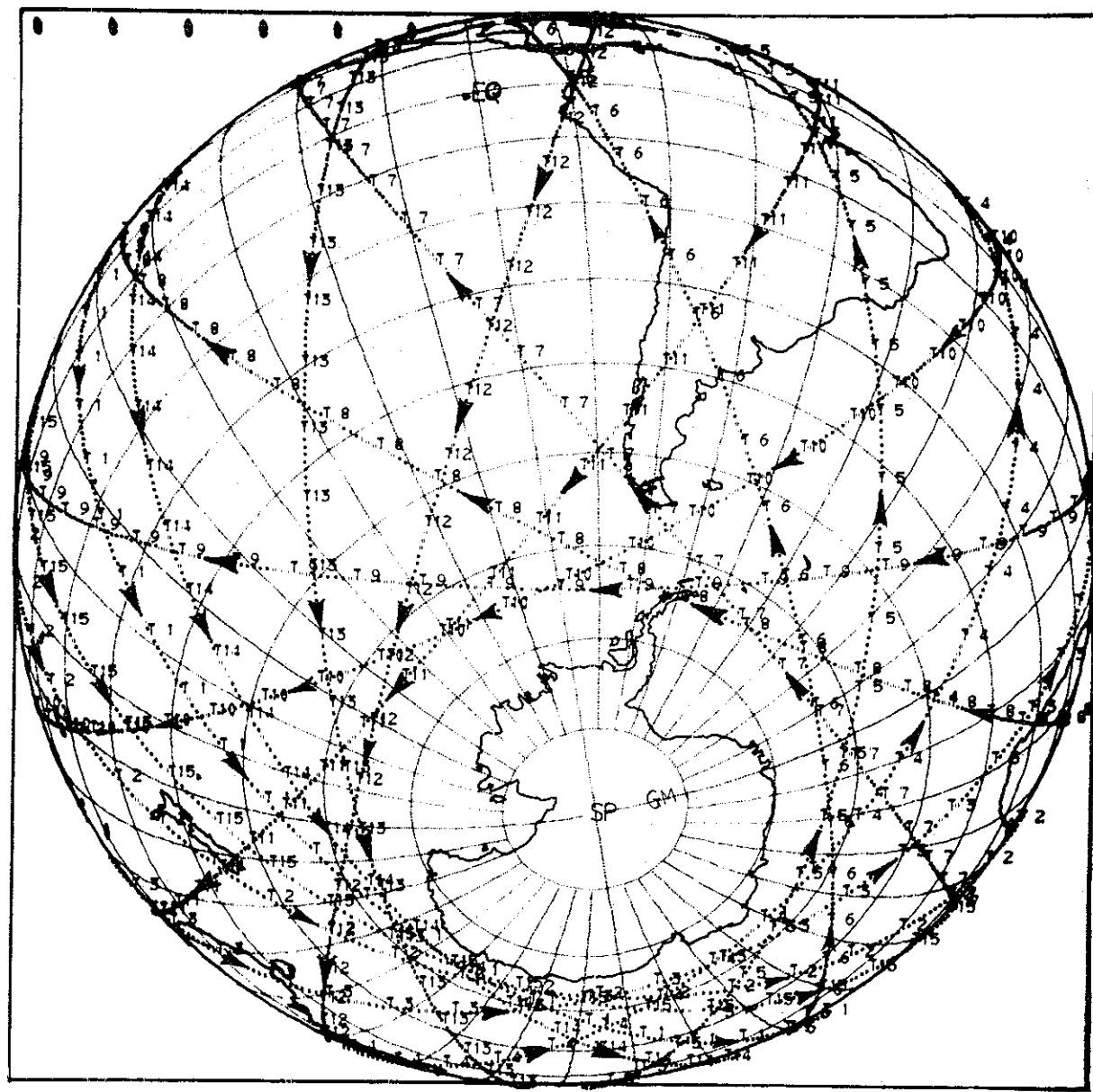


Figure 7-5. LRIR Scan Track for the Southern Hemisphere

The LRIR system block diagram is presented in Figure 7-8. The details of the diagram are self explanatory and illustrate information processing functions of both the FEU and IEU, shown in Figure 7-6.

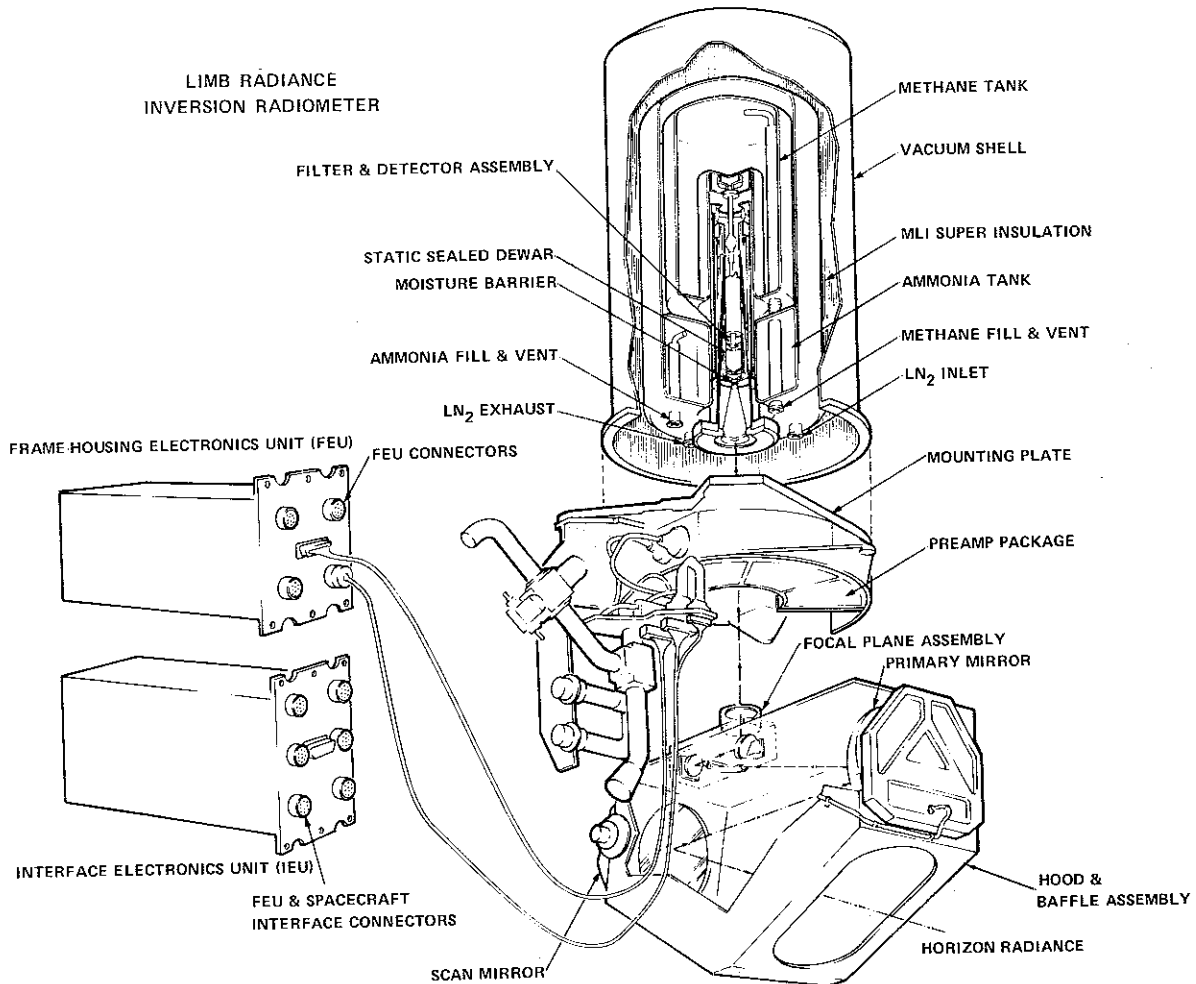


Figure 7-6. LRIR Instrument Configuration

### 7.3.3 Channel Characteristics

The optical characteristics of the four LRIR channels are presented in Table 7-2. Channels 1 and 2, the narrow ( $\text{NCO}_2$ ) and broad ( $\text{BCO}_2$ ) carbon dioxide channels, provide information on the temperature structure of the atmosphere. Channels 3 and 4 are the constituent channels for ozone and water vapor, respectively, and provide information on the vertical distributions of these trace gases.

Each channel of LRIR encompasses rather broad spectral regions about optical bands of their respective species of emitting gases. Since broad spectral

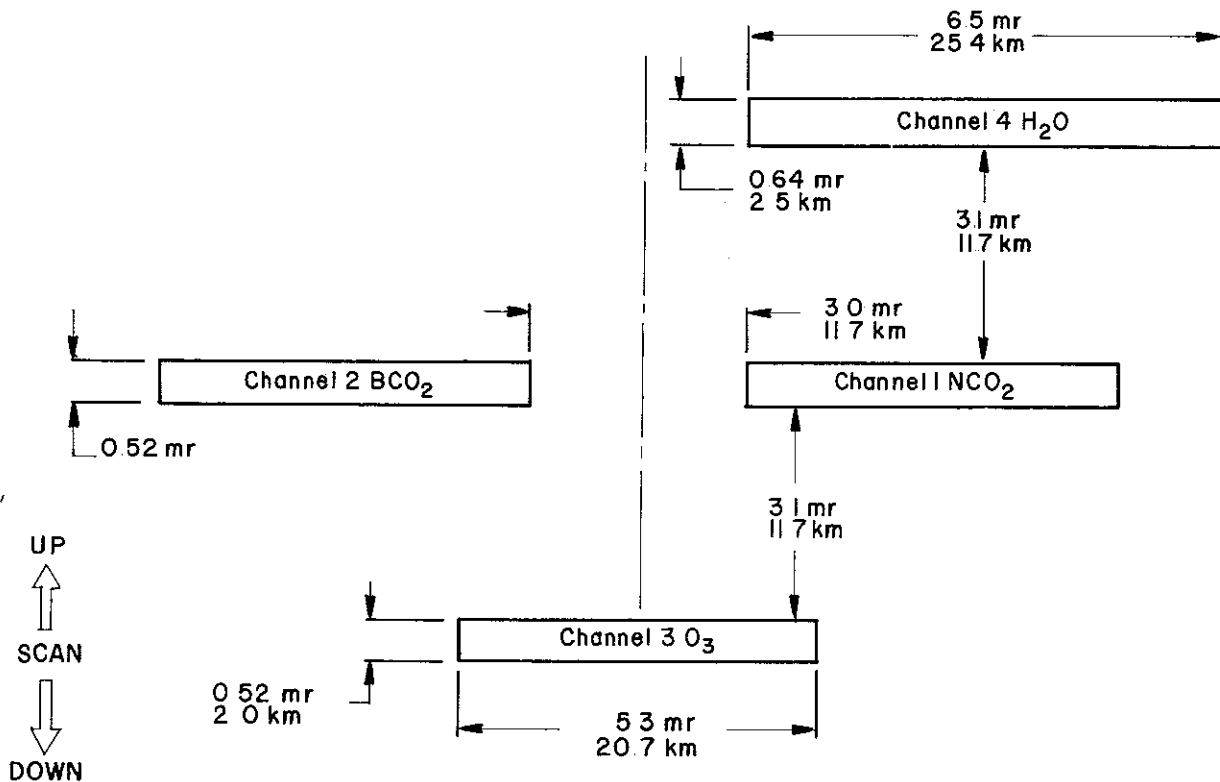


Figure 7-7. LRIR Field of View Dimensions. The IFOV arrangement is as viewed along the optical axis in the direction of the scene.

bands increase the magnitude of the received signal, the FOV can be reduced to the diffraction limit, and good vertical resolution can be obtained during the limb scan. Limb scanners use broad spectral bands with narrow angle FOV sensors to obtain altitude resolution. This philosophy of approach is different from nadir viewing experiments which employ narrow spectral bands with relatively large FOV sensors to accomplish altitude discrimination of information.

The location of the two CO<sub>2</sub> bands is not symmetrical about the 15  $\mu\text{m}$  band center, but is shifted to the short wavenumber (long wavelength) side of the spectrum. This avoids contamination by the ozone band near 14  $\mu\text{m}$ . Because each band provides a limb radiance profile (see Figure 7-2) of different character, both are utilized in the process of obtaining temperature inversion solutions. Together, they help to discriminate a unique solution to the problem (see Reference 1). Good data can be obtained solely from the BCO<sub>2</sub> channel when statistical inversion techniques are applied to the limb radiance data. However, temperature accuracy would degrade somewhat.

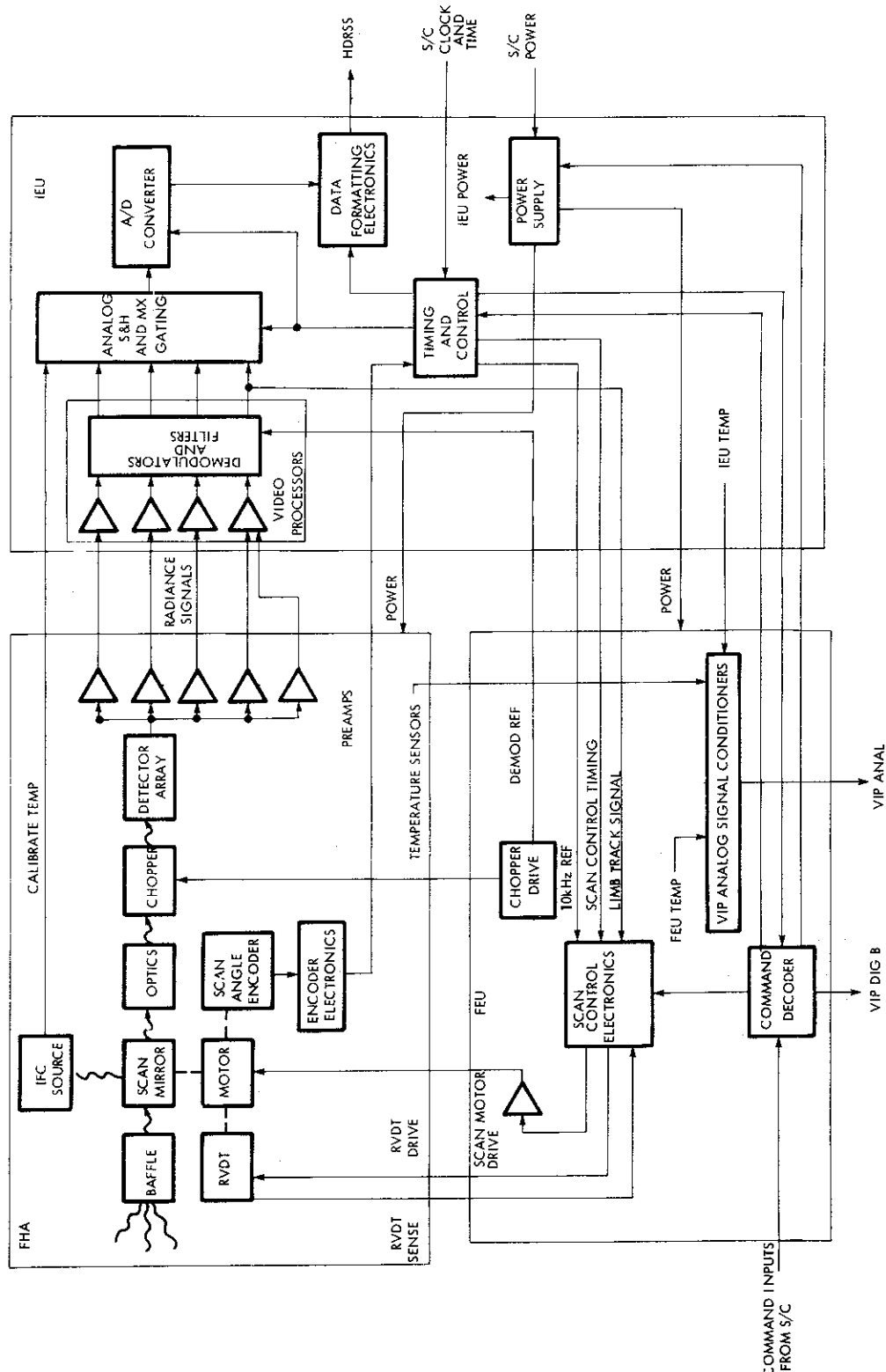


Figure 7-8. LRIR System Block Diagram

Table 7-2  
Optical Characteristics of LRIR Channels

Channel		Band Pass (50% Peak Response)	Field-of-view (km)		Random noise $\pm 1\sigma$ (watts/m <sup>2</sup> -sr)
No.	Abbrev.		Vertical	Horizontal	
1	NCO <sub>2</sub>	645-670 cm <sup>-1</sup> (14.9-15.5 $\mu$ m)	2.0	20	0.0026
2	BCO <sub>2</sub>	590-695 cm <sup>-1</sup> (14.4-16.9 $\mu$ m)	2.0	20	0.0046
3	O <sub>3</sub>	980-1165 cm <sup>-1</sup> (8.6-10.2 $\mu$ m)	2.0	20	0.011
4	H <sub>2</sub> O	370-435 cm <sup>-1</sup> (23.0-27.0 $\mu$ m)	2.5	25	0.021

The band pass for channel 3 (O<sub>3</sub>) is centered at 9.6  $\mu$ m to maximize the O<sub>3</sub> signal. The cuton wavenumber of 1165 cm<sup>-1</sup> minimizes contamination by CH<sub>4</sub> and N<sub>2</sub>O at 7.8  $\mu$ m, while the cutoff location at 980 cm<sup>-1</sup> minimizes the effects of longer wavelengths due to aerosol and HNO<sub>3</sub> emission.

For channel 4 (H<sub>2</sub>O), the cuton location of 435 cm<sup>-1</sup> was selected to minimize contamination by residual wing emission from CO<sub>2</sub> and HNO<sub>3</sub>. The long wavelength side cutoff at 370 cm<sup>-1</sup> was set by the spectral response characteristics of the detector.

Also shown in Table 7-2 is a summary of the FOV at the limb and the random noise (one sigma) of each channel. With reference to the data requirements in Table 7-1, channels 1 and 2 noise levels are well within desired specifications and channel 3 is at the desired specification. However, channel 4 is somewhat noisier than expected which diminishes the spatial resolution (both geographical and vertical) of the H<sub>2</sub>O data.

#### 7.4 Calibration

The LRIR has undergone extensive preflight calibrations in the laboratory under simulated flight environments to determine its geometric, spectral, and system responses to known magnitudes and positions of radiance sources. These calibration procedures were performed to an absolute accuracy approaching one percent.

#### 7.4.1 Preflight Calibration

The preflight calibration of LRIR may be summarized by the following five procedures.

- Determine optical characteristics of the in-flight calibration source (IFC) for all LRIR channels.
- Calibrate the encoder used to measure angular position of the plane mirror in scan space.
- Determine the response of the LRIR system to a variable blackbody radiance source for:
  - (a) Ten points over the dynamic range of all channels.
  - (b) Three different environmental temperatures of the spacecraft.
- Determine the spectral response of each LRIR channel.
- Determine the FOV response of each LRIR channel in the scan plane.

The first two procedures are critical to the absolute accuracy and interpretation of flight data. The IFC source provides a signal that establishes system response to a large (warm) radiance source. Absolute accuracy is possible only if the optical characteristics of the IFC are known and its temperature is monitored accurately. The second procedure establishes where the instrument is viewing at any time in relative scan space.

Primary calibration (see Figure 7-9) in the third procedure determines the response of all LRIR channels to varying radiance sources over the expected dynamic range of limb radiances, and for the range of possible LRIR-spacecraft temperatures anticipated for the mission. This calibration procedure establishes the linearity of instrument response to varying magnitudes of radiance signals. Once this response is established for the operating environment aboard the satellite, it is assumed to hold throughout the mission. Thus, only two calibration points are required during flight to determine absolute radiance values - a zero radiance signal (space view), and a large radiance signal (the IFC source). A linear response is assumed to hold between these two points.

The last two procedures are of less importance than the others in determining absolute radiances and their positions in scan space. However, these calibrations are important in the inversion process in understanding what is

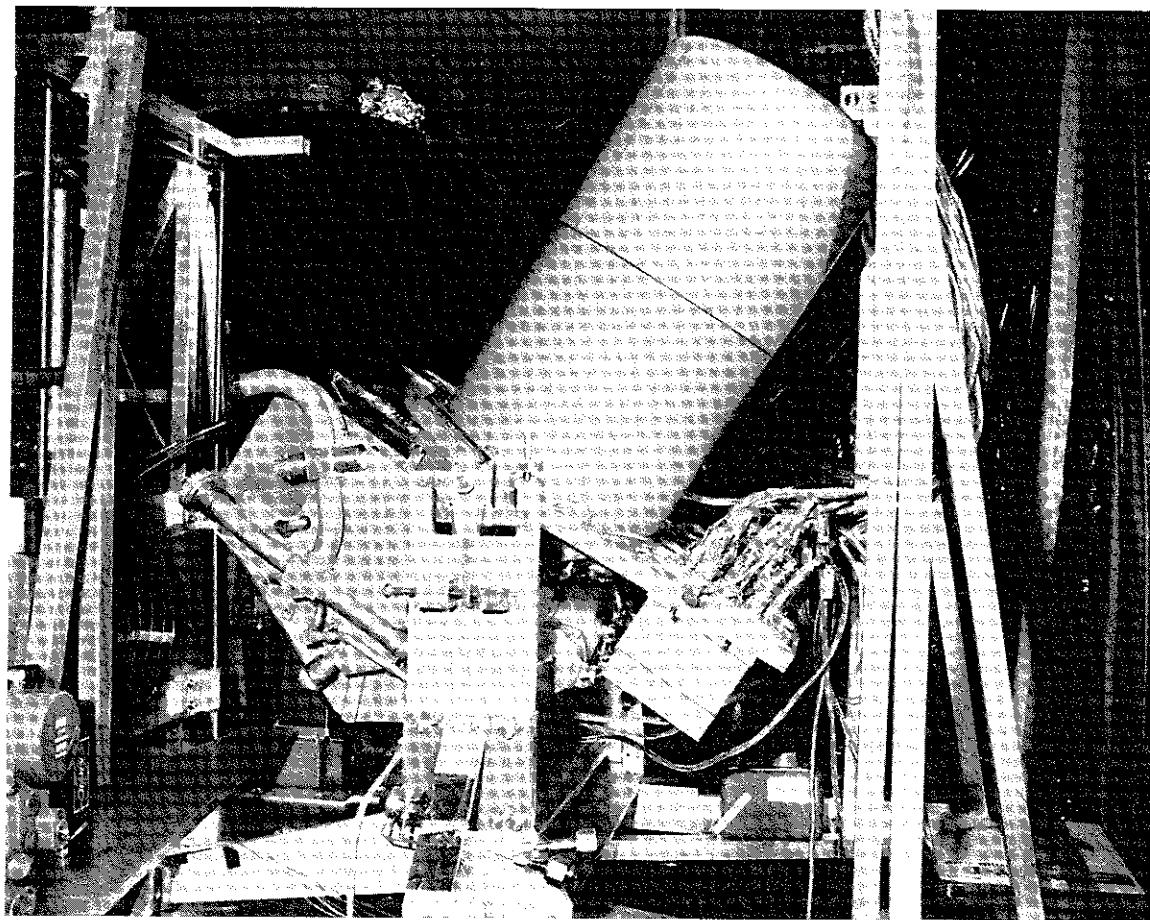


Figure 7-9. LRIR Instrumentation During Primary Calibration

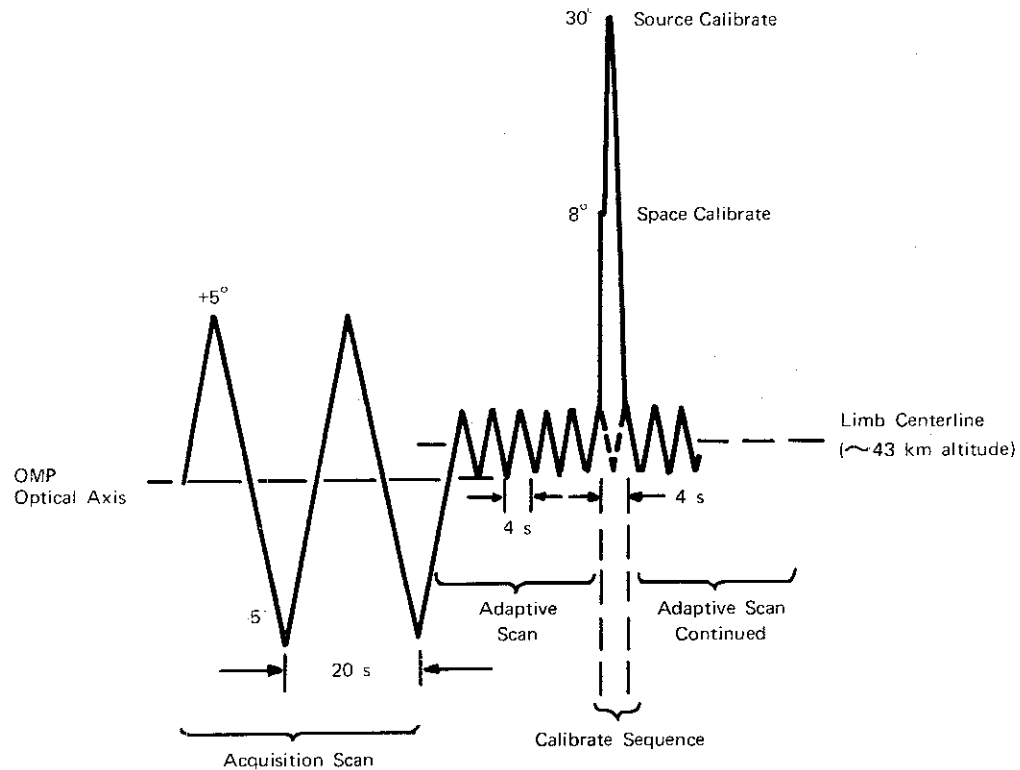
being observed optically across the band pass of each channel and how the limb radiance is being averaged spatially.

#### 7.4.2 Scan Modes and In-Flight Calibration

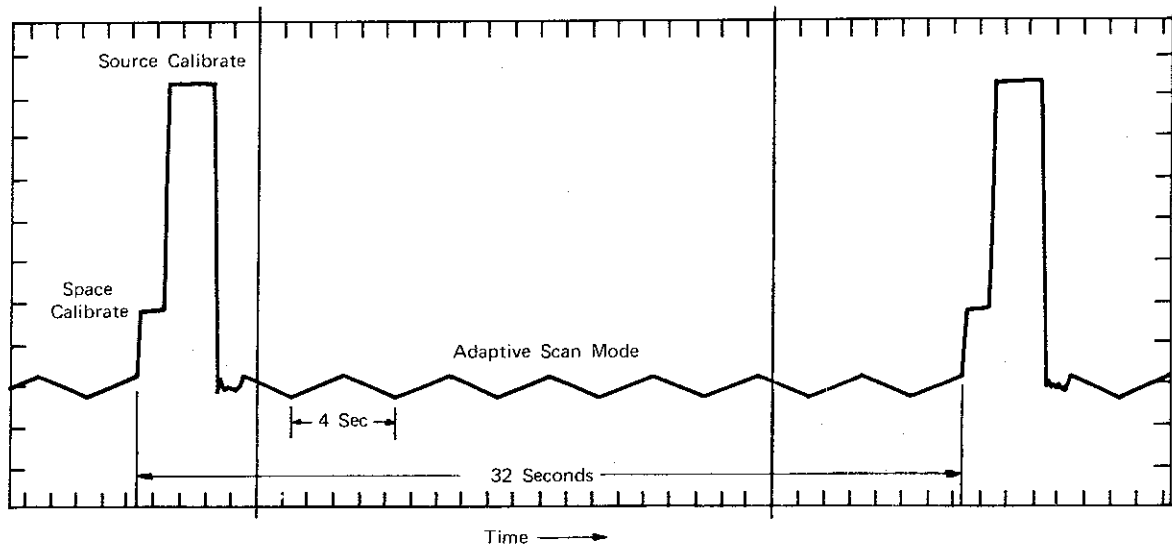
The scan mirror subsystem operates in any of five scan-calibrate modes related to limb acquisition, limb scanning, and in-flight calibration. These five modes are listed below and functionally depicted in Figure 7-10.

- Acquisition Scan

This scan generates a one degree per second line of sight (LOS) triangular sweep centered about OMP centerline. A complete period takes 20 seconds.



(a) LRIR Scan Modes - Angular Scale



(b) Analog Trace of LRIR Adaptive Scan/Calibrate Sequence Modes

**Figure 7-10. LRIR Scanning Modes During Limb Acquisition, Limb Scanning, and In-Flight Calibration Sequences**

- Adaptive Scan

This scan activates the Limb Tracking Circuit and generates a one degree per second LOS triangular sweep centered about 40 percent of the peak radiance of the narrow band CO<sub>2</sub> channel with a period of 4 seconds.

- Space Calibrate Hold

This mode generates a dc voltage to position the scan mirror at a space calibrate position within  $\pm 1/2$  degree shaft angle.

- Source Calibrate Hold

This mode drives the scan mirror to a physical stop position to look back at the In-Flight Calibration Source (IFC).

- Automatic Calibrate

This mode generates a calibrate sequence consisting of one second space calibrate hold dc level, a two second source calibrate hold dc level, and a one second return to OMP centerline to await the return to adaptive scan. This is an internally generated command.

Briefly, acquisition scan searches for the limb radiance within a  $\pm 5$  degree arc about the OMP optical axis (see Figure 7-10a). Once the limb is acquired, the scan mirror subsystem switches to adaptive scan mode during which time limb radiance profiles are recorded over a  $\pm 1$  degree scan about the limb centerline (a nominal 43 km altitude in the atmosphere). From a tangent at the earth's horizon, the range of altitude of the adaptive scan is between -25 km to 120 km. If the satellite attitude should change during successive limb scan periods (4 seconds for one down and up scan), the scan mirror will automatically adapt to the new limb centerline. This procedure continues during each limb scan period.

The automatic calibrate mode is activated during adaptive scan operation every 32 seconds while limb radiance data are being acquired. See Figure 7-10b for details. During the automatic calibrate sequence, the scan mirror rotates upward to an 8 degree angle above OMP centerline for a 1-second space (zero radiance) calibration and then to a 30 degree angle above the OMP centerline for a 2-second IFC source calibration before returning to the OMP centerline to await return to adaptive scan mode. The scan mirror can also be commanded to hold either the space calibrate or the source calibrate mode.

## 7.5 Data Processing, Archiving, and Availability

The block diagram in Figure 7-11 presents an overview of the Nimbus 6 LRIR data reduction flow. Experimental data will be archived in three forms and stored on reels of computer tapes. These are denoted as:

- Radiance Archival Tapes (RAT)

These are the most basic and complete form of experimental observations, consisting of all useful limb radiance observations for the entire mission.

- Inverted Profile Archival Tapes (IPAT)

Profiles are selected from RAT tapes with a spatial frequency of about 400 km along the scan track. These profiles are then inverted to provide parameters of temperature, ozone mixing ratio, and water vapor mixing ratio at pressure points spaced 1.5 km vertically. Parameters are interpolated to standard pressure levels and thicknesses.

- Map Archival Tapes (MAT)

Data contained on IPAT and available meteorological data in the upper atmosphere at time of observation are combined to produce objective analyses of parametric fields, interpolated both in time and space to be coincident with synoptic weather maps.

These three archival products will be stored at NSSDC. A second copy of all tapes will be available at NCAR.

The final details of data tape formats, structure, etc., are not available as of this writing but will be available to interested users once the data are processed and archived. General information concerning volume and characteristics of the archival data is presented in Table 7-3. These estimates are based on the anticipated seven-month lifetime of the instrument (cryogen cooler) and an approximate 75 percent duty cycle during this period. It is noted from this information that, from a user's standpoint, only IPAT and MAT data are feasible observations to incorporate in scientific investigations of a general nature, e.g., investigations concerning the general circulation of the stratosphere and the development of stratospheric warmings. Investigations utilizing RAT information can be carried out only at large computing centers owing to the larger number of tapes involved.

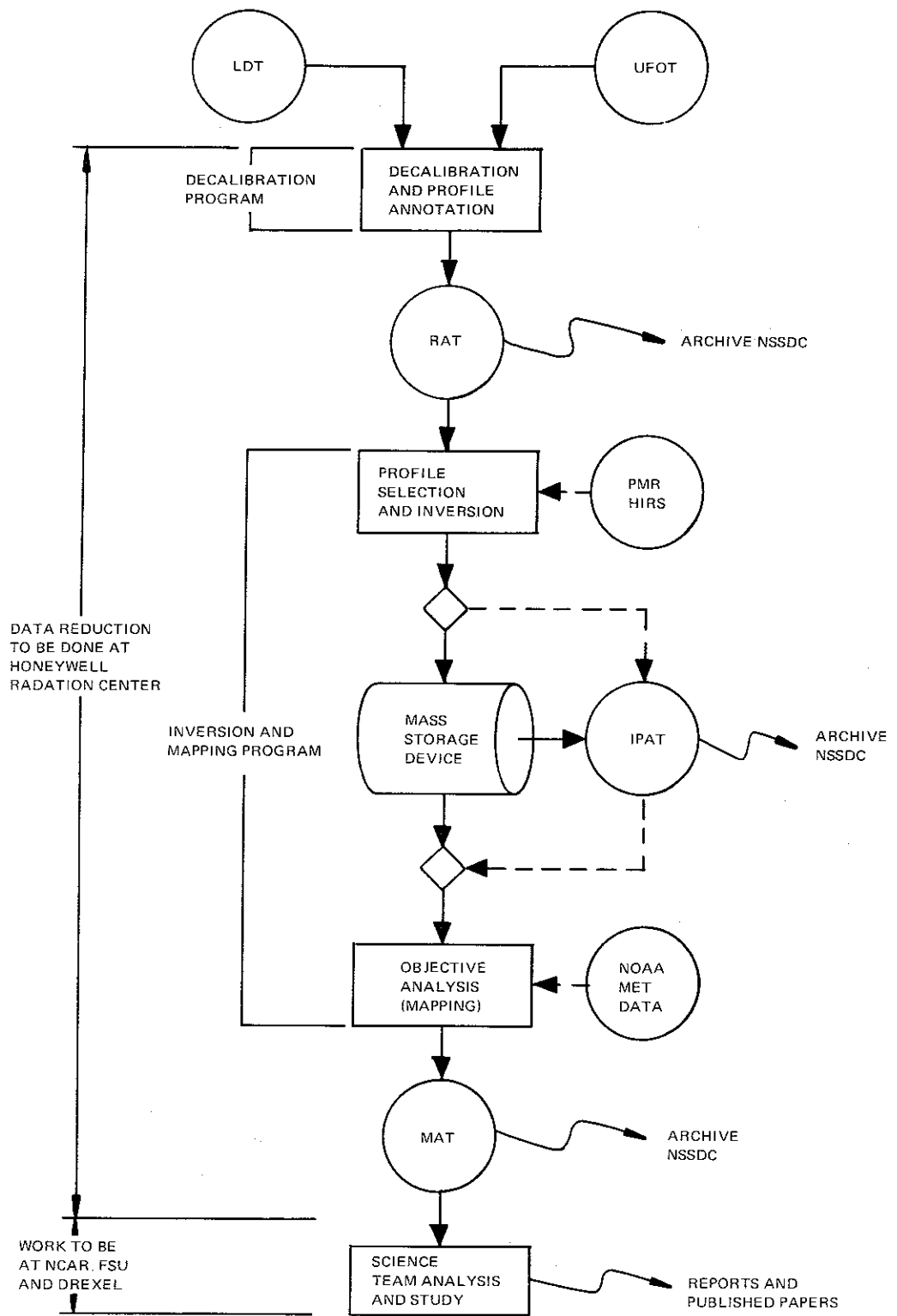


Figure 7-11. LRIR Data Reduction Flow

Table 7-3  
 Volume and Characteristics of LRIR Archival Data  
 (one reel = 2400 ft of magnetic tape)

Form	Volume (reels)	Format	Characteristics
RAT	470	7 track, 800 BPI Packed Binary	All useable limb radiance observations, as well as decalibration parameters, spacecraft status, ephemeris data, and tangent point annotators.
IPAT	23	7 track, 800 BPI Packed BCD	Inverted profiles of temperature, ozone concentration, and water vapor concentration, and water vapor concentration at pressure points spaced 1.5 km vertically (relative altitude). Parameters are interpolated for, and thicknesses computed between, the pressure levels of 100, 70, 50, 30, 10, 5, 2, 1, 0.4, and 0.1 mb.
MAT	23	7 track, 800 BPI Packed BCD	"Synoptic" maps of temperature, ozone concentration, water vapor concentration, and geostrophic winds (where possible) at the standard pressure levels of 100, 70, 50, 30, 10, 5, 2, 1, 0.4, and 0.1 mb.

Potential users of LRIR data should indicate their interest and direct their requests to:

Dr. John C. Gille  
 NCAR  
 P.O. Box 3000  
 Boulder, Colorado 80303

#### REFERENCES

1. Gille, J. C. and House, F. B.: On the inversion of limb radiance measurements I: Temperature and thickness. *J. Atmos. Sci.*, vol. 28, 1971, pp. 1427-1442.



## SECTION 8

### THE PRESSURE MODULATOR RADIOMETER (PMR) EXPERIMENT

by

J. T. Houghton  
Oxford University  
Oxford, England

#### 8.1 Scientific Objectives

The purpose of the PMR experiment is to measure the atmosphere's temperature distribution in the upper stratosphere and mesosphere (between 40 km and 85 km altitude) with as near-global coverage as is possible from each day of satellite operations. The PMR measurements will be made with a vertical resolution of about 10 km, and a horizontal resolution along the subpoint track of about 500 km. Particular scientific objectives are to:

- Monitor the atmosphere's mean structure, and the changes which occur with latitude and season at the 40 km to 85 km altitude range
- Investigate the propagation of large-scale atmospheric waves (especially stratospheric warmings) at this altitude, and to determine to what extent these disturbances are generated in the mesosphere itself
- Investigate links between ionospheric phenomena and the circulation

#### 8.2 Principles of Operation

Pressure modulation of a gas is a technique for selecting the radiation emitted by a particular molecular species. The PMR measures the emission from CO<sub>2</sub> at the top of the earth's atmosphere using this technique. A cell of CO<sub>2</sub> gas is placed in the optical path of the radiometer and the pressure of the gas is varied cyclically. Figure 8-1 shows the cell configuration for the PMR. Transmission of energy through the cell, and hence the radiation falling on the detector, is modulated at frequencies which lie within the absorption lines of the gas in the cell. The frequency component of the radiation in phase with the cell gas modulation is sensed at the detector and recovered by electronic processing. Additional, relatively simple, filtering is required to isolate the particular absorption band. Because this measuring technique requires only a single cell of gas, it is an improvement over the technique of selective chopping

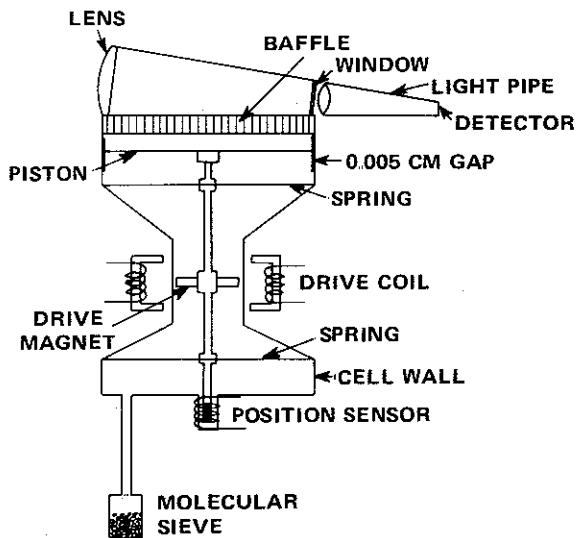


Figure 8-1. Pressure Modulator Cell Showing Method of Modulation.  
The cell is 6 cm long.

employed by the Selective Chopper Radiometer on Nimbus 4 and 5 (see Reference 2). The problems of balance inherent with a double beam system are eliminated.

The PMR uses two methods of scanning the emission lines from the atmosphere being modulated by the cell of  $\text{CO}_2$  gas. These methods are pressure scanning and Doppler scanning.

When pressure scanning, the mean  $\text{CO}_2$  cell pressure is sequenced by command to each of four pressure values. Each pressure value alters the frequency at which cell transmission modulation occurs, and thus tunes the radiometer to a different part of the atmospheric lines. Since radiation from different parts of emission lines originates at different altitudes in the atmosphere, each mean cell pressure is sensitive to a different height. Figure 8-2 shows the weighting function versus height for each of the cell pressures of the PMR.

If there is relative motion along the line of sight between the radiometer and the emitting atmosphere, a Doppler shift occurs between the atmospheric emission lines and the absorption lines of gas in the cell. Since the Nimbus satellite speed is about 20 times molecular speeds at normal atmospheric temperatures, only about 5 percent of the satellite's velocity is required to produce a Doppler shift equal to the Doppler line width. By varying the Doppler shift it is possible to scan the cell absorption lines across the atmospheric emission lines. The Nimbus 6 PMR instrument is designed so its direction of view can be altered from vertical to  $\pm 15$  degrees from the nadir along the direction of

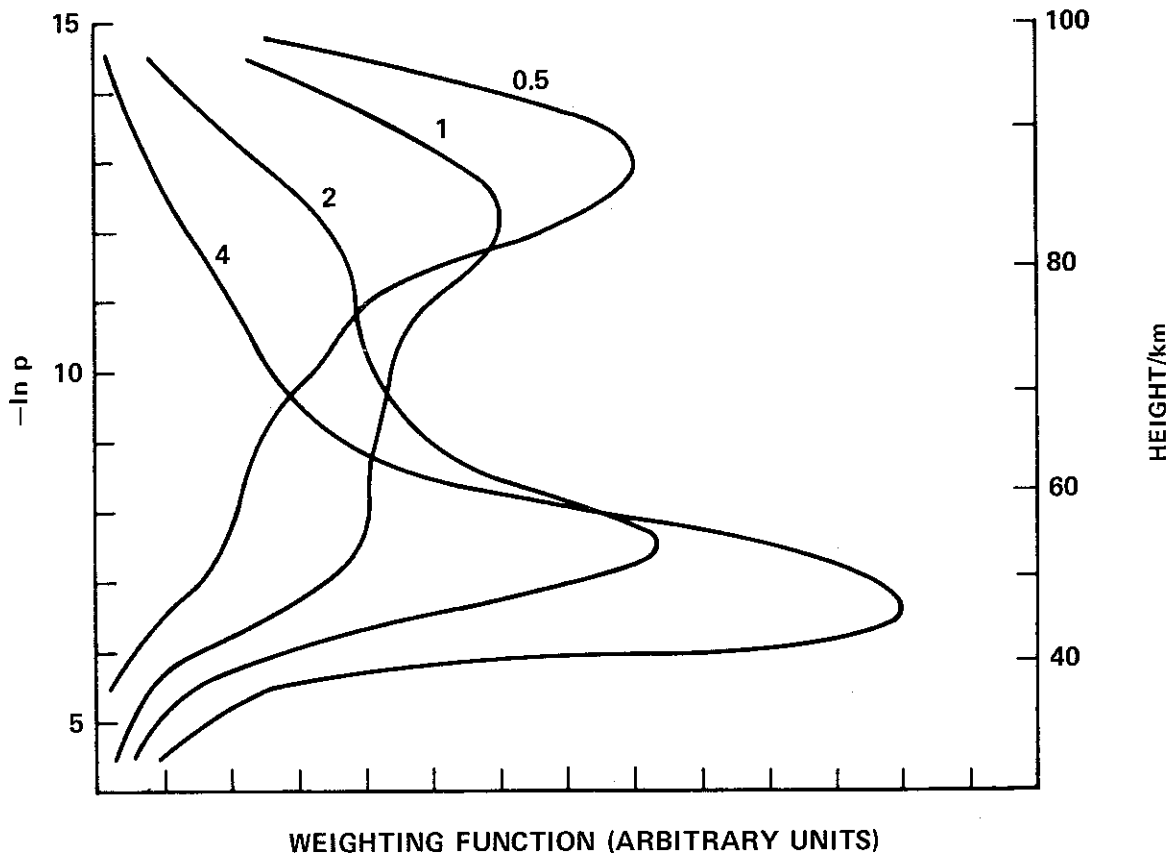


Figure 8-2. Weighting Functions for Different PMR Mean Cell Pressures. Cell pressures (in millibars) are marked on each curve.

the flight, thus introducing varying Doppler shifts. By this means the optical depth (and hence the altitude) being probed is varied. Figure 8-3 shows the weighting function for each angle of view.

Figures 8-2 and 8-3 show that by combining the techniques of pressure and Doppler scanning the altitude range between 40 km and 90 km can be probed. At levels below 80 km there is no difficulty in interpreting the measured radiances in terms of atmospheric temperature. Above 80 km, however, the  $15 \mu\text{m}$  vibration of  $\text{CO}_2$  is no longer in thermodynamic equilibrium; the measured radiances from these levels are dependent on the source function which is no longer equal to the Planck function. Therefore, corrections have to be applied to the measured radiances above 80 km before they can be interpreted in terms of atmospheric temperature.

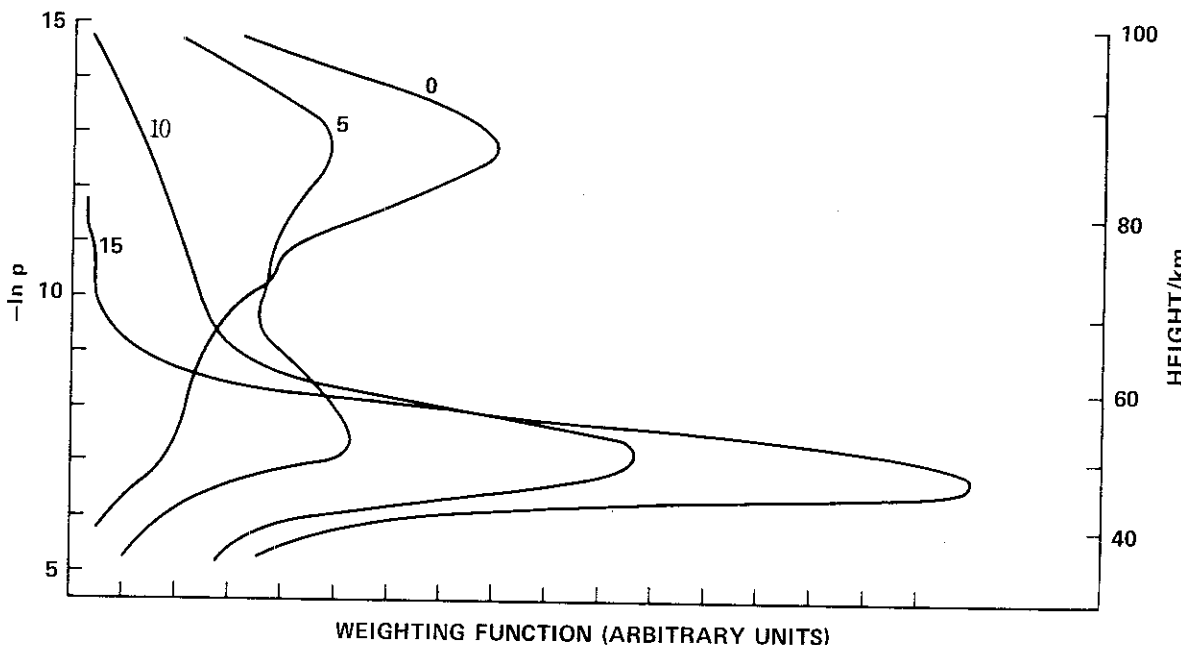


Figure 8-3. Weighting Function for the PMR Illustrating the Effect of Doppler Scanning. The number on each curve is the viewing direction in degrees from nadir.

### 8.3 The Instrument

The PMR instrument consists of two similar radiometer channels, one with a cell 1 cm long containing  $\text{CO}_2$  in the pressure range of 0.5 mb to 3 mb, and the other with a cell 6 cm long containing  $\text{CO}_2$  in the pressure range 1 mb to 4 mb. The first channel is intended to cover the 60 km to 90 km region and the second the 40 km to 60 km region. Apart from the length of cells the radiometers are identical. The package containing the radiometers measures 18 cm  $\times$  23 cm  $\times$  40 cm, weighs 12.5 kg, and consumes less than 5 watts of power. A block diagram of it (one channel only) is shown in Figure 8-4.

Each optical system consists of a plane mirror, a reference blackbody, a dc to dc power converter unit, telemetry and thermostat circuits, and command relays. The major components in one of the channels are briefly described in the following paragraphs.

The plane mirror is gold coated and mounted at 45 degrees to the velocity vector on a 90 degree stepping motor so the FOV of the channel may be directed to space or the internal reference blackbody for in-flight range and zero calibration. The motor is mounted on a pair of jewel bearings so the mirror can be rotated through  $\pm 15$  degrees from its rest position to give the required Doppler scan.

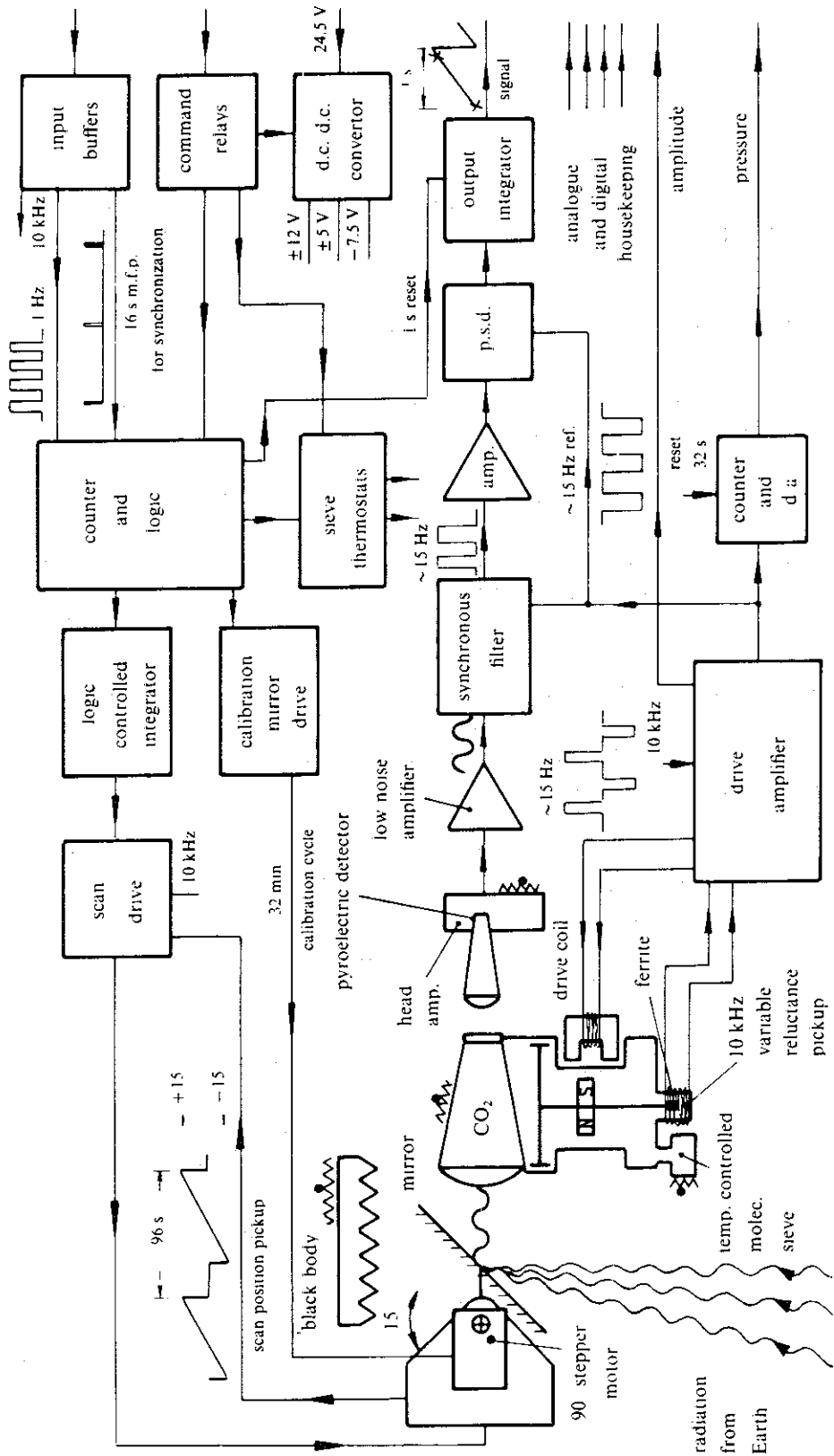


Figure 8-4. Electronics Block Diagram for One Channel of the PMR

The modulator cell is shown in Figure 8-1. The body of the cell is constructed from titanium with gold "O" ring seals. The central shaft and piston are mounted on flat beryllium-copper spider springs.

When assembled and evacuated, the natural resonant frequency of the piston on its springs is about 15 Hz. A constant piston amplitude is maintained by an active loop containing a variable reluctance position sensor, amplifier, comparator, and moving magnet drive system. Under launch vibration, the piston and spring amplitude is limited by hard stops of a shape designed to progressively limit the spring movement and to change the resonant frequency.

The cell is required to hold its CO<sub>2</sub> gas at a pressure of a few millibars for at least one year without significant loss due to leaks or outgassing contamination. Throughout each cycle the mean pressure of the gas in the cell and the frequency of modulation are such that the gas is maintained essentially isothermal.

The pressure control uses 1.56 grams of a molecular sieve material (Zeolite Union Carbide 4AXH/2) in a thermostated side arm of the cell (see Figure 8-1, lower left). For a given quantity of sieve material and a given filling of CO<sub>2</sub>, the equilibrium pressure above the sieve is a function only of temperature. Table 8-1 shows the CO<sub>2</sub> pressure corresponding to various temperature settings on the sieves. Another function of the pressure control system occurs during launch when the pressure is increased by a subsidiary system so that maximum damping will be present under launch vibration conditions.

Table 8-1  
Cell CO<sub>2</sub> Pressure Corresponding to Various Temperature  
Settings on the Sieves

Sieve Setting	Channel 1		Channel 2	
	Sieve Temperature (°C)	Cell Pressure (mb)	Sieve Temperature (°C)	Cell Pressure (mb)
1	26.5	.55	unthermostated	
2	34.8	.90	26.5	.66
3	43	1.48	37.5	1.24
4	51.3	2.43	48.5	2.32
5	59.5	4.0	59.5	4.34
6	105	>30	105	>30

The total cell pressure is deduced by measuring the frequency of oscillation of the piston assembly which changes by about 5 percent per millibar pressure change. The oscillations are counted in a 10 bit counter, which is read and reset every 32 seconds, giving an accuracy of pressure measurement of 1 percent.

The detector assembly is comprised of a lens, a condensing light pipe, and a pyroelectric bolometer flake with its associated load resistor and field effect transistor. The assembly defines the instrument FOV of 20 degrees across the line of flight and 4 degrees along the line of flight. Table 8-2 lists the noise equivalent temperature of the two radiometer channels for different mean pressures for 16 second integration times.

Table 8-2  
Noise Equivalent Temperature for  
Different Cell Mean Pressures

Path Length (cm)	Extremes of Pressure Swing (mb)	Equivalent <sup>1</sup> Width ( $\Delta W \text{ cm}^{-1}$ )	Noise Equivalent Temperature (°K)
1	0.25/0.47	0.030	1.3
1	0.68/1.27	0.056	0.7
1	1.21/2.28	0.085	0.5
6	2.5 /4.0	0.35	0.11

<sup>1</sup> Calculated from equation  $\Delta W = \int (\tau_1 - \tau_2) d\nu$ , where  $\tau_1$  and  $\tau_2$  are the transmissions at frequency  $\nu$  of band cell at the extremes of pressure occurring in the modulation.

The signal processing electronics consist of a low noise amplifier, a 15 Hz synchronous filter, an amplifier, an inverter, a phase sensitive detector, and an integrator. The ramp output is sampled twice by the spacecraft data system so its slope, which is the signal information, can be obtained. The integrator is reset every second.

The logic, constructed from low power transistor-transistor logic, provides timing waveforms derived from the spacecraft clock to control the re-setting of the integrators, the operation and repetition rate of the calibration sequences, and the scanning of the plane mirror. Other functions of the logic include the storage of the thermostat states and maintenance of synchronization of the two calibration mirrors.

The position of the scanning mirror is sensed with a variable reluctance pick off and the output is continuously compared with the voltage of the linear ramp timed by the logic. The difference signal is amplified and fed to the moving coil actuator so that the position follows the ramp.

#### 8.4 Calibration

A set of measurements of output signal versus input radiance as measured in the laboratory is shown in Figure 8-5. The PMR chops between the radiation source and the PMR cell itself. Since the PMR cell is at instrument temperature, the greatest signal was received when the blackbody radiance was at liquid nitrogen temperature (77°K) and the smallest signal was received when the radiance source was at its highest temperature (273°K). At the highest source temperature the radiance is  $107 \text{ mw/m}^2 \text{ ster cm}^{-1}$ . If the source temperature is higher than instrument temperature, the signal changes sign.

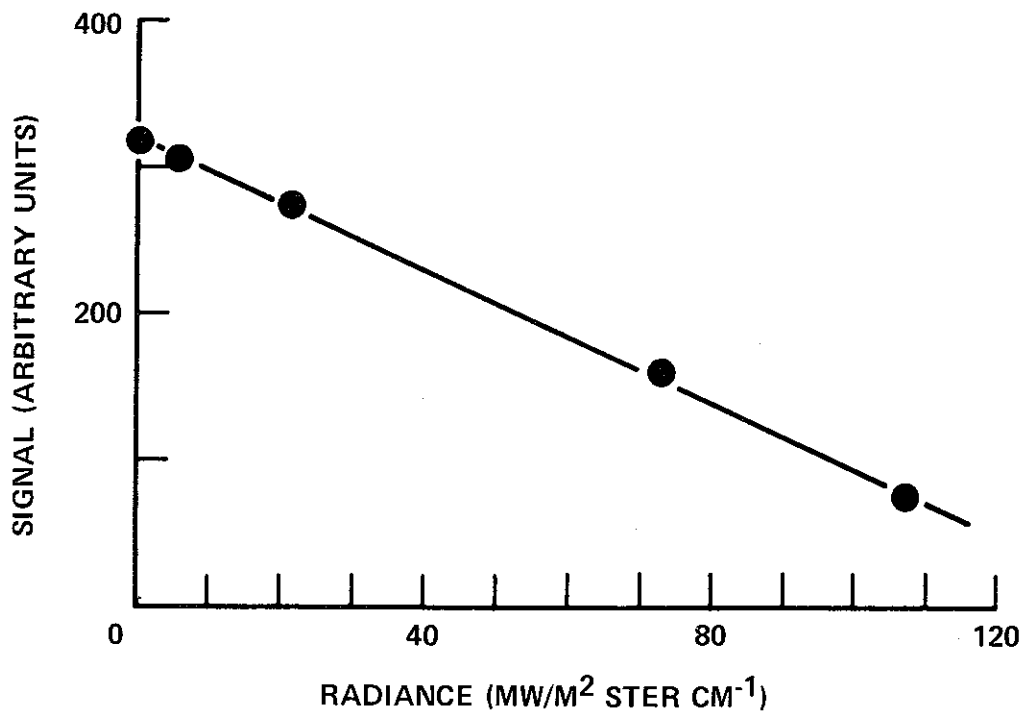


Figure 8-5. Signal versus Radiance for One of the Channels of the Engineering Model PMR

In-flight calibration is provided by views to space and an internal blackbody. Calibration sequences are programmed to occur every 32 minutes.

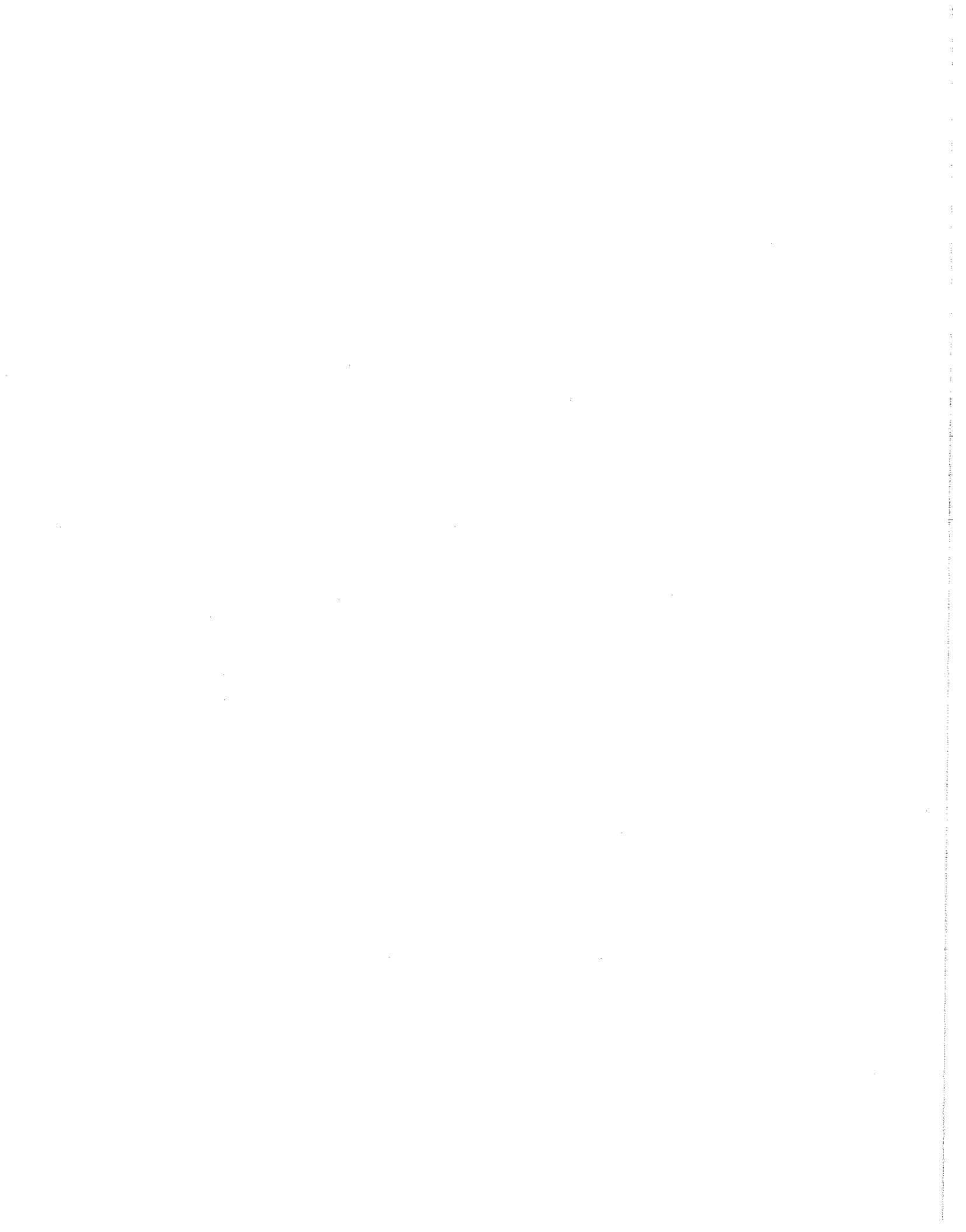
### 8.5 Data Flow and Archiving

Data from the PMR experiment is recorded by the VIP subsystem, transmitted to a STDN station, and relayed to GSFC. PMR data at GSFC will be transmitted on a daily basis via a NASCOM circuit to the PMR experimenter at the Clarendon Laboratory, Oxford, England where the scientific processing takes place.

The PMR experimenter will provide NSSDC with processed PMR data tapes for archiving and distribution to users. The format of these data tapes will be provided in a Nimbus 6 Data Catalog.

### REFERENCES AND BIBLIOGRAPHY

1. Curtis, P. D., Houghton, J. T., Peskett, G. D., and Rodgers, C. D.: Remote Sounding of Atmospheric Temperature from Satellites. To be published in Proc. Roy. Soc., 1974.
2. Houghton, J. T., and Smith, S. D.: Remote Sounding of Atmospheric Temperature from Satellites. I. Introduction. Proc. Roy. Soc., vol. 320, 1970, pp. 23-33.
3. Houghton, J. T., and Taylor, F. W.: Remote Sounding from Artificial Satellites and Space Probes of the Atmospheres of the Earth and the Planets. Rep. Prog. Phys., vol. 36, 1973, pp. 827-919.
4. Taylor, F. W., Houghton, J. T., Peskett, G. D., Rodgers, C. D., and Williamson, E. J.: Radiometer for Remote Sounding of the Upper Atmosphere. Applied Optics, vol. 11, 1972, pp. 135-141.



## SECTION 9

### THE TROPICAL WIND ENERGY CONVERSION AND REFERENCE LEVEL EXPERIMENT (TWERLE)

by

C. Cote

National Aeronautics and Space Administration  
Goddard Space Flight Center

and

P. Julian

National Center for Atmospheric Research  
Boulder, Colorado

#### 9.1 Introduction

TWERLE is a meteorological observing system using lightweight, low-cost balloons to record weather data which are transmitted to the Nimbus satellite and later transmitted to the ground for processing. The superpressure balloons, launched in tropical latitudes, carry sensing devices to measure ambient air pressure and temperature, and geometric altitude, as well as electronic equipment to transmit these data to Nimbus. On the daylight portion of each orbit, when Nimbus is within range of these balloons, the Random Access Measurement System (RAMS), which is the space-borne segment of TWERLE, detects, demodulates, and stores the Doppler signal and sensor data transmitted by each balloon platform. Processing of the Doppler signals on the ground provides the position and velocity of each platform, as well as other meteorological parameters mentioned above. These data on the upper tropical atmosphere will be used to help solve a number of scientific problems relating to GARP.

The RAMS is also used to locate and demodulate data from other platforms equipped to transmit a properly formatted signal. Signals from each platform are transmitted toward space for one second of each minute. When the satellite orbits overhead, the platform signals are detected and processed by RAMS. RAMS can handle up to eight platform transmissions simultaneously. All processed data are stored on a HDRSS for transmission to a STDN station once each orbit. Data from each platform is processed and formatted at the MDHS at GSFC and sent to the appropriate experimenter.

The RAMS system and the TWERLE balloon experiment are discussed in detail in this report. A summary of other experiments using RAMS is provided in Section 9.8 and Table 9-2.

## 9.2 Technical and Scientific Objectives

The primary design emphasis of the RAMS and the platforms is simplicity and low cost; the RAMS is a range-rate only measuring system and the platforms have a simple and inexpensive transmitter. This satellite and platform system, then, represents a considerable simplification over the range and range-rate transponder system used in the Interrogation, Recording and Location System (IRLS) on Nimbus 4.

The RAMS system was developed to cope with a multiple communications problem, since as many as 200 platforms may be simultaneously within view of Nimbus and all will be transmitting a signal intermittently.

The scientific objectives of the TWERLE balloon experiment are:

- Tropical Wind

To obtain an adequate density of wind and temperature measurements in the tropical upper troposphere with the purpose of studying the interactions of tropical circulation systems with those of middle latitudes

- Energy Conversion

To obtain data on the pressure gradients along balloon trajectories which can be related to the rate potential energy is converted to kinetic energy in the upper atmosphere

- Reference Level

To study the need for and the characteristics of an in situ measurement of pressure and temperature at a known geometric altitude. The principal use of a reference level would be to provide a fiducial point for remote atmospheric temperature sounders like HIRS such that the sounder data can be more accurately assimilated by large global atmospheric circulation models.

## 9.3 TWERLE Balloon Platform Description

Each TWERLE balloon platform consists of the meteorological sensors, solar power supply, and a transmitter-oscillator - all carried by the balloon envelope. The balloon and payload are launched by means of a mobile launch vehicle which allows the entire train to be deployed with minimum stress while running downwind. The elements of the flight train, shown in Figure 9-1, are the:

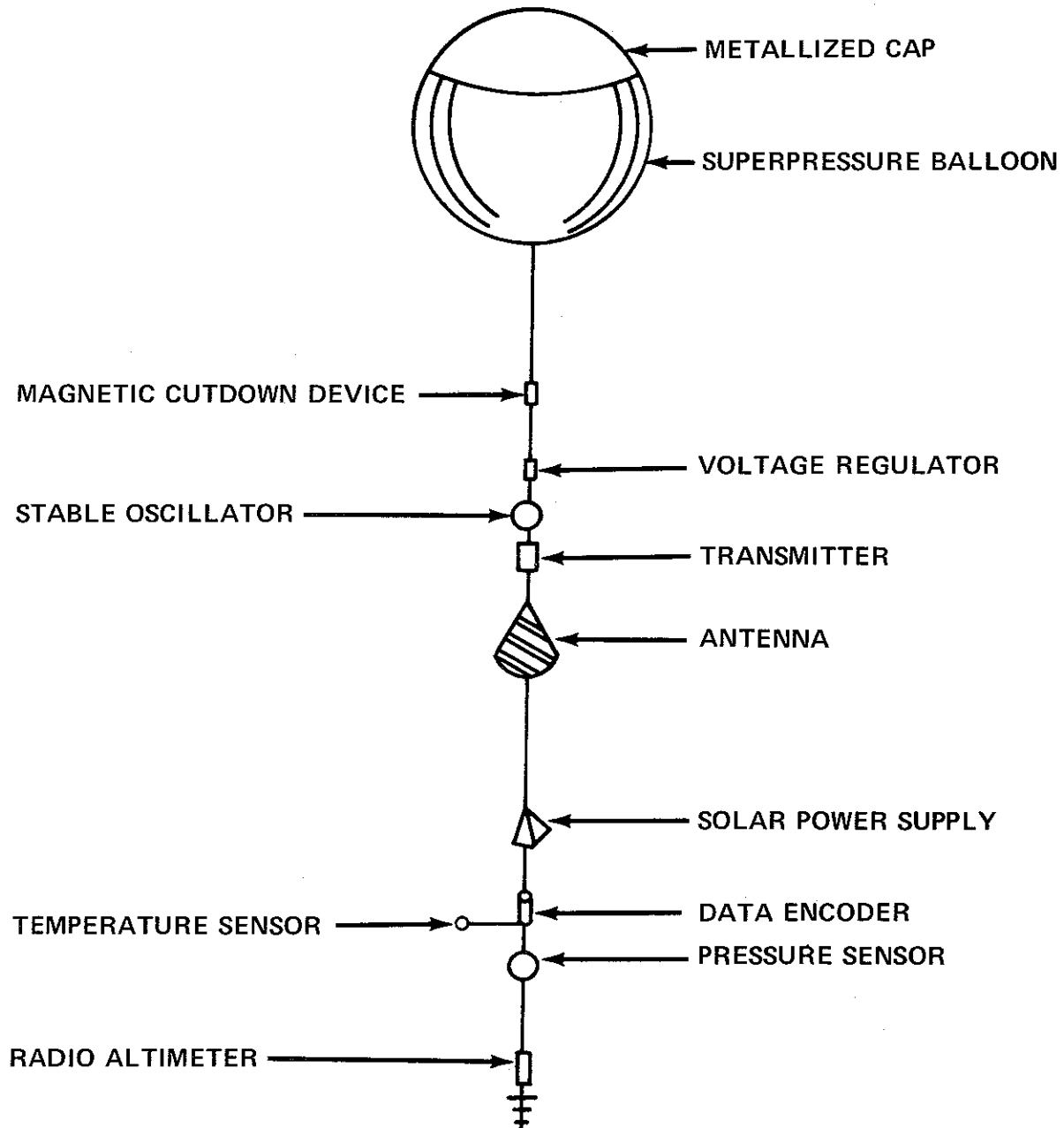


Figure 9-1. Flight Train of TWERLE Balloon System

- Balloon envelope

The balloon is a 3.5 meter diameter sphere with a metallized cap. This cap acts to prevent nocturnal formation of frost on the balloon skin by controlling the internal gas temperature.

- Magnetic cut-down device

This device senses the vertical component of the earth's magnetic field and separates the envelope and train in the event the platform drifts north of 20 degrees north magnetic latitude.

- Voltage regulator

The regulator controls voltage output from solar power supply.

- Stable oscillator-transmitter

The stable crystal oscillator is enclosed in a thermal oven to control crystal temperature within limits. Each transmitter transmits to the spacecraft on a carrier frequency of 401.2 MHz  $\pm$  5 KHz.

- Antenna

The conical helix pattern is designed to provide maximum output at low elevation angles.

- Solar power supply

The solar-cell array and reflector produces peak power outputs of 2.5 to 3.0 watts.

- Data encoder

This sequences and creates bits for the four balloon platform sensors.

- Temperature sensor

This element is a 10-mil aluminized bead thermistor in a specially-designed housing. Accuracy at flight altitude is 0.5°C rms. Resolution is 0.2°C.

- Pressure sensor

This sensor is a specially ground-calibrated aneroid pressure cell contained in a reduced-pressure chamber which opens when flight altitude is achieved. This is done to control hysteresis effects in the aneroid. Pressure accuracy is 0.5 mb rms with a resolution of 0.25 mb.

- Radio altimeter

This sensor makes use of backscatter from the ocean surface of a transmitted pulse to measure geometric altitude. The accuracy is 2 meters rms.

#### 9.4 Platform Transmissions

Each platform transmitter-oscillator is self-timed and transmits a signal for one second of each minute. Transmission is uncontrolled, occurring whenever adequate power is available from the solar cells (i. e., daytime only). Since many platforms will be within view of the satellite at any moment, the success of RAMS receiving these signals depends upon both a random set of times of transmission and a dispersion in frequency about a nominal frequency.

As the satellite passes in view, the platform signals received at the satellite are shifted in frequency by the Doppler effect (due to the satellite's orbital motion)  $\pm 8.3$  KHz about the center frequency of 401.2 MHz. The manufacturing tolerance, temperature drift, and aging of the platform crystal oscillators provide an additional  $\pm 5$  KHz of frequency dispersion. Time separation between various platform transmissions is provided by the slight differences in the period of the timer in each platform.

The format of the word transmitted by each platform is shown in Figure 9-2. After a carrier acquisition of approximately 0.34 seconds, eight bits of bit synchronization and 12 bits of frame synchronization are sent. Two mode bits follow. (On the balloon platforms these two bits are used to store the most significant bits of the radio altimeter bit count. Other environmental platforms may use these two bits to denote multiplexed subframes of sensor channel data.) The platform ID occupies 10 bits and, finally, four 8-bit channels of the sensor data are sent.

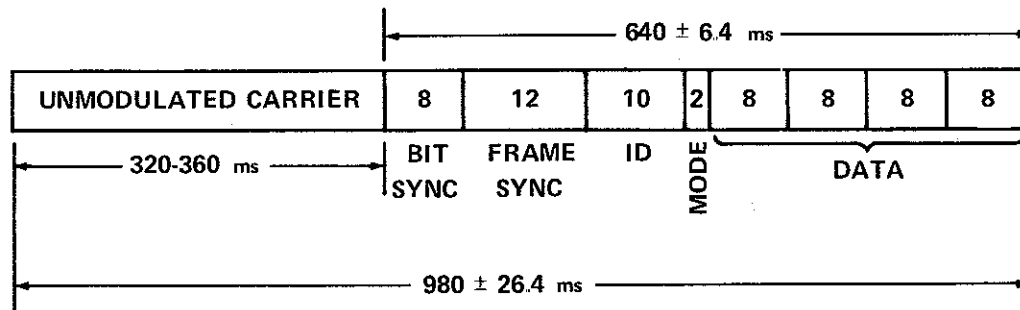


Figure 9-2. Platform Transmission Format

## 9.5 Random Access Measurement System (RAMS)

### 9.5.1 General

The RAMS detects and acquires the incoming platform transmissions, measures each received signal frequency, codes the time of each frequency measurement, demodulates and formats the sensory data. These data are output to the VIP and are then stored on a HDRSS.

If as many as 200 platforms are within satellite view at one time, the probability is 0.01 that the number of simultaneous platform transmissions will not exceed eight. Thus, RAMS was designed to allow for simultaneous reception of up to eight transmissions. On the average, 3.3 receptions per second would be expected from a field of 200 platforms.

Each platform transmits at a carrier frequency of  $401.2 \text{ MHz} \pm 5 \text{ KHz}$ . The effects of this dispersion plus Doppler shift and spacecraft receiver oscillator drifts require a 30 KHz predetection bandwidth. For RAMS to detect these transmitted signals, the 30 KHz band is effectively divided into 300 frequency resolution "cells", each 100 Hz wide, yielding a processing gain of approximately +23 dB. This signal-to-noise ratio provides a 0.95 probability of signal detection.

A signal search and locate function is performed across the received band prior to detection and acquisition. The search function is performed on sampled segments of input data that are stored and recirculated past a detector at a faster-than-real-time rate. As discussed in Section 9.5.2, this time compression technique allows the entire 30 KHz band to be searched in 120 ms.

Figure 9-3 shows the block diagram of RAMS. The platform signals are amplified and translated by the receiver from 401.2 MHz down to an IF frequency, or baseband frequency, of  $25 \text{ KHz} \pm 15 \text{ KHz}$  (10 to 40 KHz). The baseband signal is supplied to the time compressor and the eight data acquisition channels (phase-locked loops). The time compressed replica of the input is fed to the search unit where detection of signals is accomplished. Following detection, the assignment control assigns one of the eight phase-locked loops (PLLs) to acquire the signal. The frequency of the 100 Hz cell is furnished to the assigned PLL by the search unit. Following acquisition (phase lock), frequency measurement, time tagging, data demodulation, and formatting are performed. Finally, the output buffer provides temporary storage between the randomly incoming data and the Nimbus VIP data storage system.

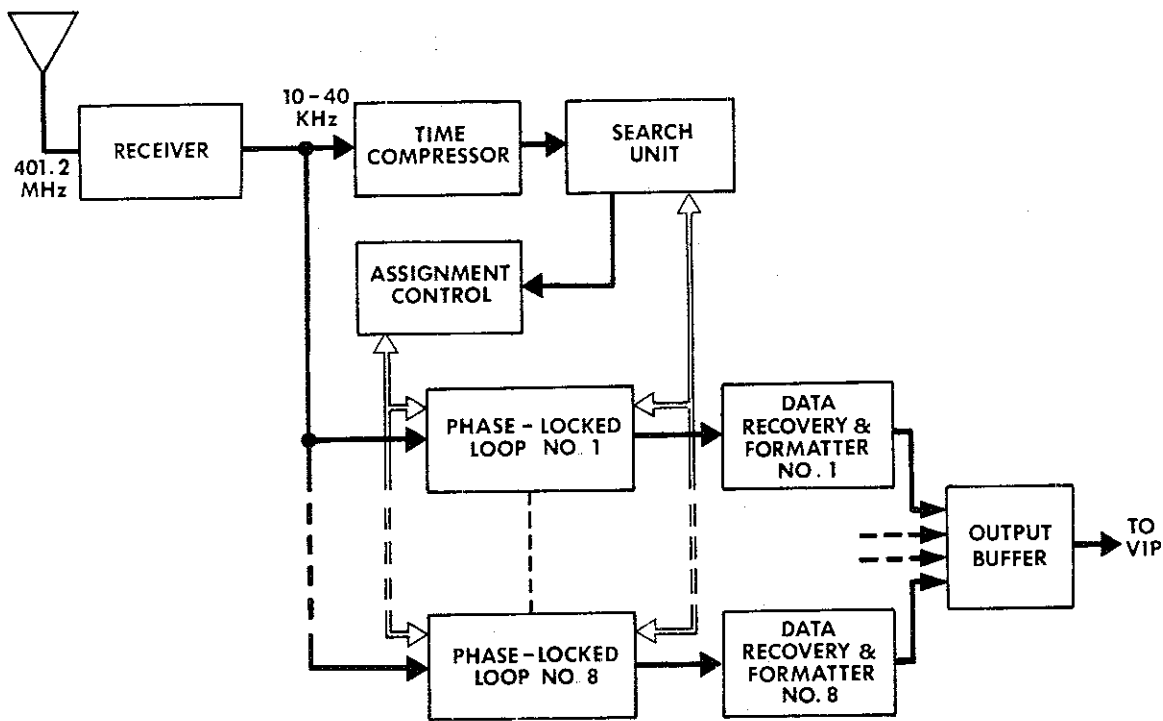


Figure 9-3. RAMS Block Diagram

#### 9.5.2 Search and Locate Function

The purpose of the search and locate function is to divide the 30 KHz bandwidth into 300 cells, determine which cells contain signals, and to assign the PLLs to those particular cells.

The time compressor is somewhat analogous to a tape recorder that stores a sample of the input signal and is then played back at a higher speed into a detector. This action would result in expansion of the signal spectrum, in the frequency domain, by the ratio of the playback to record speed, and a reduction in time by the inverse of this ratio. In RAMS, the time compressor utilizes analog-to-digital conversion of the input, and digital storage and playback as shown in Figure 9-4. The input spectrum (10 to 40 KHz) is converted into a digital format by the delta modulator at a 320 KHz sample rate, and a serial bit stream is inserted into a 128 bit register, register number 1. When filled, the first register is then connected into a long ring counter containing 23 additional 128 bit segments. The entire counter is clocked at 8 MHz (25 times the sampled rate).

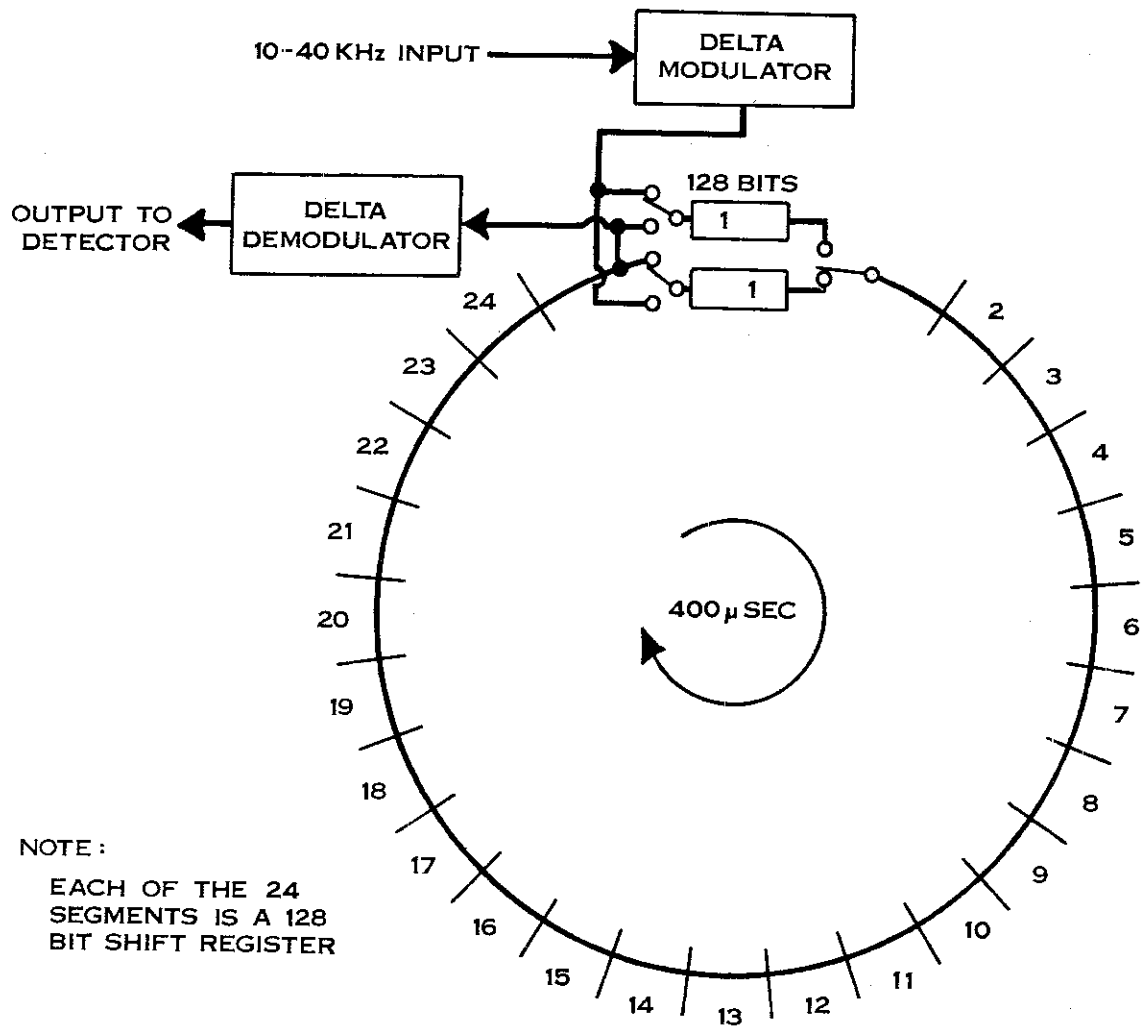


Figure 9-4. Conceptual Diagram of the RAMS Time Compressor

After 3200 clock periods, or 400 microseconds ( $\mu$ s) the contents of register number 1 are shifted completely around the ring past register number 1 and into register number 2. During this time period register number 1 is filled with new data from the delta modulator. These data are subsequently connected to the ring replacing register number 2. In this manner the contents of the ring counter are continuously updated and the oldest data segment is deleted. Since the delta modulator performs differentiation of the input, a simple integrator is utilized in the delta demodulator to provide digital-to-analog conversion of the ring counter output. The end result is that the baseband spectrum (10 to 40 KHz) is expanded in the frequency domain by a factor of 25 so that it occupies a spectrum of 250 KHz to 1.0 MHz.

The basic frequency resolution cell of 100 Hz requires at least 10 ms of dwell time to obtain sufficient energy for detection (one time constant). In speed-up time, each 100 Hz cell is 2.5 KHz wide, corresponding to a dwell time of 400  $\mu$ s. The entire baseband (of 300-100 Hz cells) may be examined in a total period of 120 ms (400  $\mu$ s dwell per cell times 300 cells). Each one second platform transmission format provides for 320 ms of unmodulated carrier prior to phase shift keying (PSK) modulation. Thus, the baseband may be examined twice for active cells during the period of one transmission, increasing the probability of detection.

#### 9.5.3 Search Unit

Signal search is performed on the time-compressed spectrum by using an incremental stepping oscillator to heterodyne the wideband spectrum and present it to a fixed-tuned bandpass filter. The filter bandwidth is 2.5 KHz corresponding to the basic frequency resolution of each cell (in speed-up time). The stepping oscillator rate is consistent with the recirculation rate, thus advancing one cell each 400  $\mu$ s. In the implementation of the stepping oscillator, digital synthesis is utilized to form frequencies presented to a mixer for the heterodyne action. Signals and noise passed by the bandpass filter are envelope detected and compared with a threshold voltage. The threshold voltage is adaptive in that it is determined by the average integrated noise level contained in the wideband spectrum over each sweep period of the search oscillator and serves to maintain a constant false alarm rate. Since the frequencies produced by the stepping search oscillator assume the form  $\sin x/x$ , spectrum spreading over adjacent cells occurs in the detection process. Also, under modulation conditions a platform signal will occupy a band of 250 Hz (2.5 cells). Thus, the decision to assign a PLL to a 100 Hz cell must take into account cell spreading. To accomplish this a digital correlator technique examines groups of five adjacent cells prior to PLL assignment. The presence of a detectable signal level in four of five adjacent cells inhibits assignment during a sweep interval. This rule also aids in masking out detection of wideband interference signals. Needless to say, if prior assignment of a PLL to a given cell has occurred, a second assignment is inhibited. PLL assignment is sequential in that all eight PLLs must be assigned at least once before reassignment of any particular loop can occur.

#### 9.5.4 Acquisition and Data Recovery

Upon recognition of a signal being present, the search unit generates a synthesized frequency representing the cell number containing the platform signal and supplies this frequency to one of the eight PLLs selected for acquisition. Using this technique the PLL only has to acquire over a  $\pm$  one cell

( $\pm 100$  Hz) bandwidth, and rapid phase lock is accomplished. The PLL demodulates the PSK modulated platform data and supplies the data to the data recovery/formatter unit. Once assignment occurs, the selected PLL dwells at the designated cell until either loss of lock occurs, as determined by a quadrature lock detector, or failure to recognize the word synchronization code occurs within 0.8 seconds. This latter feature prevents occupying a PLL on interfering signals for long periods of time.

A ringing circuit bit synchronizer is used to generate bit clock from the demodulated data and to drive an integrate-and-dump data detector. The recovered 100 bits per second data and clock are then furnished to the formatter.

#### 9.5.5 Formatting and Output Buffering

The platform transmission format includes a 12-bit frame synchronization code as shown in Figure 9-2. The formatter is enabled to search for the presence of this code in the incoming data when the PLL acquires lock. Upon recognition of the frame synchronization code, the time of the occurrence is noted by storing a time code generated by the VIP system. Also, upon recognition of the frame sync, the frequency measurement of the received signal commences (actually, the PLL oscillator frequency is measured) and zero crossings are counted for 0.3 seconds. The formatter stores the platform ID code, 2 mode bits, 32 bits of sensor data, the frequency measurement, and time measurement and converts all of this into a 90 bit message for subsequent output to the VIP.

The VIP accepts data from RAMS serially at the rate of one 90-bit message every 0.2 seconds (an effective rate of five messages per second). Since the platform transmissions are random and completely asynchronous with the VIP format, an output buffer in the RAMS provides temporary storage. The output buffer serves all eight data recovery channels and sufficient storage is included to handle peaks of eight simultaneous transmissions.

#### 9.6 Position and Velocity Determination of Balloon Platforms

At the GSFC MDHS, balloon positions and velocity parameters are derived from the relative motion between the satellite and the platforms as determined by the frequency and time measurements made by RAMS. Since the platform signal is transmitted once each minute, the RAMS can acquire and process up to 20 Doppler-shifted frequency transmissions from each platform during an orbital overpass. The position and velocity of each balloon can then be determined using the Doppler vector equation:

$$\left( \frac{c}{\Delta + g} \right) (e - \Delta) = \frac{(\bar{N} \cdot \dot{\bar{R}})(\dot{\bar{N}} - \dot{\bar{R}})}{|\bar{N} - \bar{R}|} - \frac{\bar{R} \cdot \bar{V}_e}{|\bar{N} - \bar{R}|},$$

where       $g$  = clock oscillator frequency  
                $e$  = bias or offset for platform frequency oscillator  
                $c$  = speed of light  
                $\Delta$  = observed Doppler shift  
                $\bar{N}$  = platform position with respect to the earth  
                $\dot{\bar{N}}$  = platform velocity with respect to the earth  
                $\bar{V}_e$  = velocity of earth (due to rotation) at platform location  
                $\bar{R}$  = spacecraft location  
                $\dot{\bar{R}}$  = spacecraft velocity  
 $|\bar{N} - \bar{R}|$  = slant range (platform to spacecraft)

The quantities of  $\bar{N}$ ,  $\dot{\bar{N}}$ , and  $e$  are unknown. Each minute all three of these quantities, in general, change. Some assumptions are necessary to reduce all the unknowns to a tractable number. These are:

- Platform motion is in the form of great circles during and between consecutive passes over the platform. The speed is constant.
- Oscillator bias remains constant during a pass
- Altitude is known and constant

Given these assumptions, a sufficient number of observations on two successive passes of the spacecraft are available to solve for the following six quantities:

- Speed of platform (m/sec)
- Azimuth of platform motion at the time of first received message (first pass)
- Geographic longitude of platform at time of first received message (first pass)
- Latitude of platform at time of first received message (first pass)

- Oscillator bias during first pass
- Oscillator bias during second pass

In the event that Doppler data are acquired from only a single satellite pass, only position will be estimated along with a single bias term.

System requirements place an upper limit of 5 km on position error and 2 meters/sec on velocity error. Simulation studies indicate, that for a completely noise free environment, platforms beyond 150 km from the spacecraft subtrack can be located to within 1 km of their true location. For platforms within 150 km of the subpoint the precision degrades as the platform approaches the sub-point track.

In two pass situations, velocity estimation accuracy is also affected by the platform distance from the subpoint track and the number of messages from a platform for each pass. A minimum of four or five messages, for example, is a marginal condition. Platforms beyond 600 km from the subtrack can be tracked (in the absence of noise) within a limit of 1 m/sec (east-west and north-south directions) if there are sufficient observations for each pass.

The statistical effect of noise cannot be accurately determined due to insufficient knowledge of the noise sources and their correlations. However the sensitivity of the precision due to individual known sources has been assessed in some cases. In consecutive pass cases it has been found that, in the presence of spacecraft oscillator drifts of up to 100 Hz/hr, east-west velocity accuracy is better than 1 m/sec beyond 750 km from the subtrack. For north-south velocity components the accuracy was better than 2 m/sec. For certain directions of platform motion, however, fewer observations were recorded, so that in the event the minimal four or five message groups were received the accuracy degraded beyond these limits.

## 9.7 TWERLE Balloon Platform Data Format and Availability

TWERLE balloon platform data are processed at the Nimbus MDHS and then transmitted to the National Center for Atmospheric Research (NCAR) every 12 hours for further reduction. The data transmitted to NCAR are not in final reduced form; the observed Doppler frequency and other parameters used in the determination of platform velocity are all included.

At NCAR the data are processed to a TWERLE-B format outlined in Table 9-1. In this format the data will be in a fully reduced form and no Doppler

Table 9-1  
TWERLE-B Format of Balloon Data Processed at NCAR

Word No.	Quantity	Units	Remarks
1	Platform ID	Octal	
2	Day, Time	GMT, near-est minute	Midpoint of contacts on earliest orbit
3	Location, Longitudes and Latitudes	Degrees and tenths	Midpoint of contacts on earliest orbit
4	Velocity components	m/sec	East-west and North-south components meteorological convention
5	Quality Figures	Arbitrary	1 or 2 pass data, goodness of fit of least squares solution to doppler equation
6	Sensor data $P_i$ , $T_i$ , $Z_i$	mb, degrees C, meters	For each contact $i=1 \dots n$

frequency or housekeeping data will appear. This format should be more usable for users than the MDHS-transmitted format. Both formats, however, will be available on magnetic tape in standard NCAR packed binary form. Information and utility routines allowing users to unpack and read the data are available from NCAR.

For information concerning the availability of TWERLE balloon data, and routines allowing users to unpack and read the data contact:

Dr. Paul R. Julian  
National Center for Atmospheric Research  
P. O. Box 3000  
Boulder, Colorado 80303

## 9.8 Other Experiments Using RAMS

In addition to the TWERLE balloon experiment, which is the major user of the RAMS, other experiments have been approved for participation using the Nimbus RAMS. Many of these experiments use ocean buoys which measure a variety of oceanographic and atmospheric parameters. Some use drifting balloons as support for meteorological programs. Table 9-2 lists each experiment, the address of the experimenter, and provides general information about each experiment.

**Table 9-2**  
**Nimbus RAMS Experiments**  
**(as of 15 January 1975)**

Principal Investigator	Experiment Title	Platform		
		Number	Type	Deployment Area
Mr. G. R. Cresswell Division of Fisheries & Oceanography Commonwealth Scientific & Industrial Research Organization Melbourne, Australia	Currents in East Indian Ocean	25	Drifting Buoys	Eastern Indian Ocean
A. J. Dyer CSIRO P O Box 77 Mordialloc, Vic 3195 Australia	Australian Ocean Buoy Experiment	10	Drifting Buoys	South of Australia
Professor Pierre Lacombe, Director Laboratory d' Oceanographie Museau Historie Naturelle de Paris 43 Rue Cuvier Paris, France	Participation in GARP	4	Drifting Buoys	Atlantic Ocean
Professor P. Ichernia Museum d' Historie Naturelle de Paris 43 Rue Cuvier Paris, France	A Study of the Antarctic Circum- polar Experiment	4	Drifting Buoys	Antarctic Ocean

Table 9-2 (Continued)

Principal Investigator	Experiment Title	Platform		
		Number	Type	Deployment Area
Dr. Paul R. Julian National Center for Atmospheric Research (NCAR) P.O. Box 3000 Boulder, Colorado 80303	TWERLE	441	Balloons	Tropics
Prof. Pierre Morel Assistant Director Laboratoire de Meteorologie Dynamique CNRS 24 Rue Lhomond Paris 5, France	Lagrangian Measurement of Low Level Friction Drag in the Tropics	55	Balloons and Buoys	Indian Ocean
Dr. Norbert Untersteiner, Program Director Project AIDJEX 4059 Roosevelt Way, N.E. Seattle, WA 98105	Arctic Data Buoys Arctic Ice Dynamics Joint Experiment (AIDJEX)	30	Ice Buoys	Arctic Ocean (20) Antarctica (10)
Dr. Donald V. Hansen, Director Physical Oceanography Laboratory AOWL NOAA U.S. Department of Commerce Miami, Florida	GARP Drift Experiment	32	Drifting Buoys	Atlantic Ocean
Vincent E. Lally National Center for Atmospheric Research P.O. Box 1470 Boulder, Colorado 80302	TWERLE Extension Experiment	50	Balloons	Southern Hemisphere
Vincent E. Lally National Center for Atmospheric Research P.O. Box 1470 Boulder, Colorado 80302	Carrier Balloon System	22	Balloons	Tropics

Table 9-2 (Continued)

Principal Investigator	Experiment Title	Platform		
		Number	Type	Deployment Area
John A. Knauss Graduate School of Oceanography University of Rhode Island Kingston, Rhode Island 02881	An Investigation of Gulf Stream Eddies in Western Sargasso Sea	20	Drifting Buoys	Atlantic Ocean
Arnold L. Gordon Lamont Doherty Geological Observatory Columbia University Palisades, New York 10964	Antarctic Current Experiment	25	Drifting Buoys	Antarctic Ocean
Tim P. Barnett University of California, San Diego Scripps Institute of Oceanography P.O. Box 109 La Jolla, California 92037	North Pacific Current (NPC)	20	Drifting Buoys	Pacific Ocean
D. John Garrett Marine Science, Pacific Region Environmental Canada 1230 Government Street Victoria, British Columbia Canada	Mesoscale Ocean Variability Experiment (MOVE)	10	Drifting Buoys	Pacific Ocean
R. E. Vockeroth Atmospheric Environmental Service 4905 Dufferin Street Downsview 477 (Toronto) Ontario, Canada	Canadian Buoy- Ship Experiment	4	Ship and Buoys	North Atlantic Ocean
J. Lentfer Wildlife Research U.S. Department of Interior 813 D. Street Anchorage, Alaska	Polar Bear Tracking Experiment	6	Polar Bear	Arctic
H. Brann Bureau of Meteorology Melbourne, Victoria Australia	Southern Ocean Experiment	6	Drifting Buoys	South Indian Ocean

Table 9-2 (Continued)

Principal Investigator	Experiment Title	Platform		
		Number	Type	Deployment Area
Fernando De Mendonca Instituto de Pesquisas Espaciais (INPE) P.O. Box 515 12,200 Sao Jose dos Campos San Paulo, Brazil	Satellite Remote Hydrometeorologi- cal Experiment (SHE)	25	Ground Station Buoy (1)	Brazil
Robert Kee Development Engineering Division Code 6201 U S. Naval Oceanographic Office Washington, D.C. 20390	Use of RAMS Drift Buoys for Monitor- ing Surface Current Modeling and Pre- diction	6	Drifting Buoys	Atlantic Ocean
R. R. Dickson Fisheries Laboratory Ministry of Agriculture Fisheries and Food Lowestoft, Suffolk United Kingdom	Norwegian Sea Bottom Drift Experiment and North Atlantic Deep Drift Experiment	6	Drifting Buoys	Norwegian Sea and North Atlantic Ocean
J. Nordo/C. Jensen Norwegian Meteorological Institute Neils Henrik Abelsvei 40 Blindern, Oslo 3 Norway	Meteorology in the Norwegian Sea	2	Moored Buoy and Ship	North Atlantic Ocean
C. Borge/T. Vinje Norsk Polarinstitutt Rolfstangveien 12, Postboks 158 1330 Oslo Lufthaven Norway	Ice Drift Experiment in the Svalbard Greenland Area	5	Drifting Buoys	North Atlantic Ocean
F. Anderson South African Council for Scientific & Indus- trial Research Congella, Natal, South Africa	Ocean Currents Research Experiment	6	Drifting Buoys	South Atlantic and SW Indian Ocean

Table 9-2 (Continued)

Principal Investigator	Experiment Title	Platform		
		Number	Type	Deployment Area
H. Stommel Professor of Oceanography MIT Cambridge, Massachusetts	Ocean Currents Experiment	5	Drifting Buoys	South Atlantic
B Buck Polar Research Lab. Santa Barbara California 93101	Acoustics, Ice Dynamics	6	Drifting Buoys	Arctic Ocean

As with all TWERLE balloon platforms each transmits a signal for a one-second period each minute. The one-second signal consists of a short burst of CW carrier followed by 100 bps modulation containing sync information, platform ID, and coded sensory data. The carrier frequency, including Doppler and oscillator drift, is to be within the band of  $401.2 \text{ MHz} \pm 15 \text{ KHz}$ .

Upon receipt of a signal by the satellite, the carrier frequency is measured, the time of measurement is recorded, and the platform ID and sensory data are demodulated. This information is, in turn, formatted and stored for readout once during each orbit. Following satellite data readout, processing is performed at the MDHS at GSFC to recover and format the sensor data, and to compute platform location and velocity using the same math model as for the TWERLE balloons. Velocity will always be computed even if there is no platform motion. Small velocities will always result due to spacecraft ephemeris and other parameter tolerances. These processed data are then distributed to the appropriate experimenters. The formats of data distributed (punched cards, teletype, or line printer) are discussed in Sections 9.8.1, 9.8.2, and 9.8.3.

Users who desire more information about an experiment listed in Table 9-2 should contact the experimenter directly. GSFC will not keep any record of the data output from any of these experiments. However, any experiment results presented to GSFC will be published in The Nimbus 6 Data Catalog. Also, each new platform experiment and the address of the principal investigator will be listed in The Nimbus 6 Data Catalogs in the same format as in Table 9-2.

#### 9.8.1 Platform Data Sent to Users in Punched Card Format

Five card types are used to format platform data sent to users requesting their data on punched cards. The detailed format of Card Types 3, 4, and 5 are

explained in Tables 9-3, 9-4, and 9-5, respectively. The class of information on each card type is the following:

- Card Type 1 contains the user's name and other identification (columns 02-72)
- Card Type 2 contains the user's address (columns 02-72)
- Card Type 3 contains data related to a specific platform position and/or velocity computation (columns 02-72)
- Card Type 4 contains additional data associated with the platform position (columns 02-72)
- Card Type 5 contains the platform message data at two messages per card (columns 02-72)

Card Type 1 is always first and is always followed by Card Type 2. For each platform there follows one Card Type 3 and one Card Type 4. Card Types 5 then follow, at two messages per card, until all messages from a given platform are listed. Messages from other platforms assigned to the same user follow the last Card Type 5 for the first platform listed. For each additional platform, Card Types 1 and 2 are not needed. Only Card Types 3, 4, and 5 are used as for the first platform.

The first column on each card is used to identify the Card Type number (1, 2, 3, 4, or 5). Columns 73-80 on all Card Types contain similarly formatted information. It is listed here to eliminate the need for repetition in Tables 9-3, 9-4, and 9-5.

- Columns 73-75 contain the acronym RAM
- Columns 76-77 contain the user's assigned number (01 to 50)
- Columns 78-80 are used to sequentially number all cards output from one output tape.

#### 9.8.2 Platform Data Sent to Users in Teletype Format

The teletype format is very similar to the punched card format presented in Section 9.8.1. Because each line of the teletype format is restricted to 66 characters, the last eight columns (73-80) of the punched cards are not included in each teletype line. Also the first six columns of the punched cards, containing

Table 9-3  
Format of Card Type 3 for Users Receiving Platform  
Data in Card Form

Column Block	Column(s)	Description of Item
07-19	01	Card Type
	02-05	Platform ID (octal)
	06	Blank
	07-09	GMT associated with position (or first message if number location computed)
	10-11	Day of year (1-366)
	12-13	Hour (00-23)
	14-15	Minute (00-59)
	17-19	Second (00-59)
	20-21	Millisecond (000-999)
	22-26	Blank
	27-30	Platform altitude-assumed for computation (AA. AA in km)
	31-34	Blank
	35	Assumed radius of earth (RRRR in km)
36-49	36-41	Blank
	42-43	Satellite subpoint at time of position, or first message if no location. (time from cols. 7-19)
	44-49	Latitude ( $\pm$ XX. XX in degrees, + is north)
	50-54	Longitude (XXX. XX degrees east of Greenwich)
	55-67	Blank
55-67	55-60	Oscillator bias computed by position velocity determination program. Includes any bias in S/C local oscillator. Space is provided for two biases, one for each of two passes over the platform.
	61	Bias-first pass ( $\pm$ BBBB in Hz)
	62-67	Blank
	68	Bias-second pass ( $\pm$ BBBB in Hz)
	69	Blank
	70	Point of inflection found (1) or not found (0) for each of two passes
	71	Point of inflection on first pass (1 or 0)
	72	Blank

Table 9-3 (Continued)

Column Block	Column(s)	Description of Item
73-80	71 72	Point of inflection on second pass (1 or 0) Blank Common information on all cards

Table 9-4  
 Format of Card Type 4 for Users Receiving Platform  
 Data in Card Form

Column Block	Column(s)	Description of Item
09-22	01 02-05 06 07 08	Card Type Platform ID (octal) Blank Number of passes (1 or 2) zero indicates no position computed (One pass gives two locations. Two passes give one location plus platform velocity.) Blank Platform position - first of two ambiguous positions for a single pass case - the unambiguous single position for a two pass case
24-37	09-14 15-16 17-22 23 24-29 30 31-37 38	Latitude ( $\pm$ XX. XX in degrees, + is north) Blank Longitude (XXX. XX degrees east of Greenwich) Blank Second platform position of the two positions in a single pass case. Not used in two pass case. Latitude ( $\pm$ XX. XX in degrees, + is north) Blank Longitude (XXX. XX in degrees east of Greenwich) Blank

Table 9-4 (Continued)

Column Block	Column(s)	Description of Item
39-51 53-57 59-63	39-44	Platform velocity - Velocity is only computed for two pass cases.
	45-51	North velocity ( $\pm$ XX. XX m/sec, + is north)
	52	East velocity ( $\pm$ XX. XX m/sec, + is east)
	53-54	Blank
	55	Standard error index (percent, 0 = poor 99 = excellent). This parameter indicates the quality of the fit between the observed data and the computed position and/or velocity.
	56-57	First value (used for one and two pass cases)
	58	Blank
	59-60	Second value (Only used for one pass case for ambiguous position two.)
	61	Blank
	62-63	Number of messages used in position and/or velocity computation
	64	Number of messages from first pass
	65-67	Blank
	68	Number of messages from second pass (blank for one pass case)
	69	Blank
	70	Total number of messages from platform (platform ID in cols. 2-5 on card types 3 and 4). Card type 5 gives the message data at two messages per card whether or not used in position computation. The total messages divided by two thus specifies the number of type 5 cards to follow.
		Blank
		Flag indicating whether the platform-to-satellite subpoint distance is above or below a threshold (distance is still to be defined) 0 = distance is greater than threshold. 1 = distance is less than threshold. For a two pass case, if either or both distances is less than threshold Flag = 1.
		Blank

Table 9-4 (Continued)

Column Block	Column(s)	Description of Item
73-80	71	Preferred platform position (only used for the single pass case). 0 = no preference, 1 = first position preferred (cols. 09-22), 2 = Second position preferred (cols. 24-37)
	72	Blank Common information on all cards

NOTE: If no position was computed, type 3 and 4 cards will contain only the following information:

Card Type 3 cols. 02-05 Platform ID  
cols. 07-20 GMT of first message

Card Type 4 cols. 02-05 Platform ID  
cols. 65-65 Total messages to follow on Type 5 Cards

Table 9-5  
Format of Card Type 5 for Users Receiving Platform Data  
in Card Form

Column Block	Column(s)	Description of Item
02-36	01	Card Type
	02-05	Information of the first platform message
	06	Platform ID as received by the S/C
	07-09	Blank
	10-11	Day of year message received (0-366)
	12-13	Hour message received (00-23) GMT
	14-15	Minute message received (00-59) GMT
	16	Second message received (00-59) GMT
	17-19	Blank
	20	Millisecond message received (000-999) GMT
	21	Blank
	22	Phase lock loop ID (0-7) used by the S/C hardware used to process message
		Flag (0-7) to indicate the quality of message 0 = Message good (used in position computation, if there was one)

Table 9-5 (Continued)

Column Block	Column(s)	Description of Item
25-36	22 (cont.)	<p>1 = Message used in position computation after correction of platform ID. Correction based on platform period. (ID as received is given in cols. 2-5 or in 38-41. Corrected ID is given on preceding Type 3 and 4 cards.)</p> <p>2 = Message used in position computation after correction of platform time.</p> <p>3 = Message not used. Time did not pass screening test.</p> <p>4 = Bad data. Synchronization of data from spacecraft to ground in question. May contain noise and/or data may be skewed.</p> <p>5 = Message not used. Doppler did not pass screening test.</p> <p>6 = Message used in final position computation but initial computations showed errors above a threshold</p> <p>7 = Not assigned</p>
	23	Mode (0-3)
	24	Blank
	25-27	Four 8-bit words (octal) of platform sensor data
	28-30	Word number 1
	31-33	Word number 2
	34-36	Word number 3
	37	Word number 4
	38-72	Blank
		Information on second platform message. The format is identical to columns 02-36 after the first platform message
38-72	38-41	Platform ID
	42	Blank
	43-45	Day of year
	46-47	Hour
	48-49	Minute
	50-51	Second
	52	Blank

Table 9-5 (Continued)

Column Block	Column(s)	Description of Item
	53-55 56 57 58 59 60 61-63 64-66 67-69 70-72 73-80	Millisecond Blank Phase lock loop ID Flag (0-7) Mode Blank Word 1 Word 2 Word 3 Word 4 Common information on all cards

the Card Type and the platform ID, are not given on each line of the teletype message. The first teletype line is used to give the platform ID. It is not repeated for teletype lines 2 and 3. Table 9-6 gives the detailed format of each line in a teletype message. In summary, the similarities between the teletype format and the punched card format are the following:

- Teletype Line 1 (platform ID) is of the same format as the ID given in columns 02-05 on the punched cards.
- Teletype Line 2 (platform position data) is of the same format as columns 7-71 of the Card Type 3 (Table 9-3)
- Teletype Line 3 (additional data associated with platform position) is of the same format as columns 7-71 of Card Type 4 (Table 9-4).
- Teletype Line 4 (platform message data at two messages per line) is of the same format as columns 2-72 of Card Type 5 (Table 9-5), but with the spaces in columns 16, 20, 24, 52, 56, and 59 deleted.

For the first computed platform location (lowest ID number) of a teletype message, teletype Lines 1, 2, and 3 are required, plus up to 15 lines of Line 4 information (up to 30 associated messages). Following the first group of Lines 1, 2, 3, and 4 would be lines 1, 2, 3, and 4 for the next location (in chronological order) for the same platform ID. If a user has additional platforms, information on these would follow in increasing ID order.

Table 9-6  
Teletype Format for Users Receiving Platform  
Data by Teletype

TTY Line	TTY Character(s)	Description of Item
1	01-04	Platform ID (octal)
	05	Blank
	06-10	Five periods ( . . . . )
	01-03	Day of year message received (0-366)
	04-05	Hour of platform location (00-23 in GMT) or of first message if no location is computed
	06-07	Minute of platform location (00-59 in GMT)
	08-09	Second of platform location (00-59 in GMT)
	10	Blank
	11-13	Millisecond of platform location (000-999 in GMT)
	14-15	Blank
	16-21	Assumed altitude of platform (XX. XX km)
	22-24	Blank
	25-28	Assumed radius of earth (XXXX km - integer)
	29	Blank
	30-35	Satellite subpoint latitude ( $\pm$ XX. XX degrees, + is north)
	36	Blank
	37-43	Satellite subpoint longitude (XXX. XX degrees east of Greenwich)
	44-48	Blank
2	49-54	Oscillator bias on first pass ( $\pm$ BBBB in Hz)
	55	Blank
	56-61	Oscillator bias on second pass (if applicable)
	62	Blank
	63	Point of inflection on first pass 1 = found, 0 = not found
	64	Blank
	65	Point of inflection on second pass
	66	Decimal check sum of characters 1-65 (a blank equals zero) truncated to a one decimal character.
	01	Number of passes (1 or 2) zero indicates no position computed (One pass gives two locations. Two passes give one location plus platform velocity.)

Table 9-6 (Continued)

TTY Line	TTY Character(s)	Description of Item
3 (cont.)	03-08	First latitude of platform location ( $\pm$ XX.XX in degrees, + is north)
	09	Blank
	10-16	First longitude of platform location (XXX.XX in degrees east of Greenwich)
	17	Blank
	18-23	Second latitude of platform location (for one pass - second location)
	24	Blank
	25-31	Second longitude of platform position (for one pass - second location)
	32	Blank
	33-38	North velocity ( $\pm$ XX.XX m/sec, + is north)
	39	Blank
	40-45	East velocity ( $\pm$ XX.XX m/sec, + is east)
	46	Blank
	47-48	First value of standard error index (Integer values from 0-99 indicating quality of fit. 0 = poor, 99 = excellent)
	49	Blank
	50-51	Second value of standard error index (Only applicable to one pass - second location data)
	52	Blank
	53-53	Number of messages from first pass used in location computation
	55	Blank
	56-57	Number of messages from second pass used in location computation
	58	Blank
	59-61	Total number of messages from platform (platform ID in character position 01-04 on line one). This number specifies the number of data message lines to follow at two messages per line.
	62	Blank
	63	Flag indicating whether the platform-to-satellite subpoint distance is above or below a threshold. (1 = distance is less than threshold)

Table 9-6 (Continued)

TTY Line	TTY Character(s)	Description of Item
3 (cont.)	64 65  66	Blank Preferred platform position (only used for the single pass case) 0 = no preference 1 = first position preferred (characters 03-16) 2 = second position preferred (characters 18-31) Decimal check sum of characters 1-65, truncated to a one decimal character.
4	01-32 01-04 05 06-08 09-10 11-12 13-14 15-17 18 19 20 21-23 24-26 27-29 30-32 33 34-65 34-37 38 39-41 42-43 44-45 46-47 48-50	Line 4 (and each succeeding line with the same platform ID) has space for two messages of platform data. Each message has the same format. First message of platform data Platform ID as received by the S/C Blank Day of year message received (0-366) Hour message received (00-23) GMT Minute message received (00-59) GMT Second message received (00-59) GMT Millisecond message received (000-999) GMT Phase lock loop ID (0-7) Flag (0-7) (see col. 22 Card Type 5) Mode (0-3) Word Number 1 Word Number 2 Word Number 3 Word Number 4 Blank Second message of platform data Platform ID Blank Day of year Hour Minute Second Millisecond

Table 9-6 (Continued)

TTY Line	TTY Character(s)	Description of Item
4 (cont.)	51	Phase lock loop ID
	52	Flag (0-7)
	53	Mode
	54-56	Word 1
	57-59	Word 2
	60-62	Word 3
	63-65	Word 4
	66	Decimal checksum of characters 1-65 truncated to a one decimal character

### 9.8.3 Platform Data Sent to Users in Line Printer Format

Users requesting their platform data in line printer form will receive printouts as shown in the sample format in Figure 9-5. The sample format shows the data for three cases - a position determined for two passes, and a pair of positions derived from one pass, and a case where a position was not determined from the sightings. The two-pass format is shown at the top, followed by the one-pass and no location format. The user's name and address is given in the upper left corner of the printout. Information format common to all cases is the following:

- ORBIT

The platform data was acquired during the ORBIT listed. For TWERLE only, an orbit begins and ends at the descending node (during the night portion of the orbit when TWERLE is not active). The TWERLE orbit 2, for example, begins halfway through the conventional orbit 2, which begins and ends at the ascending node.

- TIME

The time (GMT) associated with the determined position(s) is given as the day (0-366), hour, minute, second, and millisecond. Notice that the spacecraft digitizes to the nearest 0.1 second of spacecraft time, but the spacecraft GMT correction applied is to the millisecond, with an accuracy of  $\pm 10$  ms.

MR. THOMAS ON  
GENERAL ELECTRIC CO  
P.O. BOX 1555  
PHILADELPHIA, PENNSYLVANIA 19101

ORBIT = 1487

PLATFORM ID= 0005 TIME= 191/09/12/00/000 EARTH RADIUS= 6378.0 KM ALTITUDE= 14.3 STD ERR INDEX= 44

TWO PASS POS	VELOCITY-N/S	TOT	F	PLT	TIME	DATA	L	M	WD1	WD2	WD3	WD4	DATA							
LAT	LONG	NORTH EAST	MSG'S	L	ID	DDD/MM/SS/MM	WD1	WD2	WD3	WD4	L	ID	DDD/MM/SS/MM	L	M	WD1	WD2	WD3	WD4	
9.79	15.04 -0.2	1.1	15.0	0.0005	191/09/12/00/000	7	1	0.12	0.00	0.00	0.005	191/09/14/00/000	7	3	0.12	0.00	0.00	0.00	0.00	0.00
7.22	32.85 S/C SUBPT		0	0.0005	191/09/15/00/000	0	0	0.012	0.00	0.00	0.005	191/09/16/00/000	0	1	0.12	0.00	0.00	0.00	0.00	0.00
PUR PASS DATA			0	0.0005	191/09/17/00/000	0	2	0.12	0.00	0.00	0.005	191/10/05/00/000	0	1	0.12	0.00	0.00	0.00	0.00	0.00
ITEM PASS 1	PASS 2		0	0.0005	191/10/56/00/000	0	2	0.12	0.00	0.00	0.005	191/10/57/00/000	0	3	0.12	0.00	0.00	0.00	0.00	0.00
PT OF INF YES	YES		0	0.0005	191/10/58/00/000	0	0	0.12	0.00	0.00	0.005	191/10/59/00/000	1	1	0.12	0.00	0.00	0.00	0.00	0.00
MSG'S USED 5	10		0	0.0005	191/11/09/00/000	1	2	0.12	0.00	0.00	0.005	191/11/01/00/000	1	2	0.12	0.00	0.00	0.00	0.00	0.00
OSC BLAS(HZ) -4	0		0	0.0005	191/11/02/00/000	2	0	0.12	0.00	0.00	0.005	* 191/11/03/00/000	2	1	0.12	0.00	0.00	0.00	0.00	0.00
			0	0.0005	191/11/04/00/000	2	2	0.12	0.00	0.00	0.005	*								

ORBIT= 1488

PLATFORM ID= 0004 TIME= 191/10/55/00/000 EARTH RADIUS= 6377.6 KM ALTITUDE= 15.2 FVVALUE= 97.9

ONE PASS POS	STD	ERR	TOT	F	PLT	TIME	DATA	L	M	WD1	WD2	WD3	WD4	DATA	L	M	WD1	WD2	WD3	WD4
LAT	LONG	IND/PREF	MSG'S	L	ID	DDD/MM/SS/MM	WD1	WD2	WD3	WD4	L	ID	DDD/MM/SS/MM	L	M	WD1	WD2	WD3	WD4	
12.39	10.27	45 *	11.0	0.0004	191/10/55/00/000	0	0	0.12	0.00	0.00	0.004	191/10/56/00/000	0	3	0.12	0.00	0.00	0.00	0.00	0.00
9.73	35.72	41	0	0.0004	191/10/57/00/000	0	0	0.12	0.00	0.00	0.004	191/10/58/00/000	0	1	0.12	0.00	0.00	0.00	0.00	0.00
-6.99	9.59	S/C SUBPT	0	0.0004	191/10/59/00/000	1	2	0.12	0.00	0.00	0.004	191/11/01/00/000	0	0	0.12	0.00	0.00	0.00	0.00	0.00
PT OF INF YES	YES		0	0.0004	191/11/01/00/000	1	0	0.12	0.00	0.00	0.004	191/11/02/00/000	0	2	0.12	0.00	0.00	0.00	0.00	0.00
MSG'S USED 11	11		0	0.0004	191/11/03/00/000	2	2	0.12	0.00	0.00	0.004	191/11/04/00/000	2	3	0.12	0.00	0.00	0.00	0.00	0.00
OSC BLAS(HZ) -27	0		0	0.0004	191/11/05/00/000	3	0	0.12	0.00	0.00	0.004	191/11/06/00/000	3	0	0.12	0.00	0.00	0.00	0.00	0.00

202

ORBIT= 1487

\*\*\* PVD DID NOT DETERMINE A LOCATION FOR THIS SIGHTING \*\*\*

PLATFORM ID= 0012 TIME= 191/09/08/00/000 EARTH RADIUS= 6377.7 KM ALTITUDE= 0.0 FVVALUE= 0.0

ONE PASS POS	STD	ERR	TOT	F	PLT	TIME	DATA	L	M	WD1	WD2	WD3	WD4	TIME	L	M	WD1	WD2	WD3	WD4
LAT	LONG	IND/PREF	MSG'S	L	ID	DDD/MM/SS/MM	WD1	WD2	WD3	WD4	L	ID	DDD/MM/SS/MM	L	M	WD1	WD2	WD3	WD4	
0.00	0.00	0	0.0112	191/09/08/00/000	6	0	0.12	0.00	0.00	0.012	191/09/08/00/000	3	3	0.12	0.00	0.00	0.00	0.00	0.00	
0.00	0.00	0	0.0112	191/09/09/00/000	6	1	0.12	0.00	0.00	0.012	191/09/09/00/000	3	0	0.12	0.00	0.00	0.00	0.00	0.00	
-6.08	36.18	S/C SUBPT	5	0.0112	191/09/10/00/000	6	2	0.12	0.00	0.00	0.012	191/09/11/00/000	6	3	0.12	0.00	0.00	0.00	0.00	0.00
PT OF INF YES	YES		5	0.0112	191/09/11/00/000	7	0	0.12	0.00	0.00	0.012	191/09/14/00/000	7	2	0.12	0.00	0.00	0.00	0.00	0.00
MSG'S USED 10	10		5	0.0112	191/09/15/00/000	0	3	0.12	0.00	0.00	0.012	191/09/16/00/000	0	0	0.12	0.00	0.00	0.00	0.00	0.00
OSC BLAS(HZ) 0	0		5	0.0112	191/09/17/00/000	0	1	0.12	0.00	0.00	0.012	191/09/18/00/000	0	2	0.12	0.00	0.00	0.00	0.00	0.00

**Figure 9-5. Line Printer Format of TWERLE Platform Data**

- EARTH RADIUS

An a priori number for the earth radius used in computation of the platform position.

- ALTITUDE

This is the assumed platform altitude above the earth (or on the earth) used in computation of the platform position.

- STD ERR IND/PREF/FVALUE

The standard error index parameter indicates the quality of the fit between the observed data and the computed position and/or velocity. Note that two values are given in a one-pass calculation because two ambiguous positions are given. In this case an asterisk indicates which of the two positions is preferred. The FVALUE is the estimated reliability of the PREF (preference) asterisk in percent. In both cases the standard error index ranges from 0 to 100; 0 = poor fit, 99 = an excellent fit.

The platform data is given at two messages per line. The information is identical to that presented in Table 9-5 for Card Type 5. The format sequence, however, is slightly different.

- TOT MSGS are the number of messages for which data is given, whether or not they are used in the position/velocity computation.
- FL is a flag as defined for column 22 in Table 9-5.
- PLT ID is the platform ID as received by the spacecraft.
- TIME is the day, hour, minute, second, and millisecond the platform data was received at the spacecraft.
- L is the phase lock loop ID (0-7) used by the spacecraft hardware to process the message.
- M is the mode in two bits of octal, right-adjusted.
- WD1, WD2, WD3, and WD4 are the four platform words of eight bits each. All are in octal, right-adjusted.

The two-pass format of information, at the left of the figure, is the following:

- LAT LONG (and) VELOCITY-M/S NORTH EAST

These values of latitude, longitude (in degrees east of Greenwich), and velocity (in meters/second) are the computed position and velocity of the platform at the given TIME.

- S/C SUBPT

The spacecraft subpoint is the position of the satellite at the given TIME. An asterisk following indicates that on one, or both, of the passes the computed distance of the platform from the subpoint track is less than a threshold value, which is to be defined.

- MSGS USED

This is the number of platform messages used in the computation of platform position and/or velocity.

- PT OF INF

A YES or NO for each pass indicates whether or not a point of inflection of the Doppler data was found.

- OSC BIAS (HZ)

This is the computed oscillator bias (in Hertz) and is a combination of biases from the platform and spacecraft oscillators. The spacecraft oscillator bias is not given on the printout, but is available upon request.

The one-pass format of information, at the left of the figure, is the following:

- LAT LONG (and) STD ERROR INDEX/PREF

The two LAT LONG values are the two ambiguous positions of the platform. The STD ERR IND is as previously defined.

- S/C SUBPT

The spacecraft subpoint is the position of the satellite at the given TIME. An asterisk following indicates that the platform distance from the subpoint track of either computed location is less than a threshold value, which is to be defined.

- MSGS USED

This is the number of platform messages used in the computation of platform position.

- PT OF INFL (and) OSC BIAS

These values have the same meaning as for the two pass case, but there is only one value for each rather than two.

It is possible to have platform data and not compute a platform position. The format for this case would be similar to the above, but the only data given would be:

- Platform ID
- TIME of first message
- EARTH RADIUS
- Total messages
- S/C SUBPT
- Platform data for all messages

In this case, where no platform position is calculated from the messages, the flag of "O" indicates the message would have been used in a position calculation but was not due to other reasons such as not having a sufficient number of messages to compute a position.

## BIBLIOGRAPHY

1. Arndt, A. E., Burgess, John L., and Reed, David L.: System Study for the Random Access Measurement System (RAMS). NASA, X-752-70-376, October 1970.
2. Nimbus F TWERLE RAMS Platform Interface Specifications. Code 902, NASA - Goddard Space Flight Center, Greenbelt, Md., September 1973.
3. Opportunities for Participation in Space Flight Investigations. NASA Handbook NHB 8030.1A, NASA, Washington, D.C., April 1967, with memo change #43, 23 March 1972.

## SECTION 10

### THE TRACKING AND DATA RELAY EXPERIMENT (T&DRE)

by

P. E. Schmid

National Aeronautics and Space Administration  
Goddard Space Flight Center

#### 10.1 Introduction

The Tracking and Data Relay Experiment (T&DRE) is a cooperative satellite experiment utilizing both the Nimbus 6 and ATS 6 spacecraft. Both tracking data and telemetry data from the Nimbus observatory will be relayed to a ground station via the geostationary ATS 6. The experiment objectives are to:

- Determine the extent to which the orbit of a near-earth spacecraft can be established from tracking data relayed by a synchronous altitude spacecraft
- Demonstrate the technology of command and telemetry data transmission between a low altitude satellite and a ground station using a geosynchronous satellite as a communications relay

Both of the foregoing objectives are directly applicable to the forthcoming geostationary Tracking and Data Relay Satellite System (T&DRSS) which will provide operational tracking and telemetry data relay support of near-earth satellites.

#### 10.2 Telemetry Data Relay

The use of ATS as a relay of Nimbus tracking data and telemetry data requires the same basic overall system configuration. Real-time telemetry relay will be demonstrated for the following Nimbus data types:

- Versatile Information Processor (VIP)
- High Resolution Infrared Sounder (HIRS)
- Limb Radiance Inversion Radiometer (LRIR)
- Temperature Humidity Infrared Radiometer (THIR)

Extensive evaluation of this Nimbus-ATS-ground station link will be made by using a prearranged schedule of pseudo-noise (PN) code modulation, phase modulated directly onto the nominal 2 GHz carrier frequency (at bit rates of 400, 200, 100 or 50 kbs). In addition, ground station commands to Nimbus (either directly or via ATS 6) will be used to select the VIP or LRIR data at 4 kbs or the HIRS data at 3.4 kbs for transmission to the ground via ATS. This data will be phase modulated directly onto the ATS carrier. The THIR data can also be selected and in this case the THIR data frequency modulates a 43.68 KHz ( $\pm 15$  percent) subcarrier. This subcarrier phase modulates the 2253 MHz level to ATS. At ATS the subcarrier is translated to the active C-band down link. The foregoing data types will be compared with data from playback of a Nimbus tape recorder sent directly to a STDN station.

Although the telemetry data relay phase of this experiment is straightforward, it is nonetheless very important in that it will establish operational procedures and techniques directly applicable to future NASA satellite data relay programs. On the other hand, the tracking data handling and subsequent orbit computation represents a new concept inasmuch as two satellite motions are simultaneously being measured by means of range and Doppler data. Consequently, the remainder of this experiment description will focus on tracking and orbit determination. The basic transponder interrogations, and translations will, of course, be equally applicable to either telemetry or tracking data relay.

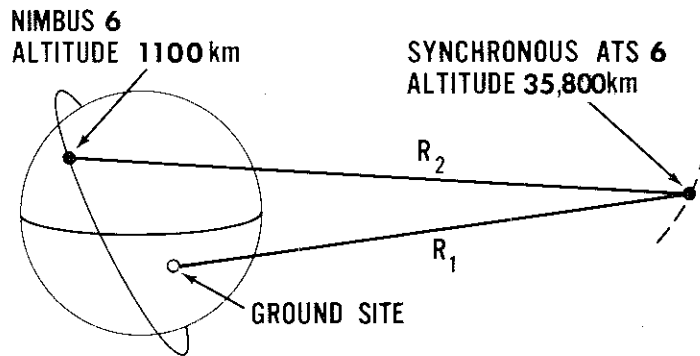
### 10.3 Tracking and Orbit Determination

The purpose of the tracking and orbit determination phase of the T&DRE can be summarized as follows:

- To demonstrate that tracking of a near-earth satellite via a geo-stationary satellite is feasible and subsequent orbit computation can be performed without the aid of multiple ground station tracking, and
- To exploit the broad tracking coverage provided by the geostationary satellite to obtain an improved geopotential solution. Selected terms in the geopotential spherical harmonic expansion will be solved, along with the position and velocity vectors of Nimbus 6 and ATS 6.

#### 10.3.1 Major System Components

ATS 6, launched on May 30, 1974, is in an earth-synchronous orbit at 35,800 km. Nimbus 6 will be in a sun-synchronous orbit at 1100 km. Figure 10-1 shows this basic geometry and the location of a ground tracking station.



MEASUREMENT TYPE	RESOLUTION	APPLICABLE FREQUENCY
RANGE ( $R_1 + R_2$ )	2 METERS	100 KHz
DOPPLER ( $\dot{R}_1 + \dot{R}_2$ )	0.05 cm/sec	2000 MHz

Figure 10-1. T&DRE Geometry

The vital ATS elements for tracking Nimbus and relaying Nimbus experiment data to the ground are a communications transponder and a 2-GHz nine-meter parabolic antenna. The transponder translates 5 GHz ground station signals into 2 GHz signals sent to Nimbus and also translates the 2 GHz signals from Nimbus into 4 GHz signals which are sent to the ground. Figure 10-2 shows these frequency links between Nimbus, ATS, and the ground. The antenna has a nominal beam width of 1.4 degrees and a gain of 36 dB. It can be electronically scanned  $\pm 5$  degrees off boresight, and has monopulse capability to track the Nimbus satellite. However, the primary ATS antenna pointing mode for the tracking experiment is for the ground station to program the ATS with computed pitch and roll commands based upon ATS and Nimbus ephemeris data.

Nimbus will observe ATS by means of an up-looking 2 GHz antenna array which has a nominal gain of 15 dB corresponding to a 3 dB beam width of 25 degrees. The system consists of the gimbaled antenna assembly, the gimbal drive electronics, the power amplifier, transponder, and the digital electronics. The gimbaled high-gain antenna is directed to ATS by programmed activation of an X/Y mechanical mount. The antenna is located on the top of the Nimbus spacecraft, as shown in Figure 1-1 in Section 1 of this report.

The tracking data recorded at the ground station consists of range and Doppler measurements in terms of time relays. The range data is elapsed

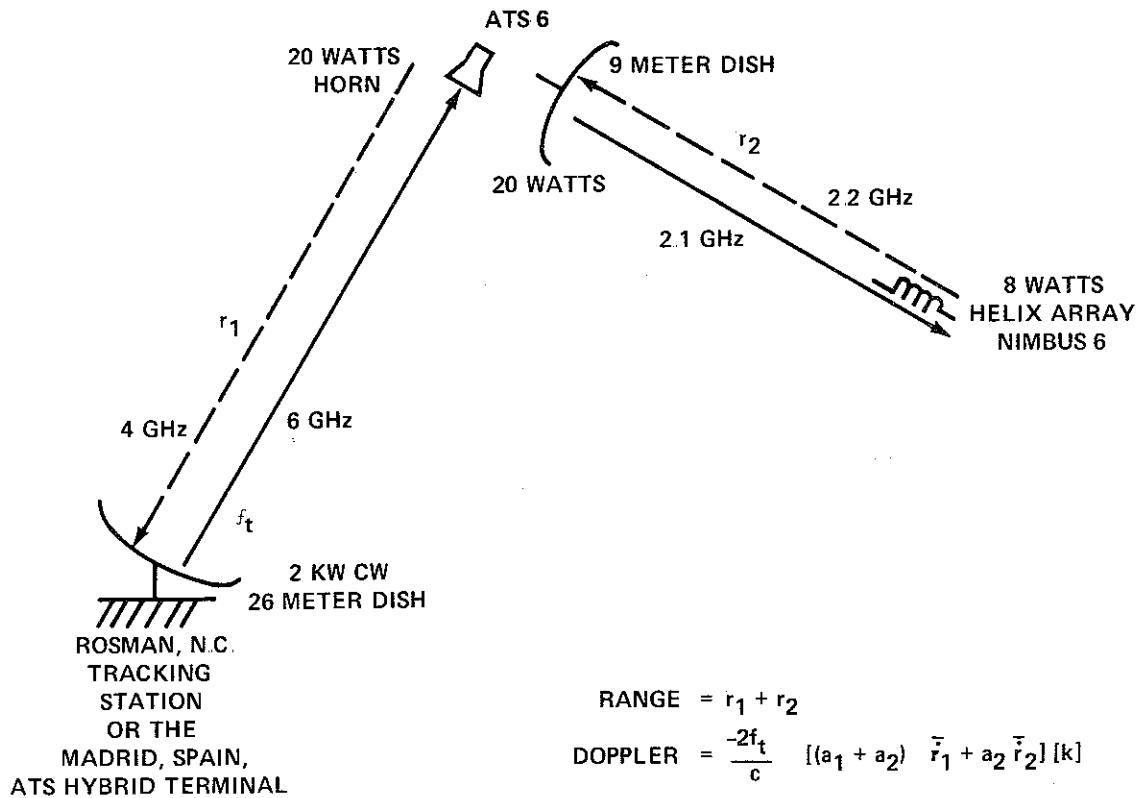


Figure 10-2. Tracking Signal Power Levels and Pointing

radio wave propagation time. The Doppler data, which is a function of range rate, is recorded as the time required to count a fixed number of cycles of two-way Doppler.

Figure 10-3 illustrates the overall tracking data processing required for this experiment.

#### 10.3.2 Overall Electronics

The overall ranging measurement consists of a measurement of the total round trip signal delay and involves:

- The interrogation station located at Rosman, North Carolina (or during later phases a transportable site at Madrid, Spain)

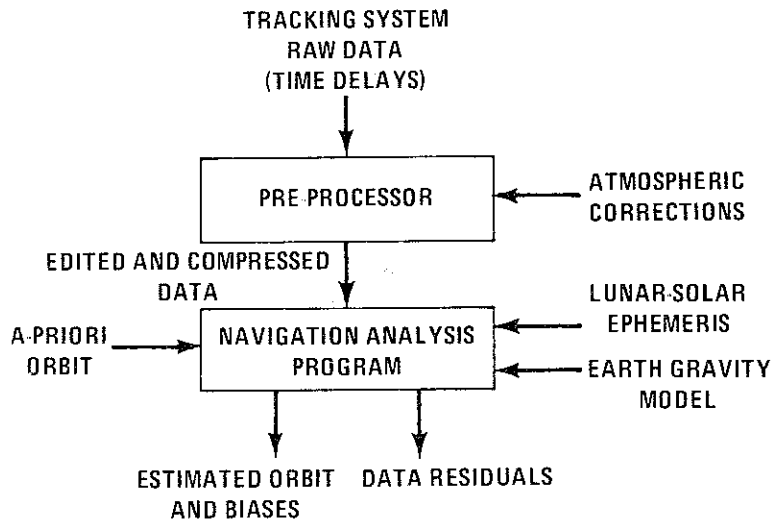


Figure 10-3. Orbit Determination Processing System Using T&DRE Data

- The phase-locked ATS translation transponder and S-Band parabolic antenna, and
- The Nimbus crystal-controlled transponder used in conjunction with the programmed S-Band helical antenna array

The rate of range change ("average range rate") is observed as a Doppler shift and necessarily involves the relative motions of the two spacecraft and the ground station.

The ground station typically will transmit at a 2 kw carrier wave (CW) level, although it is capable of transmitting up to 10 kw. The highest resolution range tone is 100 KHz with lower ambiguity resolving tones used during acquisition. The tracking signal generated at the ground station and transmitted to ATS is used for the coherent Doppler and tone ranging measurements. The signal generation is indicated in simplified form in Figure 10-4. The use of the pilot carrier at 6150 MHz permits a coherent lockup with the ATS transponder, while the tracking signal (6137.85 MHz in the case indicated) can be varied over a wide range to permit coherent tracking of other spacecraft or ground located transponders without reacquiring ATS in the frequency domain. The coherent tracking signal translation by the ATS transponder is indicated in Figure 10-5.

The Nimbus translation transponder shown in Figure 10-6 is interrogated by ATS at 2062.85 MHz. The four-element antenna subsystem is directed to ATS by programmed activation of a gimbaled X/Y mechanical mount. The

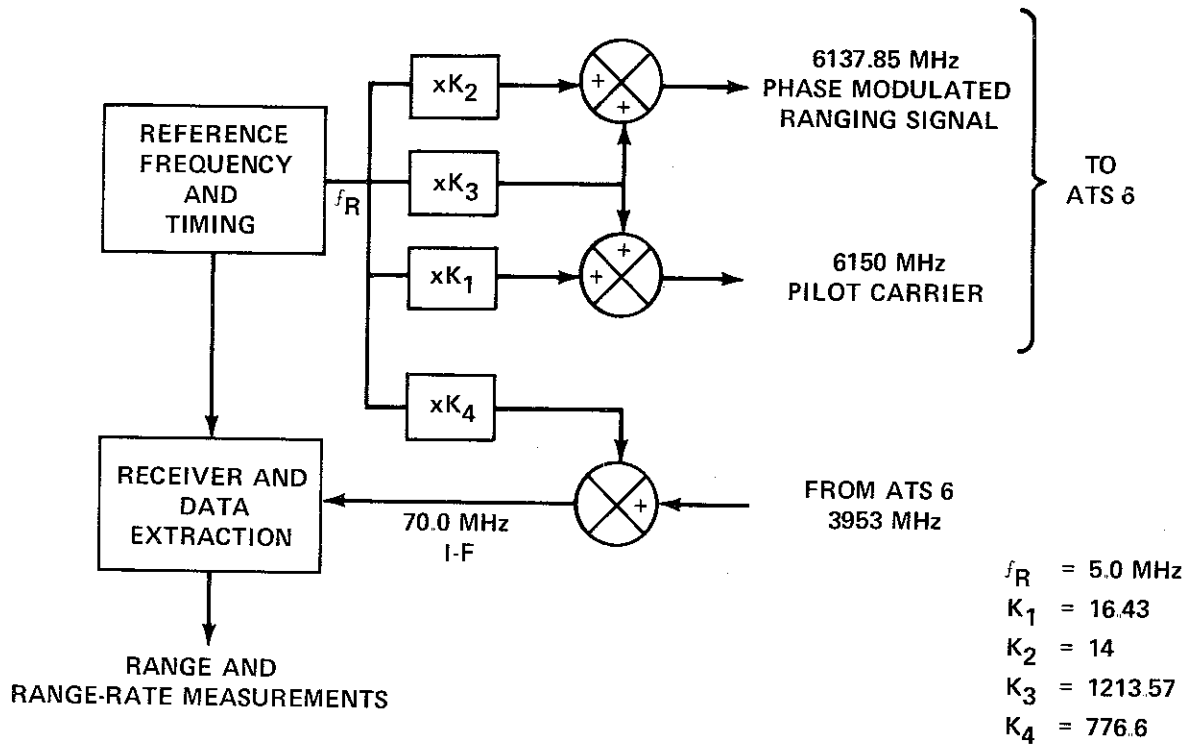


Figure 10-4. Ground Station Signal Generation to ATS 6

pointing information will normally be loaded into the T&DRE memory via VHF radio link when the spacecraft is in view of a Nimbus command site such as the Fairbanks, Alaska, STDN. The antenna can also be controlled by direct access and control via the T&DRE command system (S-band).

With reference to Figure 10-6, the incoming Doppler-shifted ATS signal is translated by a frequency derived from the Nimbus 37.550 MHz crystal oscillator. This same reference is multiplied up to S-Band (2253.0 MHz) where it serves as the carrier for the Nimbus-to-ATS eight-watt link. The translated ATS-to-Nimbus signal is phase modulated onto the 2253.0 MHz carrier at a nominal modulation index of 1.5 radians. This system is based on the Goddard Range and Range Rate concept, where a crystal-controlled relatively broadband (several hundred KHz) transponder is employed. This system is made equivalent to coherent (i.e., phase-locked transponder) operation by proper ground station processing of the transmitted carrier which is coherent with the onboard reference oscillator. The advantage of using such a transponder is that no frequency swept acquisition is required by the interrogating signal. The frequency excursion at 2 GHz due to one-way Doppler often approaches  $\pm 50$  KHz, since the linear speed of near-earth spacecraft is typically 8 km per second.

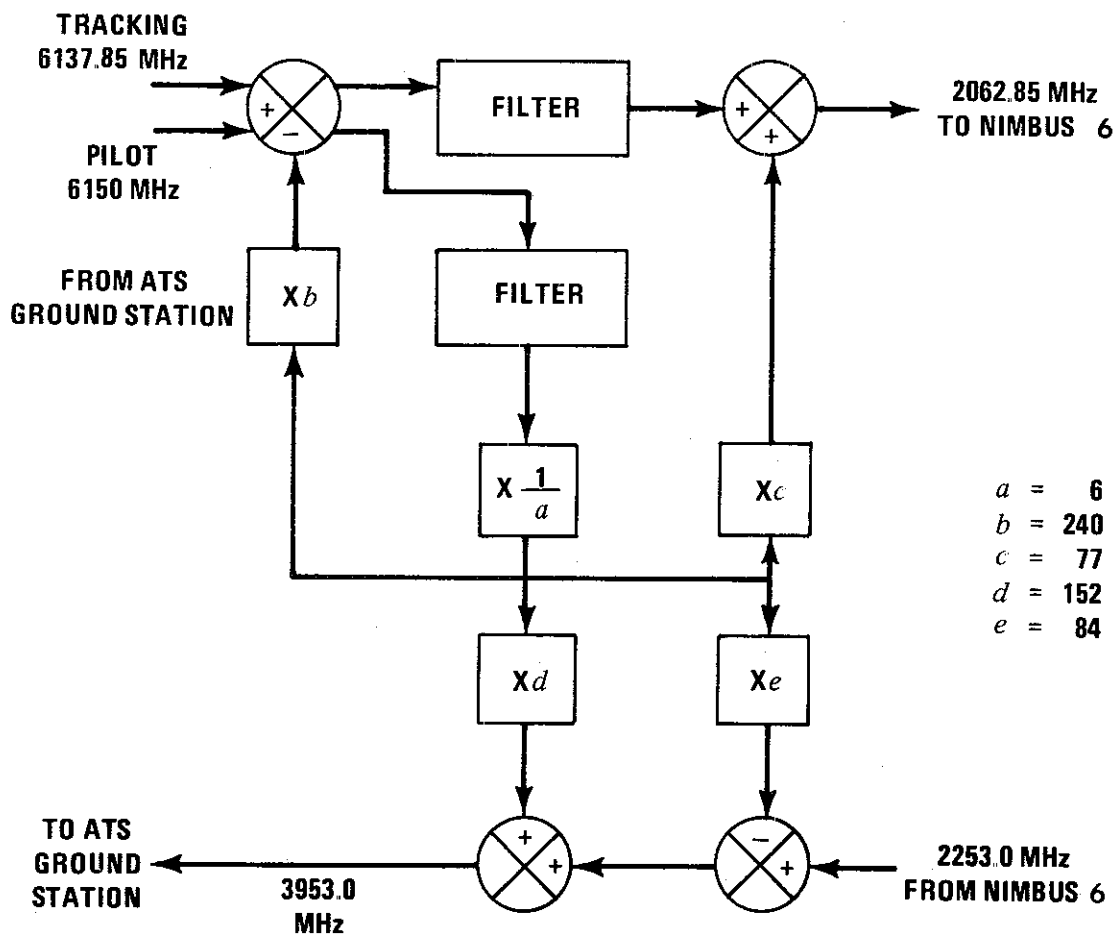


Figure 10-5. Signal Translations by the ATS 6 Transponder

Doppler data is the most accurate form of tracking data available for purposes of orbit computation because one cycle of Doppler is recorded for every half wavelength the spacecraft moves radially relative to the interrogating station. At 2 GHz this corresponds to each 7.5 cm of radial motion of Nimbus.

The group delay of the Nimbus transponder has been carefully calibrated over a wide range of frequency and temperature. Measured group delay repeatability is within  $\pm 20$  nanoseconds with a nominal delay of 2.6 microseconds. Systematic one-way ranging errors introduced by the Nimbus transponder are thus expected to be less than  $\pm 3$  meters.

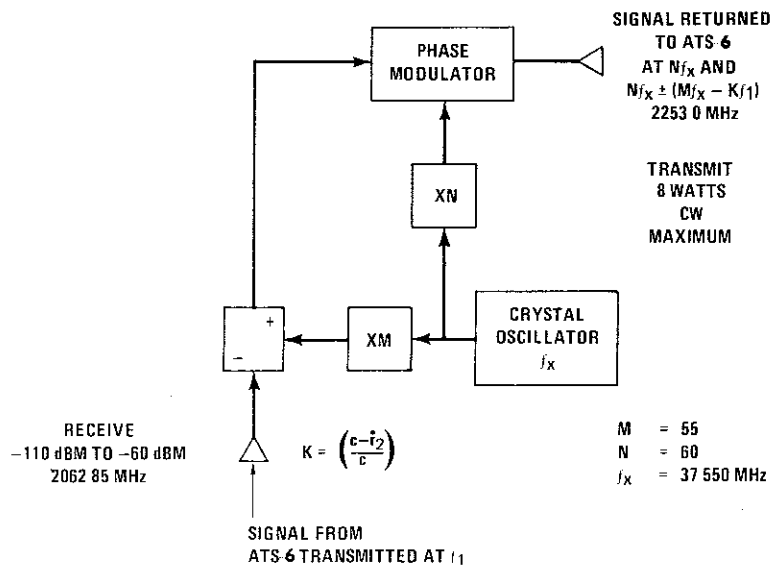


Figure 10-6. Signal Translations by the Nimbus 6 Transponder

### 10.3.3 Tracking Measurement Interpretation

The "range" measurement is performed by comparing transmitted and received tone zero crossings, the highest resolution tone frequency in this case being 100 KHz. The "range rate" measurement is performed by counting a pre-determined constant number of Doppler cycles and recording the time required to receive these cycles. Thus, both "range" and "range-rate" are recorded in terms of elapsed time. The raw data actually lists elapsed cycles of a 100 MHz clock; consequently the time readout is quantized to 10 nanoseconds.

#### 10.3.3.1 Ranging Data

The highest resolution ranging tone used in this experiment is 100 KHz. Lower frequency tones are sequentially used during acquisition for ambiguity resolution. The lower tones are at 20 KHz, 4 KHz, 800 Hz, 160 Hz, 32 Hz, and 8 Hz.

The tone ranging measurement is quite straightforward. However, its accuracy depends chiefly on the quality of preflight calibration of both the ATS and Nimbus transponder group delay. Such preflight calibration data have been taken over a range of frequencies and temperatures. Indications are that the total systematic delay error in the ranging measurement can be held to a few meters of equivalent one-way range.

### 10.3.3.2 Doppler Data

The electronics in this experiment has been so configurated that the Doppler output is maintained at the approximate value indicated in the following equation:

$$f_d = \frac{-2f_t k}{c} \left[ a_1 \bar{r}_1 + a_2 (\bar{r}_1 + \bar{r}_2) \right] \quad (1)$$

where  $f_d$  = measured average Doppler frequency

$f_t$  = uplink frequency = 6137.85 MHz

$k$  = 0.336

$a_1$  and  $a_2$  are scalar constants determined by equipment frequency multiplications (nominally  $a_1 = 0.76$  and  $a_2 = 1.00$ )

$\bar{r}_2$  = average range-rate ATS to Nimbus

In order to permit range-rate direction determination a fixed bias frequency (500 KHz) is added to the observed Doppler at the Doppler extractor. Thus the system counts the time,  $T_c$ , required to accumulate N cycles of Doppler,  $f_d$ , plus bias,  $f_b$ . That is:

$$T_c = \frac{N}{f_b + f_d} \text{ (seconds)} \quad (2)$$

where N is given in Table 10-1.

Table 10-1  
Doppler Cycle Count

N	Data Sample Rate
31995	8 per second
63990	4 per second
127980	2 per second
255960	1 per second
2559600	6 per minute

#### 10.3.4 Orbit Determination

In the actual orbit determination program (NASA-GSFC Navigation Analysis Program) the four radio propagation paths are considered separately and the final orbit solution arrived at iteratively. This analysis program is a generalized least squares parameter estimation program designed to accept and process numerous types of tracking observations, and includes algorithms for rigorous treatment of single or multi-satellite time delay and delay rate measurements. The geopotential model can be selected from any of a number of available gravity field models. One such field currently used in this program is the Goddard Earth Model-2 (GEM-2) which is given in terms of spherical harmonics up to order and degree 22. Lunar and solar perturbations are provided by means of the JPL ephemeris residing on permanent disk file at the NASA-GSFC IBM 360/95 computer facility.

Finally, many computer simulations have been performed to provide estimates of how the tracking data errors will map into orbit positions and velocity errors. Figure 10-7 shows a solution where conservative values of tracking system errors were assumed -- namely, 8 meters noise and bias ranging, and 1 cm/sec noise coupled with 0.2 cm/sec bias for range-rate measurements. The a priori Nimbus orbit was assumed in error (at  $t = 0$ ) by 20 km in position and 20 m/sec in velocity. Both ATS and Nimbus orbits are estimated simultaneously and the position error for Nimbus converges to 35 meters after continuous (except during occultation) tracking for three hours.

#### 10.4 Data Processing, Archiving, and Availability

The T&DRE tracking data acquired via ATS 6 (and used for orbit determinations and to test the satellite-to-satellite transmission system) will be received at the ATS ground station. Processing and evaluation of these data will be performed at GSFC by the Information Processing Division, the Operations Support Computing Division, and the experimenter. Telemetry data (VIP, HIRS, LRIR, and THIR) will be received at the Rosman, North Carolina, STDN station and/or the Madrid, Spain, ATS hybrid terminal and will be retransmitted to the MDHS for analysis.

Since the T&DRE is an experiment designed to test spacecraft-to-spacecraft capabilities in tracking and data relay, the data are not archived at the NSSDC. However, T&DRE-derived tapes will be processed, evaluated, and then stored by the divisions processing the data at GSFC. Users interested in using the data or in the results of this experiment should write to:

Mr. Bernard J. Trudell  
Tracking and Data Relay  
Experiment Manager  
Code 953  
Goddard Space Flight Center  
Greenbelt, Maryland 20771

The Nimbus 6 Data Catalogs will also report on the results derived from this experiment.

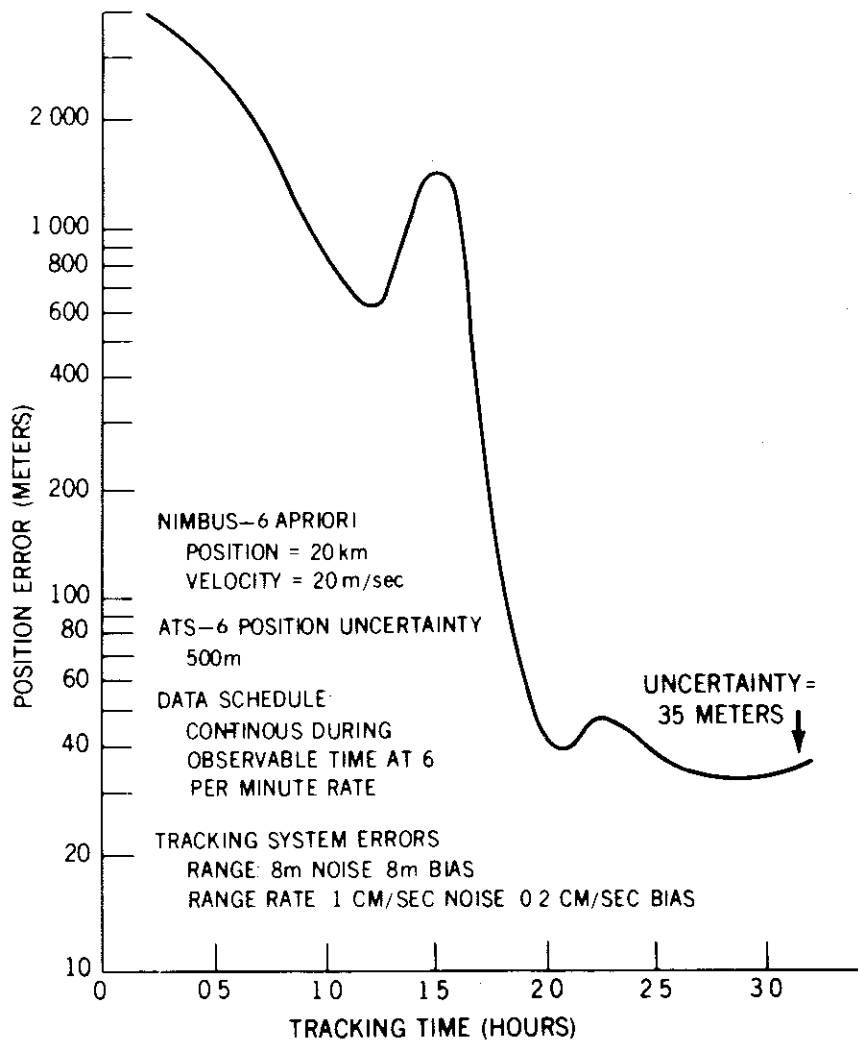


Figure 10-7. Nimbus 6 and ATS 6 Orbit Solution. The curve is the Nimbus position error relative to the earth center. (The ATS-6 position solved for.)

## BIBLIOGRAPHY

1. Buckler, T. R. : ATS-F/Nimbus F Tracking and Data Relay Experiment. NASA-GSFC, Program Plan, January 1973.
2. Filippi, C. : Range and Range-Rate Error Analysis for the ATS/Nimbus TDRS Experiment - Final Report. Magnavox Company, Advanced Systems Analysis Office, April 1971.
3. General Dynamics: ATSR Receiver Modification-Design Evaluation Report. Electro Dynamic Division, General Dynamics, September 1971.
4. Lynn, J. J. : Navigation Analysis Program, User's Guide. NASA-GSFC Contract NAS 5-11915, Old Dominion Systems, Inc., April 1973.
5. Lynn, J. J. and Schmid, P. E. : The Detection of Gravity Anomalies from Satellite-to-Satellite Tracking Data. Fifty-third Annual Meeting of the American Geophysical Union, Washington, D. C., April 17-21, 1972.
6. Schmid, P. E. : The Conversion of Tracking Data to Metric Form. NASA-GSFC X-551-69-3, January 1969.
7. VonBun, F. O. : Rotation of the Earth - The ATS/Nimbus Tracking Experiment. IAU Symposium No. 48, Morioka, Japan, May 9-15, 1971.

## SECTION 11

### THE NIMBUS 6 DATA CATALOG

Nimbus 6 Data Catalogs will be published periodically to provide a relatively current source of information required to obtain Nimbus 6 data. Each Catalog will be divided into the sections described below:

- Summary of Operations  
Section 1 will contain significant highlights of the satellite operation during the period of the catalog including any required post-launch changes in experiment description and archival tape formats as contained in preceding sections of this Guide. Performance of the various sensory systems and the spacecraft will be described, particularly when significant deviations from normal operations have been experienced.
- Orbital Elements and Daily Sensors On-Off Table  
Section 2 will give the Nimbus 6 satellite orbital elements valid for the catalog period. This section will also have a daily Sensors On-Off Table recording the times the experiments were on for the period of the catalog. The table will include ascending and descending node times and longitudes. To assist the user in determining the sensor coverage on the earth each volume will include a Subsatellite Tracks Vellum Overlay with its accompanying World Map. The subsatellite Tracks Overlay contains 14 correctly spaced tracks with the time annotations ending at the approximate day/night transitions.
- THIR Montages  
This section pictorially documents the data from the Temperature Humidity Infrared Radiometer subsystem. The montages represent the  $11.5 \mu\text{m}$  channel and the  $6.7 \mu\text{m}$  channel data obtained for each day (GMT) and are arranged in chronological order in a world montage format. Key latitudes can be read from the superimposed grids. Grid points are identified where each swath crosses  $60^\circ\text{N}$ ,  $30^\circ\text{N}$ , EQUATOR,  $30^\circ\text{S}$  and  $60^\circ\text{S}$ .

THIR transparent grid overlays (Location Guides), one for daytime montages and another for nighttime montages, will be provided as inserts to each Nimbus Catalog for general orientation with the latitude and longitude of the data presented. A THIR Time Scale, to be used for measuring time on the data strips in the daytime or nighttime montages, will be included adjacent to each montage.

- ESMR Image Data  
This section will describe the ESMR image format and present gray scale calibration information. Selected images will be shown. Complete ESMR coverage documentation will be listed in the Sensors On-Off Table.
- HIRS Image Data  
This section will describe the HIRS image format and present gray scale calibration information. Complete HIRS coverage documentation will be listed in the Sensors On-Off Table.
- SCAMS Image Data  
This section will describe the SCAMS image format and present gray scale calibration information. Complete SCAMS coverage documentation will be listed in the Sensors On-Off Table.
- Summary of Revisions and Changes to the User's Guide and Sensor Anomalies will be presented in this section with the information cumulatively carried forward from catalog to catalog.
- New TWERLE Experiments  
Catalogs will contain a table showing each new TWERLE experiment, its purpose, and its principal investigator.
- Availability of Processed Nimbus 6 Data  
Each catalog will contain an updated table of all processed Nimbus 6 experiment data that have been received at the NSSDC. These will be the data available to users as of the time of each catalog's preparation.

APPENDIX A  
ABBREVIATIONS AND ACRONYMS

ac	Alternating Current
ACS	Attitude Control System
A/D	Analog to Digital
AGC	Automatic Gain Control
ATS	Applications Technology Satellite
BCD	Binary Coded Decimal
BCO <sub>2</sub>	Broad Carbon Dioxide Channel
bpi	Bits per inch
bps	Bits per second
CBTT	Calibrated Brightness Temperature Tapes
cm	Centimeter
CW	Carrier Wave
dB	Decibel
dc	Direct Current
DEOF	Double End of File
DSAS	Digital Solar Aspect Monitor
EOF	End of File
ERB	Earth Radiation Budget
ERBCAT	ERB Compacted Archival Tape
ERBMAT	ERB Master Archival Tape
ERTS	Earth Resources Technology Satellite (now LANDSAT)
ESMR	Electrically Scanning Microwave Radiometer
FET	Field Effect Transistor
FEV	Flight Electronics Unit
FHA	Frame Housing Assembly
FM	Frequency Modulation
FOV	Field of View
GARP	Global Atmospheric Research Program
GHz	Gigahertz
GISS	Goddard Institute for Space Studies
GMT	Greenwich Mean Time
GSFC	Goddard Space Flight Center
HDRSS	High Data Rate Storage System
HIRS	High Resolution Infrared Radiation Sounder
Hz	Hertz (cycles per second)
ID	Identification
IED	Information Extraction Division
IEU	Interface Electronics Unit
IF	Intermediate Frequency

IFC	Inflight Calibration Source
IFOV	Instantaneous Field of View
IPS	International Pyrheliometric Scale
IR	Infrared
ITPR	Infrared Temperature Profile Radiometer
ITT	International Telephone and Telegraph
JPL	Jet Propulsion Lab
K	Kelvin
kbs	Kilobits per second
kg	Kilogram
KHz	Kilohertz
km	Kilometer
kw	Kilowatt
LANDSAT	Land Satellite (formerly ERTS)
LDT	LRIR Data Tape
LOS	Line of Sight
LRIR	Limb Radiance Inversion Radiometer
mb	Millibar
MDHS	Meteorological Data Handling System
MHz	Megahertz
MIT	Massachusetts Institute of Technology
mm	Millimeter
mr	Milliradian
ms	Millisecond
$\mu\text{m}$	Micrometer
$\mu\text{s}$	Microsecond
MUX	Multiplexer
NADUC	Nimbus/ATS Data Utilization Center
NASA	National Aeronautics and Space Administration
NASCOM	NASA Communications Network
NCAR	National Center for Atmospheric Research
NCO <sub>2</sub>	Narrow Carbon Dioxide Channel
NEMS	Nimbus E Microwave Spectrometer
NESS	National Environmental Satellite Service
NIP	Normal Incidence Pyrheliometer
nm	Nautical Mile
NMRT	Nimbus Meteorological Radiation Tape
NOAA	National Oceanic and Atmospheric Administration
NSSDC	National Space Science Data Center
OMP	Optical Mechanical Package
PIP	Position Pulse
PMR	Pressure Modulator Radiometer
RAMS	Random Access Measurement System

rms	Root Mean Square
rpm	Revolutions per Minute
RSM	Reference Sensor Model
S/C	Spacecraft
SCAMS	Scanning Microwave Spectrometer
SCP	Solid Cryogen Package
STDN	Spacecraft Tracking and Data Network
T&DRE	Tracking and Data Relay Experiment
THIR	Temperature Humidity Infrared Radiometer
TWERLE	Tropical Wind Energy Conversion and Reference Level Experiment
UFOT	User Formatted Output Tape
VCO	Voltage Controlled Oscillator
VDC	Volts Direct Current
VIP	Versatile Information Processor



## APPENDIX B

### A DIRECT READOUT GROUND STATION FOR NIMBUS 6 ESMR DATA

#### A. 1 Introduction

The Direct Readout Applications Group of the Sensor Evaluation Branch, Earth Observations Systems Division, Applications Directorate, at Goddard Space Flight Center is presently developing a direct readout ground system to extract the Electrically Scanning Microwave Radiometer (ESMR) data from the Nimbus 6 real-time telemetry signal transmitted by the spacecraft beacon. This work will culminate in a low-cost demonstration ground station which will produce images of the ESMR data.

#### A. 2 Background

##### A. 2. 1 Nimbus VIP and Beacon

Figure 1-3 in Section 1 of this report is a simplified block diagram of the data flow on board Nimbus 6. All data entering the Versatile Information Processor (VIP) feeds to the spacecraft beacon for real-time transmission at 136.5 MHz, and to the High Data Rate Storage Subsystem (HDRSS) for later readout to a STDN station. As Figure 1-3 indicates, the ERB, ESMR, SCAMS, TWERLE, and THIR experiments are transmitted in real time via the beacon. These experiments are described in detail in individual sections of this document.

##### A. 2. 2 Applications of ESMR Data

Currently, there are over 700 worldwide direct readout ground stations acquiring data from the highly successful National Oceanic and Atmospheric Administration (NOAA) satellites. These users receive satellite data in real time from the visible and infrared portions of the electromagnetic spectrum. The microwave data from ESMR would provide useful information not currently available to the direct readout user. Section 5 of this document and Section 4 of The Nimbus 5 User's Guide give background information on many of the applications. The ESMR data could be used for the following applications:

- Determining areas of precipitation in cloud formations
- Estimating the moisture content of clouds

- Distinguishing snow and ice cover from cloud cover
- Estimating soil moisture
- Estimating wind speeds over oceans by determining the surface roughness

The Nimbus 6 orbital characteristics (as explained in Section 1) enable the satellite to pass within line of sight of all locations at least twice each day, once near local midnight and once near local noon.

#### A. 3 Components of an ESMR Direct Readout Ground Station

The transmitting power of the Nimbus 6 beacon, although low at 0.5 watt, is estimated to be sufficient to produce a useable signal to the local user. Preliminary link calculations indicate that a receiver antenna gain of approximately 14 dB would be needed to acquire a good signal. It should be noted that ultimate system tracking requirements for the spacecraft beacon cannot be accurately defined until the spacecraft is in orbit.

The exact components of the demonstration ground station to receive and process this signal have not been specifically defined, but can be described generally. The data will be received in a serial bit stream split phase at a 4 kilobit per second rate. The data are amplitude modulated with a carrier frequency of 136.5 MHz. These data include the entire information from the VIP. The ESMR data must be extracted or decommutated from the VIP data block, which has a matrix type of format. The data must be processed by a minicomputer or special-purpose hardware and formatted properly to produce a facsimile. In summary the ground station will include the following items:

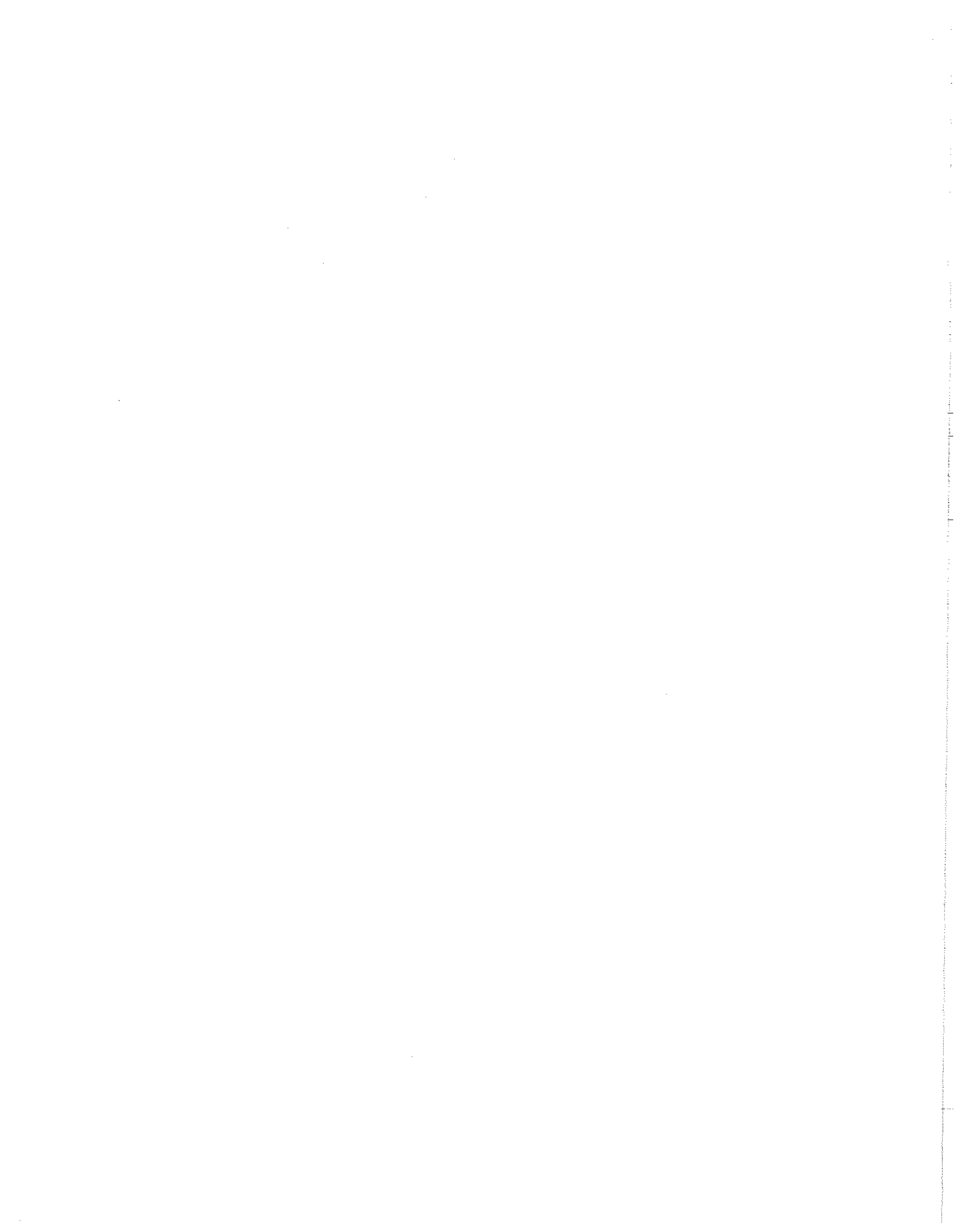
- VHF antenna and preamplifier
- VHF AM receiver
- 4.0 kilobit bit synchronizer
- Frame synchronizer
- Digital processor (minicomputer)
- Facsimile

#### A.4 Scheduled for Development and Availability of Information

It is estimated that the demonstration ground system will be completed one month after the launch of the Nimbus 6. Comments favorable or otherwise are solicited from users who can come to GSFC to examine the system, or who care to write with their suggestions. A complete ESMR Direct Readout Ground Station User's Document will be available about October 1, 1975. The document will contain sufficient detail to enable the direct readout user to construct his own direct readout system. The entire system will be modular and cost less than \$100,000. This cost estimate is based on buying all components. The system will be versatile in that other experiment data can be processed from the Nimbus 6 VIP, and similar direct readout data are presently available from the VIP on the orbiting Nimbus 5 satellite.

Individuals who want this construction document, or those who would like to comment on improving this system should write or call:

Carl P. Ashcraft  
Code 942  
Goddard Space Flight Center  
Greenbelt, Maryland 20771  
(301) 982-4487



## SECTION 5

### CORRECTIONS TO THE NIMBUS 6 USER'S GUIDE

This section presents all corrections or additions to The Nimbus 6 User's Guide, which now are known to be necessary. If additional corrections are required, they will appear in a subsequent catalog. All corrections will be carried forward cumulatively into each new catalog.

#### 5.1 THIR Corrections to the User's Guide

The THIR mirror on Nimbus 6 rotates counterclockwise. Therefore, replace lines one through four on page 14 with the following:

". . . rotation is such that, when combined with the velocity vector of the satellite, a left-hand spiral results. Therefore, the mirror scans across the earth from west to east in the daytime when traveling northward, and from east to west at night when traveling southward."

- \* The information in Figure 2-4 on page 17 is correct. However, the direction of scan is counterclockwise, and not clockwise as shown.

#### 5.2 HIRS Corrections to the User's Guide

On page 40, Table 3-2, under "Detector Summary" change LnSe to LnSb.

The CHANNEL (and) RANGE information in the swath displays for HIRS has been changed since launch, making Table 3-5 on pages 54 and 55 in the User's Guide incorrect. The table below labeled Table 5-1 provides the correct information.

#### 5.3 SCAMS Corrections to the User's Guide

The information contents of the image in the swath displays for SCAMS has been changed since launch, making Tables 4-5, 4-6, and 4-7 in the User's Guide incorrect. Thus, the table below labeled Table 5-2 replaces Tables 4-5 and 4-6 in the User's Guide, and the table labeled 5-3 replaces Table 4-7 in the User's Guide. All the images display the same parameters. Therefore, these new tables do not list all the possible displays, as were listed in the old Tables 4-5, 4-6, and 4-7.

On page 44, Figure 3-3, the SCAMS elements are shown with a right-to-left (clockwise) stepping pattern when looking in the direction of satellite motion. The SCAMS elements should be corrected to show a left-to-right (counterclockwise) stepping pattern.

This table replaces Table 3-5 on pages 54 and 55 in The Nimbus 6 User's Guide

Table 3-5

Temperature Range of Gray Scale, and Channel of HIRS Data for each Swath on each HRS Image  
Display Between Orbit 426 and 4697 (14 July 1975 through 27 May 1976)

		SWATH NUMBER									
		1	2	3	4	5	6	7	8	9	10
Coverage Period 14 July-20 July Orbits 426-513	HIRS Channel Display (channel-range)*	08-08	09-09	10-10	16-16	17-17	18-18	12-12	14-14	03-03	15-15
	Temperature Range (°K) (black to white)	300-200	290-210	260-210	310-270	100-900	0-30	290-210	260-210	240-210	280-210
Coverage Period 22 July-31 July Orbits 538-545 548-549 600-613 615-647 651-657 659	HIRS Channel Display (channel-range)*	08-08	09-09	10-10	16-16	17-17	17-17	12-12	14-14	03-03	15-15
	Temperature Range (°K) (black-white)	300-200	290-210	260-230	310-270	100-900	100-900	280-200	280-200	280-200	280-200
Coverage Period 23 July-6 Aug. Orbits 546-547 553-599 614 648-650 658 660-747	HIRS Channel Display (channel-range)*	08-08	16-16	16-21	18-18	17-17	10-10	12-12	14-14	03-03	15-15
	Temperature Range (°K) (black-white)	300-200	310-270	300-200	0-30	100-900	260-230	280-200	280-200	280-200	280-200

Table 3-5 (Continued)

Coverage Period 7 Aug. - 27 May Orbits 748-4697	HIRS Channel Display (channel-range)*	SWATH NUMBER									
		1	2	3	4	5	6	7	8	9	10
		08-08	16-16	16-21	18-18	17-17	10-10	12-12	14-14	03-03	15-15
	Temperature Range ( $^{\circ}$ K) (black-white)	310-230	310-230	310-270	0-50	100-900	280-210	300-210	300-210	240-185	300-185 ***

\*The HIRS channel number is number before the hyphen. The number after the hyphen is the computer program table used to display the data from each channel as temperatures ( $^{\circ}$ K). The range of temperatures displayed in each swath is given beneath each "HIRS Channel Display."

The 18 steps of the scale are used to represent the division of each temperature range into 18 approximately equal temperature intervals.

The central wavelength (in  $\mu$ m) of each channel on these displays is: channel 3 = 14.4, 8 = 11.0, 9 = 8.2, 10 = 6.7, 12 = 4.52, 14 = 4.40, 15 = 4.24, 16 = 3.71, 17 = 0.61, and 18 is the temperature difference between channel 16 and channel 8. The values of channel 17-17 are albedo, represented as "counts" between 100 (blackest) and 900 (whitest).

data. Table 3-1 on page 39 of the User's Guide provides detailed spectral information and the purpose of each of the HIRS channels.

\*\*14-14 temperature range changed to 270-210 on orbit 3166A (26 January 1976)

\*\*\*15-15 temperature range changed to 275-210 on orbit 3166A (26 January 1976)

Table 5-2

This table replaces Tables 4-5 and 4-6 (on pages 79 through 81) in the Nimbus 6 User's Guide and Table 5-2 in the Nimbus 6 Data Catalog Volume 4

Table 4-5 and 6

Parameter Limits of the Gray Scale for Parameters 1, 2, 3, 5, 11, 12, and 16 on the SCAMS Image Displays between Orbits 426 and 4751 (14 July 1975 and 31 May 1976)

Swath		1	2	3	4	5
Orbits 426 thru 1425 14 July 75 thru 26 Sept. 75	Parameter	3	2	16	11	12
	Gray Scale Value	black 280 °K 210	white 320 °K 100	-22	60 g/mm <sup>2</sup> 0.0	1.5 g/mm <sup>2</sup> -0.1*
Orbits 1426 thru 3675 26 Sept. 75 thru 12 Mar. 76	Parameter	3	2	16	11	12
	Gray Scale Value	black 280 °K 210	white 320 °K 100	-22	60 g/mm <sup>2</sup> 0.0	2.0 g/mm <sup>2</sup> 0.0
Orbits 3676 thru 3899 12 Mar. 76 thru 29 Mar. 76	Parameter	5	2	16	11	12
	Gray Scale Value	black 240 °K 200	white 320 °K 100	-22	70 g/mm <sup>2</sup> 0.0	2.0 g/mm <sup>2</sup> 0.0
Orbits 3900 thru 3929 29 Mar. 76 thru 31 Mar. 76	Parameter	1	1	1	5	5
	Gray Scale Value	black 220 °K 130	white 265 °K 210	300 °K 260	240 °K 200	280 °K 220
Orbits 3930 thru 4584 31 Mar. 76 thru 19 May 76	Parameter	1	1	1	2	3
	Gray Scale Value	black 220 °K 130	white 265 °K 210	300 °K 260	320 °K 100	280 °K 220
Orbits 4585 thru 4751 19 May 76 thru 31 May 76	Parameter	1	1	1	5	3
	Gray Scale Value	black 220 °K 130	white 260 °K 200	290 °K 245	240 °K 180	280 °K 220

\*1.6 to 0.0 between orbit 426 and 477

Parameters 1, 2, 3, 5, and 16 represent uninverted antenna temperatures for channels 1 (22.24 GHz), 2 (31.65 GHz), 3 (52.85 GHz), and 5 (55.45 GHz). Parameter 16 is the temperature difference between channels 2 and 3. Parameters 11 and 12 represent inverted antenna temperatures of integrated atmospheric water vapor (channel 11) and integrated liquid water from clouds or precipitation.

Table 5-3

This table replaces Table 4-7 (on pages 82 and 83) in The Nimbus 6 User's Guide

Table 4-7

Contour Program Options used for Parameters 13, 14, and 15  
on the SCAMS Image Display

Contour options	Parameters			Valid for orbits
	13 Mean temperature between 1000 mb and 500 mb	14 Mean temperature between 500 mb and 250 mb	15 Mean temperature between 250 mb and 100 mb	
Contour interval	4°K	4°K	4°K	426-851
Contour thickness	1°K	1°K	1°K	(14 July- 14 Aug. 1975)
Contour interval	4°K	4°K	4°K	852-4751
Contour thickness	2°K	2°K	2°K	(14 Aug.-1975-31 May 1976)

Section 4.5.3 "Tape Format" on page 83 of the User's Guide states that each tape will have "five files, i.e., a short header file. . . and four data files, . . ." There will not be a header file on the archival tape. The sentence should be changed to read: "The tapes will be standard 9-track 1600 BPI tapes, each containing four data files, one for each of four days."

In Table 4-8 on page 80 the "Pitch error" and "Roll error" "Dimensional Units" should be changed to counts (from Deg) and the "Multiplier Used" should be changed to 1 (from 32). In the same table the "Playback orbit" should be followed by one "I\*2 Spare", and then by the "Reference orbit", which should be changed to I\*4 (rather than I\*2). (Reference orbit = year \* 100,00 + day \* 100 + finish hour.) The "Dimensional Units" for the "Geopotential thicknesses" on page 85 of the same table should be changed to "°K" (from DM).

The following SCAMS information has been edited by the experimenter and briefly outlines the current status of data availability, retrieval methods, and a current table of theoretical brightness temperature values.

The SCAMS instrument operated from June 15, 1975 to May 31, 1976. The data from this experiment has been processed and can be obtained from the National Space Science Data Center at GSFC. The digital data, including instrument output, calibrated antenna temperatures, deconvolved brightness temperatures, and retrieved atmospheric parameters, are recorded on a set of 87 9-track tapes. With three exceptions, each

tape contains four contiguous days of data. Channel 1 and 2 brightness temperatures and five atmospheric parameters from these tapes have been dumped in a condensed format on microfiche. A typical fiche contains somewhat less than two days of data. Photographic images for individual orbits are also available.

At this time, the archived data represent the "first cut" at retrievals, and can be improved with respect to calibration of the oxygen band channels and inversion of the H<sub>2</sub>O channels. Data prior to January 2, 1976 was calibrated by assuming the radiometric temperatures of the calibration targets to be equal to their physical temperatures. Comparisons with radiosondes indicated that a more accurate calibration would be obtained with an offset of -1.2°K on the oxygen band target. The archived data starting with January 2, 1976 incorporates this correction. Strictly speaking, the previous data should be recalibrated and reinverted, but for most purposes an adequate approximation can be obtained by simply subtracting 1° from the oxygen band antenna and brightness temperatures and the retrieved temperature profile. No corrections were made to the H<sub>2</sub>O targets, for lack of evidence that any was necessary.

All of the archived water vapor and liquid water retrievals were obtained by a linear algorithm. Improved retrievals, particularly in humid regions, can be obtained by use of the following nonlinear equations:

$$\text{vapor (mm)} = 72 + 12\alpha$$

$$\text{liquid (mm)} = 0.4\beta$$

where

$$\alpha = \left[ 7.34 \ln \left( \frac{280 - T_{01}}{280 - T_{B1}} \right) - 3.75 \ln \left( \frac{280 - T_{02}}{280 - T_{B2}} \right) \right] \cos \theta$$

$$\beta = \left[ -3.34 \ln \left( \frac{280 - T_{01}}{280 - T_{B1}} \right) + 9.71 \ln \left( \frac{280 - T_{02}}{280 - T_{B2}} \right) \right] \cos \theta$$

T<sub>B1</sub> and T<sub>B2</sub> are the measured brightness temperatures at 22.23 and 31.65 GHz, and T<sub>01</sub> and T<sub>02</sub> are brightness temperatures computed for a tropical model atmosphere containing 72 mm precipitable water vapor; the latter are listed in table 5-4 as a function of view angle θ.

The following information, describing how the antenna temperatures are computed from the SCAMS instrument digital data, should be added after SCAMS Section 4.5 of the User's Guide.

Table 5-4

Theoretical brightness temperatures for a saturated tropical troposphere with no clouds and a smooth ocean surface.

(Valid for period 2 January 1976 - 31 May 1976)

$\theta$ view angle	$T_{01}$	$T_{02}$
0	225.6	178.2
8°	225.9	177.9
17°	226.9	177.3
26°	229.2	177.5
34°	233.9	180.1
44°	242.0	187.4
53°	254.5	203.0

#### 4.6 Post-launch Calibration

Antenna temperatures are computed from the SCAMS Instrument digital data for each of the five channels by the equation:

$$T_A = T_{AS} + \frac{T_{AC} - T_{AS}}{d_{T_C} - d_s} (d - d_s)$$

where  $T_A$  is antenna temperature for the earth (positions 0-12),  $T_{AS}$  is the space antenna temperature (position 13),  $T_{AC}$  is the calibration target antenna temperature (position 14),  $d$  is earth data in counts,  $d_s$  is space data in counts, and  $d_c$  is calibration target data in counts. The digital data matrix is described in Table 4-2 of the Nimbus 6 User's Guide. The space calibration antenna temperature is assumed constant at 3° K for all five channels. The target antenna temperature is computed by

$$T_{AC} = T_C + T_{CO}$$

The constant offset  $T_{CO}$  is currently zero for channels 1 and 2. The target temperatures ( $T_C$ ) are given by

Table 5-5

This table accompanies Section 4.6 "Post-launch Calibration",  
and should be added to the end of the SCAMS section of the User's Guide.

Table 4-9

Thermistor Calibration Constants  
used to Calculate the SCAMS Target Temperatures

channel constant	1	2	3,4,5
$a_0$	298.16		
$a_1$	.46485	.46535	.46814
$a_2$	$3.0 \cdot 10^{-5}$	$2.9 \cdot 10^{-5}$	$3.0 \cdot 10^{-5}$
$R_{25}$	603.75	602.98	599.71
$R_1$	495.6		
$R_2$	603.4		
$d_R$ (word no.)	1	11	2
$d_{R1}$ (word no.)	61		62
$d_{R2}$ (word no.)	71		72

Table 5-6

This table replaces Table 4-9 in Section 4.6 "Post-launch Calibration" and should be added to the end of the SCAMS section of the User's Guide.

Table 4-9a

Thermistor Calibration Constants  
used to Calculate the SCAMS Target Temperatures

channel	1	2	3, 4, 5
constant			
$a_0$		298.16	
$a_1$	.46485	.46535	.46814
$a_2$	$3.0 \cdot 10^{-5}$	$2.9 \cdot 10^{-5}$	$3.0 \cdot 10^{-5}$
$R_{25}$	603.75	602.98	599.71
$R_1$		495.6	
$R_2$		603.4	
$d_R$ (word no.)	1	11	2
$d_{R1}$ (word no.)		61	62
$d_{R2}$ (word no.)		71	72
$T_{CO}$	0		-1.2°K

$$T_C = a_0 + a_1 (R - R_{25}) + a_2 (R - R_{25})^2$$

where the thermistor resistances ( $R$ ) are computed by

$$R = R_1 + \frac{R_2 - R_1}{d_{R2} - d_{R1}} (d_R - d_{R1})$$

and values of the other constants are listed in Table 4-9a. Note that channels 3, 4, and 5 share the same calibration target. Also listed in Table 4-9a are word numbers in the digital data matrix containing data values  $d_R$ ,  $d_{R1}$ ,  $d_{R2}$ , and the recent addition of the  $T_{CO}$  value for channels 3, 4, and 5.

Figure 5-1 below replaces Figure 4-2 (page 64) in  
The Nimbus 6 User's Guide.

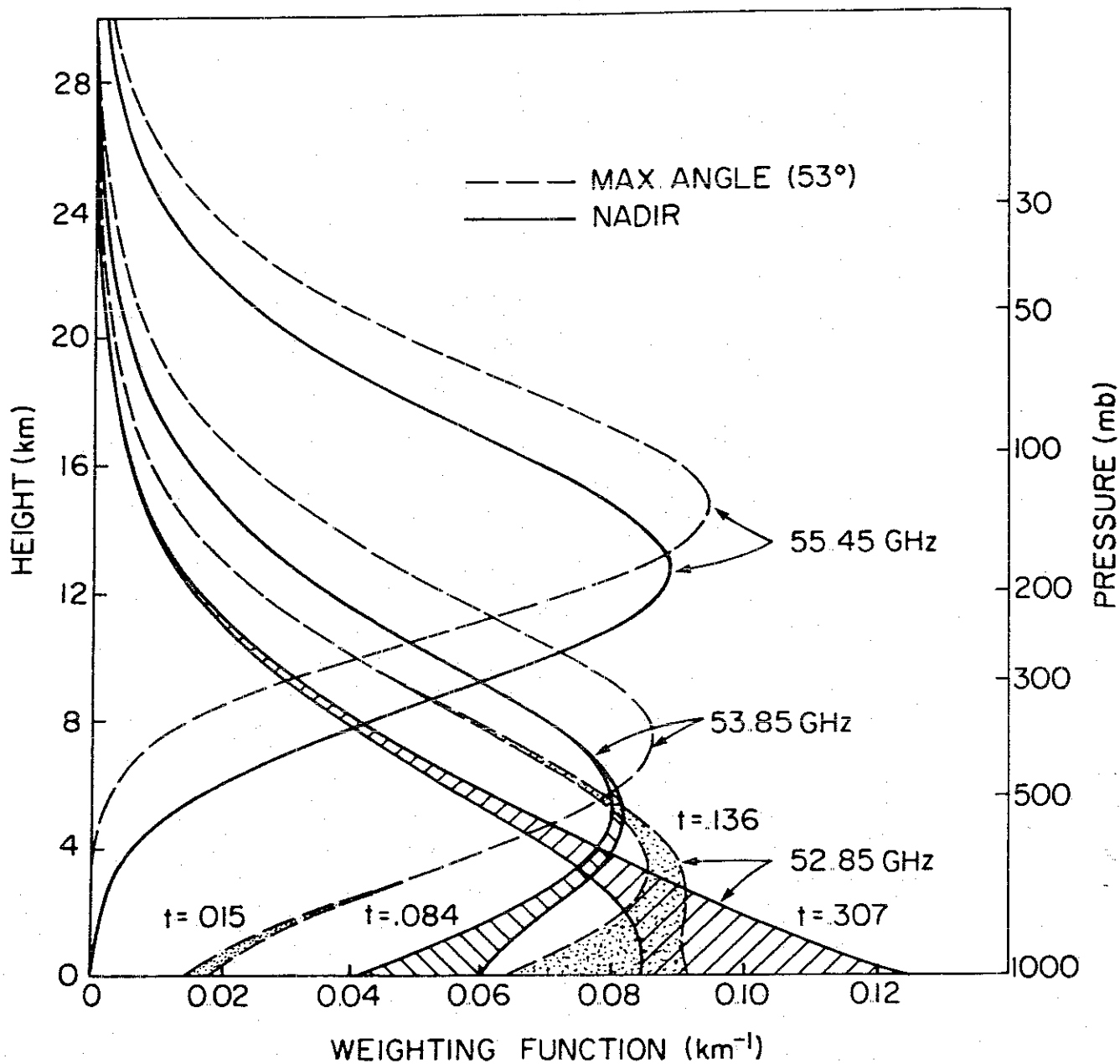


Figure 5-1. Weighting functions for the SCAMS oxygen-band channels, at two view angles. The shaded area within each weighting function represents the reflected contribution when the surface is smooth seawater ( $t = e^{-\tau_v}$ , transmittance of the atmosphere). The calculations used the 1962 U. S. Standard Atmosphere temperature profile with  $2 \text{ g/cm}^2$  water vapor. The oxygen absorption coefficient was computed as in References 1 and 2.

## REFERENCES

1. Rosenkranz, P.W.: Shape of the 5 mm Oxygen Band in the Atmosphere. IEEE Trans. Antenn. Propag., vol. AP-23, No. 4, 1975, pp. 498-506.
2. Liebe, H.J., Gimmestad, G.G., and Hopponen, J.D.: Atmospheric Oxygen Microwave Spectrum - Experiment versus Theory. IEEE Trans. Antenn. Propag., vol. AP-25, no. 3, 1977, pp. 327-335.

### 5.4 ESMR Corrections to the User's Guide

The following are corrected equations for the ESMR Section of the User's Guide:

page 90

$$X \text{ (km)} = (636 + 10.8P - 0.32P^2) R_j$$

page 96

$$T_B = T_A - (T_A - T_C) \frac{(C - C_A)}{(C_C - C_A)}$$

page 101

$$\frac{T_{\text{Horizontal}}}{\text{True}} = 1 + a \frac{T_{\text{Horizontal}}}{\text{Nominal}} - \frac{T_{\text{Vertical}}}{\text{Nominal}}$$

$$\frac{T_{\text{Vertical}}}{\text{True}} = 1 + b \frac{T_{\text{Vertical}}}{\text{Nominal}} - b \frac{T_{\text{Horizontal}}}{\text{Nominal}}$$

page 106

$$N_j = 256 (T_{Hi} - 100) + T_{Vi} - 100$$

The following information supplements Section 5.3.2 in the User's Guide.

The display format and temperature ranges of the images in the swath displays for ESMR has been changed twice since launch. The first revision occurred after orbit 3932 in which each ESMR scan line is displayed once prior to orbit 3932 and twice after orbit 3933. Similarly, each of the 71 scan-spot elements is displayed once through orbit 3932 and twice after orbit 3933.

Through orbit 3932 (31 March) the ESMR displays contained 20 swaths of data, as shown in the ESMR image displays up to orbit 3932 in Section 3.3. The swaths are numbered (numbers not shown) from 1 on the left to 20 on the right. Each of the ten swaths on the left has the same geographic coverage. However, each swath displays either horizontally or vertically polarized data at a temperature range as listed in Table 5-5a. The right set of ten swaths has a similar format, and displays the earliest recorded data. If the right swaths were cut and placed above the group on the left, the new display would show the continuous coverage recorded for that orbit. Swaths 1 and 11 have the same polarization and temperature range. Similarly, swaths 2 and 12, 3 and 13, etc., are the same. The tables here labeled 5-8 and 5-9 replace Table 5-5 on page 105 of the User's Guide.

As stated above, the ESMR display format was modified at orbit 3933 (31 March 1976) and again at orbit 6185 (15 September 1976). From orbit 3933 through orbit 6184, the following format was used:

The new displays contain ten swaths of data plus a geographic grid overlay for each swath, as shown in the ESMR image displays after orbit 3933 in Section 3.3, of the Nimbus 6, Data Catalog, Volume 5.

The swaths are numbered (numbers not displayed) from 1 on the left to 10 on the right. Each of the five swaths on the left has the same geographic coverage. However, each swath displays either horizontally or vertically polarized data at a temperature range as listed in Table 5-5b. The right set of five swaths has a similar format, and displays the latest recorded data. If the right swaths were cut and placed below the group on the left, the new display would show the continuous coverage of that display.

Swaths 1 and 6 display the same parameter. That is, the temperature range and polarization for swaths 1 and 6 are the same. Similarly, swaths 2 and 7, 3 and 8, 4 and 9, and 5 and 10 display the same parameters. Table 5-5b is set up to show this duplication of parameter information.

Data time (GMT) references for the left set of five swaths are shown adjacent to the vertical line at the left. Time tick marks are every five minutes with hour and minute annotation every fifteen minutes. Data time references for the right set of five swaths are shown in a similar manner adjacent to the vertical line at the right.

The center portion of the display contains two swaths of grid overlay information: the left grid for overlay on each of the five swaths on the left, and the right grid for overlay on each of the five swaths on the right. The grid longitudes are generated at ten degree intervals between 55 degrees south and 55 degrees north, and at 20 degree intervals from 55 degrees to the Poles. Latitude grids are generated every five degrees. All grid lines consist of a series of dots at one degree intervals. Latitudes are labeled at  $60^{\circ}$ S,  $30^{\circ}$ S, EQ,  $30^{\circ}$ N, and  $60^{\circ}$ N. Longitude labels are normally placed next to each latitude label.

Table 5-7  
This table replaces Table 5-5 on page 105 in the User's Guide

Table 5-5

Brightness Temperature Value for each Step of the Gray Scale on ESMR Image Displays for Orbit 426 through 827 (14 July through 12 August 1975)

Gray Scale Number	Swath Number and ESMR Display Parameter						$T_H + T_V$ $\frac{T_H + T_V}{2}$	$T_H$ $\frac{T_H + T_V}{2}$	$T_V$ $\frac{T_H + T_V}{2}$	$T_H$ $\frac{T_H + T_V}{2}$	$T_V$ $\frac{T_H + T_V}{2}$	$T_H$ $\frac{T_H + T_V}{2}$	$T_V$ $\frac{T_H + T_V}{2}$
	1 and 11 ( $T_H$ )	2 and 12 ( $T_V$ )	3 and 13 $T_H + T_V$ $\frac{T_H + T_V}{2}$	4 and 14 ( $T_H$ )	5 and 15 ( $T_V$ )	6 and 16 $T_H + T_V$ $\frac{T_H + T_V}{2}$							
(black)	> 200			> 250						> 300			
1	1 and 11 ( $T_H$ )	2 and 12 ( $T_V$ )	3 and 13 $T_H + T_V$ $\frac{T_H + T_V}{2}$	4 and 14 ( $T_H$ )	5 and 15 ( $T_V$ )	6 and 16 $T_H + T_V$ $\frac{T_H + T_V}{2}$	same as 1 and 11	same as 1 and 11	same as 1 and 11	same as 1 and 11	same as 1 and 11	same as 1 and 11	same as 1 and 11
2	196-200	same as 1	246-250	243-246	240-243	237-240	234-237	231-234	228-231	225-228	221-225	218-221	215-218
3	193-196	same as 2	243-250	240-243	237-240	234-237	231-234	228-231	225-228	221-225	218-221	215-218	212-215
4	190-193	same as 3	243-246	240-243	237-240	234-237	231-234	228-231	225-228	221-225	218-221	215-218	212-215
5	187-190	same as 4	240-243	237-240	234-237	231-234	228-231	225-228	221-225	218-221	215-218	212-215	209-212
6	184-187	same as 5	237-240	234-237	231-234	228-231	225-228	221-225	218-221	215-218	212-215	209-212	206-209
7	181-184	same as 6	234-237	231-234	228-231	225-228	221-225	218-221	215-218	212-215	209-212	206-209	203-206
8	178-181	same as 7	231-234	228-231	225-228	221-225	218-221	215-218	212-215	209-212	206-209	203-206	200-203
9	175-178	same as 8	228-231	225-228	221-225	218-221	215-218	212-215	209-212	206-209	203-206	200-203	< 200
10	171-175	same as 9	225-228	221-225	218-221	215-218	212-215	209-212	206-209	203-206	200-203	< 200	< 200
11	168-171	same as 10	221-225	218-221	215-218	212-215	209-212	206-209	203-206	200-203	< 200	< 200	< 200
12	165-168	same as 11	218-221	215-218	212-215	209-212	206-209	203-206	200-203	< 200	< 200	< 200	< 200
13	162-165	same as 12	215-218	212-215	209-212	206-209	203-206	200-203	< 200	< 200	< 200	< 200	< 200
14	159-162	same as 13	212-215	209-212	206-209	203-206	200-203	< 200	< 200	< 200	< 200	< 200	< 200
15	156-159	same as 14	209-212	206-209	203-206	200-203	< 200	< 200	< 200	< 200	< 200	< 200	< 200
16	153-156	same as 15	206-209	203-206	200-203	< 200	< 200	< 200	< 200	< 200	< 200	< 200	< 200
17	150-153	same as 16	203-206	200-203	< 200	< 200	< 200	< 200	< 200	< 200	< 200	< 200	< 200
(white)	18	same as 17	200-203	< 200	< 200	< 200	< 200	< 200	< 200	< 200	< 200	< 200	< 200

$T_H$  = Brightness temperature derived from the ESMR horizontal polarization channel data

$T_V$  = Brightness temperature derived from the ESMR vertical polarization channel data

Table 5-8

This table follows the new Table 5-6 (above), which replaced  
Table 5-5 on page 105 in the User's Guide

Table 5-5a

Brightness Temperature Value for each Step of the Gray Scale on ESMR Image Displays  
for Orbit 828 through 3932 (13 August 1975 through 31 March 1976)  
(Brightness Temperatures are in °K)

Gray Scale Number	1 and 11 ( $T_H$ )	2 and 12 ( $T_V$ )	3 and 13 $T_H + \frac{T_V}{2}$	4 and 14 ( $T_H$ )	5 and 15 ( $T_V$ )	6 and 16 $T_H + \frac{T_V}{2}$	7 and 17 ( $T_H$ )	8 and 18 ( $T_V$ )	9 and 19 $T_H + \frac{T_V}{2}$	10 and 20 ( $T_V - 0.6T_H$ )
(black)	1 > 200 2 196-200 3 191-196 4 187-191 5 183-187 6 178-183 7 174-178 8 169-174 9 165-169 10 161-165 11 156-161 12 152-156 13 148-152 14 143-148 15 139-143 16 134-139 17 130-134 (white) 18 < 130	> 230 226-230 223-226 219-223 215-219 211-215 208-211 204-208 200-204 196-200 193-196 189-193 185-189 181-185 178-181 154-158 150-154 < 130	> 210 206-210 203-206 199-203 195-199 191-195 188-191 184-188 180-184 176-180 173-176 169-173 165-169 161-165 158-161 154-158 150-154 < 150	> 250 246-250 243-246 239-243 235-239 231-235 228-231 224-228 220-224 216-220 213-216 209-213 205-209 201-205 198-201 194-198 190-194 < 190	> 270 267-270 264-267 261-264 258-261 254-258 251-254 248-251 245-248 242-245 239-242 236-239 233-236 229-233 226-229 223-226 220-223 < 220	> 250 247-250 244-247 241-244 238-241 234-238 231-234 228-231 225-228 222-225 219-222 216-219 213-216 209-213 206-209 203-206 200-203 < 200	> 290 287-290 284-287 281-284 278-281 274-278 271-274 268-271 265-268 262-265 259-262 256-259 253-256 249-253 246-249 243-246 240-243 < 240	> 300 298-300 295-298 293-295 290-293 288-290 285-288 283-285 263-265 260-263 258-260 255-258 253-255 250-253 248-250 245-248 243-245 240-243 < 260	> 280 278-280 275-278 273-275 270-273 268-270 265-268 263-265 260-263 258-260 255-258 253-255 250-253 248-250 245-248 243-245 240-243 < 260	> 140 136-140 133-136 129-133 125-129 121-125 118-121 114-118 110-114

$T_H$  = Brightness temperature derived from the ESMR horizontal polarization data  
 $T_V$  = Brightness temperature derived from the ESMR vertical polarization data

Table 5-9

This table follows the new Table 5-5a (above), which replaced  
Table 5-5 on page 105 in the User's Guide

Table 5-5b

Brightness Temperature Value for each Step of the Gray Scale on ESMR Image Displays for Orbits 3933 through 6184 (31 March through 30 June 1976)

(Brightness Temperatures are in °K)

Gray Scale Number	Swath Number and ESMR Display Parameter				
	1 and 6 (T <sub>H</sub> )	2 and 7 (T <sub>H</sub> )	3 and 8 (T <sub>H</sub> )	4 and 9 (T <sub>V</sub> )	5 and 10 $\left(\frac{T_H + T_V}{2}\right)$
(black) 1	>200	>230	>210	>250	>270
2	196-200	296-230	206-210	246-250	267-270
3	191-196	223-226	203-206	243-246	264-267
4	187-191	219-223	199-203	239-243	261-264
5	183-187	215-219	195-199	235-239	258-261
6	178-183	211-215	191-195	231-235	254-258
7	174-178	208-211	188-191	228-231	251-254
8	169-174	204-208	184-188	224-228	248-251
9	165-169	200-204	180-184	220-224	245-248
10	161-165	196-200	176-180	216-220	242-245
11	156-161	193-196	173-176	213-216	239-242
12	152-156	189-193	169-173	209-213	236-239
13	148-152	185-189	165-169	205-209	233-236
14	143-148	181-185	161-165	201-205	229-233
15	139-143	178-181	158-161	198-201	226-229
16	134-139	174-178	154-158	194-198	223-226
17	130-134	170-174	150-154	190-194	220-223
(white) 18	<130	<170	<150	<190	<220

T<sub>H</sub> = Brightness temperature derived from the ESMR horizontal polarization data

T<sub>V</sub> = Brightness temperature derived from the ESMR vertical polarization data

Table 5-10

Brightness Temperature Value for each Step of the Gray Scale on ESMR Image Displays for Orbits 6185 (15 September 1976) through the present Catalog period

(Brightness Temperatures are in °K)

Gray Scale Number	Swath Number and ESMR Display Parameter				
	1 and 6 (T <sub>V</sub> )	2 and 7 (T <sub>V</sub> )	3 and 8 (T <sub>V</sub> )	4 and 9 (T <sub>V</sub> )	5 and 10 (T <sub>V</sub> )
(black) 1	>240	>254	>270	>280	>300
2	236-240	251-254	266-270	277-280	296-300
3	233-236	248-251	263-266	274-277	293-296
4	230-233	245-248	260-263	271-274	290-293
5	227-230	242-245	257-260	268-271	287-290
6	224-227	239-242	254-257	265-268	284-287
7	221-224	236-239	251-254	262-265	281-284
8	218-221	233-236	248-251	259-262	278-281
9	215-218	230-233	245-248	256-259	275-278
10	212-215	227-230	242-245	253-256	272-275
11	209-212	224-227	239-242	250-253	269-272
12	206-209	221-224	236-239	247-250	266-269
13	203-206	218-221	233-236	244-247	263-266
14	200-203	215-218	230-233	241-244	260-263
15	197-200	212-215	227-230	239-241	257-260
16	193-197	208-212	223-227	237-239	253-257
17	190-193	205-208	220-223	235-237	250-253
(white) 18	<190	<205	<220	<235	<250

T<sub>V</sub> = Brightness temperature derived from the ESMR vertical polarization data

From orbit 6185 (15 September 1976) through the current data catalog period, the new ESMR image display has the following format:

Since an anomaly renders the Horizontal channel unuseable, the new ESMR format was devised to display the Vertical channel with five different temperature ranges and polarization for each individual swath. That is, the temperature range and polarization for swaths 1 and 6 are the same. Swaths 2 and 7, 3 and 8, 4 and 9, and 5 and 10 display the same parameters. Thus, four additional swaths of data are dedicated to the Vertical channel display for a total of 5 swaths as described above.

Data time (GMT) references and grid overlay information remain unchanged. Please refer to Table 5-10 for new parameter information.

## 5.5 ERB Corrections to the User's Guide

Post-launch calibration procedures are described below. While the numbers are not for the period of this catalog, the calibration procedure is valid for all data. This information can be added as section 6.5a to the User's Guide and would fit on page 134.

### 6.5a Post-launch Calibration

The observations from the wide angle channels (11 and 12), which measure the total energy ( $< 0.2 \mu\text{m}$  to  $> 50 \mu\text{m}$ ) emitted and reflected by the earth, depend on the prelaunch calibration and pertinent instrument temperatures. Assuming unit emissivity for the target scene, the irradiance from the scene is given by,

$$H_T = [\Delta W - \epsilon_s F_s \sigma T_s^4 + \epsilon_d F_d \sigma (T_d + K_v)^4]$$

where

$\Delta W$  = effective thermopile irradiance ( $\text{w m}^{-2}$ )

$\sigma = 5.6697 \times 10^{-8} \text{ w m}^{-2} (\text{deg. K})^4$

$\epsilon_s$  = emissivity of FOV stop = 0.965

$F_s$  = view factor of the FOV stop = 0.18892

$T_s$  = temperature ( $^{\circ}\text{K}$ ) of the FOV stop

$\epsilon_d$  = emissivity of the thermopile = 0.977

$F_d$  = view factor of the thermopile = 0.80461

$T_d$  = temperature ( $^{\circ}\text{K}$ ) of the thermopile base

$K$  = factor relating thermopile base temperature to thermopile surface temperature =  $0.0031^{\circ}\text{K}$  per count

$v$  = thermopile output in digital counts

The effective thermopile irradiance ( $\Delta W$ ) is obtained from the thermopile output ( $v$ ) as follows:

$$\Delta W = a_0 (T_m) + a_1 (T_m) \cdot v$$

where

$$a_0 = C_0 + C_1 T_m,$$

and

$$a_1 = d_0 + d_1 T_m$$

are derived from prelaunch calibrations and depend on the module temperature ( $T_m$ , °C). The coefficients  $C_0$ ,  $C_1$ ,  $d_0$ ,  $d_1$  are given below. In calibrating channel 11 and channel 12 (W) with the FOV stop out, the quantity  $F_s$  in the equation for  $H_I$  is set to zero.

	<u>Ch. 11</u>	<u>Ch. 12 (W)</u>	<u>Ch. 12 (N)</u>
$C_0$ :	9.86	10.4	8.38
$C_1$ :	0.18358	0.23235	0.18483
$d_0$ :	0.6042	0.6035	0.6014
$d_1$ :	$-8.254 \times 10^{-4}$	$-6.109 \times 10^{-4}$	$-5.879 \times 10^{-4}$

The observations from the other two wide-angle channels (13 and 14), which measure the shortwave radiation ( $0.2 \mu m$  to  $4.0 \mu m$ ), and ( $0.7 \mu m$  to  $3.0 \mu m$ ), are transformed to irradiance (H) by,

$$H = \frac{(V - V_o)}{S_I}$$

where  $V$  is the digital counts,  $V_o$  is the offset (in counts) observed from dark FOV's, and  $S_I$  is the sensitivity ( $w m^{-2} count^{-1}$ ) obtained from the equation:  $S_I = S_0(1+(0.01) \cdot (T-25) \cdot STC)$ , where  $S_0$  is the sensitivity at  $25^\circ C$ ,  $T$  is the detector temperature ( $^\circ C$ ), and  $STC$  is the sensitivity temperature coefficient (percent per degree C). These constants are given below:

<u>Ch</u>	<u><math>V_o</math></u>	<u><math>S</math></u>	<u><math>STC</math></u>
13	-41	2.004	0.04
14	-44	3.989	0.03

The interpretation of digital counts (V) from the shortwave scanning channels (15-18) gives the radiance ( $w m^{-2} sr^{-1}$ ) of the scene ( $N_s$ ) by,

$$N = \frac{(V - V_0)}{S_I}$$

where  $V_0$  is the offset (counts) obtained during views of the internal blackbody or space. The sensitivity  $S_I$  at temperature  $T(^{\circ}\text{C})$  is obtained using the equation for  $S_I$  described above, and the constants given below.

<u>Ch</u>	<u><math>V_0</math></u>	<u>S</u>	<u>STC</u>
15	-3	3.155	0.0
16	0	3.275	0.03
17	-1	3.116	-0.01
<u>18</u>	<u>15</u>	<u>2.963</u>	<u>-0.05</u>

A series of checks on the sensitivity of these channels, using the on-board diffuse target, indicated no noticeable degradation over the July-August 1975 period of operation.

The longwave scanning channels (19-22) have had numerous inflight calibrations which have remained essentially unchanged since 3 July. The calibration coefficients,  $a_0$  and  $a_1$  relate digital counts ( $V$ ) to the scene radiance  $N$  ( $\text{w m}^{-2} \text{ sr}^{-1}$ ) as follows:

$$N_s = N_m + a_0 + a_1 \cdot V$$

where  $N_m$  is the radiance of the detector module. The radiance  $N_s$  is the actual radiance measured within the spectral limits of the filter ( $4.5 \mu\text{m}$  to  $50 \mu\text{m}$ ). The calibration coefficients, obtained from inflight calibrations on 3 July 1975, are as follows:

<u>Ch</u>	<u><math>a_0</math></u>	<u><math>a_1</math></u>
19	-0.82	0.09583
20	-0.60	0.10535
21	-1.26	0.10168
<u>22</u>	<u>-0.29</u>	<u>0.10338</u>

The deviations of these calibration coefficients as derived from inflight calibrations from 29 July to 20 August are shown in Table 6-6a. The only change which indicates a need for updating the calibration coefficients is the change in the intercept of channel 20.

Periodic checks of the electronic gains of channels 1 through 14 have shown that the electronic gains have remained within 0.5 percent of the prelaunch values, with few exceptions. Table 6-6a shows the percentage of maximum deviation in the gain ratios (current/prelaunch) for the three steps in the calibration staircase voltage. The 6.5 percent change in the high-level gain of channel 2 and the gain changes in channels 6, 7, and 8 are believed to be caused by radio-frequency interference with the electronic calibration circuit and is neither a real change in the electronic gain nor nonlinearities of the channels.

Table 5-11

This table is part of the new Section 6.5a "Post-launch Calibration"  
to be added to the ERB section of the User's Guide

Table 6-6a

Stability of Calibration of the  
ERB Longwave Scanning Channels  
(between 29 July and 20 August 1975)

Date	Channel 19		Channel 20		Channel 21		Channel 22	
	$\Delta a_0$	$\Delta a_1$						
7/29	-0.07	-0.4	1.12	0.5	-0.07	-0.4	0.36	-0.3
8/5	0.50	-0.3	1.22	0.1	0.08	-0.3	0.11	-0.2
8/8	0.68	-0.4	1.33	0.1	0.04	-0.2	-0.003	-0.1
8/12	-0.06	-0.2	0.74	-0.4	-0.09	-0.3	0.17	-0.2
8/17	0.69	-0.3	1.49	0.2	0.20	-0.3	0.16	-0.2
8/20	-0.22	-0.3	1.53	0.2	0.04	-0.2	0.13	-0.4

$\Delta a_0$  = change in intercept ( $w m^{-2} sr^{-1}$ )

$$= (a_0)_{\text{current}} - (a_0)_{7/3/75}$$

$\Delta a_1$  = change in slope (%  $w m^{-2} sr^{-1} ct^{-1}$ )

$$= \frac{[(a_1)_{\text{current}} - (a_1)_{7/3/75}]}{(a_1)_{7/3/75}} \times 100$$

Table 5-12

This table is part of the new Section 6.5a "Post-launch Calibration"  
to be added to the ERB section of the User's Guide

Table 6-6b

Percentage Change of the Maximum Deviation in the Gain  
Ratio between Post-launch and Prelaunch Gain Values for  
ERB channels 1 through 14 (20 June and 17 August 1975)

Ch	G <sub>0-39</sub>	G <sub>30-60</sub>	G <sub>60-90</sub>
1	-0.2	0.2	-0.1
2	0.1	-0.3	-6.5
3	±0.1	-0.1	-0.2
4	±0.1	-0.2	-0.1
5	±0.1	-0.2	0.2
6	2.6	1.8	-2.1
7	1.3	2.1	-0.6
8	1.6	1.3	-0.9
9	0.4	-0.6	±0.1
10	0.7	-0.5	±0.2
11	-0.4	0.3	0.4
12	0.2	-0.2	0.4
13	-0.3	0.2	0.3
14	+0.2	-0.1	0.3

Table 6-7, the ERB Compacted Archival Tape Format, on pages 136 through 139 of the User's Guide, should be changed as follows:

Directory Record (Page 136)

Delete last line of section A which reads:

"135-340      Zero fill                                  1"

and add the following:

135-149      Orbital Elements

135	Day of Epoch	1
136	Year of Epoch	1
137	Hours	1
138	Minutes (including fraction)	100
139	Eccentricity	10 <sup>5</sup>
140	Argument of Perigee (integer part)	1
141	Argument of Perigee (fraction part)	10 <sup>3</sup>
142	Right Ascension (integer part)	1
143	Right Ascension (fraction part)	10 <sup>3</sup>
144	Inclination (integer part)	1
145	Inclination (fraction part)	10 <sup>3</sup>
146	Semimajor Axis (km, integer part)	1
147	Semimajor Axis (km, fraction part)	10 <sup>3</sup>
148	Mean Anomaly (integer part)	1
149	Mean Anomaly (fraction part)	10 <sup>3</sup>
150	Sun-Earth Distance (A. U.)	10 <sup>4</sup>
151-340	Zero fill	1

Orbital Summary Record (Page 139)

Delete last line of table, which reads:

17-340      Zero fill                                  1"

and add the following:

17-26	Solar Irradiances (Chs. 1-10) Normalized to mean sun-earth distance	Chs. 1-5:10 Chs. 6-10:100
27	Solar Channels Assembly Gamma Angle (positive to right of track)	1
28-340	Zero fill	1

## 5.6 LRIR Corrections to the User's Guide

Table 5-13

Post-launch analysis of relative spectral response data and orbital data leads to the following corrected values for Table 7-2, on page 154 of the User's Guide

Table 7-2

### Optical Characteristics of LRIR Channels

Channel		Band Pass (50% Peak Response)	Field-of-view (km)		Random noise in orbit* $\pm 1\sigma$ (watts/m <sup>2</sup> -sr)
No.	Abbrev.		Vertical	Horizontal	
1	NCO <sub>2</sub>	649-672 cm <sup>-1</sup> (14.9-15.4 $\mu$ m)	2.0	20	0.0023
2	BCO <sub>2</sub>	592-700 cm <sup>-1</sup> (14.3-16.9 $\mu$ m)	2.0	20	0.0040
3	O <sub>3</sub>	984-1169 cm <sup>-1</sup> (8.6-10.2 $\mu$ m)	2.0	20	0.011
4	H <sub>2</sub> O	412-446 cm <sup>-1</sup> (22.4-24.3 $\mu$ m)	2.5	25	0.008

\*Noise will gradually increase as the detector temperature increases during the useful life of the experiment.

## 5.7 PMR Corrections to the User's Guide

There are no PMR corrections to the User's Guide.

5.8 TWERLE Corrections to the User's Guide

Table 5-14

The following are address changes to Table 9-2  
on page 186 in the User's Guide

Table 9-2

Nimbus RAMS Experiments - Address Changes

Address Changes

<u>OLD</u>	<u>NEW</u>
Mr. G. R. Cresswell Division of Fisheries & Oceanography Commonwealth Scientific & Industrial Research Organization Melbourne, Australia	Mr. G. R. Cresswell Division of Fisheries & Oceanography CSIRO P. O. Box 21 Cronulla, N. S. W. 2230 Australia
A. J. Dyer CSIRO P. O. Box 77 Mordialloc, Vic 3195 Australia	Dr. A. J. Dyer Division of Atmospheric Physics CSIRO Station Street ASPENDALE 3195 Victoria, Australia
Professor Pierre Lacombe, Director Laboratory d'Oceanographic Museau Historie Naturelle de Paris 43 Rue Cuvier Paris, France	Professor Pierre Lacombe, Director Laboratoire d'Océanographie Physique Muséum National d'Histoire Naturelle 43-45 Rue Cuvier 75005 Paris, France
Professor P. Tchernia Muséum d'Histoire Naturelle de Paris 43 Rue Cuvier Paris, France	Professor P. Tchernia Laboratoire d'Océanographie Physique Muséum National d'Histoire Naturelle 43-45 Rue Cuvier 75005 Paris, France

Table 9-2 (Continued)

Dr. Norbert Untersteiner, Program Director Project AIDJEX 4059 Roosevelt Way, N.E. Seattle, WA 98105	Dr. Norbert Untersteiner AIDJEX Coordinator University of Washington 4059 Roosevelt Way, N.E. Seattle, Washington 98105
Dr. Donald V. Hansen, Director Physical Oceanography AOWL NOAA U. S. Department of Commerce Miami, Florida	Dr. Donald V. Hansen, Director Physical Oceanography Laboratory AOML/NOAA 15 Rickenbacker Causeway Virginia Key Miami, Florida 33149
Vincent E. Lally National Center for Atmospheric Research P.O. Box 1470 Boulder, Colorado 80302	Mr. Vincent E. Lally National Center for Atmospheric Research P.O. Box 3000 Boulder, Colorado 80302
J. Lentfer Wildlife Research U. S. Department of Interior 813 D. Street Anchorage, Alaska	Mr. Jack W. Lentfer Fish and Wildlife Service Department of Interior 4454 Business Park Blvd. Anchorage, Alaska 99503
H. Brann Bureau of Meteorology Melbourne, Victoria Australia	Mr. H. N. Brann Bureau of Meteorology P.O. Box 1289K Melbourne, Victoria 3001 Australia
Robert Kee Development Engineering Division Code 6201 U. S. Naval Oceanographic Office Washington, D.C. 20390	Mr. Robert Kee Code 6220 U. S. Naval Oceanographic Office Washington, D.C. 20373

Table 9-2 (Concluded)

F. Anderson South African Council for Scientific & Industrial Research Congella, Natal, South Africa	Mr. Frank P. Anderson CSIR, Institute for Technology P.O. Box 17001 Congella 4013 South Africa
H. Stommel Professor of Oceanography MIT Cambridge, Massachusetts	Professor Henry Stommel Department of Meteorology Room 54-1416 Massachusetts Institute of Technology Cambridge, Massachusetts 02139
B. Buck Polar Research Lab. Santa Barbara California 93101	Mr. B. M. Buck, President Polar Research Laboratory, Inc. 123 Santa Barbara Street Santa Barbara, California 93101
John A. Knauss Graduate School of Oceanography University of Rhode Island Kingston, Rhode Island 02881	Dr. P. L. Richardson Woods Hole Ocean Institute Woods Hole, Massachusetts 02543

5.9 T&DRE Corrections to the User's Guide

There are no T&DRE corrections to the User's Guide.

Table 5-15

The following are new TWERLE users, added since launch.  
 This information should be added to Table 9-2  
 (Nimbus RAMS Experiments) on page 186 in the User's Guide.

Principal Investigator	Experiment Title	Platforms		
		Number	Type	Deployment Area
Mr. Kalinowski Centre National Pour L'Exploitation Des Oceans COB 29 N-Plouzane B-T 337 29273 Brest CEDEX, France	Drifting Buoys in Bay of Biscay, France	10	Drifting Buoys	Bay of Biscay, France
Mr. James L. Baker 4 Beach Road Sherwood Forest, Maryland 21405	Distress Communication and Location System for Small Craft	2	Ships	Chesapeake Bay and Gulfstream between Florida and Cape Hatteras
Mr. Michael Metge Imperial Oil LTD. 339 50th Ave., S.E. Calgary, Alberta Canada T2G 2B3	Surface Drifter Buoys, Davis Strait	24	Drifting Buoys	Davis Strait
Mr. Ronald J. Lynn NOAA/NMFS Southwest Fisheries Center P.O. Box 271 La Jolla, California 92038	Albacore Oceanography Drifter Study	9	Drifting Buoys	Eastern Pacific Ocean
Dr. Julian Pike NCAR, P.O. Box 3000 Boulder, Colorado 80307	Mountain Wind Project	4	Meteorological Platforms	Rocky Mountains
Mr. Jorgen Taagholt Ionosphere Laboratory University of Denmark Building 349 Dk. 2800 Lyngby, Denmark	Greenland Meteorological Experiment	3	Meteorological Platforms	Northeast Greenland
Dr. A. D. Kirwan, Jr. Department of Oceanography College of Geosciences Texas A&M University College Station, Texas 77843	Anomaly Dynamics Study (ADS)	32	Drifting Buoys	North Pacific
Mr. Jan Dietrich Danish Hydraulic Institute Agern Alle 5 DK 2970 Horsholm, Denmark	Iceberg Tracking in Davis Strait	4	Buoy Transmitter	Davis Strait

Table 5-15 (Continued)

Mr. Gale Woods NOAA National Marine Fisheries Service NSTL Bay St. Louis, Mississippi 39520	Porpoise Tracking System Project	5	Antenna and Transmitter	San Diego, California
Mr. David F. Thomas, Jr SATD-MEB-SDS, Mail Stop 322 NASA Langley Research Center Hampton, Virginia 23665	Air-droppable In Situ Platforms for Long Duration Measurements near Hurricanes	10	Ocean Platforms	Western Atlantic near North America
Dr. P. Roger Williamson Department of Applied Physics & Information Science University of California - San Diego La Jolla, California 92037	Stratospheric Monitoring with Long-term Balloon Flights	3	Super-pressure Balloons	Southern Hemisphere
Mr. J. C. O'Rourke Canadian Marine Drilling, Ltd. P.O. Box 200 Calgary, Canada T2P 2H8	Arctic Ice Dynamics	24	Sea Ice Platforms	Beaufort Sea
Dr. J. Michael Hall NOAA Data Buoy Office National Space Tech Office Bay St. Louis, Mississippi 39520	East Coast Drifting Experiment	24	Drifting Buoys	Atlantic Ocean
	High Impact Detection and Determination on Large Buoys	10	Buoy	Atlantic Ocean, Gulf of Mexico, & North Pacific Ocean
	Reliability Enhancement Experiment	3	Buoy	Santa Barbara, California & Arctic Ocean
Mr. Robert Ochlkers University of Wisconsin Space Science and Engineering Center 1225 W. Dayton St. Madison, Wisconsin 53706	Buoy Experiments in Lake Michigan	10	Buoy	Lake Michigan
Capt. E. A. Delaney USCG Oceanographic Unit Bldg. 159E Navy Yard Navy Yard Annex Washington, D.C. 20590	North Atlantic and Labrador Current Studies	1	Drifting Buoys	North Atlantic, Labrador Coast
Dr. R. H. Goodman Innovative Ventures, Ltd. 4632 11th St. Calgary Alberta, Canada T2E2W7	Ice Monitoring in the Canadian Arctic and Labrador Region	2	Drifting Buoys	Canadian Arctic, Labrador

Table 5-15 (Continued)

Mr. L. Brooks Chevron Oil Field Research Co. P.O. Box 446 La Habra, California 90631	Current Flow and Iceberg Drift in Davis Strait	4	Buoys	Davis Strait
Dr. John D. Cochrane Department of Oceanography Texas A&M University College Station, Texas 77843	North Equatorial Counter-current Experiment	3	Buoys	Pacific Ocean
Dr. F. M. Vukovich P.O. Box 12194 Research Triangle Institute Research Triangle Park North Carolina, 27709	Gulf Stream Eddies	4	Drifting Buoys	Gulf Stream
Dr. Donald R. Sheldon Drug Enforcement Administration D E A 1405 I St. N.W. Washington, D.C. 20537	Tracking Concealed RAMS Transmitters	10	Beacon	Washington, D.C.
Dr. D. Halpern NOAA Pacific Marine Env. Labs Univ. Washington WB10 Seattle, Washington 98195	Ocean Circulation Studies and Pacific Equatorial Waters	3	Drifting Buoys, Moored Buoys	Mid-Pacific Equatorial
M. Petit, Project Marisonde Cerain, Magny Les Hameaux 78470 Saint Remy, France	Project Marisonde	7	Meteoro- logical Buoys	10°W-15°W 44°N-46°N
Dr. John J. Kelly Naval Arctic Research Lab. Barrow, Alaska 99723	NARL Buoy Program	10	Buoys	Arctic Ocean

